NUI MAYNOOTH

Ollscoil na hÉireann Má Nuad

AN ASSESSMENT OF THE RELATIONSHIP BETWEEN GLACIER MASS BALANCE AND SYNOPTIC CLIMATE IN NORWAY:

LIKELY FUTURE IMPLICATIONS OF CLIMATE CHANGE

Rowan Fealy

Dr. John C. Sweeney

Thesis submitted for the degree of Ph.D.

Department of Geography,

Faculty of Arts,

National University of Ireland, Maynooth

October 2004

An assessment of the relationship between glacier mass balance and synoptic climate in Norway: likely future implications of climate change

Rowan Fealy

Abstract

Regional variations in temperature and precipitation from selected European stations are found to be significantly related to large-scale modes of atmospheric variability in the North Atlantic. Increased westerlies over Europe, particularly since the 1970s, are shown to significantly contribute to increases in temperature and precipitation over northern Europe while suppressing the penetration of warm, moist air into more southern European locations. These regional variations, primarily resulting from changes in the atmospheric circulation, are found to largely explain the divergent response evident in glacier mass balance, between Scandinavia and the Alps, over the last 30 years.

To further examine these linkages, a Temporal Synoptic Index (TSI) was derived for a number of locations in Norway. Principal Components Analysis (PCA) and subsequent clustering of component scores is used to classify days for both winter and summer seasons over the period 1968-1997. Findings indicate that the occurrence of 'warm' type air masses during the summer months have increased in frequency, particularly since the late 1980s. However, temperatures were also found to be decreasing in these clusters. A general decrease in the frequency of 'cold' cluster types during the winter months is evident until the early 1990s. These decreases were largely compensated for by increases in the frequency of 'warm' types, with an increased moisture carrying capacity, particularly since the late 1970s. The frequency occurrence of these key air mass types was shown to be significantly related to glacier mass balance during both the accumulation and ablation season. Winter air mass types from maritime source regions act to enhance accumulation and suppress ablation, while summer continental source types suppress accumulation and enhance ablation.

Statistically downscaled output from the HadCM3 GCM for two locations in southern Norway indicate mean winter temperatures are likely to increase by ~1.25°C by the end of the present century with the largest increases occurring during December and January. Summer increases are suggested to be in the region of ~2.5°C, with a more marked increase of up to ~3.5°C during the month of August. Based on these scenarios, a Temporal Synoptic Index for the period 1997-2099 is constructed. This index is then used to predict glacier mass balance, used as input into an ice-flow model for Rembesdalskåka, in southern Norway, to assess likely future changes in glacier behaviour as a consequence of anthropogenic climate change.

Results from the ice-flow model indicate that the equilibrium line altitude (ELA) of Rembesdalskåka is likely to increase in altitude from its average 1968-1997 position of 1650 metres to 1750 metres by end of century resulting in a retreat of front position of nearly 3km. Despite a decreasing glacier net balance which commences around 2010, increases in summer ablation only become a significant contributor to net balance after 2040, resulting in an advance of the glacier front of up to 1km during the first few decades of the century. These findings suggest that the hydroelectric power industry in Norway is likely to be a beneficiary of the projected changes in glacier behaviour arising from climate change.

Acknowledgements

To my parents, who first set me on this path when they brought me by the hand to my first day at school, and for letting me know that no matter what, I don't have too far to reach out and their supporting hand will still be there. To Rea, who over the course of this thesis (and my life!), has provided immeasurable support both on a work level and in keeping me sane, for which I am eternally grateful. To Ros, for being a brother when I needed him and slipping me the odd 20 quid when I was a poor student! I would also like to thank a more recent addition to my family, Orpha, for her patience, support and friendship.

Emma, to whom a simple thanks will never cover all that she has done (seen and unseen) and put up with me during this thesis, particularly during the last year, when even the limits of her patience were tested on a daily basis. From the bottom of my heart, I would like to thank you, for being you.

I would also like to thank my extended family and friends for knowingly, or unknowingly, providing support and for their friendship, which I may have tested on occasion.

There is an endless number of people who have provided assistance and support and without whom I would not have been able to carry out this research. Eirik Førland in DNMI for his kindness and advice on the Norwegian meteorological data and to Asta Guttormsdottir for sorting out the data for me. I would also like to thank Liss Marie Andreasson, Bjarne Kjøllmoen and Elvehøy Hallgeir from NVE who provided invaluable assistance and advice on glaciers in Norway. I am also indebted to W. Brian Whalley (QUB) who willingly donated his extensive library of reports on glaciers in Norway. W.H. Theakstone also provided support and advice to the early stages of this research which was invaluable. I am also very grateful to Rob Wilby for his advice and guidance on statistical downscaling.

Physical geographers tend to require regular data 'fixes', two providers of which I would like to particularly thank- Ian Harris at CRU for providing access to the NCEP reanalysis data which was sourced from NOAA-CIRES Climate Diagnostics Center, Boulder, Colorado, USA and providing essential follow up support and David Viner who facilitated many a query on the HadCM3 data which was supplied by the Climate Impacts LINK Project (DEFRA Contract EPG 1/1/154) on behalf of the Hadley Centre and U.K. Meteorological Office.

I am also very grateful to Jason Doran who gave endlessly of his time and computer programming skills, without which I would probably be still writing this! I would also like to thank you for your friendship and support over the all the years I have known you. I would also like to thank Mark Maguire for his help and advice and being a great friend.

I would also like to take this opportunity to thank all the staff of the Geography Department for all their help and support over the years that I have studied and worked in the department- Jim W, Paddy, Rob, Brendan, Mary, Gay, Jim K., Dot, Fran and a more recent addition, Ronan. A special mention for Dennis and Shelagh who provided endlessly of their time and patience while trying to explain basic

statistics to me! Ro, for advice on modelling issues and Paul for his advice and support, particularly over the last few months when he had to suffer reading this. I would also like to thank all the postgrads, past and present, who have contributed enormously to my time in Maynooth.

A special thank you to five in particular who have endured me and tried to humour me during my time here, but more importantly have given freely of their friendship and for that I am grateful. Martina, for your friendship and (nearly always) good humour; Conor, who has the dubious pleasure of sharing an office with me and consequently has suffered more than others! your friendship means a lot to me; Una, your friendship and openness has helped put things in perspective when needed, long may it continue; Laura, I would like to say thanks for your friendship and patience, particularly over the last (almost) year and normalising the whole surreal experience of doing a thesis (this ***is*** the last thesis Thursday ***ever***!!). Finally, to AK, whose endless willingness to help people resulted in my *conversion* to geography and ultimately to my doing this thesis. Adrian has also had the very dubious pleasure of sharing an office with me from which I think I was the net beneficiary. Thank you all for your support, help and more importantly, your friendship throughout out our time here.

I owe a debt of gratitude to one individual in particular, John Sweeney, who has given freely and willingly of his time while sheparding me through this whole process. I am indebted to you for all your time, patience, help, support, advice and friendship without which this thesis would now be a long forgotten idea! It is a privilege to have studied under your guidance and direction.

Rowan

CONTENTS

List of figures *(i)*
List of plates *(iv)*
List of tables *(v)*

Chapter I: Climate-glacier interaction studies: an introduction

1.1 Introduction 1

1.2 Climate-glacier interaction studies: A brief review 4

1.3 Aims and Objectives 7

1.4 Contemporary climate change: A future for glaciers? 9

1.5 Study location and glacier selection 12

1.6 Thesis outline 17

Chapter II: Accounting for climate variability in the North Atlantic: the influence of atmospheric circulation

2.1 Introduction 19

2.2 North Atlantic Oscillation (NAO) 20
2.2.1 NAO and temperature 22
2.2.2 NAO and precipitation 25
2.2.3 Statistical analysis of the relationship between atmospheric modes and climate elements 26

2.3 Conclusion 39

Chapter III: Long-term fluctuations in temperature and precipitation in Europe: can they be explained by atmospheric variability?

3.1 Introduction 42

3.2 Evidence for trends in the European temperature and precipitation series? 43

3.3 A change point analysis of the climate series 49
3.3.1 Cumulative sums of deviations (CUSUMS) 49
3.3.2 Evidence for change points in the atmospheric modes of variability 58

3.4 Conclusions 63

Chapter IV: An examination of regional mass balance in Europe from selected glaciers: the role of atmospheric variability and regional climate

4.1 Introduction 66

4.2 Components of glacier mass balance 67

4.3 Climate-glacier interactions 74
4.3.1 Regional variation in mass balance trends 74
4.3.2 The relationship between long-term variations in mass balance and climate 76

4.4 Conclusion 80

Chapter V: Regional climate indices and Scandinavian glacier mass balance

5.1 Introduction 82

5.2 Regional climate and mass balance 83
5.2.1 Circulation Indices 83
5.2.1.1 Zonal air flow 84
5.2.1.2 Meridional air flow 87
5.2.1.3 Localised atmospheric circulation index 88
5.2.2 The local climate dimension 92

5.3 Discussion 98
5.3.1 Evidence of a non-stationary response to climate? A note of caution 100

5.4 Conclusion 103

Chapter VI: Temporal synoptic classification methodology

6.1 Introduction 105

6.2 Synoptic climatological literature: A review of relevant classification techniques 106

6.3 Methodology 115
6.3.1 Data 115
6.3.2 Synoptic typing 118
6.3.2.1 Principal Components Analysis 118
6.3.2.2 Normalisation Constraints 125
6.3.2.3 Clustering Procedure 126

6.4 Conclusion 129

Chapter VII: Temporal Synoptic Index results

7.1 Introduction 130

7.2 Results from temporal synoptic index 130
7.2.1 Principal Components 130
7.2.2 Cluster characteristics 132
7.2.2.1 Winter 133
7.2.2.2 Summer 144
7.2.3 Conclusion 153

7.3 Relationship between air mass frequencies and glacier mass balance 154

7.4 Case study of Rembesdalskåka, an outlet glacier from Hardangerjøkulen 160

7.5 Conclusion 165

Chapter VIII: Statistical downscaling: a synoptic classification for the 21st century

8.1 Introduction 167

8.2 Statistical downscaling: a brief review and highlighting of some issues raised 174

8.3 Methodology 178
8.3.1 Data 180
8.3.2 Development of transfer functions 184

8.4 Results 186
8.4.1 Calibration and verification 186
8.4.2 Scenario Generation 194
8.4.3 Downscaled Temporal Synoptic Index 1968-2100 198
8.4.4 Results from the downscaled Temporal Synoptic Index 202
8.4.5 The effects of changing cluster frequency occurrence on glacier mass balance 208

Chapter IX: Ice flow model

9.1 Introduction 212

9.2 Review of mass balance and ice flow model literature 213

9.3 Glacier Model 218
9.3.1 Model Outline 218
9.3.2 Model Inputs 222
9.3.3 Glacier ice flow model 224
9.3.4 Model initialisation 224
9.3.5 Implications for Rembesdalskåka 229

9.4 Discussion 232

Chapter X: Conclusions: Summary of findings, research limitations and some future perspectives

10.1 Introduction 234

10.2 A brief overview and discussion of findings 235

10.3 Limitations of Research 239

10.4 Directions for further research 240

10.5 Future perspectives 241

Bibliography 244

Appendices

Appendix I: Recode values for horizontal visibility at surface I-1

Appendix II: Principal component matrices
Winter II-1
Summer II-5

Appendix III: Mean sea level pressure maps
Flesland III-1
Skabu III-3

Appendix IV: Percentiles of GCM and NCEP predictor variables
Winter III-1
Summer III-4

Appendix V: Flow diagram of methodological steps V-1

Appendix VI: Programme-Ice flow model IV-1

List of Figures

Figure 1.4.1 Variations of the Earth's surface temperature over the last 140 years and the last millennium. 10
Figure 1.4.2 Glacier front positions for a selection of global glaciers. 11
Figure 1.5.1 Map of glaciers in the mountain area of Jotunheimen from before 1853. 15
Figure 2.2.1 North Atlantic Oscillation. 20
Figure 2.2.2 North Atlantic Oscillation Index 1830-2000 23
Figure 2.2.3 Observed December-March surface temperature anomalies associated with a high NAO index; the period 1981-1995, when the NAO was high, relative to the period 1951-1980, when the NAO was low. 24
Figure 2.2.4 1981-1995 average precipitation anomalies expressed as departures from 1951-80 mean, from station data in Eischeid et al. (1991) data set 26
Figure 2.2.5 Location map of temperature and precipitation stations. 28
Figure 2.2.6 Scatter diagrams of the NAO ± 2d with temperature and precipitation for a selection of stations. 36
Figure 3.2.1 Winter Temperature for Alpine and Scandinavian stations. 45
Figure 3.2.2 Winter Precipitation for Alpine and Scandinavian stations. 46
Figure 3.2.3 Summer Temperature for Alpine and Scandinavian stations. 47
Figure 3.2.4 Summer Precipitation for Alpine and Scandinavian stations. 48
Figure 3.3.1 CUSUMS (cumulative sums of deviations) of NAO, EA-JP and summer temperatures for Alpine Stations. 51
Figure 3.3.2 CUSUMS (cumulative sums of deviations) of NAO, EA-JP and summer temperatures for Scandinavian Stations. 51
Figure 3.3.3 CUSUMS (cumulative sums of deviations) of NAO and winter temperatures for Alpine Stations. 52
Figure 3.3.4 CUSUMS (cumulative sums of deviations) of NAO and winter temperatures for Scandinavian Stations. 53
Figure 3.3.5 CUSUMS (cumulative sums of deviations) of NAO, EA-JP and summer precipitation for Alpine Stations. 55
Figure 3.3.6 CUSUMS (cumulative sums of deviations) of NAO, EA-JP and summer precipitation for Scandinavian Stations. 55
Figure 3.3.7 CUSUMS (cumulative sums of deviations) of NAO and winter precipitation for Alpine Stations. 57
Figure 3.3.8 CUSUMS (cumulative sums of deviations) of NAO and winter precipitation for Scandinavian Stations. 58
Figure 3.3.9 CUSUMS and Pettitt test of the annual NAO (Hurrell PC) 1900-2000. 60
Figure 3.3.10 CUSUMS and Pettitt test of winter NAO (Hurrell PC) 1900-2000. 60
Figure 3.3.11 CUSUMS and Pettitt test of summer NAO (Hurrell PC) 1900-2000. 61
Figure 3.3.12 Annual and Winter NAO with an 11-year moving average highlighting the negative phase in the NAO between 1930-1960 and the gradual increase after 1970. 62
Figure 3.3.13 Summer (JJA) NAO (1900-2000) and EA-JP (1946-2000) indices. 63
Figure 4.2.1 Location of the four long-term monitored glaciers 68
Figure 4.2.2 Winter, summer and annual net balance for Storbreen 1949-1999. 69
Figure 4.2.3 Winter, summer and annual net balance for Hintereisferner 1953-1999. 70
Figure 4.2.4 ELA versus net balance for Hintereisfernier 1953-1999 70
Figure 4.2.5 ELA versus net balance for Storbreen 1949-1999 71
Figure 4.2.6 ELA versus net balance for Storglaciaren 1946-1999 71
Figure 4.2.7 Area-elevation Distribution for Hintereisferner 1964 and 1995 73
Figure 4.2.8 Area-elevation Distribution for Storbreen 1996 73
Figure 4.2.9 Area-elevation Distribution for Storglacieran 1981 and 1996 74
Figure 4.3.1 Cumulative Net Balance (m w.eq) of four European glaciers over their length of record. 75
Figure 4.3.2 5-year averages of deviations of mean summer temperature from the

long term mean, areal mean of deviations and NAO_{JJA}. 76
Figure 4.3.3 5-year centred moving average of the standardised mean net balance of eleven Alpine glaciers (Alps) and ten Scandinavian glaciers (Scandinavian) from 1948-2000. The annual NAO is also plotted 77
Figure 5.1.1 Cumulative net balance of selected Norwegian glaciers (including Storglaciaren) 82
Figure 5.2.1 Location of Indices and glaciers 83
Figure 5.2.2 Correlation between glacier mass balance and the NAO indicating a decreasing relationship with increasing continentality of glacier location (1-6 Southern Norway; 7-8 Northern Scandinavia; 9-10 Svalbard). 86
Figure 5.2.3 Mean winter, summer and net balance of the Norwegian glaciers (1968-1999). ELA of the glaciers is displayed on the right hand axis. 86
Figure 5.2.4 Cumulative net balance of both long-term monitored Scandinavian glaciers. Also plotted are the cumulative deviations of the annual NAO derived from the 1st principal component of pressure. 91
Figure 5.2.5 Winter temperature from Laerdal and winter balance from Ålfotbreen. 93
Figure 5.2.6 Winter precipitation from Skjaak and winter balance from Ålfotbreen. 93
Figure 5.2.7 NI Index, between, Ona and Utsira-Fyr, and winter balance from Ålfotbreen. 94
Figure 5.2.8 Winter temperature from Laerdal and winter balance from Nigardsbreen. 95
Figure 5.2.9 Winter precipitation from Skjaak and winter balance from Nigardsbreen. 95
Figure 5.2.10 NI Index, between, Ona and Utsira-Fyr, and winter balance from Nigardsbreen. 96
Figure 5.2.11 Summer temperature from Laerdal and summer balance from Ålfotbreen. 97
Figure 5.2.12 NI Index, between, Ona and Utsira-Fyr, and summer balance from Ålfotbreen. 97
Figure 5.2.13 BS Index and summer balance from Ålfotbreen. 98
Figure 5.3.1 DJF NAO correlations (Pearson's r) with "increasing length of time series" 1980-1999 and winter balance. 100
Figure 5.3.2 EA-JP correlations (Pearson's r) with "increasing length of time series" 1980-1999 and summer balance. 101
Figure 5.3.3 BS Index correlations (Pearson's r) with "increasing length of time series" 1980-1999 and summer balance. 102
Figure 6.3.1 Stations locations and their position relative to monitored Norwegian glaciers. 116
Figure 6.3.2 Scree Plot for Flesland DJF. 123
Figure 6.3.3 Scree plot of cluster centres for Flesland. 128
Figure 7.2.1 Flesland cold (TSI 3). 139
Figure 7.2.2 Orlandet cold (TSI 2 +5+9). 139
Figure 7.2.3 Skabu cold (TSI4-coldest (▲) and TSI1-second coldest(●)). 139
Figure 7.2.4 Flesland warm (TSI 7 +12). 139
Figure 7.2.5 Orlandet warm (TSI 6+8). 139
Figure 7.2.6 Skabu DJF warm (TSI 3 +10). 139
Figure 7.2.7 Nordstraum cold (TSI 1b+1c). 140
Figure 7.2.8 Bodo cold (TSI 4). 140
Figure 7.2.9 Nordstraum warm (TSI 6+7). 140
Figure 7.2.10 Bodo warm (TSI 5 + 10). 140
Figure 7.2.11 Mean temperature of cold cluster (TSI3) from Flesland. 141
Figure 7.2.12 Mean temperature of cold cluster (TSI3b and TSI 3c) from Flesland. 141
Figure 7.2.13 Mean temperature of cold cluster (TSI4) from Bodo. 142
Figure 7.2.14 Mean temperature of cold cluster (TSI 1c) from Nordstraum. 143
Figure 7.2.15 Mean temperature of warm cluster (TSI 7) from Nordstraum. 143
Figure 7.2.16 Bergen JJA warm (TSI 1). 149
Figure 7.2.17 Bodo JJA warm (TSI 2). 149
Figure 7.2.18 Flesland JJA warm (TSI 1+9). 149
Figure 7.2.19 Nordstraum JJA warm (TSI 3+6). 149
Figure 7.2.20 Orlandet JJA warm (TSI 10-14). 149
Figure 7.2.21 Skabu JJA warm (TSI 3). 149
Figure 7.2.22 Mean temperature of warm clusters (TSI 1 & 9) from Flesland. 150

Figure 7.2.23 Mean temperature of warm clusters (TSI 3, 10 & 11) from Orlandet. 150
Figure 7.2.24 Mean temperature of warm clusters (TSI 3a) from Skabu. 151
Figure 7.2.25 Mean temperature of warm clusters (TSI 2) from Bodo. 151
Figure 7.2.26 Mean temperature of warm clusters (TSI 5) from Nordstraum. 152
Figure 7.2.27 Mean daily temperatures for JJA for all stations (1968-1998). 152
Figure 7.3.1 Location of synoptic stations (▲) and glaciers (●). 154
Figure 7.4.1 Mass balance for Hardangerjøkulen 1963-2000. 161
Figure 7.4.2 Observed and modelled mass balance for winter based on a split sample. 164
Figure 7.4.3 Observed and modelled mass balance for summer based on a split sample. 164
Figure 8.1.1 Temperature change by 2100 depending on emissions scenario. 167
Figure 8.1.2 Modelled output with natural forcing only. 168
Figure 8.1.3 Modelled output with natural and anthropogenic forcing. 168
Figure 8.1.4 Conceptual 3-Dimensional structure of a GCM. 169
Figure 8.1.5 GCM land-sea mask and output resolution for the European domain. Grid box locations selected for downscaling are shown as black boxes. The selected sub-domain for each station is illustrated by the box outlines. 170
Figure 8.1.6 Temperature for the period 2040-2069. 171
Figure 8.1.7 Precipitation for the period 2040-2069. 172
Figure 8.3.1 Organisation of grid points used in calculation. The grid P5 represents the grid box containing the surface station. 182
Figure 8.4.1 Verification for downscaled temperature-Flesland (1983-1996). 189
Figure 8.4.2 Verification for downscaled temperature variance-Flesland (1983-1996). 189
Figure 8.4.3 Verification of downscaled specific humidity-Flesland (1983-1996). 190
Figure 8.4.4 Verification of downscaled specific humidity variance-Flesland (1983-1996). 190
Figure 8.4.5 Verification of downscaled *uu*-scalar - Flesland (1983-1996). 191
Figure 8.4.6 Verification of downscaled *uu*-scalar variance-Flesland (1983-1996). 191
Figure 8.4.7 Verification of downscaled temperature-Skabu (1983-1996). 192
Figure 8.4.8 Verification of downscaled temperature variance-Skabu (1983-1996). 192
Figure 8.4.9 Verification of downscaled specific humidity-Skabu (1983-1996). 193
Figure 8.4.10 Verification of Skabu specific humidity variance (1983-1996). 193
Figure 8.4.11 Verification of Skabu *uu*-scalar (1983-1996). 194
Figure 8.4.12 Verification of downscaled *uu*-scalar variance-Skabu (1983-1996). 194
Figure 8.4.13 Winter temperature (December, January and February) for Flesland 1968-2100, downscaled from the HadCM3 GCM. 195
Figure 8.4.14 Mean Summer temperature (June, July and August) for Skabu 1968-2100, downscaled from the HadCM3 GCM. 196
Figure 8.4.15 Flesland winter temperature-$GCM_{control}$ (1968-1996) and GCM_{future} (2068-2096) 197
Figure 8.4.16 Skabu summer temperature-$GCM_{control}$ (1968-1996) and GCM_{future} (2068-2096). 197
Figure 8.4.17 Flesland specific humidity-$GCM_{control}$ (1968-1996) and GCM_{future} (2068-2096). 198
Figure 8.4.18 Skabu specific humidity-$GCM_{control}$ (1968-1996) and GCM_{future} (2068-2096). 198
Figure 8.4.19 Comparison between winter air mass occurrence frequencies for Flesland. Observed (1968-1996), modelled current (1968-1996) and modelled future (2068-2096). 202
Figure 8.4.20 Mean daily winter temperature for clusters 1-3 for Flesland. 203
Figure 8.4.21 Comparison between summer air mass occurrence frequencies for Skabu. Observed (1968-1996), modelled current (1968-1996) and modelled future (2068-2096). 204
Figure 8.4.22 Histogram of wind direction from the observed NCEP Reanalysis data and HadCM3 GCM data. 205
Figure 8.4.23 Mean daily summer temperature for clusters 1-4 for Skabu. 207
Figure 8.4.24 Modelled frequencies of TSI 3 and 4 for winter, based on downscaled data from Flesland. 208
Figure 8.4.25 Modelled frequencies of TSI 3 and 4 for summer, based on downscaled data from Skabu. 209
Figure 8.4.26 Modelled glacier mass balance for Rembesdalskåka based on relationships

derived between the frequency occurrence of observed air mass types at Flesland and Skabu, 1968-2099 210
Figure 8.4.27 Observed relationship between the measured equilibrium line altitude (ELA) and net balance for Rembesdalskåka (1968-1997) 211
Figure 8.4.28 Effect of reducing net balance on the ELA of Rembesdalskåka 1968-2099 211
Figure 9.3.1 Surface and bed elevation data for Rembesdalskåka. Also, the flowline from which the data used as input to the glacier model was extracted from. 221
Figure 9.3.2 Cross section extracted from the profile line in Figure 9.3.1, displaying the bed elevation, glacier surface and nunatuk. 222
Figure 9.3.3 Altitudinal distribution of winter, summer and net balance for Hardangerjøkulen averaged over the 1963-1997 period. 225
Figure 9.3.4 Modelled glacier surface after 50 years, starting from initial conditions of zero ice 226
Figure 9.3.5 Modelled glacier surface after 100 years, starting from initial conditions of zero ice 226
Figure 9.3.6 Modelled glacier surface after 250 years, starting from initial conditions of zero ice 227
Figure 9.3.7 Present observed glacier surface (---) and modelled glacier surface (—) after 500 years, starting from initial conditions of zero ice 227
Figure 9.3.8 Present observed glacier surface and modelled glacier surface after 1000 years starting from initial conditions of zero ice 228
Figure 9.3.9 Adjusted mass balance series 1968-2099 229
Figure 9.3.10 Modelled front position 1990-2100 (The model was run past 2100 to estimate likely front position for after this period, assuming the 2100 decadal forcing does not change) 230
Figure 9.3.11 Ice flow model output for a steady state surface, based on the observed mass balance profile 1968-1997, and modelled scenario surface based on an ELA value of 1750 metres, representative of end of century conditions. 231
Figure 9.4.1 Measured front position changes for Rembesdalskåka 1998-2003. 233

Figure III-1 Daily mean sea level pressure for air mass clusters-Flesland (DJF) 1968-1997 III-1
Figure III-2 Daily mean sea level pressure for air mass clusters-Skabu (DJF) 1968-1997 III-3
Figure IV-1 Comparison of GCM and NCEP percentiles of mslp. IV-1
Figure IV-2 Comparison of GCM and NCEP percentiles of the westerly component IV-1
Figure IV-3 Comparison of GCM and NCEP percentiles of the southerly component IV-2
Figure IV-4 Comparison of GCM and NCEP percentiles of westerly shear IV-2
Figure IV-5 Comparison of GCM and NCEP percentiles of southerly shear IV-3
Figure IV-6 Comparison of GCM and NCEP percentiles of total shear IV-3
Figure IV-7 Comparison of GCM and NCEP percentiles of mslp IV-4
Figure IV-8 Comparison of GCM and NCEP percentiles of the westerly component IV-4
Figure IV-9 Comparison of GCM and NCEP percentiles of the southerly component IV-5
Figure IV-10 Comparison of GCM and NCEP percentiles of the westerly shear IV-5
Figure IV-11 Comparison of GCM and NCEP percentiles of southerly shear IV-6
Figure IV-12 Comparison of GCM and NCEP percentiles of total shear IV-6
Figure V-1 Flow diagram illustrating steps employed in methodology V-1

List of Plates

Plate 1.5.1 Rembesdalskåka photographed in 1955. 16
Plate 1.5.2 Rembesdalskåka photographed on the 14th October 2003. 16

List of Tables

Table 1.6.1 Relationship between climate-glacier interactions (after Meier, 1965) 17
Table 2.2.1 List of long-term temperature and precipitation stations from various European locations used in the analysis. Stations are listed on a south to north axis. 27
Table 2.2.2 Correlations between the North Atlantic Oscillation and long-term temperature data from various European stations (PC- Principal Component (Hurrell), GI- Index between Gibraltar and Iceland). 29
Table 2.2.3 Correlations between the North Atlantic Oscillation and long-term precipitation data from various European stations (PC- Principal Component (Hurrell), GI- Index between Gibraltar and Iceland). 30
Table 2.2.4 Correlations between the East Atlantic-Jet Pattern (EA-JP), Arctic Oscillation (AO) and long-term temperature data from various European stations. 32
Table 2.2.5 Correlations between the East Atlantic-Jet Pattern (EA-JP), Arctic Oscillation (AO) and long-term precipitation data from various European stations. 33
Table 2.2.6 Correlations with winter season NAO (Principal Component), NAO_{DJF} and individual winter months, $NAO_{DEC-JAN-FEB}$, and European temperature series for NAO ± 1d. 34
Table 2.2.7 Correlations with winter season NAO (Principal Component), NAO_{DJF}, and individual winter months, $NAO_{DEC-JAN-FEB}$, and European precipitation series for NAO>± 1d. 35
Table 2.2.8 Mean of temperature (°C) and precipitation (mm) during winter months when the NAO is in extreme mode. 37
Table 2.2.9 Correlations with summer season NAO (Principal Component), NAO_{JJA} and EA-JP, $EAJP_{JJA}$, and individual summer months (Gibraltar/Iceland), $NAO_{JUN-JUL-AUG}$, and $EAJP_{JUN-JUL-AUG}$, with European temperature series for NAO ± 1d. 38
Table 2.2.10 Correlations with summer season NAO (Principal Component), NAO_{JJA} and EA-JP, $EAJP_{JJA}$, and individual summer months (Gibraltar/Iceland), $NAO_{JUN-JUL-AUG}$, and $EAJP_{JUN-JUL-AUG}$, with European precipitation series for NAO>± 1d. 38
Table 3.2.1 Significance (Kendall's τau-b) and direction (+/-) of trends in seasonal temperature and precipitation data from Alpine and Scandinavian stations (1900-2000). 44
Table 4.1.1 Location, elevational range, length, area and aspect of glaciers. 67
Table 4.3.1 Relationship between the NAO (DJF) and EA-JP (JJA) and winter (Bw), summer (Bs) and net (Bn) mass balance from the four long term European glaciers. 78
Table 4.3.2 Mean of the Alpine winter temperature series 1900-2000 and values pre- and post- 1970. 78
Table 5.2.1 Glacier Mass Balance for a selected number of Scandinavian glaciers and the NAO (seasonal average between Dec-Mar) and the East Atlantic Jet Pattern. The ratio of winter balance to net balance (bw/bn) and summer balance to net balance (bs/bn) are also included. 85
Table 5.2.2 Bodo- Stykkisholmur (Meridional) Index (normal 1890-1999) 87
Table 5.2.3 Norwegian Index between Tromsoe and Hammerodde Fyr 88
Table 5.2.4 Norwegian Index between Ona and Utsira Fyr 90
Table 6.3.1 Correlation Matrix used as input to Principal Components Analysis for Bergen-Florida DJF 121
Table 6.3.2 Component matrix for Flesland with six extracted components. 122
Table 6.3.3 % Explained variance of each extracted component 124

Table 7.2.1 Flesland mean winter diurnal range of meteorological variables 134
Table 7.2.2 Orlandet mean winter diurnal range of meteorological variables 135
Table 7.2.3 Skabu mean winter diurnal range of meteorological variables 136
Table 7.2.4 Bodo mean winter diurnal range of meteorological variables 137
Table 7.2.5 Nordstraum mean winter diurnal range of meteorological variables 138
Table 7.2.6 Flesland mean summer diurnal range of meteorological variables 144
Table 7.2.7 Orlandet mean summer diurnal range of meteorological variables 145
Table 7.2.8 Skabu mean summer diurnal range of meteorological variables 146
Table 7.2.9 Bodo mean summer diurnal range of meteorological variables 147
Table 7.2.10 Nordstraum mean summer diurnal range of meteorological variables 148
Table 7.3.1 Flesland 14 cluster solution for winter 156
Table 7.3.2 Bodo 18 cluster solution for winter 156
Table 7.3.3 Nordstraum 12 cluster solution for winter 157
Table 7.3.4 Skabu 18 cluster solution for winter 157
Table 7.3.5 Flesland 19 cluster solution for summer 158
Table 7.3.6 Bodo 12 cluster solution for summer 158
Table 7.3.7 Nordstraum 9 cluster solution for summer 159
Table 7.3.8 Skabu 13 cluster solution for summer) 159
Table 7.4.1 Correlations and significance levels (two-tailed) for Rembesdalskåka's winter balance and winter synoptic index for Flesland and summer balance and summer synoptic index for Skabu (n=30). 162
Table 7.4.2 Partial correlations for TSI 3 and TSI4 and winter balance at Rembesdalskåka. 162
Table 7.4.3 Partial correlations for TSI 3 (with TSI 4 and TSI 5 held constant) and summer balance at Rembesdalskåka. 163
Table 8.3.1 Location of stations 181
Table 8.3.2 Primary and derived predictor variables 184
Table 8.4.1 List of selected predictors for Flesland (ns) and Skabu (nn). 187
Table 8.4.2 % explained variance (R^2) for each variable and location. 188
Table 8.4.3 Component matrix for Flesland DJF (1968-2100) with six extracted components. 199
Table 8.4.4 Component matrix for Skabu JJA (1968-2100) with six extracted components. 200
Table 10.1.1 Relationship between climate-glacier interactions (after Meier, 1965) 234

Table I-1 Recode values for horizontal visibility at surface I-1
Table II-1 Bodo Component matrix with six extracted components. II-1
Table II-2 Orlandet Component matrix with six extracted components. II-2
Table II-3 Skabu Component matrix with five extracted components. II-3
Table II-4 Nordstraum Component matrix with four extracted components. II-4
Table II-5 Bodo Component matrix with six extracted components. II-5
Table II-6 Flesland Component matrix with seven extracted components. II-6
Table II-7 Nordstraum Component matrix with four extracted components. II-7
Table II-8Orlandet Component matrix with six extracted components. II-8
Table II-9 Skabu Component matrix with five extracted components. II-9

Chapter I

Climate-glacier interaction studies: an introduction

1.1 Introduction

The Earth has undergone repeated glacial and interglacial cycles as a consequence of climatic fluctuations between cold, glacial, and warm, interglacial periods during the Quaternary Period (<2 million years). During glacial periods, approximately one-third of the Earth's surface was covered by ice sheets up to 3 kilometres in thickness (Benn and Evans, 1998). These glacial-to-interglacial sequences are primarily driven by changes in solar radiation receipt as a consequence of periodicities inherent in the Earth's orbit around the Sun. Three orbital cycles of importance have been identified, namely: eccentricity, or the shape of the Earth's orbit around the sun which varies from near circular to near elliptical every 100,000 years, obliquity, or the tilt of the Earth's axis which fluctuates on a 41,000-year cycle, and precession, which is the direction of the Earth's axial tilt relative to fixed stars, which varies on a 23,000 year cycle (Benn and Evans, 1998).

The astronomical theory of ice ages, which suggested that these periodicities were causally connected to glacial cycles, was first developed by James Croll, a Scottish scientist, in the 1860s, but was later elaborated on by Milutin Milankovitch, a Serbian mathematician, in the early 20th century. However, it is only since the 1950s that the astronomical theory of ice ages has become widely accepted. This has primarily been due to the uncovering of new evidence from marine and terrestrial sources that verified the synchronicity in timing between the glacial/interglacial sequences and the astronomical periodicities, thereby confirming the hypothesis that changes in the orbital cycles are the primary forcing mechanism for climate change over the Quaternary Period (Nesje and Dahl, 2000a).

These orbital cycles affect climate by causing variations in the seasonal and latitudinal amount of solar radiation received at the Earth's surface. These

variations in turn have a dramatic effect on the global climate system producing climatic fluctuations between cold, glacial conditions, resulting in the development of ice sheets, and warm, interglacial periods, with a much reduced ice cover. Once established, these large ice sheets exert considerable influence on the regional climate, which would in turn act to regulate their existence (Benn and Evans, 1998), and also on the global climate, partly due to the increased albedo resulting from the enlarged areal extent of ice cover.

Terrestrial storage of water as ice and snow had a dramatic effect on global sea levels during glacial periods. Evidence from proxy sources suggest that sea level was approximately 120 metres lower than present during the last glacial maximum (Benn and Evans, 1998). At present, glaciers and ice sheets cover about 10% of the Earth's surface which if melted, would raise present day sea levels by approximately 70 metres (Nesje and Dahl, 2000a).

After the last glacial maximum, c. 18 kyr ago, a period of glacier readvance occurred during the Younger Dryas, a cold interstadial which occurred around 11-10 kyr ago, after which rapid retreat of the northern hemisphere ice sheets occurred. The onset of this retreat marked the beginning of the present interglacial, known as the Holocene Epoch, and within 1,000 years, the North American Laurentide ice sheet had been reduced to remnants, some of which still exists today on Baffin Island. The Scandinavian ice sheet underwent similar rates of retreat during this episode also.

Periods of neoglaciation, which refer to the readvance or regrowth of glaciers after attaining their minimum extent during the Holocene (Nesje and Dahl, 2000a), occurred as early as 8 kyr ago (Benn and Evans, 1998). Research from Scandinavia suggests that most, if not all, Scandinavian glaciers completely melted at least once during the Holocene (Nesje and Dahl, 2000a). The most recent period of neoglacial activity, known as the Little Ice Age, commenced during the late 16^{th} century and continued up until the middle of the 19^{th} century, was marked by temperature reductions of up to 1.0 - 1.5°C, most likely resulting from a reduction in sunspot activity and increased volcanic activity during this time.

On shorter timescales, radiative forcing, resulting from the difference between incoming and outgoing solar radiation received at the Earth's surface, is the primary process that drives daily changes in the global climate system. The midday sun is near vertical at the equator concentrating large amounts of radiation over a relatively small area, while at the poles a larger radiation footprint results from the more oblique sun angle. This results in an energy surplus at the equator and a deficit at the poles. The subsequent redistribution of this surplus heat energy at the equator is mobilised polewards through atmospheric and oceanic circulation which produce spatial and temporal variations in climate. As a consequence of the reduced solar radiation received at more northerly latitudes, glaciers tend to be more extensive in these regions. However, glaciers do exist close to the equator, but only at high elevations, in marked contrast to some high latitude glaciers that terminate at sea level. This elevational difference gives rise to the concept of regional *glaciation levels* or threshold elevations above which glaciers could form. However, it is this interaction between regional climate, namely temperature and effective precipitation (solid precipitation), and local topography that determines where glaciers can actually form and their dependency on the survival of snow and ice through the subsequent ablation season is primarily climatically controlled.

Glaciers adjust to both these short-term seasonal and longer-term annual or decadal changes in climate through a variety of responses. Short-term seasonal variations in climate, resulting in increases or decreases in temperature or precipitation, affect the mass balance or gains and losses of snow and ice from the surface of a glacier. Longer-term changes in climate produce changes in glacier behaviour, which tend to lag climate over much longer time scales (10^1-10^2 years). In determining the degree to which glaciers are affected by climate and climate change, it is necessary to uncover the dominant climatic controls that exert an influence on glaciers and hence, glacier behaviour.

The mass balance of a glacier is largely a response to climate forcing on a variety of scales from localised, short duration to large, hemispherical and planetary scale teleconnections. It has been suggested that these large-scale atmospheric teleconnections may be responsible for spatially distributed co-varying responses

evident for some glacier annual net balances (Dyurgerov, 2002). However, the linkages that exist between mass balance and climate at the various scales still remain unclear. In an attempt to examine some of these linkages, this research will initially endeavour to determine the extent to which dominant large-scale atmospheric forcing mechanisms affect the regional climate of Europe, paying particular attention to two glaciated regions. The two regions, the Alpine region and Scandinavia, are of particular interest in terms of glacier mass balance because of their recent contrasting behavioural changes. Alpine glaciers have been marked by mass wastage and subsequent retreat in the last number of decades, while the response of a number of Scandinavian glaciers over the same period has been largely positive. The positive net balances currently being recorded on Scandinavian glaciers are in stark contrast to many other parts of the world where glacier recession now prevails (Figure 1.4.2).

It is intended that the approach adopted should provide a mechanism through which changes in mass balance can be linked to variations in large scale forcing, through variations in the regional climate variables. It is also intended that, in subsequent chapters, the results will be used in conjunction with long-term glacier mass balances records from four glaciers, in Alpine Europe and Scandinavia, to examine possible reasons for the divergent responses between these two regions. A later chapter will focus in greater detail on Scandinavian glaciers in order to examine the positive net balances currently being recorded on these glaciers.

1.2 Climate-glacier interaction studies: A brief review

Most climate-glacier studies to date have concentrated on localised interactions at or near the glacier surface (Laumann and Reeh, 1993; Vincent and Vallon, 1997; Greuell and Böhm, 1998). These studies typically involve amassing detailed glaciological measurements over hours, days or seasons, which are then related to on-site, or nearby, meteorological measurements. They are generally conducted on a glacier specific basis and, while they are useful, they suggest little about the large-scale controls that exert an influence on glacier mass balances regionally or at the hemispherical scale.

A number of studies have tried to link glacier mass balance with larger scale synoptic events (Yarnal, 1982; Alt, 1987), the wider atmospheric circulation (Hoinkes, 1968; McCabe and Fountain, 1995; Tvede and Laumann, 1997; Bitz and Battisti, 1999; Lamont *et al.*, 1999) and the North Atlantic Oscillation (Pohjola and Rodgers, 1997a; Washington *et al.*, 2000; Nesje *et al.*, 2000b). Yarnal (1982), in an analysis of the relationship between synoptic scale atmospheric circulation and glacier mass balance in south western Canada, related the height of the 500 hPa surface to the mass balance from three glaciers: Peyto, Alberta and Sentinel. Yarnal classified days using an objective synoptic typing technique outlined by Kirchhofer (1973) on two data sets. The first consisted of a high density grid of 500 hPa heights, termed "smallgrids", and the second involved a more generalised synoptic scale set of 500 hPa heights with a reduced number of points covering a larger spatial area, termed "biggrids". The technique employed classified days (grids) based on row and column similarity of their data matrix. This particular technique is an example of a map pattern classification technique. The resulting classes were then characterised according to their dominant climatological characteristics, such as, "efficient moisture carriers", "inefficient carriers", "warm" or "cold". Frequencies of occurrence of the classified types were calculated and related to the mass balance of the selected glaciers. Yarnal (1982) found that a large proportion of variance in the winter balance could be explained by fluctuations in the frequency of particular synoptic types. Cyclonic type flows enhanced accumulation, while anticyclonic flows, which were less efficient bearers of moisture, acted to suppress accumulation during the accumulation period. During the ablation period, synoptic scale circulation was found to only partially contribute to the ablation.

McCabe and Fountain (1995) in a similar study analysed the relationship between the variability of the 700 hPa heights over western Canada and glacier mass balance. Approximately 60% of the variation in winter mass balance could be explained by variations in the height of the 700 hPa surface. Large winter balances occurred when negative height anomalies dominated western Canada and much of the western United States. They attributed diminishing winter mass balances of South Cascade Glacier evident since the 1970s to increasing 700 hPa heights over

western Canada, which resulted from a deepening of the Aleutian Low, causing a shift in the storm track locations to more southerly locations. These changes, coupled with an increase in the 700 hPa height surface over western Canada, increased subsidence, and produced a warming and drying of the air over this region. The warmer temperatures and reduction in moisture resulted in reduced winter mass balances being recorded since the mid-70s. These reductions in winter mass balances of glaciers in the western United States recorded during the mid-70s were in contrast to increasing winter balances over the same period for glaciers in Alaska. McCabe and Fountain (1995) suggested that the atmospheric conditions producing reduced or negative winter balances over the western United States acted to increase the intrusion of warm moist air into Alaska resulting in more positive balances being recorded there.

Hoinkes (1968) analysed the relationship between the deviation of the 500 hPa surface and glacier mass balance during the ablation period for a selection of glaciers from Scandinavia and the Alps. His results showed that positive or balanced glacier budgets in the Alps were possible with both a low-index circulation, characterised by a meridional flow, with cyclonic tracks shifted southwards, and high index circulation, characterised by zonal flow off the Atlantic predominantly towards north-western Europe. The latitude of the zero deviation was the determining factor.

Relating synoptic controls to the surface energy budget regime of an ablating fast ice surface or sheet of land-fast ice that forms in early winter and by spring extends by up to 50 km seawards, Crane (1979) identified two clearly defined energy budget regimes that were related to the stage of decay of the fast ice. Days with similar turbulent fluxes within each of the regimes were clustered and in each set, one group of days was found to enhance ablation while the other was identified as suppressing ablation. The groupings, which were found to be statistically significant, could all be differentiated in terms of pressure patterns, direction of airflow and average temperature (Crane, 1979).

Brazel *et al.* (1992) examined synoptic conditions on West Gulkana Glacier, Alaska, over the period 1948-1986, to interpret possible long-term changes in ablation based on relationships developed between daily surface energy budgets and the prevailing synoptic situation for a summer melt season. Their findings suggest that the synoptic conditions found to enhance ablation had significantly increased over the 1957 to 1992 period. Sensible heat flux contributions to summer melt, related to specific regional synoptic conditions, were also found to be a major source of variability in ablation (Brazel *et al.*, 1992).

In a similar analysis of the energy balance of a melting snow pack in the Southern Alps, New Zealand, Neale and Fitzharris (1997) also found that different synoptic situations produced distinctive energy budgets with radiation dominating during large scale anticyclonic patterns while sensible heat flux was found to be important during north-westerly patterns. Melt periods lasting up to a week were associated with the passage of troughs and anticyclones across New Zealand (Neale and Fitzharris, 1997).

1.3 Aims and Objectives

While these studies demonstrate the importance of synoptic-scale climate on glacier mass balance, there still exists large gaps in our understanding of the interactions between both of these systems and the scales at which these interactions operate. They also act to highlight the complexity of the relationship that exists between mass balance and climate. With the exception of Yarnal (1982), who highlighted the need to assess the influence of the various scales at which climate operates, these studies have confined themselves to specific scales of analysis, spatially and temporally, thereby somewhat limiting their potential usefulness and broader applicability.

The principal objective of this research will be an examination of the effects of climate, operating at various scales, on glaciers. An analysis, encompassing both the accumulation and ablation seasons and focusing on European glaciers, will be conducted to determine the linkages that exist between climate and glacier mass

balance. This will involve an initial examination of the large-scale atmospheric modes of climate in the North Atlantic, particularly the North Atlantic Oscillation, a key driver of hemispherical scale climate variability, and their influence on temperature and precipitation, two key determinants of glacier mass balance. Long term variations in both the large- and local- scale climate will also be assessed for changes that are likely to impact glacier mass balance. An improved understanding of the links between large-scale atmospheric circulation and long-term variability of the local climate elements should assist in an analysis of long-term variations in glacier mass balance, particularly of European glaciers.

A methodology will be developed to facilitate an analysis of the links between climate and glaciers, which is cost effective, transferable and utilises readily available meteorological data, remote from the glacier, in an attempt to further our understanding of the interaction between glaciers and climate through the critical link of glacier mass balance. The development of such a methodology should play an important role in attempting to understanding these interactions, particularly in mountainous regions where there is a serious lack of glacier specific meteorological data.

These indices of large-scale climate variability will also be incorporated into an analysis of the relationship between low frequency changes and mass balance variability. Within the large-scale fluctuations, changes in circulation and air mass types would also be expected to occur. An analysis of this smaller scale variability will be facilitated by an examination of spatially reduced circulation indices and air mass types derived from data from synoptic stations. The second component of the analysis and main objective of the research, will concentrate on selected glaciers from Scandinavia, primarily because these glaciers are currently experiencing advancing front positions in marked contrast to the global glacier signal which has been dominated by mass wastage and retreat in recent decades.

A second objective of this research, based on a satisfactory outcome from the above analysis - that climate variability can be used to explain glacier mass balance changes - is to derive a scenario of future climate change which will be used to

suggest possible future changes in glacier mass balance. This module of the research will utilise output from a global climate model (GCM) to derive scenarios of climate change for Norway for the 21st century. These scenarios will then be used to determine likely changes in the mass balance for a particular glacier, Rembesdalskåka, an outlet glacier from Hardangerjøkulen, to suggest likely changes in its behaviour as a consequence of anthropogenic climate change.

Climate change over the course of the present century is likely to have a large impact on glaciers and hence glacier meltwater. Seasonal meltwaters from glaciers in Norway add a significant contribution to base flows during the summer months on rivers that are used for the generation of hydropower. Currently, electricity generated by hydropower in Norway accounts for 99% of total energy production and it is the sixth largest producer of hydropower in the world (http://www.norway.org.uk/facts/energy/electricity/electricity.htm). However, during the winter of 2003, Norwegian electricity production fell by 18% as a consequence of a reduced energy content of the hydropower reservoirs, coupled with a reduction in snow accumulation, resulting in lower than average inflow to rivers during the spring and summer. To meet electricity consumption demands, Norway had to import almost 8 TWh (terawatt-hours) in 2003, while in the previous year there had been a net surplus of 9.7 TWh (http://www.nve.no). Therefore, any variation in climate that is likely to have an effect on glaciers and their ability to store water, coupled with a change in the distribution and receipt of precipitation, is likely to have a large impact on the countries capability to generate electricity from hydropower over the long term.

1.4 Contemporary climate change: A future for glaciers?

This research takes place in the context of the current scientific consensus which attributes most of the increase in global temperature experienced since the middle of the 20th century, to anthropogenic activities (Figure 1.4.1) (IPCC, 2001b). This increase is associated with increasing atmospheric concentrations of greenhouse gases, primarily CO_2, from pre-Industrial Revolution levels of 280 p.p.m.v. (parts per million volume) to their current levels of 380 p.p.m.v. The present day

concentration of CO_2 is at a level that has not been exceeded during the past 420,000 years and most likely not during the past 20 million years (IPCC, 2001b).

The natural greenhouse effect, which results from naturally occurring quantities of greenhouse gases, acts to raise the temperature of the Earth's surface by ~21°C; thereby making the planet habitable. However, as a consequence of the increasing concentrations of these gases in the atmosphere, primarily attributed to human activity such as, the burning of fossil fuels, it is likely that global temperatures will increase significantly during the course of the present century.

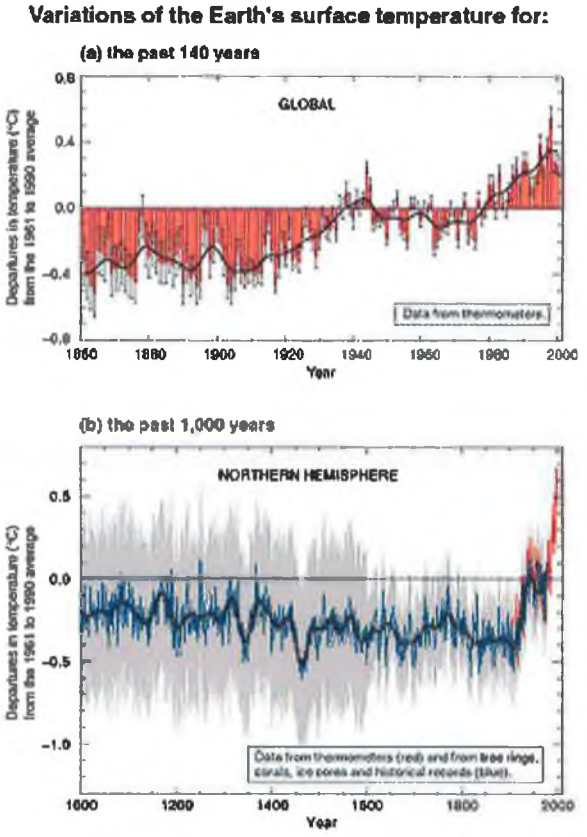

Figure 1.4.1 Variations of the Earth's surface temperature over the last 140 years and the last millennium (IPCC, 2001).

Records of surface temperatures from the Northern Hemisphere, compiled from various sources and proxy data, suggest that, globally, 1998 was the warmest year of the warmest decade of the warmest century of the last millennium (Figure 1.4.1) (IPCC, 2001b). These increases in temperature have been accompanied by decreases in snow cover and retreat of mountain glaciers (Figure 1.4.2) and as a

consequence a rise in sea level of between 10-20 cm since 1900, reductions in the sea-ice thickness of the Arctic and increases in precipitation over the land masses of temperate regions of between 0.5-1.0% (IPCC, 2001b).

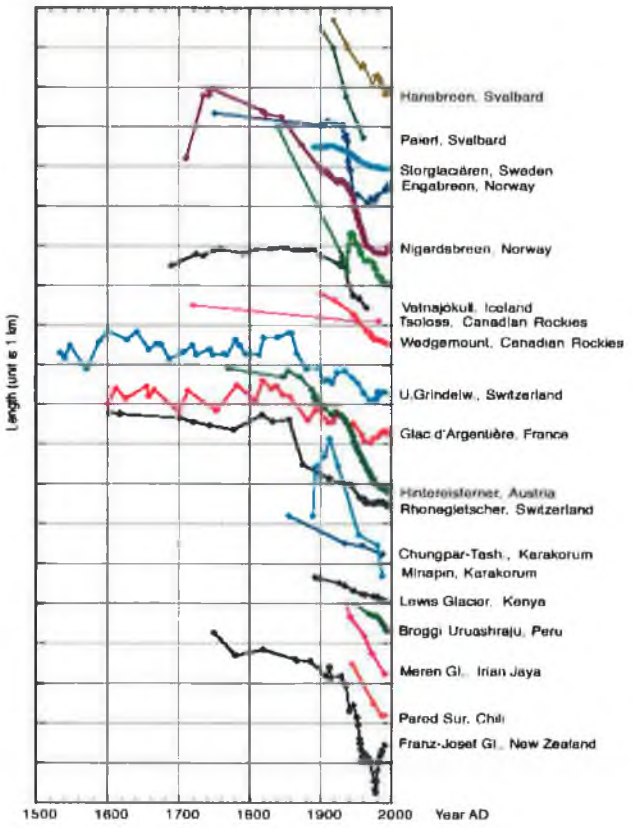

Figure 1.4.2 Glacier front positions for a selection of global glaciers (Source: Haeberli, 2004)

If emissions of greenhouse gases were to continue increasing at current rates, a doubling of atmospheric concentrations of CO_2 is likely to occur by the end of the present century. Global climate model (GCM) simulations of the climate system suggest that increases in global temperature in the order of between 1.4 to 5.8°C by 2100 are likely as a consequence. These temperature increases are unlikely to be uniformly distributed and there is likely to be a large degree of regional variation in the spatial distribution of these increases.

Any change in the amount or distribution of temperature or precipitation will directly affect glacier accumulation and ablation and therefore the behaviour of glaciers. Globally, glaciers are in retreat mode, partly as a response to the return to warmer conditions after the last neoglacial period during the Little Ice Age, but

also due to the continued increases evident in global temperature since then. The timing of specific glacier responses will be dependent on glacier size and the sensitivity of individual glaciers to any changes that may occur in climate.

1.5 Study location and glacier selection

Glaciers from two locations in Europe were selected for the present study. Alpine glaciers are currently responding in a manner consistent with global trends and are undergoing volume loss and retreat of front positions, while Scandinavian glaciers, particularly maritime ones, have been advancing or maintaining equilibrium in recent years. Thus, these glaciers present an opportunity to examine the regional response in glacier mass balance resulting from the same large-scale climate forcing, that of the North Atlantic Oscillation.

The primary analysis will focus on Scandinavian and in particular Norwegian glaciers as they provide a unique opportunity to examine the direct effects of climate and climate change on glacier mass balance due to their advancing front positions. Over the course of the last two centuries Norwegian glaciers have undergone repeated phases of advance and retreat of front positions primarily as a consequence of climate fluctuations. During the 19th century, climate variations resulted in a strong regional component to glacier fluctuations, with some advancing, while others were retreating. However, during the 1880s, a synchronous retreat of all the glaciers began (Hoel and Werenskiold, 1962). Phases of glacier advance and retreat occurred over the next four decades, until the 1930s, after which a marked retreat began again. After the 1950s a number of glaciers show evidence of advancing in response to a deterioration in climate during the 1940s (Hoel and Werenskiold, 1962). Ahlmann (1953) suggests that this deterioration was primarily as a result of a decrease in winter temperatures that occurred during the 1940s, of which 1940, 1941 and 1942 were 'remarkably cold' (Ahlmann, 1953:25). Despite these decreases in winter temperatures, spring and autumn temperatures were found to be increasing (Ahlmann, 1953).

Between 1846 and 1955, Hardangerjøkulen glacier, a maritime glacier located in southern Norway which will be used as a case study glacier in this research to examine the effects of climate on glacier behaviour, reduced in size by approximately 44 km^2 (Hoel and Werenskiold, 1962). Prior to this, at its Little Ice Age maximum around 1750, its equilibrium line altitude (ELA) may have been 130 metres lower than present (Nesje and Dahl, 1991).

Importantly from the point of view of this research, data exist for a number of glaciers that have been monitored on a long-term basis. Furthermore, the Norwegian glacier monitoring network was expanded greatly during the 1960s, substantially increasing the number of monitored glaciers. Norway also has a large number of well-distributed meteorological stations with high quality data, a fundamental requirement for any climate-glacier interaction study. This intensive glacier monitoring effort in Norway largely reflects the importance of glaciers to the economy in terms of meltwater contributions to base flows on rivers used in the generation of hydroelectric power. Electricity production from Norwegian hydropower plants is estimated to be about 119 TWh/year and, in addition to other natural resources, has been an important contribution to continued economic growth (Paaske, 2002). In 2000, the power supply sector accounted for approximately 2.3% of GDP in Norway, corresponding to NOK 24.7 billion (Paaske, 2002).

Historically, there has been a long tradition of economic exploitation of Norwegian glaciers. As far back as 1834, substantial quantities of glacier ice, mainly from Folgefonni, Strupbreen and Øksfjordjøkulen was quarried and exported to England, where it was sold in London for use in refrigeration. In one particular shipment in 1925, up to 90 tons were exported to Scotland for use in preserving salmon (Hoel and Werenskiold, 1962). However, trade between Scotland and Norway was discontinued after a local dispute broke out.

Norwegian land taxes have also been found to fluctuate in accordance with the climate. During years in which produce was abundant, taxes were raised. Thus, recorded land taxes can also be used as indirect proxy evidence for glacier front

position reconstruction work. For example, in 1667, land taxes were raised in the Jostedal region suggesting an increase in prosperity as a consequence of a relatively mild climate. This suggests that glaciers in the region were not posing a threat to the farmsteads in the region, and thus the glaciers were in a diminished state (Hoel and Werenskiold, 1962).

Proxy evidence from other documentary sources suggests that glaciers in Nordfjord were at a similar extent to the present during the 1600s. Neoglacial activity during the Little Ice Age has also been recorded in documentary sources, written during the 17th century, when a marked advance of glacier front positions occurred. Mean ELAs for glaciers in Jostedalsbreen were estimated to have been 70 metres lower than their position in 1993 (Torsnes *et al.*, 1993). As a consequence of the depressed ELAs and resultant advances of front positions, during which agricultural land was overrun by ice and debris and in which some farmhouses were swept away, a lowering of taxes and rents was required (Forbes, 1853; Hoel and Werenskiold, 1962). Compiled evidence suggests that glacial advances began between 1660-1700; glaciers prior to this advance were at a minimum extent (Hoel and Werenskiold, 1962).

Glacier fluctuations can also cause additional hazards. Lake Demmevatnet is a lake damned by Rembesdalskåka (Plate 1.5.1,Plate 1.5.2), an outlet glacier from Hardangerjøkulen, from which a number of jøkulhlaups or glacier outburst floods have caused catastrophic flooding in Simadalen in 1813, 1861, 1893, 1937 and 1938 (http://www.nve.no; Elvehøy *et al.*, 2002). These jøkulhlaups occurred when the lake drained through a subglacial tunnel. Prior to 1899, overtopping of the glacier by the lake surface and subsequent melting of a channel on the glacier, resulted in annual flooding, lasting for weeks in the late summer (http://www.nve.no). The annual flooding was prevented after this time by the incision of drainage tunnels in the glacier. A number of other Norwegian glaciers have associated glacial dammed lakes that pose an increased risk, both economically and as a human hazard, as a consequence of glacier fluctuations resulting from climate change.

MAP OF THE GLACIERS OF THE YMESFIELD
in lat. 60°40.

Figure 1.5.1 Map of glaciers in the mountain area of Jotunheimen from before 1853 (Forbes, 1853)

Rembesdalsskaki, an outlet glacier of Hardangerjokulen.
(Photo: B. Luncke, Norsk Polarinstitutt, 1955.)

Plate 1.5.1 Rembesdalskåka photographed in 1955 (Source: Hoel and Werenskiold, 1962).

Plate 1.5.2 Rembesdalskåka photographed on the 14th October 2003. Photo: Hallgeir Elvehøy (Source: http://www.nve.no)

Research on Norwegian glaciers, with a view to furthering our understanding of the linkages between climate and glaciers, is clearly justified for a number of reasons, some of which have been outlined. In addition, their location relative to a warm body of water, and hence moisture source from the North Atlantic, may mean that the Norwegian glacier response to climate change may continue to be in contrast with global trends over the course of the present century.

1.6 Thesis outline

The chapters in this thesis follow, loosely, the framework proposed by Meier (1965) outlining the interaction between climate and glaciers (Table 1.6.1). Climate, as defined by Meier, is further subdivided for the purposes of this study to include both large- and local- scale climate variability.

Climate	→	General Meteorological Environment	→	Net Mass Balance of Glacier	→	Dynamic response of glacier	→	Lasting evidence of glacier margin position

Table 1.6.1 Relationship between climate-glacier interactions (after Meier, 1965)

The primary concern of Chapter II will be an examination of the large-scale modes of atmospheric variability to determine if low frequency changes result in long-term changes in temperature and precipitation which will be the subject of chapter III. Chapter III will also examine the climate series for change points that may have occurred. These change points may be significant as some previous studies have suggested that the relationship between climate and glaciers may alter after a climate change point has occurred (Vincent and Vallon, 1997).

If long-term changes are evident in these variables, Chapter IV will examine these in the context of long-term mass balance measurements to determine if they explain the divergent mass balance signals evident between southern and northern European glaciers. The impact of any change-points in the climate series on glacier mass balance will also be assessed.

Chapter V will then focus on shorter-term changes in mass balance which will be examined in the context of more regional scale climate variability. The focus of this chapter will be on mass balance from Scandinavian glaciers but in particular Norwegian glaciers. Localised indices of atmospheric variability will also be examined to determine the linkages that exist at the smaller scale.

Chapter VI will outline a synoptic classification methodology employed to derive a regional circulation index for Norway, based on five synoptic stations. Results derived from the synoptic index will be examined in Chapter VII. An examination of synoptic categories will also be undertaken to determine if any changes have occurred within the air mass types. A crucial component of the thesis will also be outlined in this chapter, which seeks to examine glacier mass balance in the context of seasonal frequencies of the derived synoptic categories. A more detailed analysis will be undertaken for one particular glacier, Rembesdalskåka, an outlet glacier from Hardangerjøkulen.

Chapter VIII proposes to derive climate change scenarios for the present century, employing a statistical downscaling methodology to downscale output from a global climate model. The downscaled data will be used to determine changing circulation frequencies for the present century and their effect on glacier net balance, as a consequence of climate change. In Chapter IX, following the proposed framework of Meier (1965), a 1-Dimensional ice flow model will be used to determine the dynamic response of Rembesdalskåka to the modelled changes in net balance suggested in Chapter VIII.

Chapter X will conclude with a critical overview of the research and how the findings relate to the theoretical framework of the discipline to date. Research limitations and requirements for future work will also be briefly discussed.

Chapter II

Accounting for climate variability in the North Atlantic: the influence of atmospheric circulation

2.1 Introduction

Climate variability in the North Atlantic results from numerous interactions: between the troposphere, stratosphere, ocean, adjacent land masses, the Arctic, the Tropics and remote forcing from the Pacific (Marshall *et al.*, 2001). This variability results primarily from the interaction of three interrelated phenomena; the Tropical Atlantic Variability (TAV), fluctuating tropical Atlantic sea surface temperatures which straddle the intertropical convergence zone (ITCZ), the North Atlantic Oscillation (NAO), which represents fluctuating sea level pressure between the Azores and Iceland, and the Atlantic Meridional Overturning Circulation (MOC) or thermohaline circulation (Marshall *et al.*, 2001). These phenomena interact on a variety of timescales, from interannual to decadal, and over a large spatial area, vertically integrating the ocean and atmosphere.

In the mid-latitudes, the North Atlantic Oscillation accounts for 37% of the variability of the winter 500 hPa heights over the North Atlantic (Marshall *et al.*, 2001). It is the leading mode of climate variability, particularly in winter when it is most pronounced in amplitude (Marshall *et al.*, 2001). The NAO is also linked to the leading annular mode of climate variability in the Northern Hemisphere, the Arctic Oscillation (AO).

Fluctuations in the NAO have also been found to co-vary with fluctuations in temperature and precipitation, two key variables that affect glacier mass balance. A greater understanding of the linkages that exist between these series is crucial, as predicted changes in atmospheric circulation as a consequence of climate change are likely to have an effect on the NAO (Marshall and Kushnir, 1997; Marshall *et al.*, 2001). Therefore, there are a number of reasons that justify a detailed examination of the NAO in the context of examining the relationship between large-scale modes of atmospheric variability and glacier mass balance.

2.2 North Atlantic Oscillation (NAO)

The NAO represents a large-scale mode of atmospheric variability operating over interannual to decadal time scales in the Northern Hemisphere (Marshall and Kushnir, 1997). Its effects were first commented on more than two centuries ago by missionaries who noted that year to year fluctuations in air temperatures on both sides of Iceland were often out of phase with one another (Marshall *et al.*, 2001). Evidence from the Greenland Ice Sheet Project (GISP-2) suggests that the NAO is the only circulation mode of variability that is 'coherent with periodic behaviour in the 700 year stable isotope record' derived from the ice cores taken from Central Greenland (Marshall and Kushnir, 1997).

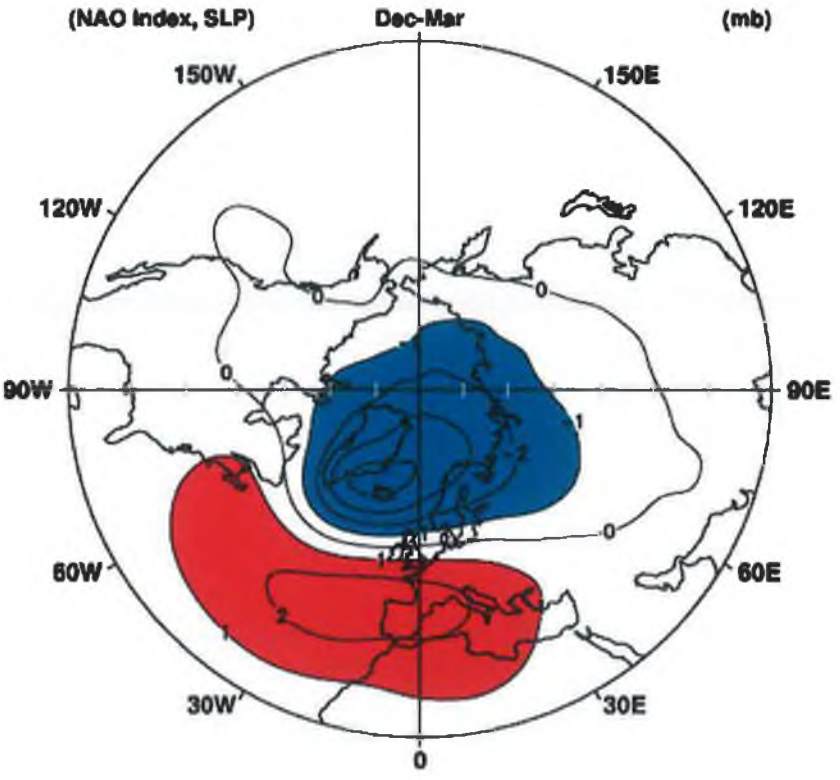

Figure 2.2.1 North Atlantic Oscillation. Blue represents below average SLP anomalies, Red represents above average SLP anomalies (Source: Hurrell 1995).

The NAO is characterised by a meridional or north-south pressure gradient between the semi-permanent low pressure centred over Iceland (Icelandic Low) and the semi-permanent high pressure centred over the Azores (Azores High) (Figure 2.2.1). It is instrumental in the large-scale transfer and redistribution of

atmospheric mass between the equator and the North Pole and is associated with changes in westerly airflow over the North Atlantic onto Europe (Hurrell, 1995). It is most pronounced during the boreal winter months of December, January and February, when it accounts from more than one-third of the total variance in sea-level pressure (SLP) over the North Atlantic, but is present throughout the whole year (Marshall and Kushnir, 1997; Hurrell and Dickson, 2001).

The NAO fluctuates between positive and negative modes. Positive modes are associated with stronger than average westerlies due to a large pressure gradient between the Icelandic Low and Azores High. Negative modes result from a diminished gradient between Iceland and the Azores. An index of the NAO can be calculated from the pressure differences between these two regions and is defined as the difference between the normalised mean sea level pressure (SLP) measured at Lisbon, Portugal and Stykkisholmur, Iceland (Marshall and Kushnir, 1997).

Fluctuations between positive and negative phases of the NAO (Figure 2.2.2) have pronounced impacts on the strength and direction of Atlantic storm tracks, sea-ice distribution, marine ecosystems and regional wintertime temperatures and precipitation across Europe, Eurasia and the East Coast of the United States. Thus, its effects are far reaching.

As a consequence of the large meridional pressure gradient experienced during positive phases, the NAO has a direct influence on wind speed and direction over the surface of the Atlantic, and thus on air-sea interaction. It therefore has a significant impact on ocean circulation and in particular the formation and location of the Meridional Overturning Circulation (MOC) (Hurrell, 1995; Hurrell and Dickson, 2001; Marshall and Kushnir, 2001). The MOC accounts for a large proportion of the oceanic heat exchange between the equator and the pole and it has been suggested that the strength of the MOC is linked with abrupt changes in past climate (Marshall *et al.*, 2001) due to increased freshening and warming of the sub-polar seas. Such a situation occurred during the Younger Dryas when it was initially suggested that melting continental land ice draining in to the North Atlantic dramatically reduced the density of the North Atlantic ocean surface

water, resulting in a shut down of North Atlantic Deep Water formation (Appenzeller, 1997). More recent work has focused on the role played by the drainage of Lake Agassiz via the Great Lakes and St. Lawrence River diverting the North Atlantic Drift to a more southerly location (Benn and Evans, 1998). Irrespective of the mechanism involved, the role of the MOC, its location and intensity, appears crucial in moderating Northern Hemisphere temperature and hence climate.

Although controversial, a weakening and possible collapse of the MOC has been projected by some Global Climate Models (GCMs) as a consequence of global warming. While this would result in overall cooling of the North Atlantic region, due to the large degree of uncertainty associated with how the MOC is likely to respond to anthropogenic climate change, this is considered a high impact, low risk event.

2.2.1 NAO and temperature

Global average surface temperature has increased by 0.6 ±0.2°C over the course of the 20th century (IPCC, 2001b). The global temperature record displays a large degree of variability, but does suggest that most of this warming occurred between two specific periods, 1910-1945 and 1970-2000. In the Northern Hemisphere, the 1990s was the warmest decade and 1998 was the warmest year since reliable global instrumental records began in 1861 (IPCC, 2001b). Proxy records indicate that the temperature increases recorded during the 20th century in the Northern Hemisphere resulted in it being the warmest century in the last millennium. Much of this warming has occurred in the winter, spring and autumn seasons (Jones *et al.*, 2001).

In a study of long-term temperature trends in Western Europe over the 20th century, Moses *et al.* (1987) detected a greater magnitude of change at higher latitudes reflecting the sensitivity of high-latitudes to climate change. This increased sensitivity at these latitudes primarily results from ice-albedo feedback

mechanisms. The detection of this increased temperature trend at high-latitudes is consistent with current global climate model predictions on global warming.

In a similar study of long-term trends in temperature in the Norwegian Arctic, Hanssen-Bauer and Førland (1998a) concluded that decadal fluctuations in the temperature record were connected to variations in atmospheric circulation. Moses *et al.* (1987) suggested a similar connection between temperature variations, in particular winter temperature, and changes in circulation and extreme modes of the NAO. However, both studies indicated that not all of the variability in the temperature records could be attributed to atmospheric circulation changes alone and suggested that additional mechanisms must also play an important role.

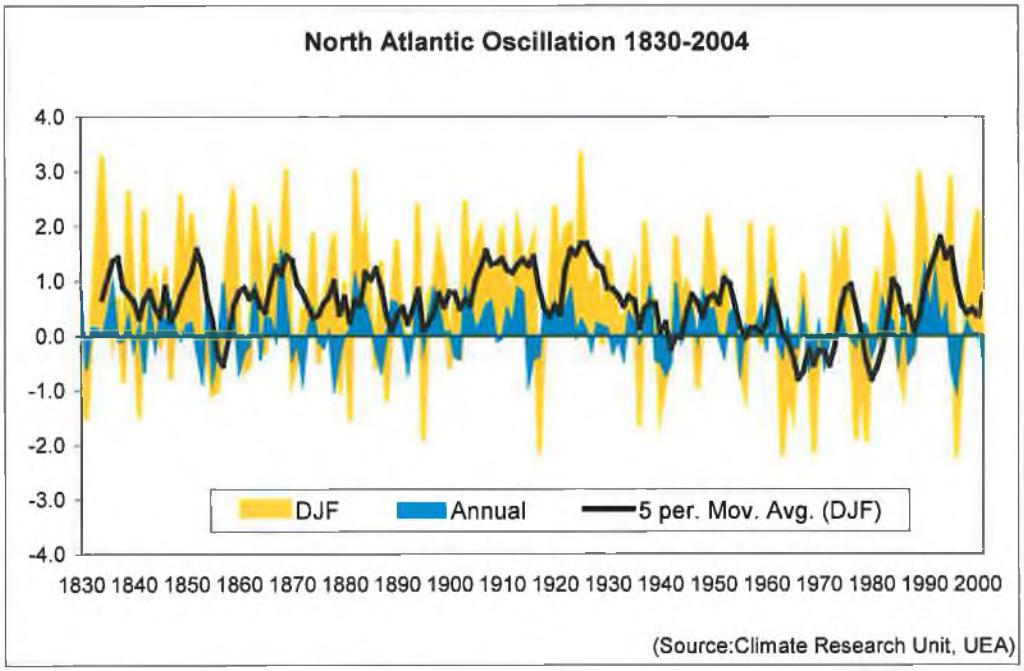

Figure 2.2.2 North Atlantic Oscillation Index 1830-2000. (Annual Index – Blue; DJF – Yellow Line; Black Line – 5-year running mean on DJF Index.)

It is evident that the NAO exhibits considerable variability (Figure 2.2.2). The annual index tends to be dampened due to the inclusion of non-winter months, when the NAO is present but less active. The averaged December, January, and February (DJF) index (Yellow) see-saws between strongly positive and strongly negative modes. While the fluctuations do not appear to adhere to any regular

pattern, which may reflect the underlying stochasticity of climate, there are periods when the NAO has persisted for a number of years in a particular mode.

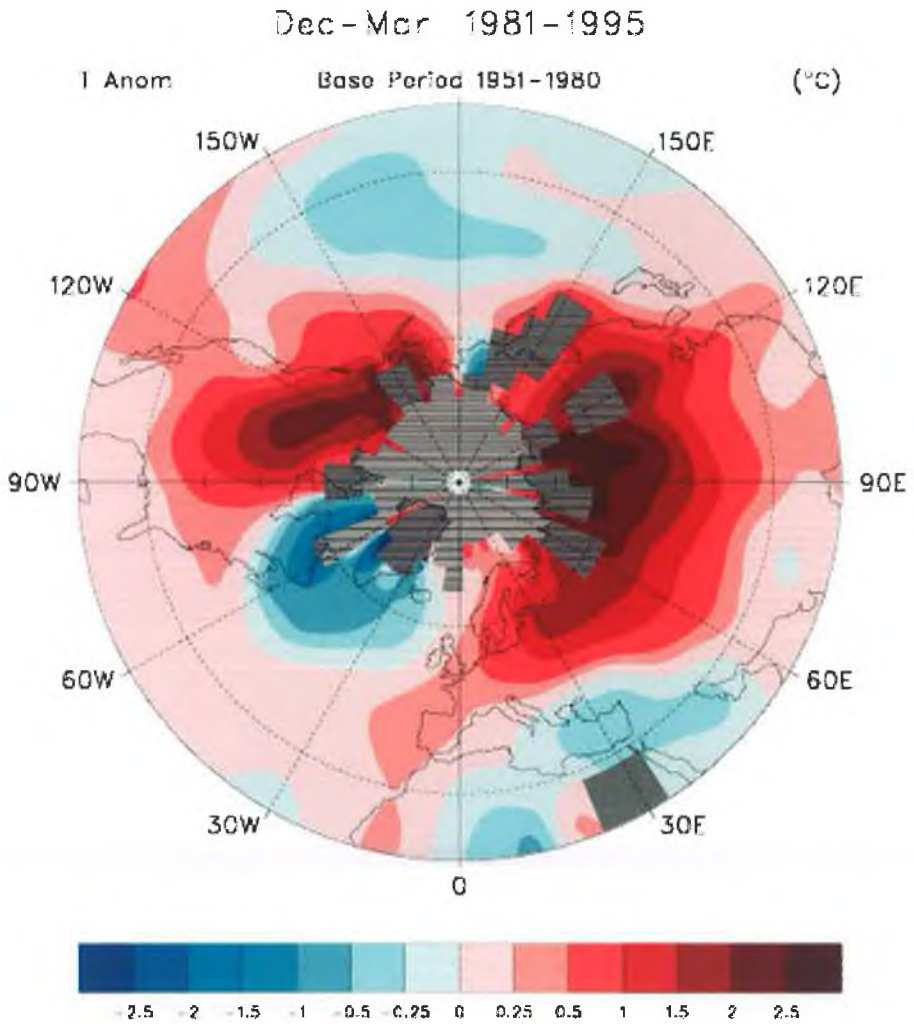

Figure 2.2.3 Observed December-March surface temperature anomalies associated with a high NAO index; the period 1981-1995, when the NAO was high, relative to the period 1951-1980, when the NAO was low (after Hurrell, 1996) (Source: CLIVAR IPO).

From the turn of the 19th century to the early 1930s, the NAO was largely in a positive phase. While from the 1940s to the 1970s it tended towards a more negative phase. The timing of this negative phase corresponds with the mid-century cooling experienced by many of the countries bordering the North Atlantic. Before the 1940s temperatures had been increasing since the turn of the century.

Positive phases of the NAO produce a tendency towards higher winter temperatures in Northern Europe due to an intensification of westerlies

transporting oceanic heat onto the European Continent (Figure 2.2.3). As a consequence, recent wintertime temperature trends have been associated with high index phases of the NAO (Marshall *et al.*, 2001).

2.2.2 NAO and precipitation

There is evidence to suggest that regional changes in precipitation amounts, intensity and location have also occurred over the course of the 20th century (IPCC, 2001b). Annual precipitation over the 20th century has displayed an increasing trend in the mid- to high-latitudes in the order of approximately 0.5-1.0% per decade (IPCC, 2001b), while in the sub-tropical Northern Hemisphere land areas, precipitation has decreased by 0.3% per decade (IPCC, 2001b). Associated with these precipitation increases in the mid- to high- latitudes is a tendency towards an increase in the frequency of more intense precipitation events (IPCC, 2001b). An increasing frequency of more intense events can occur due to a number of factors, such as, changes in humidity, atmospheric circulation patterns and increased storm activity.

Positive phases of the NAO result in a change in storminess and storm track location (Rogers, 1990; Hurrell, 1995) which in turn produce changes in synoptic scale eddy transfer of warm, moist air between the equator and pole (Hurrell, 1995).

Thus, European precipitation patterns tend to exhibit a strong association with the NAO, with drier than average conditions over much of central and southern Europe and wetter than average conditions being experienced over northern Europe during high index phases (Figure 2.2.4) (Marshall and Kushnir, 1997; Marshall *et al.*, 2001). Precipitation during this phase exhibits a strongly north-south gradient, with positive anomalies associated with northern Europe and negative anomalies associated with southern Europe. The recent high index phase has been associated with a number of positive mass balance years on maritime glaciers in western Norway, while in the Alps, mass balance values were among the lowest recorded.

These variations in precipitation, resulting from various modes of the NAO may help explain long-term variations in European glacier mass balance.

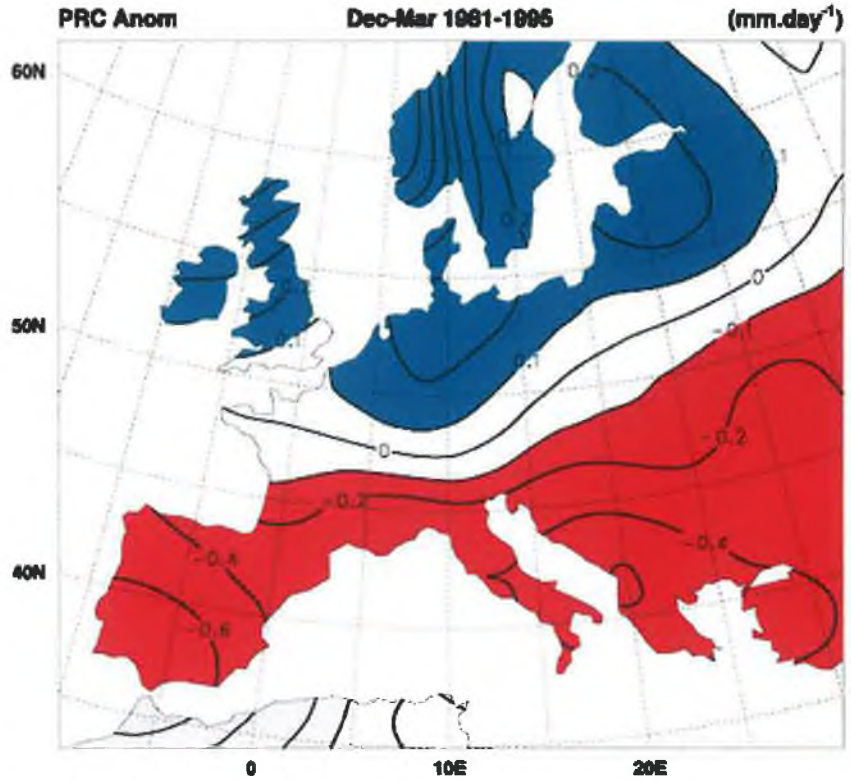

Figure 2.2.4 1981-1995 average precipitation anomalies expressed as departures from 1951-80 mean, from station data in Eischeid *et al.* (1991) data set (courtesy of J. Hurrell) (Source:CLIVAR IPO)

2.2.3 Statistical analysis of the relationship between atmospheric modes and climate elements

To analyse the relationship between circulation and the primary climatic variables, long-term (~90 years) monthly temperature and precipitation data, for a selection of stations, on a south to north axis over Europe, was compiled from two sources (Table 2.2.1). Data for northern Europe was obtained from the North Atlantic Climatological Dataset (NACD) (Frich *et al.*, 1996) and updated with the Nordklim Dataset 1.0 (Tuomenvirta *et al.*, 2001) while data from the rest of Europe was obtained from the European Climate Assessment (Klein Tank *et al.*, 2002). Preference in selecting stations was given to those with long-term records. The selection was also intended to capture a range of spatially diverse responses to

atmospheric variability as outlined in the previous sections. An additional requirement was that the datasets were homogenised and quality controlled.

These criteria resulted in the following stations being selected: for Nordic countries, Kalmar, Oslo-Blindern, Bergen-Florida, Ona, Reykjavik, Stykkisholmur, Bodoe and Kiruna. Valentia, Malin Head and Stornoway were deemed representative of Western Europe, while Genoa, Bologna, Lugano, Innsbruck, Sonnblick and Saentis were selected to represent the Alpine region (Table 2.2.1).

Country	Station Name	Latitude	Longitude	Elevation (m)
Italy	Genoa	44°24N	09°00E	53
Italy	Bologna	44°29N	11°15E	60
Switzerland	Lugano	46°00N	08°58E	273
Austria	Sonnblick	47°03N	12°57E	3106
Switzerland	Saentis	47°15N	09°21E	2490
Austria	Innsbruck	47°16N	11°24E	577
Ireland	Valentia	51°56N	10°15W	9
Ireland	Malin Head	55°22N	07°20W	20
Sweden	Kalmar	56°43N	16°17E	15
Great Britain	Stornoway	58°13N	06°19W	15
Norway	Oslo-Blindern	59°57N	10°43E	94
Norway	Bergen-Florida	60°23N	5°20E	12
Norway	Ona	62°52N	6°32E	13
Iceland	Reykjavik	64°08N	21°54W	52
Iceland	Stykkisholmur	65°05N	22°44W	8
Norway	Bodoe	67°16N	14°26E	11
Sweden	Kiruna	67°49N	20°20E	442
Norway	Tromsoe	69°39N	18°56E	100

Table 2.2.1 List of long-term temperature and precipitation stations from various European locations used in the analysis. Stations are listed on a south to north axis.

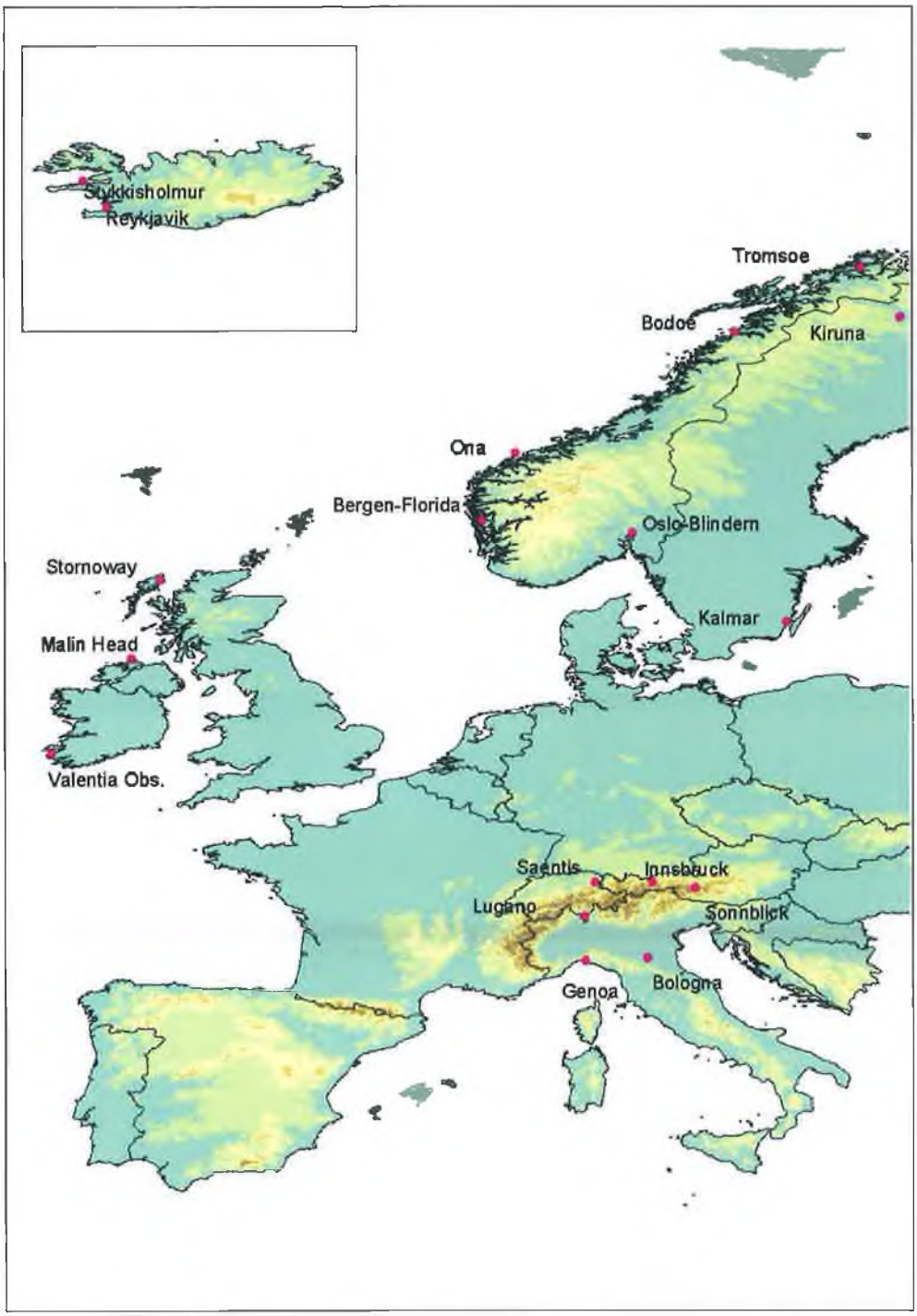

Figure 2.2.5 Location map of temperature and precipitation stations.

As the NAO is most pronounced during the boreal winter months of December, January and February (DJF), the highest correlations with temperature and precipitation were found with these months; both when seasonally averaged (DJF) and on a monthly basis (Table 2.2.2). Correlations between the NAO and temperature during the boreal summer months of June to August were less

conclusive. Weak or insignificant relationships with the NAO during the boreal summer are expected due to a much weakened, and in some cases altogether absent, NAO during these months.

Station	DJF_{PC}	Dec_{GI}	Jan_{GI}	Feb_{GI}	JJA_{PC}	Jun_{GI}	Jul_{GI}	Aug_{GI}
Bologna	0.37**	0.36**	0.37**	0.54**		0.21*		
Lugano	0.37**	0.23*	0.35**	0.59**	0.21*	0.30**		0.35**
Sonnblick	0.39**	0.25*	0.41**	0.54**	0.23*			
Innsbruck	0.23*	0.24*	0.36**	0.47**				0.26**
Saentis	0.44*		0.37**	0.57**	0.23*			0.31**
Valentia	0.63**	0.63**	0.75**	0.76**	0.27**	-0.25**		
Malin Head	0.64**	0.45**	0.69**	0.62**	0.39**			
Stornoway	0.63**	0.45**	0.62**	0.56**	0.42**			
Reykjavik				-0.18*		-0.27**	-0.21*	
Kalmar	0.69**	0.58**	0.67**	0.66**	0.50**			
Oslo-Blindern	0.73**	0.53**	0.68**	0.61**	0.44**			
Bergen-Florida	0.73**	0.59**	0.71**	0.69**	0.23*	-0.20*		
Ona	0.68**	0.44**	0.64**	0.65**	0.36**			
Tromsoe	0.56**	0.24*	0.41**	0.42**	0.24*	0.27**	0.27**	

** (*) Correlation is significant at the 0.01(0.05) level (2-tailed).

Table 2.2.2 Correlations between the North Atlantic Oscillation and long term temperature data from various European stations (Data compiled from Frich *et al.*, 1996 and Klein Tank *et al.*, 2002) (PC- Principal Component (Hurrell), GI- Index between Gibraltar and Iceland).

A general trending south-north gradient is evident from Table 2.2.2 in the relationship between the seasonally averaged winter NAO (DJF) and temperature. This gradient is also evident during the months of December (Dec_{GI}) and January (Jan_{GI}). The strength of the gradient appears to diminish during the month of February (Feb_{GI}). This may partially be a response to sea-surface temperatures (SSTs), which are at an annual minima during the month of February which coupled with a westerly airflow may act to suppress temperatures and thereby diminish the gradient apparent in the previous months. The correlations between the NAO and the northernmost station, Tromsoe, although significant are less than

could be anticipated and would appear to indicate a northern latitudinal boundary to the influence of the NAO on temperature during the winter months.

A much-weakened NAO still appears to exert an influence on temperature during the seasonally averaged summer months of June, July and August (JJA_{PC}). However, the relationship is less clear when the NAO is related to the individual summer months of June (Jun_{GI}), July (Jul_{GI}) and August (Aug_{GI}).

Station	DJF_{PC}	Dec_{GI}	Jan_{GI}	Feb_{GI}	JJA_{PC}	Jun_{GI}	Jul_{GI}	Aug_{GI}
Genoa	-0.43**		-0.34**			-0.24*		
Lugano	-0.37**	-0.21*	-0.30**		-0.23*	-0.25*		-0.33**
Sonnblick				0.29**				-0.37**
Innsbruck		0.23*		0.29**				-0.21*
Saentis		0.29**	0.32**	0.43**	-0.24*			-0.30**
Malin Head		0.46**	0.38**	0.50**	-0.35**			0.22*
Stornoway	0.66**	0.58**	0.65**	0.68**		0.48**	0.28**	0.42**
Stykkisholmur	0.51**		0.30**		0.47**	0.27**		
Kalmar	-0.46**		-0.32**					
Oslo-Blindern		0.34**	0.35**	0.46**	-0.31**			
Bergen-Florida	0.81**	0.34**	0.65**	0.65**	0.21*	0.43**	0.46**	0.54**
Kiruna						0.30**	0.37*	
Tromsoe	0.45**				0.33**	0.22*		

** (*) Correlation is significant at the 0.01 (0.05) level (2-tailed).

Table 2.2.3 Correlations between the North Atlantic Oscillation and long term precipitation data from various European stations (Data compiled from Frich *et al.*, 1996 and Klein Tank *et al.*, 2002) (PC- Principal Component (Hurrell), GI- Index between Gibraltar and Iceland).

A south-north gradient in the strength of the correlations between the NAO and precipitation during the boreal winter is also evident (Table 2.2.3). However, in the case of precipitation, reductions in precipitation receipt at the low-lying (<300 m) southern European stations appears to be weakly, but significantly, related to an increase in the strength of the NAO during the winter months, while the southern European stations at elevation (>550 m) are weakly but positively correlated with the NAO.

Aspect, more than elevation, is likely to be the more important factor influencing precipitation receipts at Alpine stations during high index events; Genoa and Lugano are on the windward side of the Alps with a westerly airflow. However, orographic enhancement would also occur at the high elevation stations acting to increase receipts. Kalmar, in Sweden, and Oslo, in Norway, appear to be the exception during winter and summer, respectively, to the south-north gradient. The change in sign of the correlations with the NAO for these stations may reflect their more continental location away from a moisture source.

Again, the relationship with the NAO is less clear when precipitation is related to the individual months of June, July and August. As was the case with temperature, the relationship between precipitation at Tromsoe and the NAO is less evident, again suggesting a northern latitudinal boundary to its influence.

Overall, there is a consistent seasonal signal between the winter and summer with reductions in precipitation receipt apparent in the alpine region. Receipts increase northwards with a positive NAO. Thus, a stronger NAO acts to suppress/diminish moisture from penetrating into central and southern Europe diverting it on a more northerly trajectory.

Based on the findings from Table 2.2.2 and Table 2.2.3, it was decided to assess the influence of additional large-scale modes of atmospheric variability that occur during the summer months, on temperature and precipitation. As a result, two modes of variability, the East Atlantic-Jet Pattern (EA-JP) which is one of the primary modes of atmospheric variability occurring between April and August, and the Arctic Oscillation (AO), which is closely related to the NAO, were examined in conjunction with these variables. Positive phases of both modes reflect an intensification of westerlies over Europe during these months.

Table 2.2.4 and Table 2.2.5 display the significant correlations between, seasonally averaged and individual monthly, values of EA-JP and the AO and temperature and precipitation, respectively. A positive phase of the EA-JP is moderately related to temperatures for the Alpine stations, while weakly to moderately, negatively

correlated with temperatures in Northern Europe. A positive AO is weakly but positively related to temperature for Alpine and Northern European stations, with the exception of Reykjavik.

Station	JJA_{EAJP}	Jun_{EAJP}	Jul_{EAJP}	Aug_{EAJP}	JJA_{AO}	Jun_{AO}	Jul_{AO}	Aug_{AO}
Bologna	0.65**	0.49**	0.36**	0.57**				
Lugano	0.53**	0.49**		0.55**	0.27**		0.27**	0.32**
Sonnblick	0.40**			0.54**	0.30**	0.23*	0.26**	0.24*
Innsbruck	0.44**		0.36**	0.51**	0.23*		0.22*	0.29**
Saentis	0.42**			0.54**	0.28**		0.27**	0.33**
Valentia								0.40**
Malin Head					0.38**	0.24*	0.25*	0.45**
Stornoway					0.44**	0.27**	0.24*	0.42**
Reykjavik						-0.28**		
Kalmar		-0.44**			0.44**	0.45**		0.42**
Oslo-Blindern	-0.33*	-0.59**		-0.46**	0.33**	0.22*		0.32**
Bergen-Florida		-0.50**		-0.40**	0.23*			
Ona		-0.47**			0.32**	0.35**		
Tromsoe					0.31**	0.43**		

** (*) Correlation is significant at the 0.01 (0.05) level (2-tailed).

Table 2.2.4 Correlations between the East Atlantic-Jet Pattern (EA-JP), Arctic Oscillation (AO) and long term temperature data from various European stations (Data compiled from Frich *et al.*, 1996 and Klein Tank *et al.*, 2002)

The relationship between the EA-JP and temperature are in contrast to those of the NAO (Table 2.2.2) indicating a decreasing relationship with increasing latitude with a westerly circulation. This can be explained by the location of the centres of action of the EA-JP. A high pressure cell centred over the eastern Mediterranean acts to draw warm air from the African Continent and circulate it onto continental Europe enhancing the continental summer temperatures, while a low pressure cell centred over the Eastern North Atlantic/Northern Scandinavia would draw cooler air down from higher latitudes.

Station	JJA_{EAJP}	Jun_{EAJP}	Jul_{EAJP}	Aug_{EAJP}	JJA_{AO}	Jun_{AO}	Jul_{AO}	Aug_{AO}
Genoa		-0.29*		-0.35*				
Lugano				-0.31*	-0.24*			-0.25*
Saentis								-0.24*
Malin Head	0.62**	0.36*	0.34*	0.50**				
Stornoway	0.60**		0.38*	0.49**		0.27*		
Stykkisholmur	-0.44**	-0.29*	-0.39**		0.30**	0.31**	0.23*	0.34**
Oslo-Blindern				0.35*				
Bergen-Florida	0.37**		0.41**	0.58**	0.27**	0.44**	0.36**	
Kiruna	0.38*			0.42**				
Tromsoe						0.22*		0.27**

** (*) Correlation is significant at the 0.01 (0.05) level (2-tailed).

Table 2.2.5 Correlations between the East Atlantic-Jet Pattern (EA-JP), Arctic Oscillation (AO) and long term precipitation data from various European stations (Data compiled from Frich *et al.*, 1996 and Klein Tank *et al.*, 2002).

In terms of the relationship between the EA-JP and precipitation, conclusions are again difficult to arrive at due to the reduced number of significant correlations. There is a general trend for a weak and negative relationship with precipitation receipts at Alpine stations, strong positive correlations with Western European stations and diminished, but significant and positive correlations with Northern European stations. Iceland is again the exception.

A more discriminating measure of the relationship between the atmospheric variability indices and temperature and precipitation considers only values that are greater than one standard deviation from normal, which in this case is defined as the period between 1876-2000. Table 2.2.6 and Table 2.2.7 display Spearman correlation coefficients between the NAO and temperature and precipitation, respectively, by season mean and individual winter months where the NAO is greater than one standard deviation above or below the mean.

The Spearman correlation coefficient was employed in this instance, as it is less sensitive to the effect of outliers than the previously used Pearson's correlation

coefficient, is non-parametric and is therefore considered to be more robust to deviations from linearity (Wilks, 1995)

Station	NAO_{DJF}	$NAO_{DEC-JAN-FEB}$
Bologna	0.61**	0.58**
Lugano	0.69*	0.55**
Sonnblick	0.70**	0.60**
Innsbruck	0.41*	0.59**
Saentis	0.70**	0.57**
Valentia	0.74**	0.80**
Malin Head	0.77**	0.72**
Stornoway	0.74**	0.66**
Kalmar	0.80**	0.77**
Oslo-Blindern	0.83**	0.75**
Bergen-Florida	0.82**	0.78**
Ona	0.77**	0.68**
Tromsoe	0.62**	0.47**

** (*) Correlation is significant at the 0.01 (0.05) level (2-tailed).

Table 2.2.6 Correlations with winter season NAO (Principal Component), NAO_{DJF}, and individual winter months, $NAO_{DEC-JAN-FEB}$, and European temperature series for NAO $\geq \pm 1\delta$ (Data compiled from Frich *et al.*, 1996 and Klein Tank *et al.*, 2002).

It is evident from Table 2.2.6 that extreme index events (>1δ) are positively and significantly correlated to European temperatures. An increase in winter temperatures is associated with high index events while a reduction in winter temperatures is associated with low index events. The pattern of precipitation receipts displayed in Table 2.2.7 is similar to that of Table 2.2.3, but the correlations are higher. High index events are associated with reduced precipitation in low-lying Alpine stations, accounting for 15-18% of explained variance, with very slight increases at elevated Alpine stations, accounting for 5-8% of the explained variance. The exception is Saentis which shows increases in precipitation associated with high index events. Substantial increases are evident for the Western European and coastal Scandinavian stations, accounting for 30-50% of the variance explained.

Station	NAO_{DJF}	$NAO_{DEC-JAN-FEB}$
Genoa	-0.59**	-0.39**
Lugano	-0.47*	-0.42**
Sonnblick		0.24*
Innsbruck		0.29**
Saentis		0.50**
Malin Head		0.55**
Stornoway	0.82**	0.76**
Stykkisholmur	0.61**	0.29**
Kalmar	-0.65**	
Oslo-Blindern		0.58**
Bergen-Florida	0.86**	0.72**
Tromsoe	0.68*	

** (*) Correlation is significant at the 0.01 (0.05) level (2-tailed).

Table 2.2.7 Correlations with winter season NAO (Principal Component), NAO_{DJF}, and individual winter months, $NAO_{DEC-JAN-FEB}$, and European precipitation series for NAO $\geq \pm 1\delta$ (Data compiled from Frich *et al.*, 1996 and Klein Tank *et al.*, 2002).

Extreme index events, when the NAO $\geq \pm 2\delta$, would be expected to enhance the above findings. However, due to the reduction in size of the dataset as a consequence of selecting these extreme events (rendering significance testing unreliable in this instance) it was decided to plot the results to allow for a visual examination of the data (Figure 2.2.6). For temperature, the effects of a small number of cases and the potential negative impact of outliers does not appear to have too much of an effect on the relationships, while for precipitation the impacts are less clear.

What is clear from the scatter plots are that extreme high index occurrences are associated with high temperatures across Europe and enhanced precipitation in Western Europe and Scandinavia and suppressed precipitation in southern alpine Europe. The difference in temperature between individual winter months recording an extreme high index and the long-term mean winter (DJF) temperature range from an increase of just under 3^0C at Sonnblick to 4.3^0C at Oslo (Table 2.2.8).

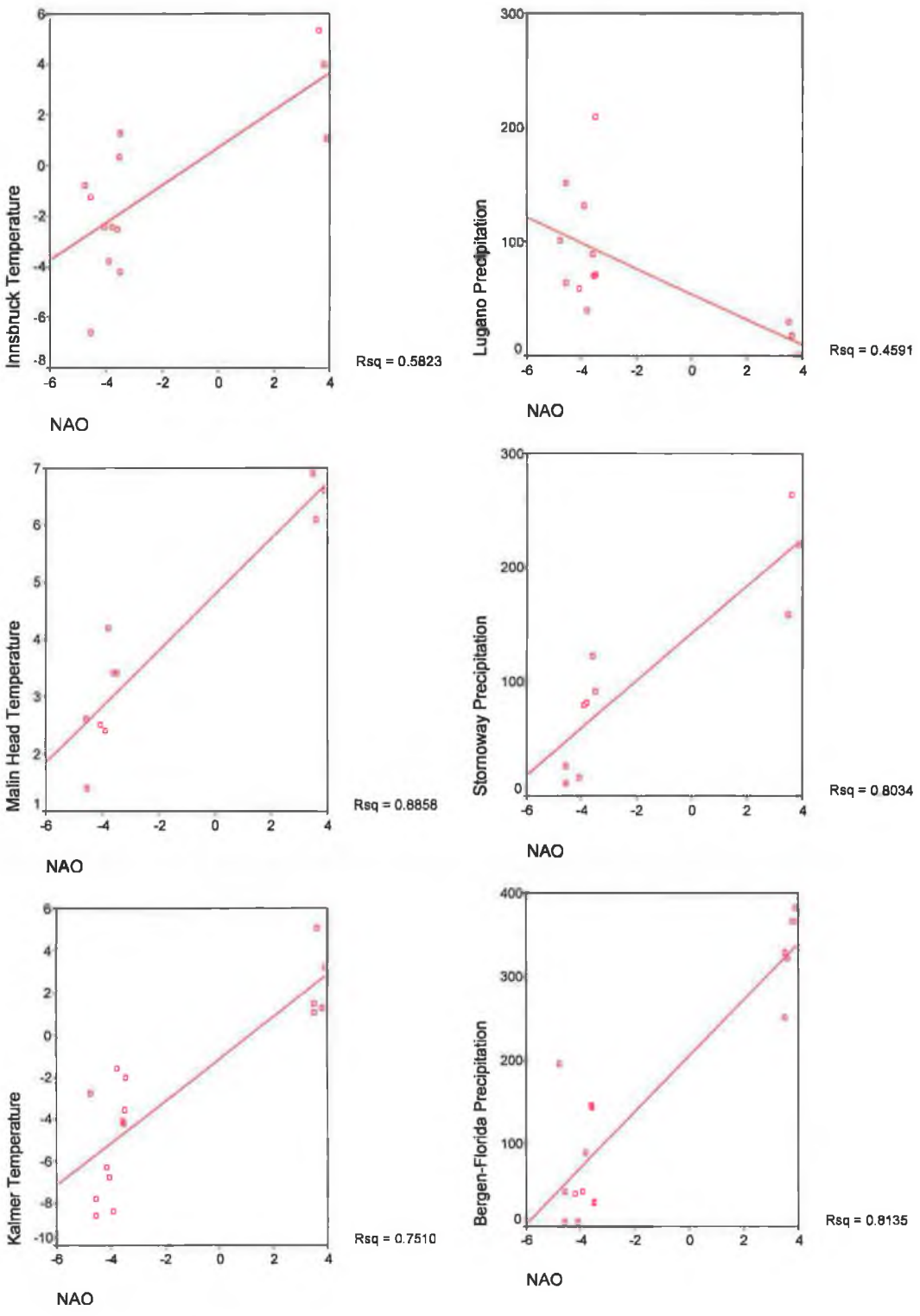

Figure 2.2.6 Scatter diagrams of the NAO ≥ ± 2δ with temperature and precipitation for a selection of stations

Reductions of up to 43 mm are found in precipitation receipts measured at Genoa between averages of high index months and the long-term mean winter (DJF)

precipitation, while for Stornoway, in northern Scotland, increases of 100 mm above the mean are apparent for similar years.

Station	Units	Mean	$\leq \pm 2\delta$	$\geq \pm 2\delta$
Bologna	^{0}C	3.7	1.7	**6.1**
Sonnblick	^{0}C	-12.3	-13.6	**-9.4**
Innsbruck	^{0}C	-0.6	-2.2	**3.5**
Malin Head	^{0}C	5.6	2.8	**6.5**
Oslo-Blindern	^{0}C	-3.6	-8.2	**0.7**
Bergen-Florida	^{0}C	1.8	-2.2	**4.0**
Tromsoe	^{0}C	-3.5	-4.5	**-2.2**
Genoa	mm	113.0	**151.1**	69.4
Sonnblick	mm	113.6	86.3	**137.5**
Innsbruck	mm	47.7	39.1	**70.5**
Stornoway	mm	114.3	60.9	**214.2**
Oslo-Blindern	mm	48.6	17.0	**53.1**
Bergen-Florida	mm	193.8	69.3	**330.2**
Tromsoe	mm	84.5	**103.2**	92.2

Table 2.2.8 Mean of temperature (^{0}C) and precipitation (mm) during winter months when the NAO is in extreme mode (Underlined figures indicate below average, *Bold* figures indicate above average values) .

A similar approach was undertaken to assess the influence of extreme modes of the NAO and EA-JP during the summer months. An intensification of westerlies during the summer season was found to be positively related to increases in temperature across all European stations (Table 2.2.9). However, the individual monthly correlations with the Scandinavian stations suggest that increases in westerlies during the summer months are associated with a cooling of more northern latitudes.

Diminished/suppressed precipitation receipts are again evident with high index modes for Alpine Stations (Table 2.2.10). While, for Western European and Scandinavian stations, precipitation increases are evident.

Station	NAO_{JJA}	$EAJP_{JJA}$	$NAO_{JUN-JUL-AUG}$	$EAJP_{JUN-JUL-AUG}$
Bologna		0.81**		0.38**
Lugano		0.66**	0.36**	
Sonnblick		0.53*	0.22*	
Innsbruck		0.60**	0.27**	0.32*
Saentis	0.39*	0.51*	0.26*	
Malin Head	0.61**			
Stornoway	0.57**			
Reykjavik			-0.22*	
Kalmar	0.63**			-0.32*
Oslo-Blindern	0.56**			-0.51**
Bergen-Florida			-0.23*	-0.41**
Ona	0.57**			
Tromsoe			0.30**	

** (*) Correlation is significant at the 0.01 (0.05) level (2-tailed).

Table 2.2.9 Correlations with summer season NAO (Principal Component), NAO_{JJA} and EA-JP, $EAJP_{JJA}$, and individual summer months (Gibraltar/Iceland), $NAO_{JUN-JUL-AUG}$ and $EAJP_{JUN-JUL-AUG}$, with European temperature series for NAO Index ≥ ± 1δ (Data compiled from Frich *et al.*, 1996 and Klein Tank *et al.*, 2002).

Station	NAO_{JJA}	$EAJP_{JJA}$	$NAO_{JUN-JUL-AUG}$	$EAJP_{JUN-JUL-AUG}$
Lugano			-0.41**	
Sonnblick			-0.30**	
Saentis			-0.22*	
Malin Head	-0.62**	0.73**	0.22*	0.42**
Stornoway			0.49**	0.37*
Stykkisholmur	0.61**	-0.51*	0.31**	-0.33*
Oslo-Blindern	-0.44*			
Bergen-Florida			0.58**	0.38**
Kiruna			0.33**	0.31*
Tromsoe	0.49**			

** (*) Correlation is significant at the 0.01 (0.05) level (2-tailed).

Table 2.2.10 Correlations with summer season NAO (Principal Component), NAO_{JJA} and EA-JP, $EAJP_{JJA}$, and individual summer months (Gibraltar/Iceland), $NAO_{JUN-JUL-AUG}$ and $EAJP_{JUN-JUL-AUG}$, with European precipitation series for NAO Index ≥ ± 1δ (Data compiled from Frich *et al.*, 1996 and Klein Tank *et al.*, 2002).

On examination of the scatter plots for precipitation with the EA-JP $\geq \pm 1\delta$ (not included) some of the results shown in Table 2.2.10 may be unduly impacted by the effect of outliers. For example, with the removal of just one outlier from the correlation between the EA-JP and Stornoway, the relationship becomes significant (0.01). However, during the summer months the association between high index events and reduced precipitation receipts for the Alpine stations does appear to hold.

2.3 Conclusion

This chapter examined the relationship between large-scale atmospheric modes of circulation over the North Atlantic and its impact on the spatial distribution of European temperature and precipitation. The resulting relationships were shown to be both seasonally and spatially variable. While the nature of the link was quite different for both climate variables, the overall effect was one of increased temperatures over the entire European domain during the months of December, January and February with an above average index. Concurrent reductions in precipitation were found for the southern alpine stations. These results are consistent with those of Hurrell (1995) and Brunetti *et al.* (2001). Brunetti *et al.* (2001) show similar reductions in total precipitation for stations in Northern Italy, which they attribute to a strengthening of the NAO, resulting in increased advection of warm and moist air over central and northern Europe.

While for Western European stations, increases in precipitation were evident, Northern Europe also experienced increases in precipitation receipt but to a lesser extent than the Western European stations. For years recording above or below average/extreme indices, the above relationships are further enhanced resulting in greater spatial divergence between the regions in terms of temperature and precipitation.

The relationship between the NAO and temperature during the months of June, July and August are less conclusive due to a diminished NAO during this season and also indicating the influence of a more continental type circulation regime on

temperature during these months. Results for precipitation were slightly more conclusive during these months, despite the NAO being greatly diminished and sometimes absent during the boreal summer. Reductions in precipitation across Alpine European stations with increases in Western and Northern Europe, reflecting the underlying deflection of moist maritime air away from central to more northerly locations in Europe.

The results also indicate that there is a latitudinal boundary zone above which the association between the NAO and climate diminishes. This appears to relate to the extent of effective advection of heat by westerlies (Chen and Hellström, 1999). Correlations between the NAO and the two northernmost stations, Tromsoe and Kiruna, would indicate that the maximum latitude lies close to the latitude of these stations. However, this may also be an artefact of the spatial domain from which the NAO is calculated. Therefore, use of the Arctic Oscillation may be more advisable when comparisons are being conducted on stations with a large latitudinal range.

These seasonal and spatial changes are more pronounced when an analysis of the more extreme values of the NAO is undertaken, further highlighting the discrepancies in amounts and receipts between the regions of interest.

Atmospheric modes of variability and in particular the North Atlantic Oscillation play a crucial role in determining the regional climate of Europe. Its effects are most pronounced in winter when it accounts for the major source of variability in atmospheric circulation in the North Atlantic region. Contrasting regional effects in climate are apparent between southern and northern Europe during both high and low index phases of the NAO. During high index events, zonal or westerly airflow becomes dominant with the resultant advection of heat and moisture onto northern Europe. This produces milder and, crucially from the point of view of glacier mass balance, wetter winters than would otherwise be experienced. During low index events, meridional type circulation becomes dominant, due to a weakening of both the Icelandic low and Azores high. This results in drier and colder than average conditions in northern Europe and warm moist air being diverted over southern

Europe. Despite the high degree of interannual variability of the NAO, anomalous high or low circulation patterns can persist for a number of years (Hurrell, 1995). There has also been the suggestion that recent temperature anomalies are strongly associated with recent persistent phases in the NAO (Hurrell, 1995).

While regional differences in the response of the local climate to the large-scale circulation indicate a mechanism by which spatial differences in mass balance may be explained, in order to assess their long-term variations, an analysis of the temporal characteristics of the European climate series and the impact of fluctuations of the NAO on these variables is required. Subsequent chapters will integrate both these components

Chapter III

Long-term fluctuations in temperature and precipitation in Europe: can they be explained by atmospheric variability?

3.1 Introduction

In an analysis of meteorological controls on the mass balance of Glacier de Sarennes, Vincent and Vallon (1997) demonstrated that summer temperature and ablation were highly correlated over the period 1949-1973, with temperature accounting for as much as 80% of the explained variance. However, when additional data up to 1991 were included in the analysis, the explained variance decreased to 60%. When the period prior to 1973 was excluded from the analysis, the correlation with temperature deteriorated to just 30%. They suggested that inclusion of the state of the glacier surface (snow/ice) over successive years is necessary in order to account for albedo changes when relating mass balance to temperature. This requirement may suggest additional controls influencing the relationship between the local climate and glaciers. Vincent and Vallon (1997) point to this factor as being the result of a much greater interannual and seasonal variability in temperature and precipitation, where consecutive extreme seasons may leave the glacier surface more prone to the effects of temperature depending on the surface conditions of the glacier.

This alteration in the relationship between temperature and ablation, as outlined by Vincent and Vallon (1997), which occurred in the early 1970s, corresponds with a shift in seasonal zonal frequency as described by Bardossy and Caspary (1990). They indicate that while the overall annual frequencies of zonal circulation remained constant, the seasonal frequencies were changing from about 1973, with increased frequencies apparent in December and January and decreases in April and May. These changes were associated with relatively warmer and more humid winters in central Europe. This increase in zonal circulation also corresponds to a shift in the NAO from being predominantly negative to being positive, a phase the NAO has largely persisted in since the 1970s.

The beginning of the 1970s also saw substantial increases in the decadal mean residence times of Grosswetterlagen types W (west) and CW (clustered west) over north western Europe (Werner *et al.*, 2000). They suggested that, up to the beginning of the 1970s, no correspondence was apparent between surface temperatures in the northern hemisphere and residence times of these Grosswetterlagen types. However, after this period both variables were found to increase at similar rates. An outlier test of the decadal behaviour of the climate state signal identified the decade 1981-1990 as the onset of climate change in the North Atlantic area with a trend commencing in the early 1970s (Werner *et al.*, 2000).

A number of other studies have also pointed to a change point in climate as having occurred during the 1970s (Hoppe and Kiely, 1999), resulting in increases in precipitation in Ireland (Kiely, 1999) and Scotland (Smith, 1995); increasing precipitation intensity in Italy (Brunetti *et al.*, 2001); increasing temperature at 300 hPa in the lower and middle latitudes (Weber, 1997) and increasing 700mb heights over western Canada (McCabe and Fountain, 1995).

Increasing or decreasing seasonal trends in either temperature or precipitation are likely to have a large impact on glacier mass balance. Long-term trends in either series may also help explain the differences evident in mass balance between European and Scandinavian glaciers. The initial focus of this chapter will be an assessment of the regional climate series for temporal changes such as, increasing or decreasing trends, which will be evaluated in the context of changes in the NAO. Any trends evident in these series will be examined for obvious change points, which have been identified in a number of previous studies. The influence of large-scale factors on change points identified will also be examined.

3.2 Evidence for trends in the European temperature and precipitation series?

The winter temperature series and 10-year moving averages displayed in Figure 3.2.1 indicate a significant (sig. <0.01) and rising trend in winter temperatures for all the Alpine stations, while a similarly increasing trend does not appear to exist in

the Scandinavian temperature series over the same period (Table 3.2.1). A comparison of moving averages between stations would seem to suggest a large degree of internal regional coherence within the temperature series, indicating synchronous fluctuation points. An illustration of this is the increasing trend evident in the winter Alpine series from the late 1960s onwards, while for the Scandinavian series, the decreasing trend until the mid 1960s is apparent in all series along with the subsequent changes in direction evident in the 1960s and again in the early 1980s.

Temperature					**Precipitation**				
Station	**DJF**		**JJA**		**Station**	**DJF**		**JJA**	
Bologna	+	0.00	+	0.01	Genoa	+		+	
Lugano	+	0.00	+	0.03	Lugano	+		-	0.09
Sonnblick	+	0.01	+	0.00	Sonnblick	+		+	0.00
Innsbruck	+	0.00	+	0.04	Innsbruck	-		+	
Saentis	+	0.00	+	0.03	Saentis	-		-	0.01
Kalmer	+		+		Kalmer	+	0.01	+	
Oslo	+		+		Oslo	+		-	
Bergen	+		+		Bergen	+		+	
Ona	+		+	0.07	Kiruna	+	0.00	+	
Tromsoe	-		+	0.00	Tromsoe	+	0.00	+	0.04

Table 3.2.1 Significance (Kendall's τau-b) and direction (+/-) of trends in seasonal temperature and precipitation data from Alpine and Scandinavian stations (1900-2000).

While the Alpine stations experienced increasing winter temperatures, there is no evidence of a similar trend in the Alpine winter precipitation series (Figure 3.2.2). With the exception of Oslo, winter precipitation in Scandinavia appears to have increased. These increases, which are significant (sig. <0.01) at a number of stations are marked, especially since the 1980s (Figure 3.2.2).

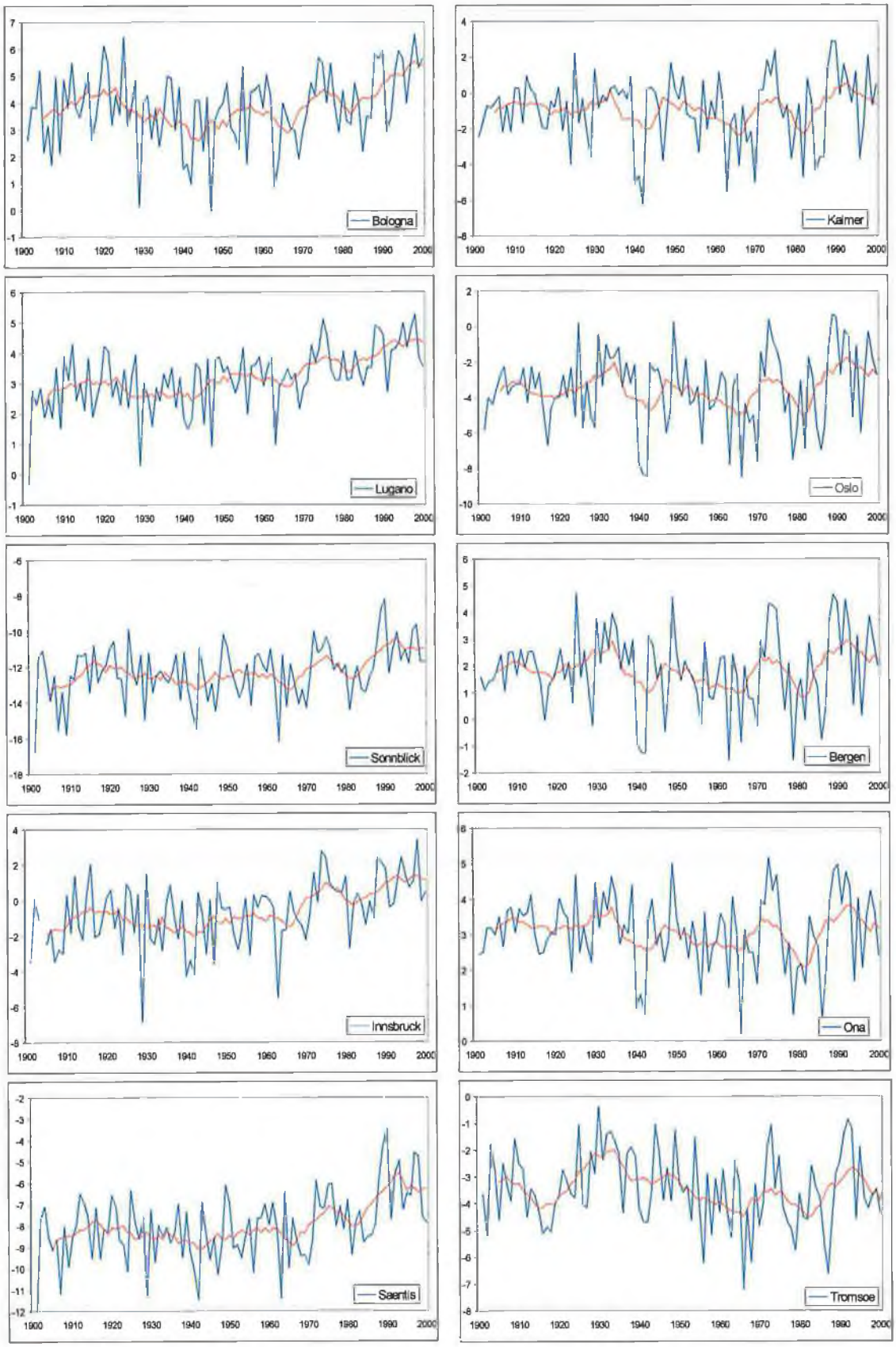

Figure 3.2.1 Winter Temperature for Alpine (left) and Scandinavian stations (right)

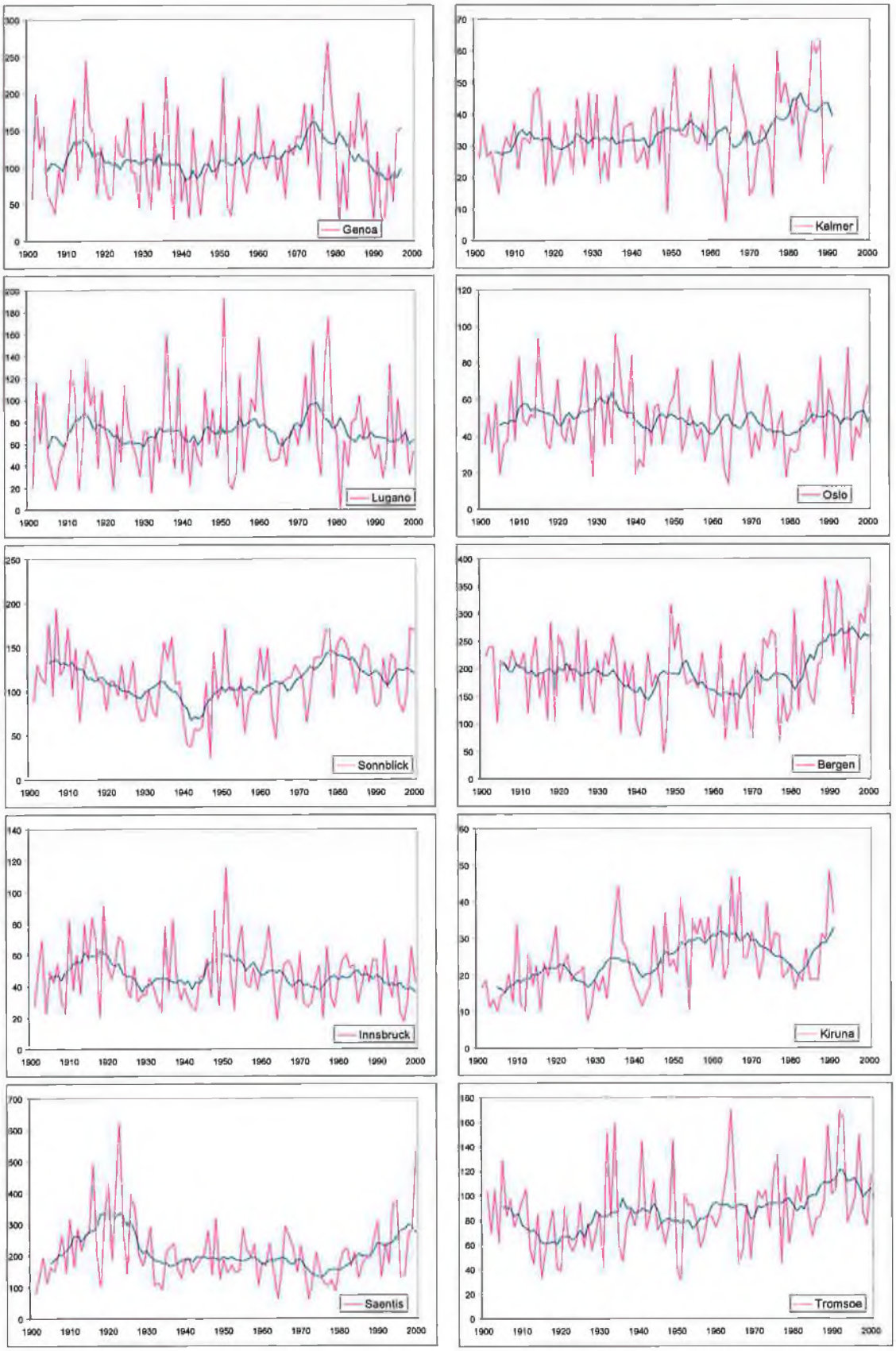

Figure 3.2.2 Winter Precipitation for Alpine (left) and Scandinavian stations (right)

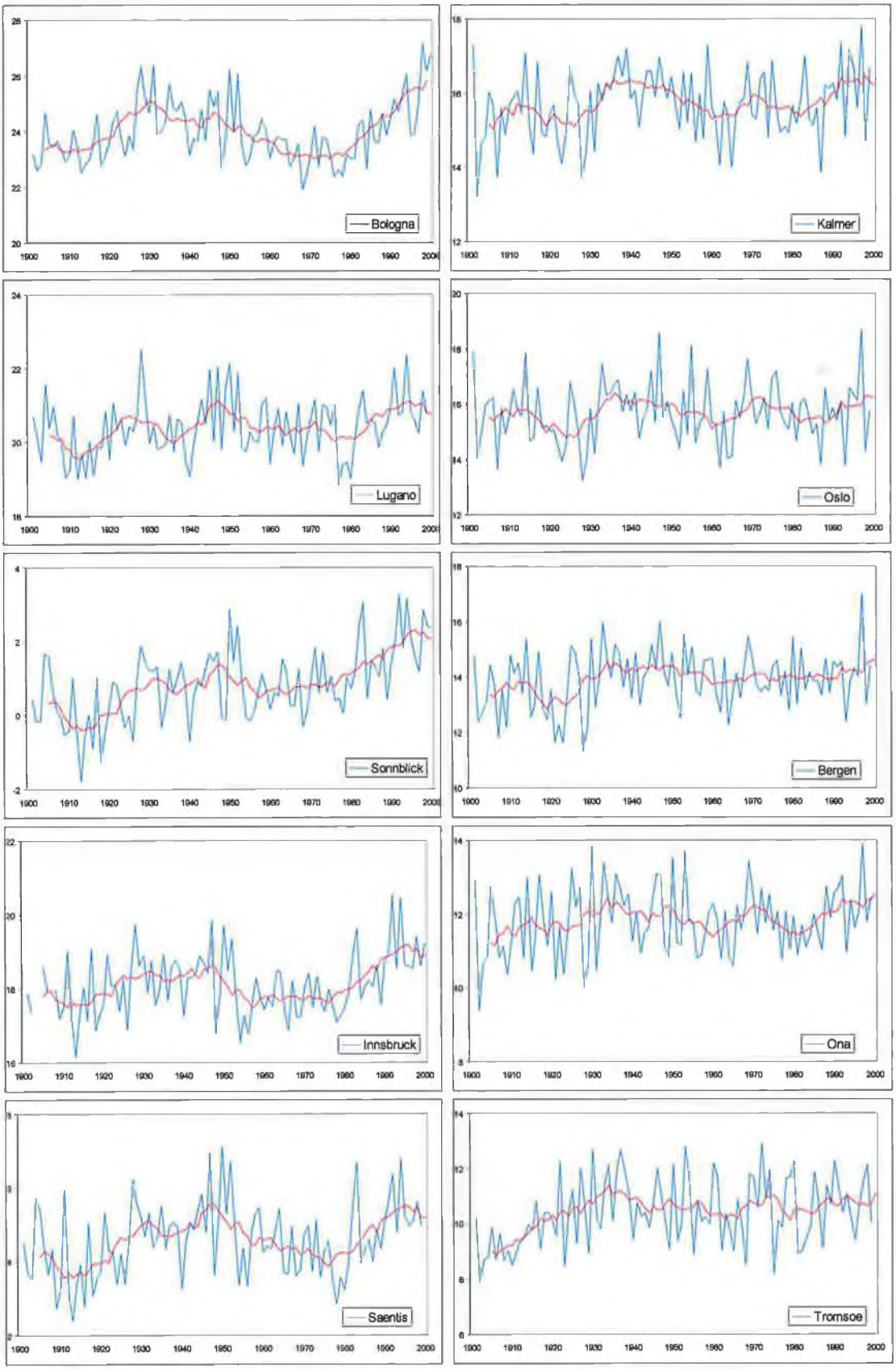

Figure 3.2.3 Summer Temperature for Alpine (left) and Scandinavian stations (right)

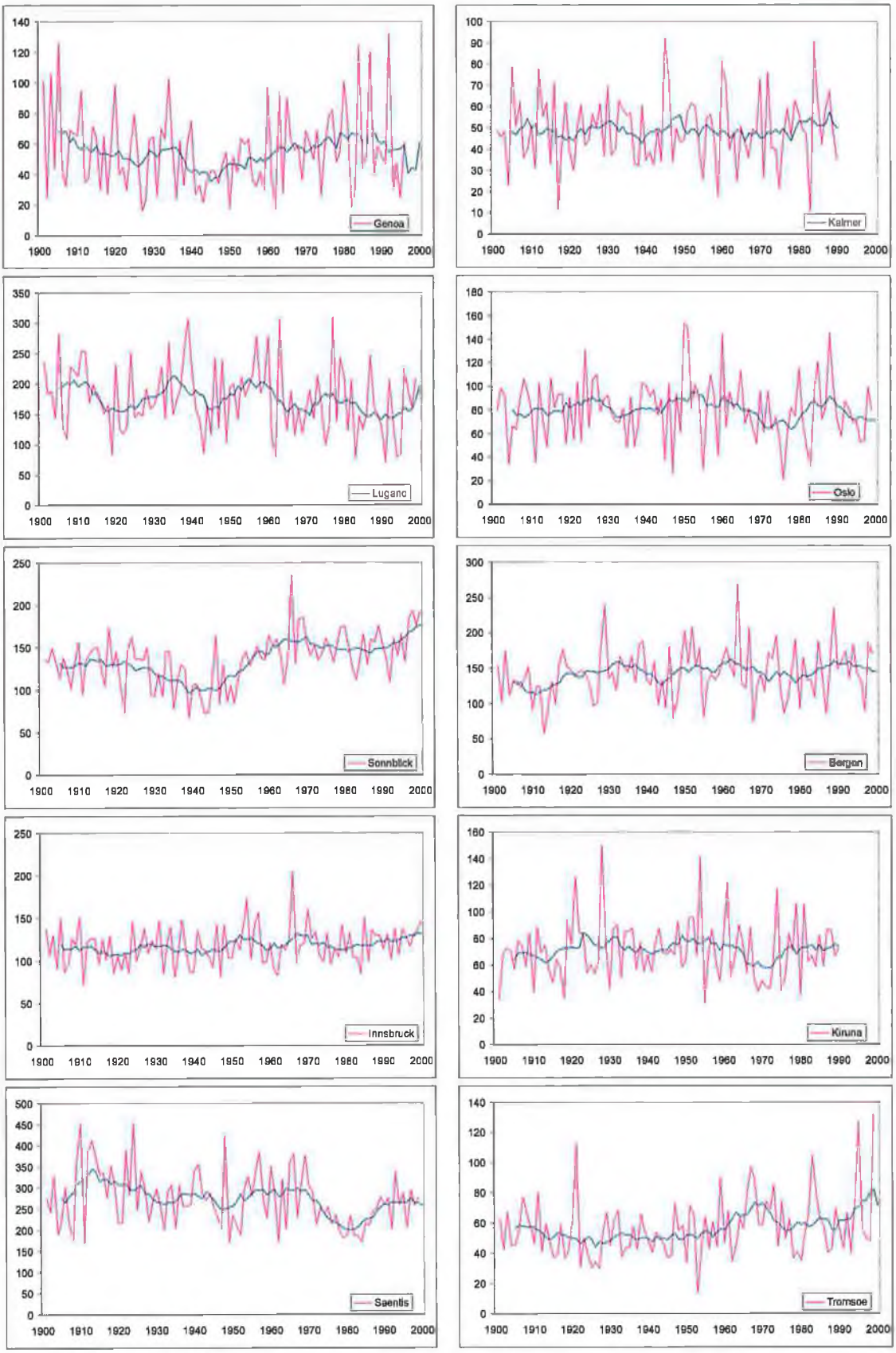

Figure 3.2.4 Summer Precipitation for Alpine (left) and Scandinavian stations (right)

The Alpine summer temperature series also displays evidence of an increasing trend over the last century, with all stations indicating significant increases (sig.<0.05) (Figure 3.2.3). While there are a number of fluctuations in the records, the timing of the increases are consistent at all stations. In comparison, the Scandinavian temperature series, which appear to have been increasing up to the 1930s, have maintained relative stability since then, with only two stations showing slight increases (sig. <0.1) (Figure 3.2.3).

The summer precipitation series from Figure 3.2.4 is a little more difficult to interpret. Increasing precipitation at Sonnblick (sig.<0.00) is evident, while, Genoa has recovered from a mid century decline. Receipts at Lugano (sig.<0.1) and Saentis (sig. <0.01), show decreases, with no change apparent at Innsbruck. Similarly with the Scandinavian series, with the exception of Tromsoe, which is increasing (sig. <0.05), little or no overall trend is apparent in the fluctuations within the series.

The similarity in the long-term regional response, which is most obvious in the winter and summer temperature series for both the Alpine and Scandinavian series, would seem to indicate that the fluctuations are influenced by an external forcing mechanism. As was suggested previously, the NAO and its summer time equivalent, the EA-JP, are significantly related to both these variables. The following sections will examine for the presence of change points in both the climate series to determine if the synchronicity evident in the regional response can be associated with changes in the NAO. The timing of any change points will then be investigated with the presence of change points in the NAO

3.3 A change point analysis of the climate series

3.3.1 Cumulative sums of deviations (CUSUMS)

A cumulative sums of deviations (CUSUM) analysis was performed on both the summer and winter temperature and precipitation series (Figure 3.3.1-Figure 3.3.8) to determine if any changes have occurred in these series which in turn may be

reflected in the glacier mass balance series from Europe. The method consists of calculating the cumulative sum of deviations or anomalies from the long-term mean for each series of interest (Sneyers, 1992). This method has been used in a number of previous studies to identify change points in climate series (Sneyers, 1992; Kiely, 1999; Hoppe and Kiely, 1999) and has also been used to detect inhomogeneities in climate series (Sneyers, 1992). However, it is sensitive to the effect of outliers.

The Cusum is defined as follows:-

$$S_i = \sum_{i=n}^{i} (x_i - k),$$

where k is the average of the time-series.

The hypothesis of no change in the mean value is rejected if max | S_i | becomes too large (Kiely, 1999).

The summer Alpine temperature series from Figure 3.3.1 indicate three change points that are consistent across all bar one station, namely Sonnblick. The first two change points, in 1920 and 1926, mark a period of increasing temperatures after a number of years of below average conditions. After this time period, temperatures briefly drop for a number of years before they begin to increase again until the late 1940s/early 1950s. The third change point in 1981 marks a return to increasing temperatures which continues to the end of the records in 2000. These findings are consistent with those discussed in the previous section and with those of Böhm *et al.* (2001), in a study of regional temperature variability in the European Alps. They found that Alpine temperatures during the 20th century were characterised by rising temperatures towards a first maximum in 1950 and a second in the 1990s. However, their analysis also highlighted the seasonal differences within the series studied.

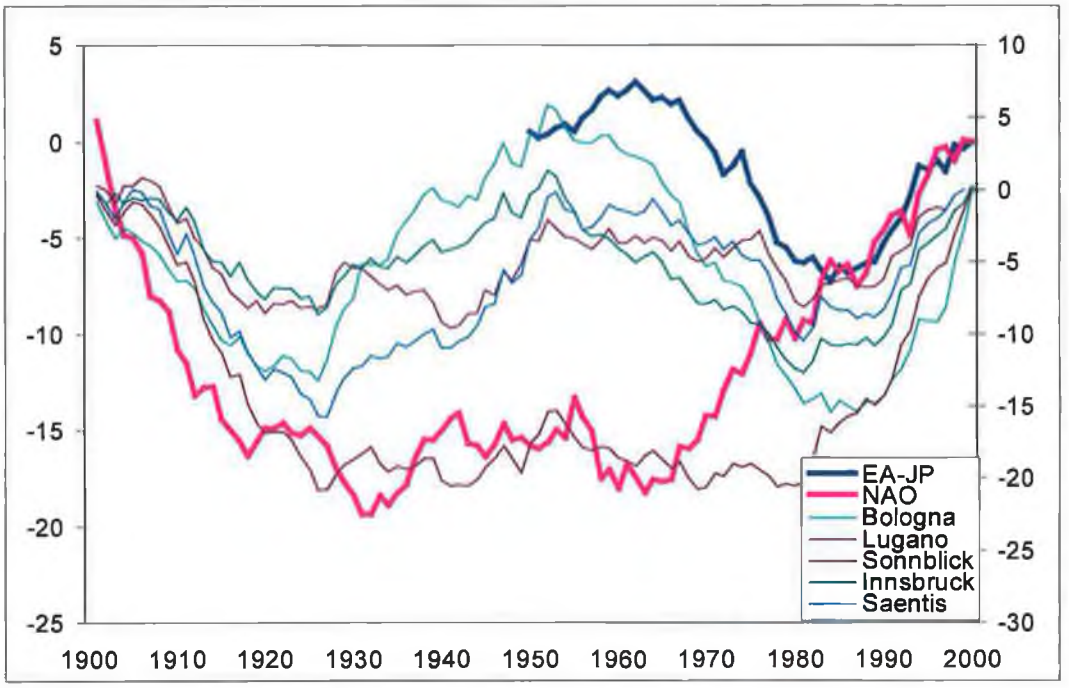

Figure 3.3.1 CUSUMS (cumulative sums of deviations) of NAO, EA-JP and summer temperatures for Alpine Stations.

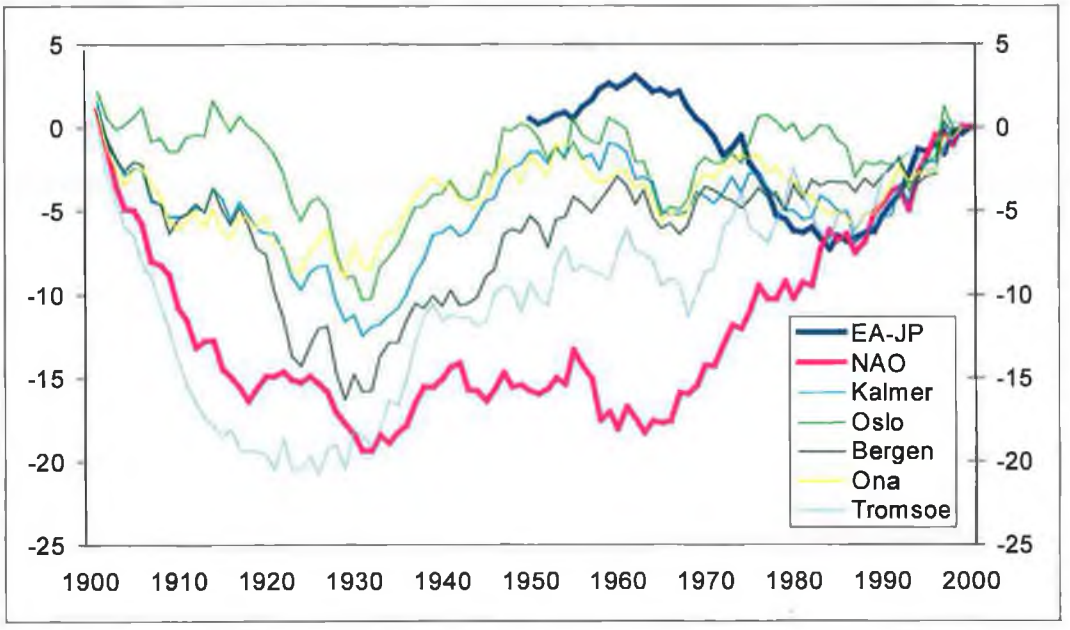

Figure 3.3.2 CUSUMS (cumulative sums of deviations) of NAO, EA-JP and summer temperatures for Scandinavian Stations.

The Scandinavian summer temperature series also display a number of change points, three of which occur in the first three decades of the early 20th century. The first change point occurs around 1909/1910, the second, around the mid-1920s, a little earlier than the change point evident in the Alpine series and the third around

the end of the 1920s to the beginning of the 1930s, which marks an early century temperature maximum. After the 1930s maximum, Scandinavian summer tend to decrease slightly, in response to the mid century cooling which is also evident in the Alpine series, until a third maximum is attained after a 1965 change point.

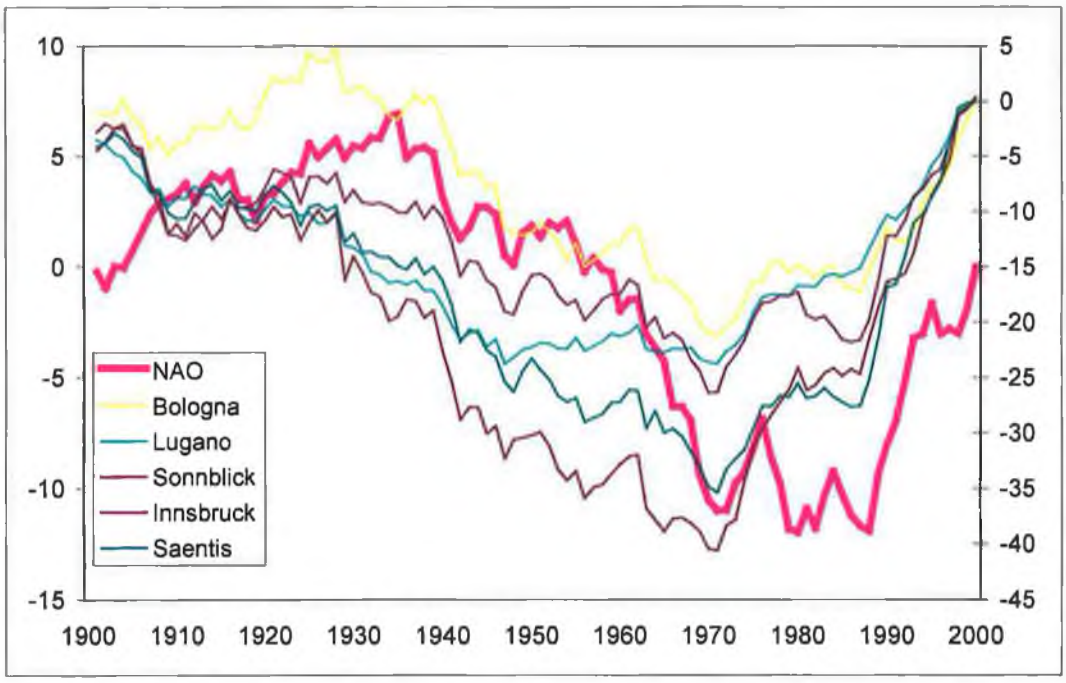

Figure 3.3.3 CUSUMS (cumulative sums of deviations) of NAO and winter temperatures for Alpine Stations.

An analysis of change points in the winter temperature series for the Alpine stations displays little temporal coherence to those of the change points located in the summer temperature series, findings which are similar to those of Böhm et al (2001), while at a number of Scandinavian stations, 1929 is identified as a possible change point. The CUSUMs for the Alpine region again identifies a number of possible change points. The most obvious change point is located in 1971, with a second in 1987. These two change points represent periods of increasing or substantially increased temperatures, with some stations demonstrating increases of up to 2-3^{O}C. However, the Alpine series also demonstrate a number of possible change points before 1971.These change points occur around 1944, 1947/48 and 1956 and again illustrate periods of increasing or increased temperatures, but not to the same degree as the changes evident after 1971 (Figure 3.3.3).

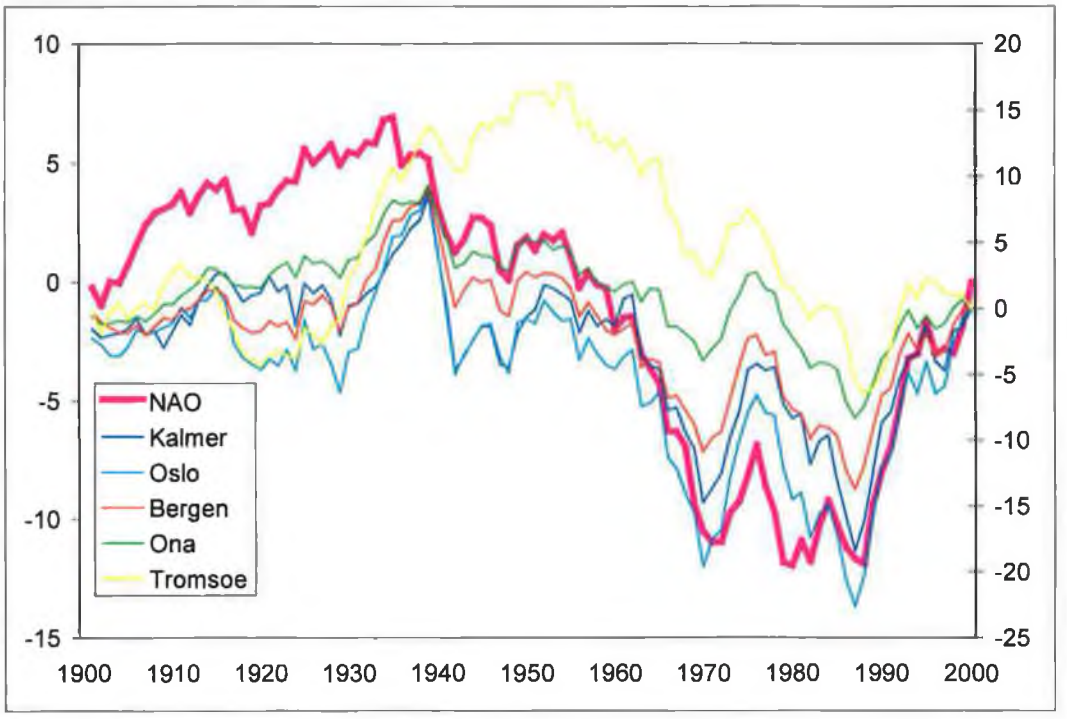

Figure 3.3.4 CUSUMS (cumulative sums of deviations) of NAO and winter temperatures for Scandinavian Stations.

The CUSUMs of the Scandinavian winter temperature series indicate a change point in the late 1920s/early 1930s, after which, below average conditions prevail until a second change point in 1970 marks a second maximum in temperatures. This period of above average temperatures lasts only a few years and is followed by another return to below average conditions up to the early 1980s. A third maximum is attained after 1987 (Figure 3.3.4).

A CUSUMs analysis of summer precipitation displays a number of change points in the Alpine series over the period of record. The CUSUMs of the Saentis series indicates three change points as having occurred at 1927, 1944 and 1971, from Figure 3.3.5 (a), while at Lugano, four change points are suggested at 1915, 1940, 1960 and 1980. While the overall trend for precipitation, at both these stations during the period 1900-2000 is decreasing, the change point locations represents a change from years with above average conditions followed by periods of below average conditions. In comparison to Saentis and Lugano, precipitation at Genoa has increased since the late 1940s, while Innsbruck has maintained around average precipitation over the course of the century. The Genoa series (Figure 3.3.5 (b))

indicates a number of change points in the first half of the century, 1911,1920 and 1935, with only one occurring in the second half in 1962. The early century change points again represent periods of increased precipitation prior to decreases, while the 1962 change point marks a return to increasing precipitation, which had been declining up to the late 1940s. For Innsbruck (Figure 3.3.5 (b)), the change points largely represent changes between periods of above average precipitation and below average precipitation. Sonnblick undergoes a large cumulative decrease from the start of the series to the 1950s after which precipitation increases until the end of the records (Figure 3.3.5 (a)).

The CUSUMS analysis of the Scandinavian summer precipitation series do not display any convincing evidence of containing any significant change points from Figure 3.3.6, with the exception of a possible change point around the mid-1960s.

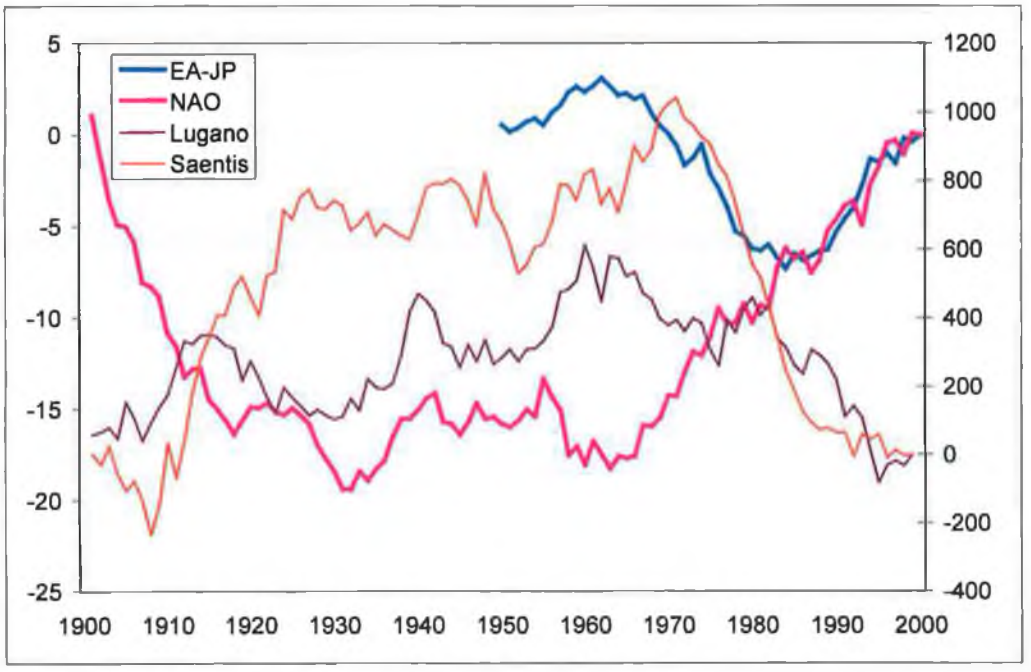

(a)

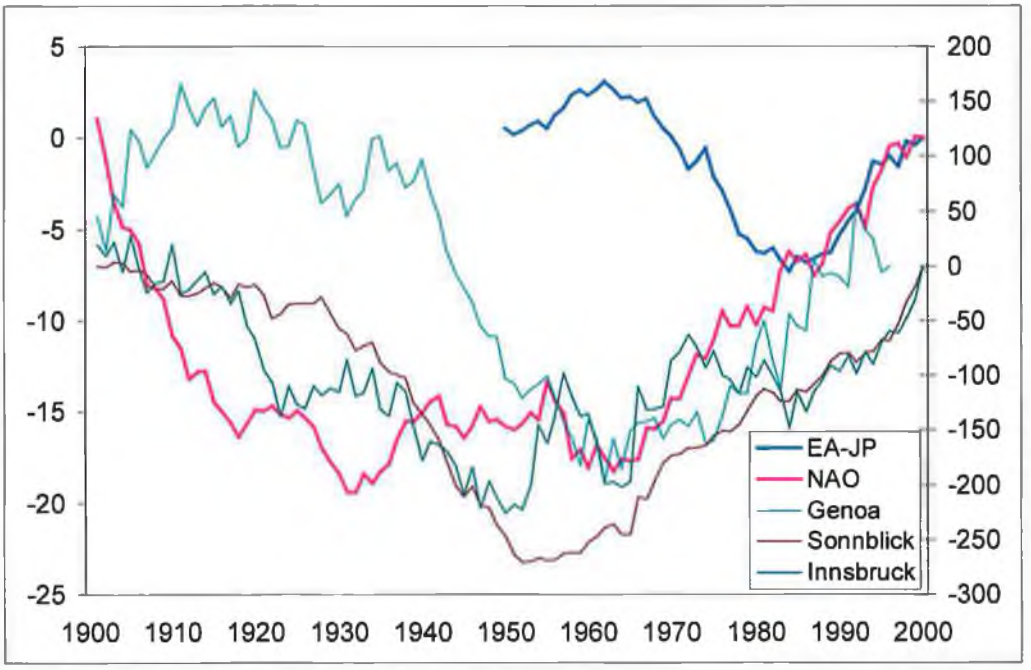

(b)

Figure 3.3.5 CUSUMS (cumulative sums of deviations) of NAO, EA-JP and summer precipitation for Alpine Stations (Sonnblick scaled by a factor of 3).

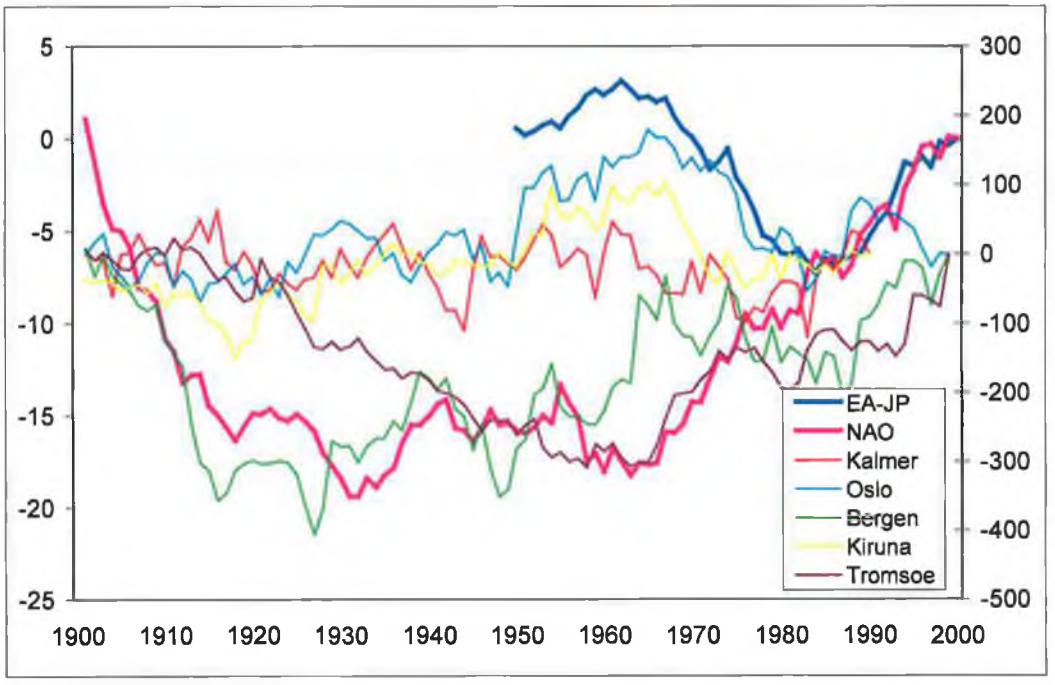

Figure 3.3.6 CUSUMS (cumulative sums of deviations) of NAO, EA-JP and summer precipitation for Scandinavian Stations (Kalmer increased by a factor of 2).

Hanssen-Bauer and Førland (1998b) in their analysis found reductions in summer precipitation between 1960 and 1975 that may explain the possible identification of

this change point around the mid-1960s. However, these reductions were only found for stations in the southern half of Norway.

Tromsoe, from Figure 3.2.4 and Figure 3.3.6, in northern Norway is consistent with their findings for the more northern stations of an increasing trend over the century, resulting in below average conditions in the first half of the century and above average conditions in the latter half. However, Kiruna, in northern Scandinavia appears to respond in a manner similar to the more southern stations.

The CUSUMs, from Figure 3.3.7 (a) and (b), indicates the occurrence of an early century change point in winter precipitation in the Alps around 1910. The change point for Innsbruck and Saentis indicate slightly later occurrences than the other Alpine stations, around 1924 and 1931 respectively. Sonnblick, Genoa and Innsbruck show decreasing receipts after this period until the mid-1940s, while precipitation at Lugano remains constant over the same period. Records from Genoa and Lugano display a second change point during the 1950s; a period during which, increasing or increased precipitation receipts are evident. Innsbruck, in contrast to Genoa, Lugano and Sonnblick, displays largely decreasing precipitation over this period.

A third change point in the Alpine series around the late 1960s and early 1970s marks an end to the increasing precipitation trend evident since the 1950s. After this period, reductions in Alpine winter precipitation are evident. However, the 1970s change point at Saentis demonstrates the beginning of a period of increasing receipts despite the overall decreasing trend as suggested by Kendall's τau-b analysis (Table 3.2.1). The series from Genoa and Lugano suggest a probable change point occurring around the early 1980s, while the series from Sonnblick, indicates the late 1980s as being the location of a probable change point.

A change point analysis of precipitation at the Scandinavian stations during the winter months (Figure 3.3.8) indicates the occurrence of a change point during the 1930s for a number of stations. After this period, Tromsoe, Kiruna and Kalmer display increasing precipitation receipts, while receipts at Oslo and Bergen display

slight decreases. A second change point is evident for a number of stations during the 1970s with Kiruna, Bergen and Oslo, demonstrating decreasing precipitation after this period. A third change point during the 1980s marks a return to a period of increased precipitation.

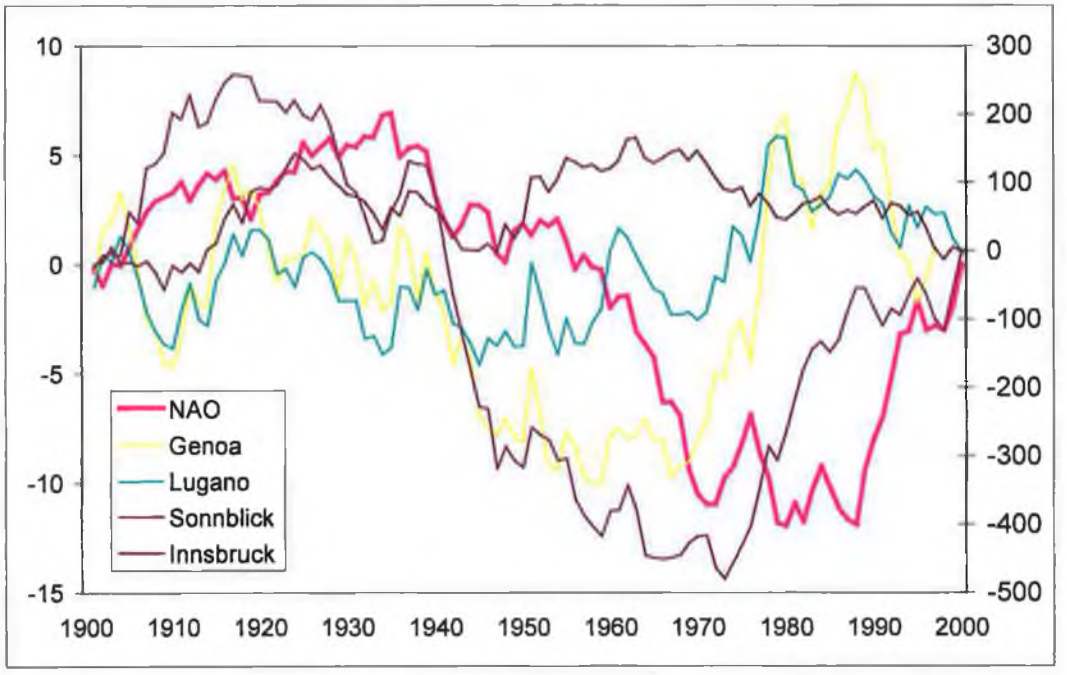

(a)

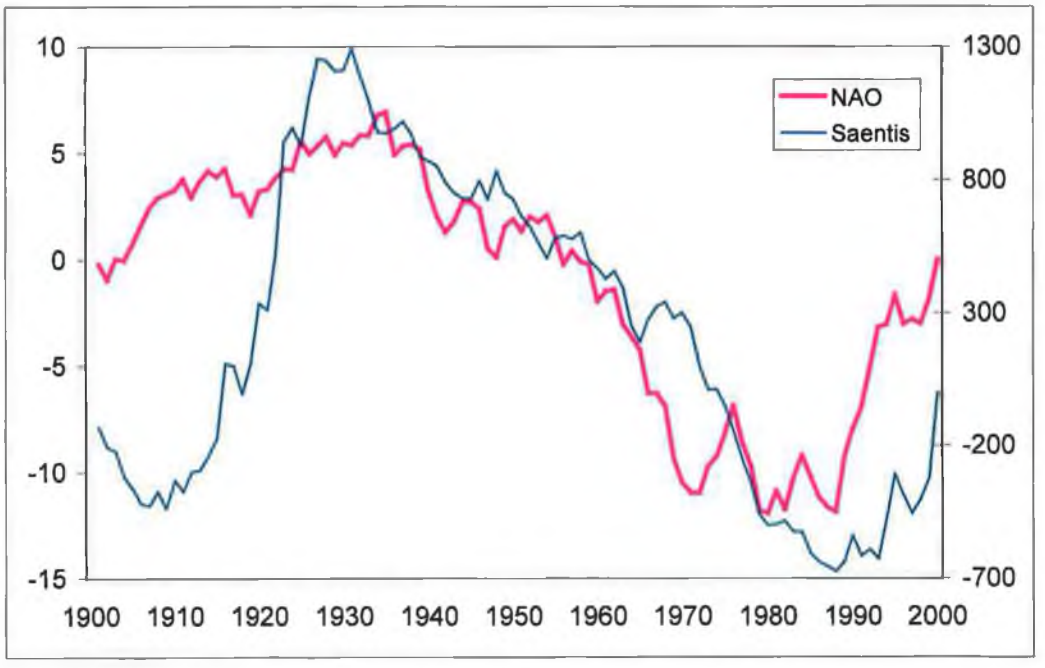

(b)

Figure 3.3.7 CUSUMS (cumulative sums of deviations) of NAO and winter precipitation for Alpine Stations.

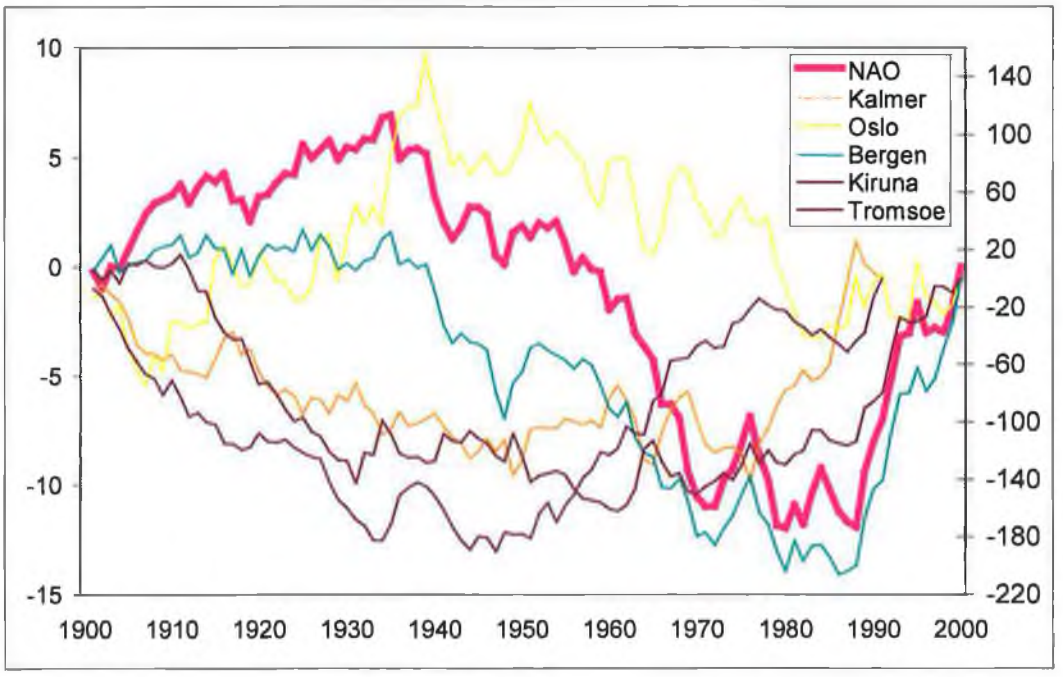

Figure 3.3.8 CUSUMS (cumulative sums of deviations) of NAO and winter precipitation for Scandinavian Stations (Tromsoe scaled by 3, Bergen scaled by 5).

3.3.2 Evidence for change points in the atmospheric modes of variability

The change point analysis of the temperature and precipitation series, outlined above, suggests a large degree of variability both within, and between, the regions examined. Some of this variability may be explained by the underlying stochastic variability that is inherent in any climate series reflecting localised conditions. However, a large degree of coherence is also suggested by the change point analysis. This coherence within both the regional series would seem to indicate the influence of a large-scale control affecting the variability of both climate series.

In addition to the CUSUMS analysis, used in the previous section, the non-parametric Pettitt test (Pettitt, 1979) was also applied to the annual and seasonal NAO index values from 1900-2000 in order to determine if (i) any change points occur within the records (ii) these change points coincide with the change points determined in the temperature and precipitation series (Figure 3.3.1 - Figure 3.3.8) and (iii) change points are detected to establish the probability of a particular year being a change-point.

The Pettitt test considers a time series as two samples represented by $x_1 \ldots x_t$ and $x_{t+1} \ldots x_T$. For continuous data the indices V(t) and U(t) can be calculated from the following formula

$$U_{t,T} = U_{t-1,T} + V_{t,T}$$

for t = 2,…,T,

$$V_{t,T} = \sum_{j=1}^{T} \operatorname{sgn}(x_t - x_j)$$

sgn(x) = 1, for x > 0,
sgn(x) = 0, for x = 0,
sgn(x) = -1, for x < 0.

The most significant change point is found where the value $| U_{t,T} |$ is maximum. The approximate significance probability, p(t), of a change point can be calculated from

$$p(t) = 1 - \exp\left(\frac{-6U_{t,T}^2}{T^3 + T^2}\right)$$

(Pettitt, 1979; Kiely, 1999)

The CUSUMS and Pettitt analysis of the NAO, annual, winter and summer indices, from Figure 3.3.9-Figure 3.3.11, indicates a probable change point as having occurred during 1910 - 1920. This change point appears consistent across both the annual and seasonal NAO indices. Even though it appears as a lower probability change point for the annual and winter NAO series, change points during this period are also found in the temperature and precipitation series. Stations from both regions also indicate the occurrence of a change point in the summer temperature series during this period. The decline evident in the Alpine summer temperature series ceases, while the Scandinavian temperature series display a decreasing trend

during this period (Figure 3.3.4). Decreasing winter precipitation is evident at the Alpine stations after this period (Figure 3.3.7 (a), (b)).

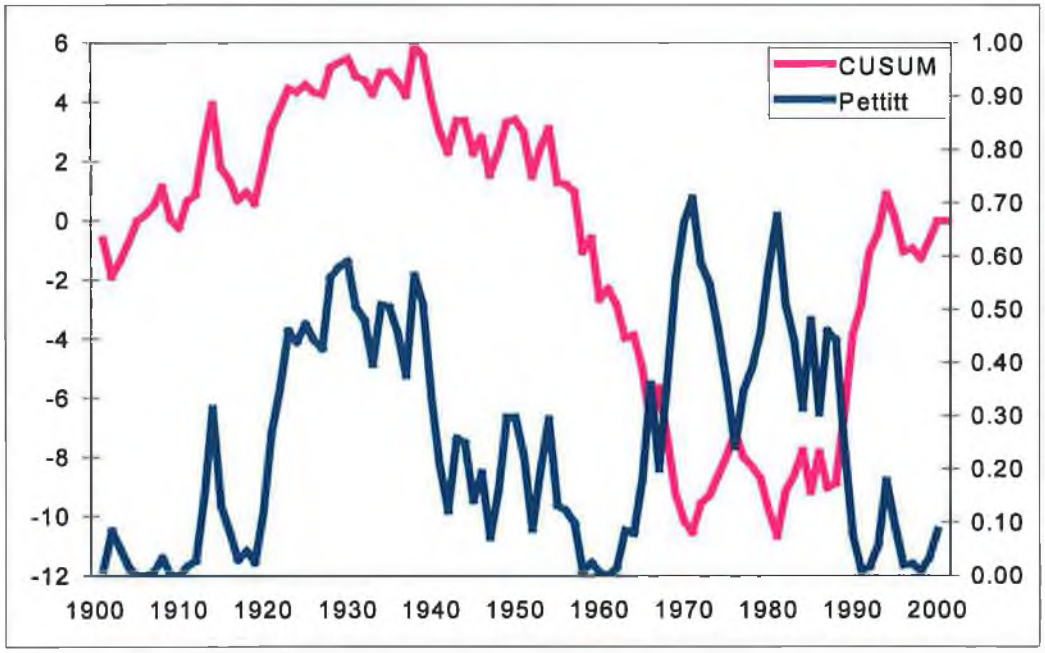

Figure 3.3.9 CUSUMS and Pettitt test of the annual NAO (Hurrell PC) 1900-2000.

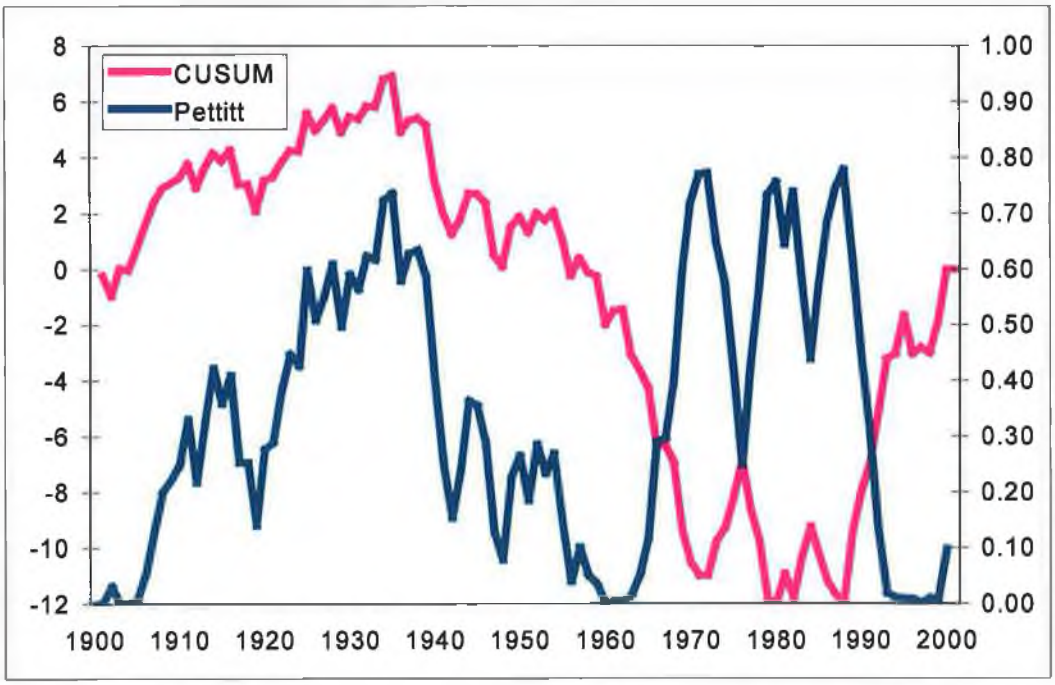

Figure 3.3.10 CUSUMS and Pettitt test of winter NAO (Hurrell PC) 1900-2000.

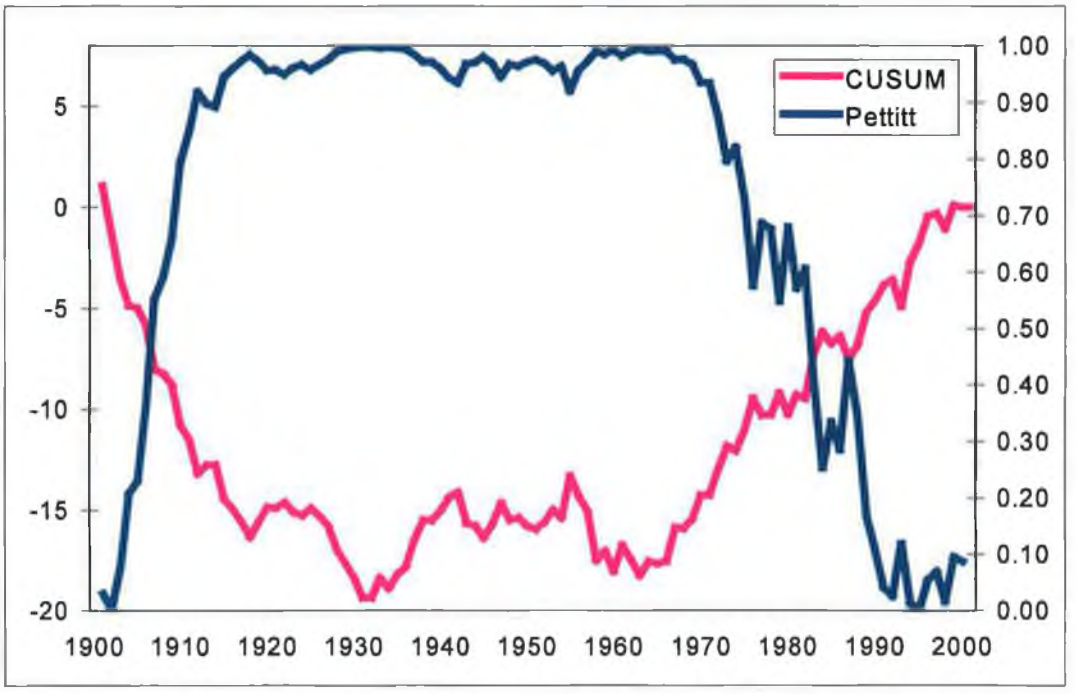

Figure 3.3.11 CUSUMS and Pettitt test of summer NAO (Hurrell PC) 1900-2000.

A higher probability change point occurs in the annual and winter NAO series during the 1920s – 1940s. Summer temperatures from both regions display an increasing trend until the late 1920s to early 1930s, while Alpine winter temperatures show evidence of a decline during this period. Scandinavian winter temperatures reach a maximum during the 1930s after which, a gradual decline commences and continues until the mid 1960s. Winter precipitation at the Alpine stations show marked declines up until the 1930-1940s.

The annual and winter NAO exhibit a largely decreasing trend from the 1930s – 1960s (Figure 3.3.12). The summer index, although less pronounced, also exhibits a decreasing trend over this period which coincides with mid-century cooling. This decrease in the NAO index is reflected in winter temperatures in the Scandinavian series and summer temperatures in the Alpine series. Winter precipitation from the Alpine series is also shown to increase during this negative phase of the NAO.

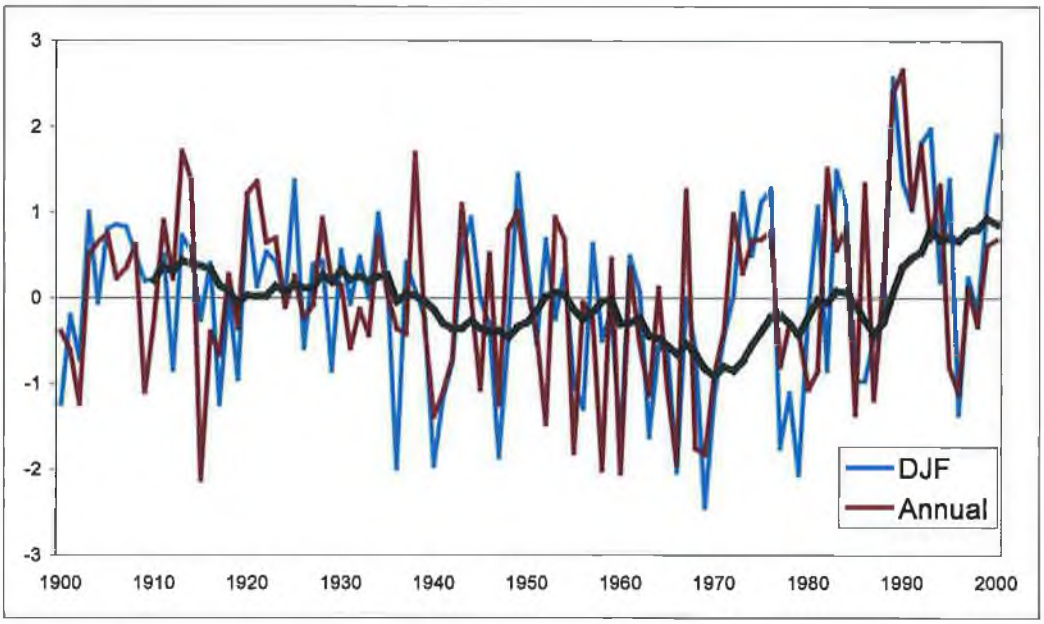

Figure 3.3.12 Annual and Winter NAO with an 11-year moving average highlighting the negative phase in the NAO between 1930-1960 and the gradual increase after 1970.

There are a number of significant change points in the annual and winter NAO index from the 1970s to 1990s. The 11-year moving average from Figure 3.3.12 illustrates that, while the overall-increasing trend is towards a more positive phase of the NAO from the 1970s onwards, this increasing trend is interspersed with a number of negative phase years. There are two probable change points in the annual index, 1971 and 1981 (Figure 3.3.9), while the winter index indicates three change points of near-equal probability, 1972, 1980 and 1988 (Figure 3.3.10).

These change points are consistent with the increases in winter temperature, outlined in the previous section, from the 1970s to 2000. The increases are very marked in both regions and are consistent across all stations. While the signal is not as consistent as that found with winter temperature, there is also evidence for co-variation between the NAO and winter precipitation during this period. Precipitation receipts from Genoa and Lugano, which are negatively correlated with the NAO, largely reflect this inverse relationship during the 1970-2000 period. While increases in precipitation at Sonnblick, coincide with the first change point in the early 1970s; increases in precipitation at Seantis coincide with the later change point around 1988. Change points in the Scandinavian winter precipitation

series at Bergen most closely correspond with the change points in the winter NAO.

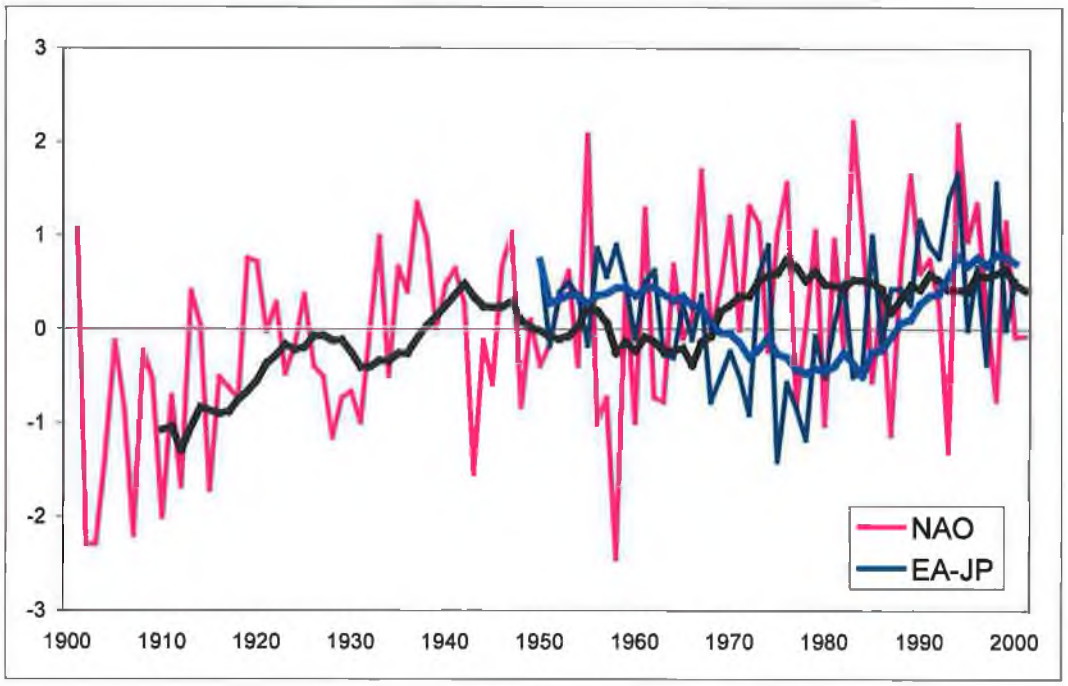

Figure 3.3.13 Summer (JJA) NAO (1900-2000) and EA-JP (1946-2000) indices. Thick lines show the 11-year moving average.

A CUSUMS and Pettitt analysis of the summer index indicates two change points in this series, the first around the 1930s and the second during the mid-1960s. Four Scandinavian stations indicate the period between 1929-1931 as being probable change points in the summer temperature series (Figure 3.3.4), while two Alpine stations suggest the period between 1926-1927 as being a probable change point.

3.4 Conclusions

The previous chapter established that leading modes of atmospheric circulation in the North Atlantic were related to the regional climate of Europe. Persistent high index phases producing an intensification of westerlies with consequent increases in the advection of warm and moist maritime air onto northern Europe act to suppress the penetration of moisture in southern Europe. This results in both seasonal and interannual differences in the receipt and amount of precipitation across Europe, particularly during the winter months. Similarly, seasonal and

interannual differences in temperature were also evident during persistent phases of the NAO.

These persistent phases were found to impact on the variability of the regional climate series examined. Significant positive trends in temperature for both winter and summer were found for all the Alpine stations over the period of measurement (1900-2000). Ona and Tromsoe were the only stations in Scandinavia to display significant positive trends in summer temperature. Significant positive trends were also found for winter and summer precipitation for a number of Scandinavian stations. Sonnblick was the only Alpine station to display a positive and significant trend in summer precipitation. Significant and decreasing trends in summer precipitation were found at Lugano and Saentis. There is a strong correspondence between winter temperatures and the NAO, particularly evident at Scandinavian stations since the mid 1970s. These findings are compatible with those of Bardossy and Caspary (1990) and Werner *et al.* (2000).

The identification of a second possible change point, which occurred during 1988/1989, was also highlighted. The scale and effect would suggest that it is at as significant as that detected in the early 1970s. Other authors also highlight this year as being significant; in the Arctic summer ice cover (Chapman and Walsh, 1993; Maslanik *et al.*, 1996); change in convection in the Labrador Sea (Rhines, 1994); statistically significant change in glacier regime (Dyurgerov, 2003) and a decline in cod recruitment in the Atlantic since the mid 1980s linked to rising temperatures (Beaugrand *et al.*, 2003). Also during this period, Mysak and Power (1991) found large positive sea ice anomalies occurring in the Greenland Sea, which had been preceded by above average runoff from North America into the western Arctic. They suggested that this sequence is part of a self-sustained climatic oscillation in the Arctic, occurring with a period of approximately 15-20 years, and hence is a component of interdecadal climate variability. However, observations linking atmospheric circulation and precipitation are scarce, so no significant conclusions can be made with regards to the proposed climate oscillation (Holland, 1995). Despite the lack of a significant conclusion, sea ice does appear to be an important component in interdecadal climate variability (Holland, 1995).

The regional climate is largely a response to the forcing provided by atmospheric circulation, which reflects an interaction between ocean-atmosphere-land over large areas and integrating over long time scales, from interannual to decadal. Having established that linkages existed between circulation and the regional climate, the present chapter sought to clarify these links in order to establish if the long-term variations in the mass balance of European glaciers could be explained in the context of variability in both the regional and large-scale atmospheric circulation. An examination of long-term variations in glacier mass balance in the context of these findings will form the central theme of the next chapter.

Chapter IV

An examination of regional mass balance in Europe from selected glaciers: the role of atmospheric variability and regional climate

4.1 Introduction

A number of previous studies have linked atmospheric modes of variability to European glacier mass balance (Pohjola and Rodgers, 1997a,1997b; Washington *et al.*, 2000; Nesje and Dahl, 2000b; Nesje *et al.*, 2000; Six *et al.*, 2001). These studies have predominantly focused on individual or regional glacier mass balances with the exception of Six *et al.* (2001) who compared Alpine and Scandinavian annual mass balance variations to the North Atlantic Oscillation. They found that the year to year coherence between these two variables was weak and that smoothing was required to filter noise from the relationship. Nesje and Dahl (2000b) and Nesje *et al.* (2000) in a study of Scandinavian glaciers found that the highest correlations were between winter balances, for the more maritime glaciers, and a seasonally averaged wintertime NAO. They also found that correlations decreased with increasing continentality and latitude. These results again reflect a limiting factor in the effectiveness of advection from westerlies as suggested by Chen and Hellström (1999). Similar findings were highlighted in preceding chapters.

In order to assess the influence of climate on European glacier mass balance, previous findings are related to mass balance components for a selection of glaciers. Initially, four glaciers were selected, from Scandinavia and the Alps, which fulfilled the criteria of having long-term mass balance measurements. The selected glaciers are also currently undergoing large changes in mass. Recent studies on glacier mass balance suggest that, globally, glaciers have been experiencing net losses since the 1970s, with an accelerating trend since the end of the 1980s (Dyurgerov, 2002), which is largely attributed to climate change. However, Scandinavian glaciers, predominantly those in maritime locations, have been experiencing net gains since the 1970s in direct contrast to that of the global

trends. This chapter will conclude with a more detailed examination of these glaciers.

Glacier name	Country	Lat	Long	Max (m)	Min (m)	Length (km)	Area (km^2)	Aspect (acc/abl)	Period
Sarennes	France	45°07'N	06°10'E	3190	2830	1.5	0.83	S/S	1949-99
Hintereisferner	Austria	46°48'N	10°46'E	3710	2426	7.13	8.72	E/NE	1953-99
Storbreen	Norway	61°34'N	08°08'E	1970	1380	3.0	5.35	NE/NE	1949-99
Storglaciaren	Sweden	67°54'N	18°34'E	1828	1125	3.7	3.24	E/E	1946-99

Table 4.1.1 Location, elevational range, length, area and aspect of glaciers.

The location of the four glaciers selected for the initial analysis are displayed in Figure 4.2.1. Their elevational range, length, area and aspect of accumulation and ablation zones are displayed in Table 4.1.1. With the exception of Hintereisfernier, in Austria, all records start before the 1950s. Storglaciaren in Sweden has the longest record with measurements commencing in 1946. As glaciers respond to slight variations in climate and therefore are considered to be sensitive indicators of climate (Nye, 1960; Oerlemans and Fortuin, 1992), the divergent response evident in the mass balance of these glaciers over recent years may, in fact, indicate a climate change signal.

4.2 Components of glacier mass balance

The mass balance components of a glacier are comprised of spatially averaged mass gains or losses measured over the glacier surface, during one glaciological year, which in the Northern Hemisphere is considered from 1st October to the 30th September. The glaciological year is then subdivided into two seasons, winter (1st October to 31st May) and summer (1st June to 30th September) (Dyurgerov, 2002). The measurement of snow (ice and firn) accumulated on the surface of the glacier at the end of the winter season, winter mass balance (bw), minus the ablation of snow and ice at the end of the summer season, summer mass balance (bs), is termed the annual or net balance (bn).

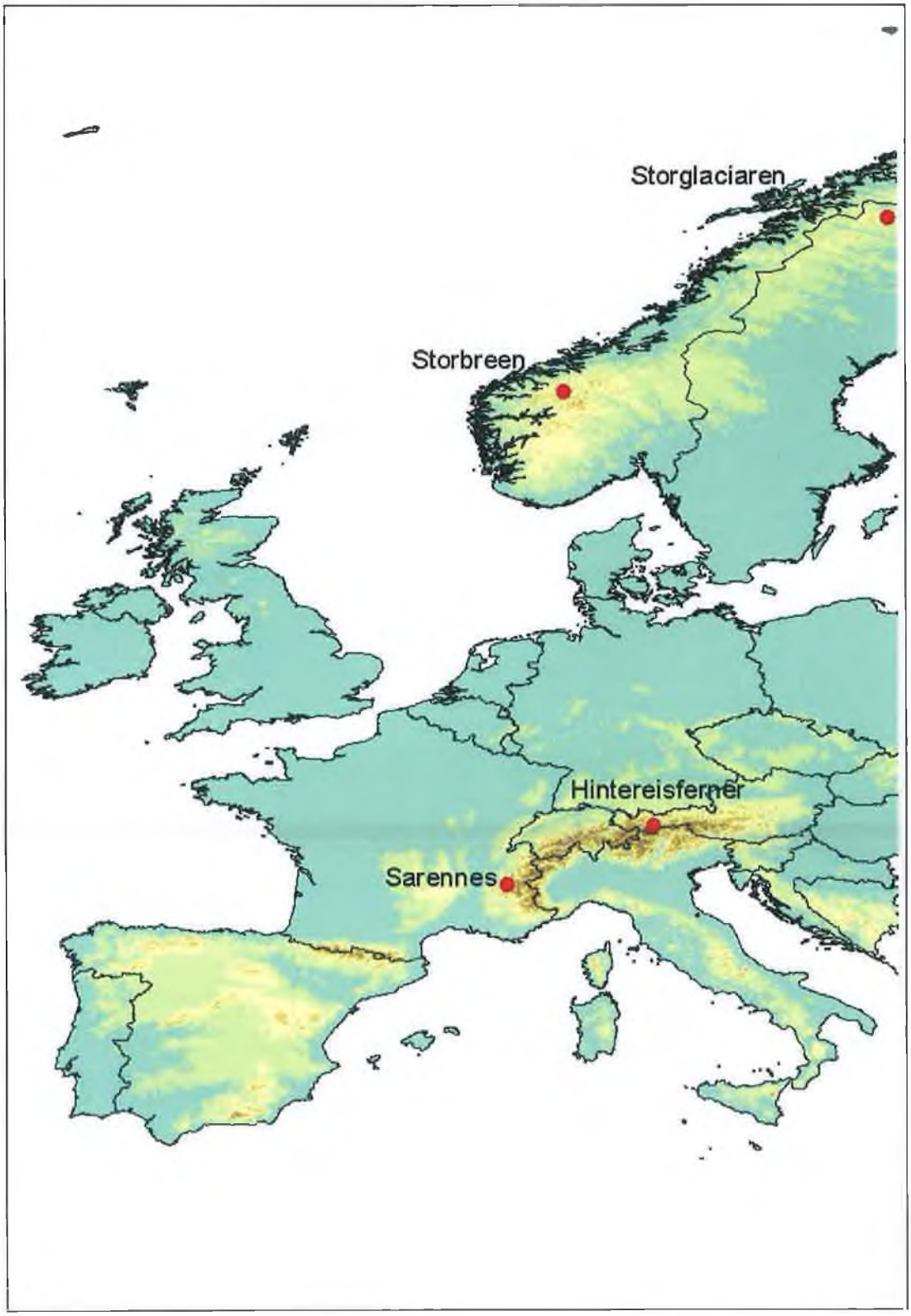

Figure 4.2.1 Location of the four long-term monitored glaciers

$$bn = bw - bs$$

(±) Net Balance = (+) Winter Balance – (-) Summer Balance

The net balance is largely an expression of the health of the glacier at the end of the glaciological year. A positive net balance indicates that summer ablation was less than the previous winters accumulation and results in an overall mass gain in volume to the glacier. When losses due to summer ablation are greater than the previous winters accumulation, a negative net balance results.

Positive net balances lead to an expansion of the accumulation zone and a lowering of the equilibrium-line altitude (ELA) (Benn and Evans, 1998), the altitude of a line that separates the accumulation zone from the ablation zone on a glacier. In terms of glacier-climate interactions, a change in the elevation of the ELA is a direct response of the glacier to climate conditions over the glaciological year. Figure 4.2.2 and Figure 4.2.3 display winter (bw), summer (bs) and annual net balance (bn) for Storbreen and Hinteresiferner over the period of measurement. It is clear that the annual balances of Hintereisferner have been quite negative since the mid-1970s.

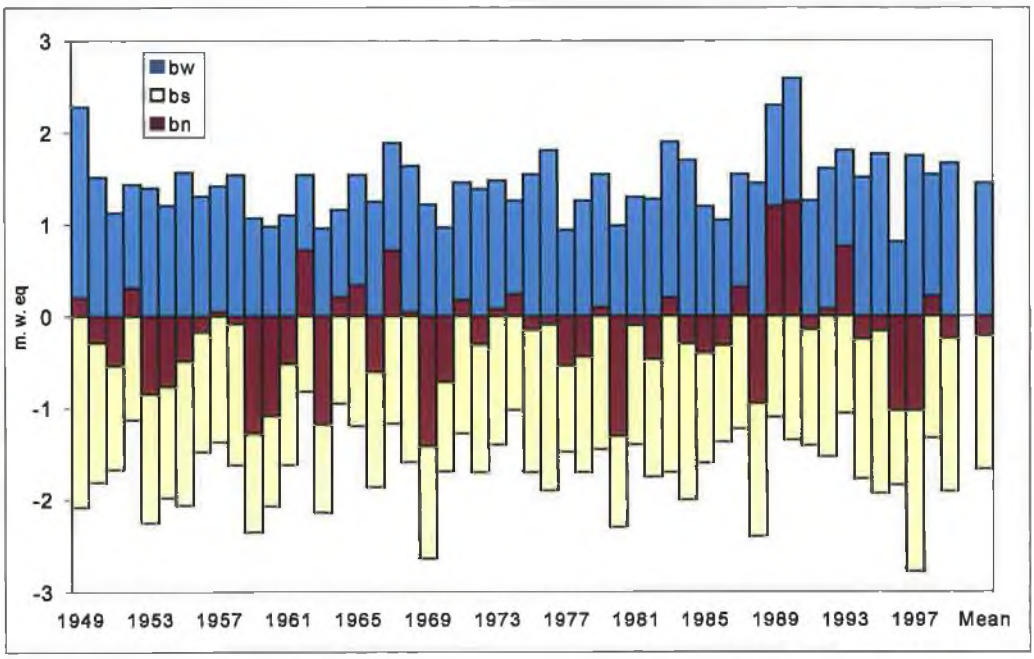

Figure 4.2.2 Winter, summer and annual net balance for Storbreen 1949-1999.

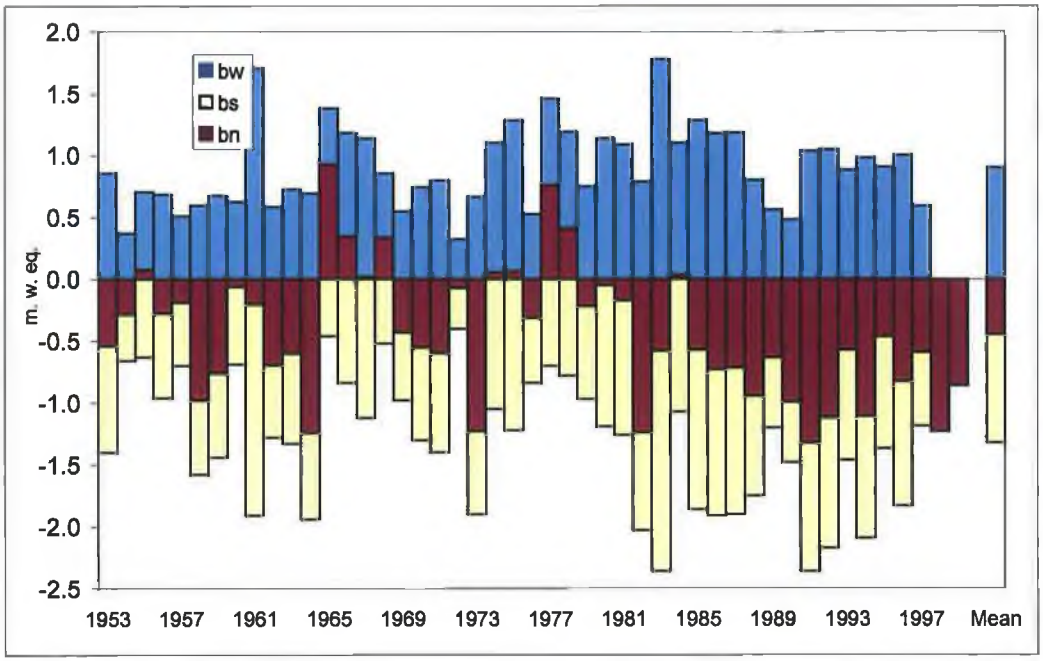

Figure 4.2.3 Winter, summer and annual net balance for Hintereisferner 1953-1999.

During years in which the net balance is negative, there is an expansion of the ablation zone and the ELA moves up the glacier reflecting the diminished area of the accumulation zone. Depending on the glaciers area/elevation distribution or hypsometry, a lowering or rising of the ELA can have a large impact on glacier mass. Glaciers with a large area at or near the ELA will demonstrate the largest changes in response to interannual climate variations (Benn and Evans, 1998).

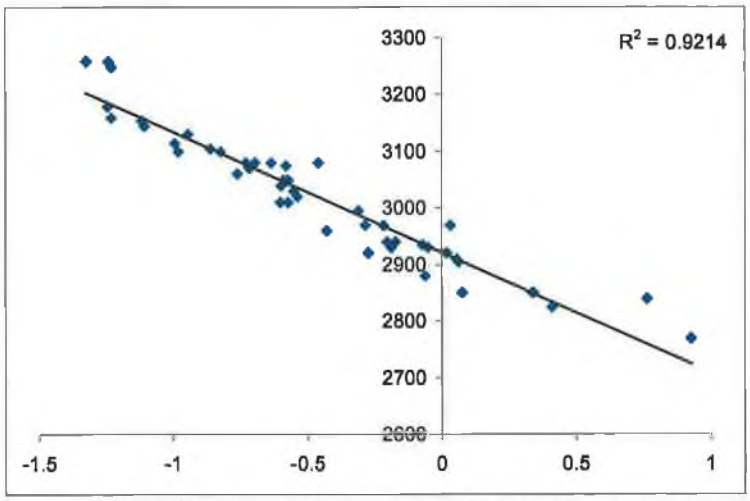

Figure 4.2.4 ELA versus net balance for Hintereisfernier 1953-1999

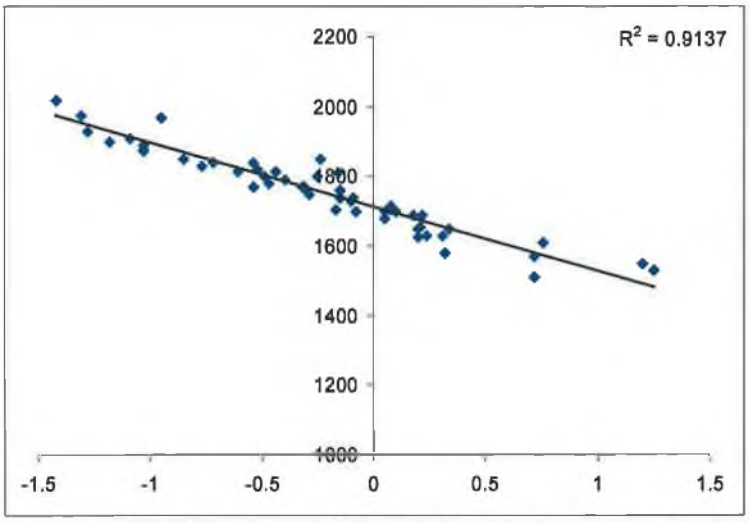

Figure 4.2.5 ELA versus net balance for Storbreen 1949-1999

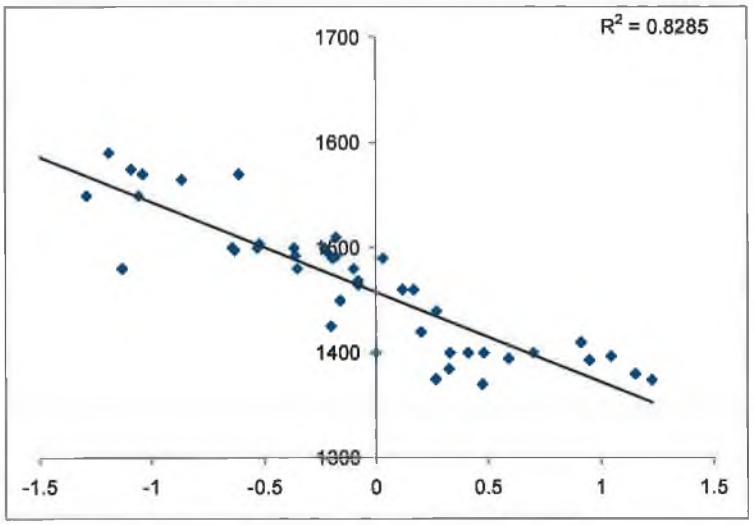

Figure 4.2.6 ELA versus net balance for Storglaciaren 1946-1999

The relationship between net balance and the ELAs for three of the four glaciers are shown in Figure 4.2.4, Figure 4.2.5 and Figure 4.2.6. The correlations between both these variables are very high for all three glaciers, with R^2 values of 92 %, 91% and 82 % respectively for Hintereisfernier, Storbreen and Storglaciaren. As the ELA is closely connected to precipitation and temperature (Benn and Evans, 1998) a number of studies have used these variables to reconstruct ELAs and annual net balances (Tangborn, 1980; Raper et al, 1996; Kerschner, 1997; Kuhn *et al.*, 1997). However, subsequent research has indicated the importance of additional climatic parameters, such as, albedo (Vincent and Vallon, 1997). ELAs have also been directly related to atmospheric circulation patterns (Lamont *et al.*, 1999; Hooker and Fitzharris, 1999).

The hypsometric curve or area elevation distributions of the selected glaciers are shown in Figure 4.2.7, Figure 4.2.8 and Figure 4.2.9. Hintereisferner, with an altitudinal range of ~1300 metres and located at high elevation, is currently in retreat and has decreased in area from 9.06 km^2 in 1961 to 8.72 km^2 in 1995. Storbreen has a smaller altitudinal range of 650 metres and is 5.35 km^2 which up until 1988 was retreating, when its front position was more than 1 km from its recorded position in 1900, after the climatic deterioration during the Little Ice Age. Its maximum elevation lies almost 350 metres lower than Hintereisferner's minimum elevation reflecting the difference in regional glaciation threshold levels, primarily due to latitudinal variations between these two locations. Storglacieran, with an altitudinal range of 550 metres, has increased in area from 3.0 km^2 to 3.24 km^2, in direct contrast to Hintereisferner.

No data were available to derive a hypsometric curve for Glacier de Sarennes. However, based on an analysis of documentary sources, Valla and Piedallu (1997) were able to quantify volumetric variations of the glacier. They estimated that the volume of the glacier in 1991 represented only 20% of that in 1850. The front position had retreated more than 1 km and the surface area had decreased from 1.6 to 0.5 km^2. They estimated if the current trend in the mass balance of Glacier de Sarennes continued, that the glacier would disappear within half a century.

The hypsometric curves of Hintereisferner and Storbreen suggest that these glaciers have a relatively large area between the minimum and maximum-recorded ELA elevations. This suggests that a change in the elevation of the ELA of either of these glaciers would result in large volume changes. The area of Hintereisferner, between the recorded upper and lower ELA elevations, is approximately 6.6 km^2, while for Storbreen, approximately 5.0 km^2 lies within this region suggesting that both these glaciers may be sensitive to any changes that might occur in climate. This is in contrast to Storglaciaren which has only a small percentage of its area, approximately 1.6-1.7 km^2, between its upper and lower ELA boundaries.

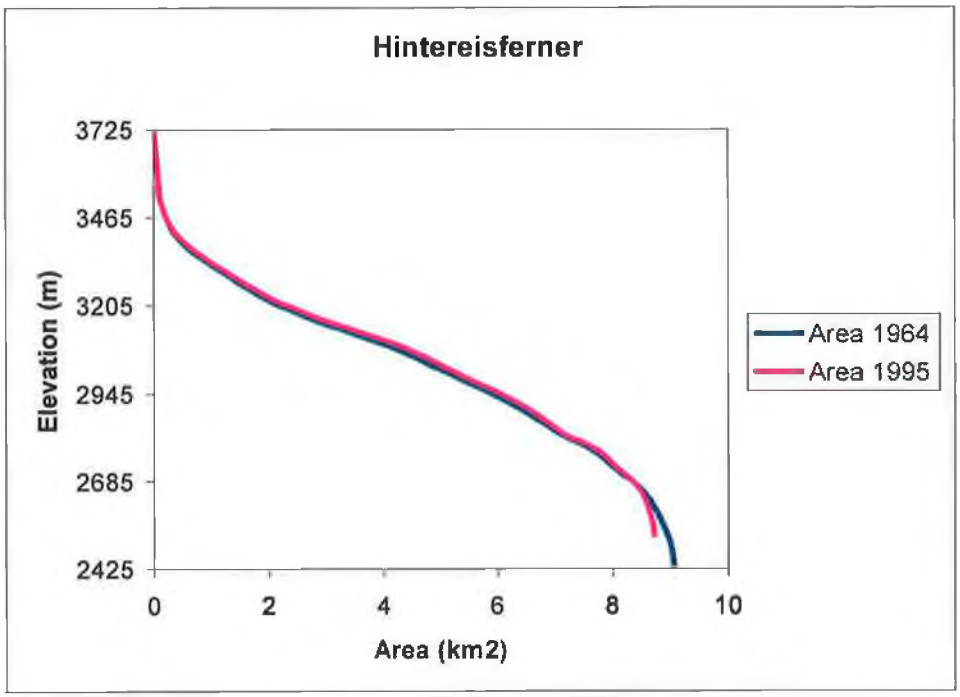

Figure 4.2.7 Area-elevation Distribution for Hintereisferner 1964 and 1995

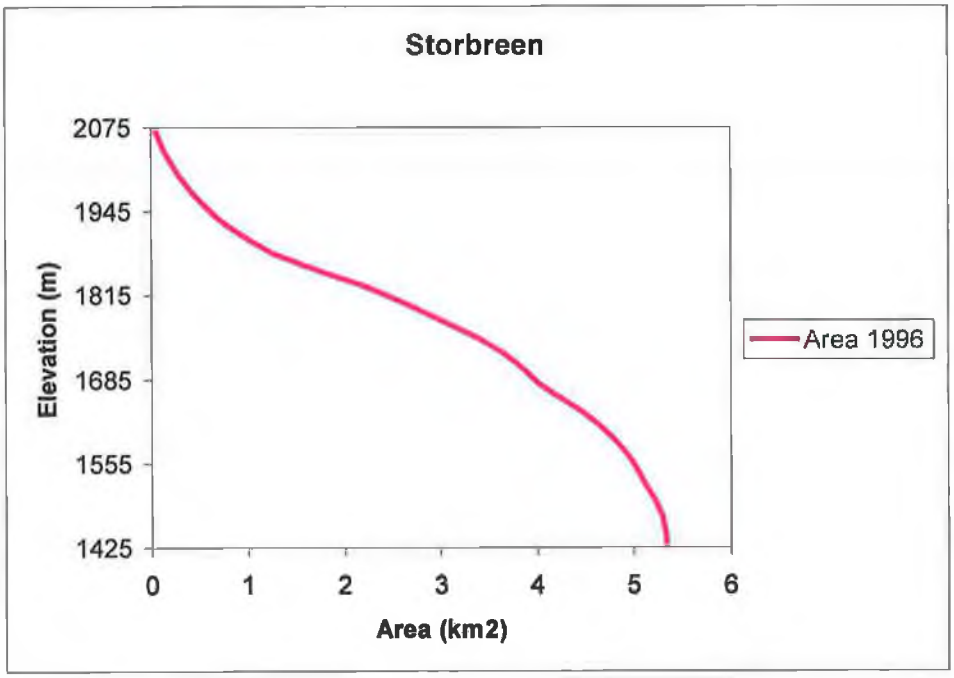

Figure 4.2.8 Area-elevation Distribution for Storbreen 1996

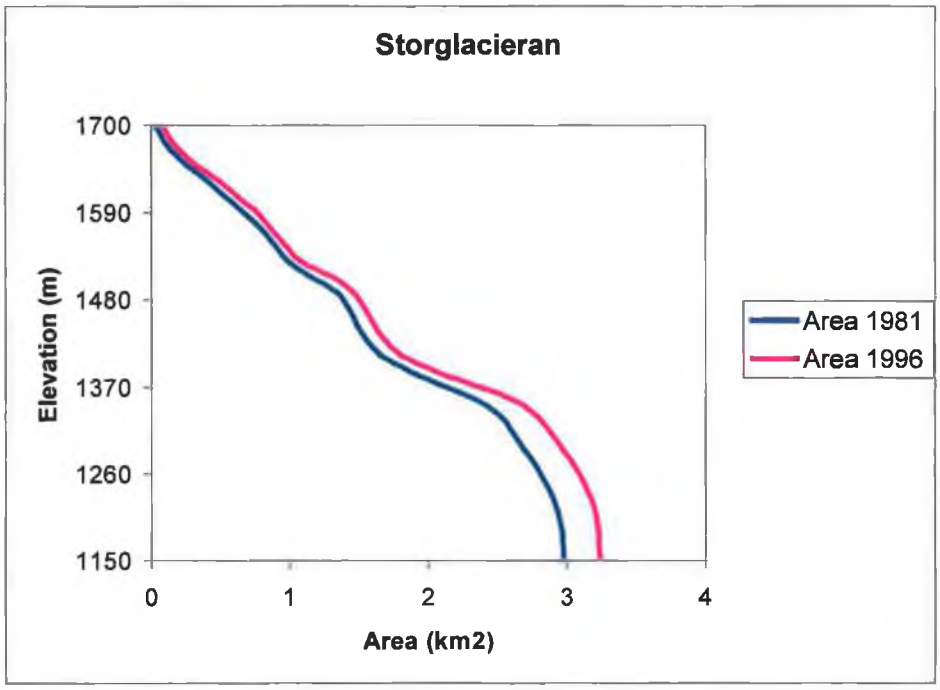

Figure 4.2.9 Area-elevation Distribution for Storglacieran 1981 and 1996

4.3 Climate-glacier interactions

4.3.1 Regional variation in mass balance trends

Winter accumulation and summer ablation rarely balance. Thus some years record mass gains while others, mass losses (Benn and Evans, 1998). If, when averaged over a number of years, the net gains balance the net losses, the glacier is said to be in a near constant state of equilibrium or steady state. If however, years of mass gains or losses occur consecutively, resulting in significant changes to mass, then the glacier will respond to these variations through an advance or retreat of its front position. While the ELA reflects year to year variations in climate, the cumulative net balance, derived by adding successive years net balances, reflects long term trends in glacier mass balance (Benn and Evans, 1998).

A comparison of the cumulative net balance curves between the Alpine and Scandinavian glaciers highlight the difference in the long-term mass balance trends between these regions (Figure 4.3.1). All glaciers show a marked synchronous decline in mass from the start of the records to the early 1970s. From the early

1970s to the late 1980s, Storglacieran's mass maintains an equilibrium, while Storbreen's decline continues until 1988. The cumulative net balance of the Alpine glaciers display evidence of increasing slightly during this period.

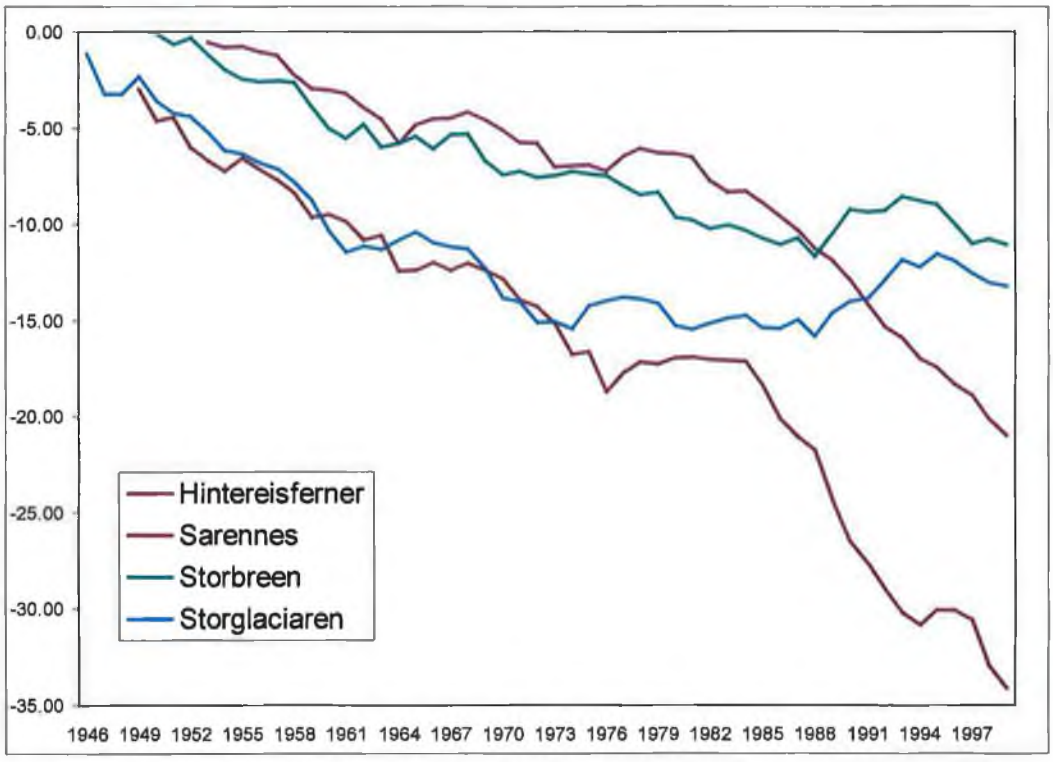

Figure 4.3.1 Cumulative Net Balance (m w.eq) of four European glaciers over their length of record.

Similar increases have been found for glaciers in the central Italian Alps during this period. Pelfini and Smiraglia (1997), in a study conducted on glacier fronts in the Lombard region, found an almost synchronous advance occurring at a number of glaciers from the early 1970s to the middle of the 1980s, after which glacier recession becomes dominant again. Pelfini and Smiraglia (1997) suggest that this advance phase could be linked to the 'mid-century cooling' or the 1955-1984 cold phase identified by them as deviations of mean summer temperatures falling below the long term mean during this period (Figure 4.3.2). The NAO Index is also shown for the summer season, which corresponds visually with the deviations of summer temperatures, recorded at the Alpine stations.

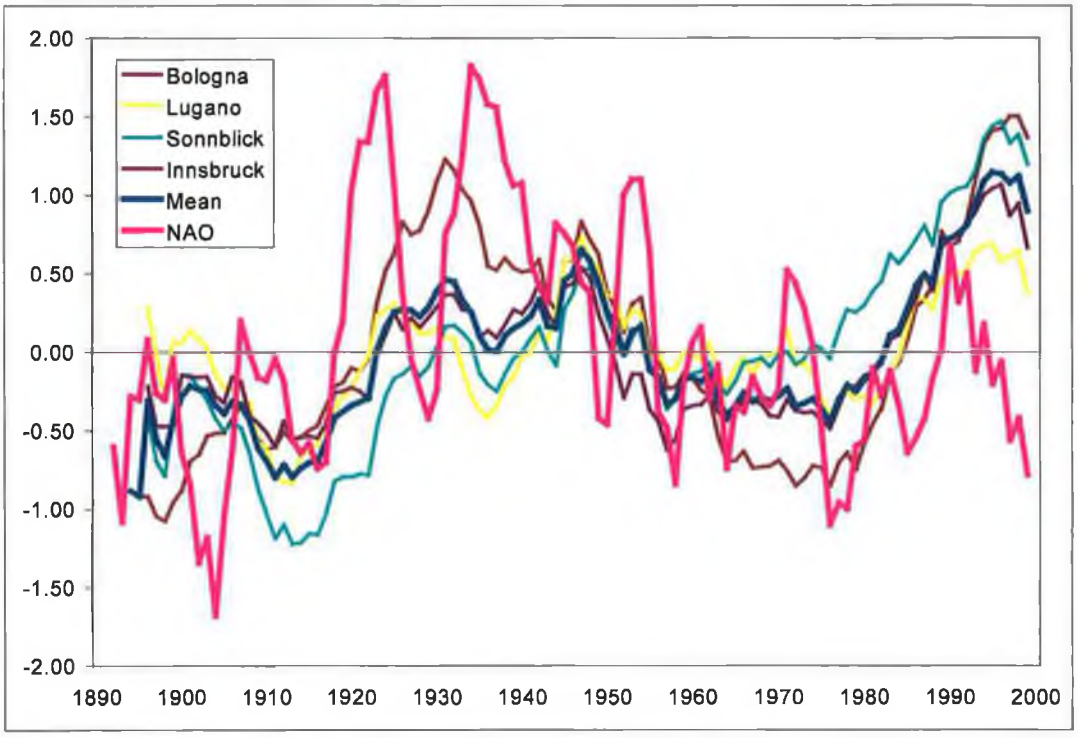

Figure 4.3.2 5-year averages of deviations of mean summer temperature from the long term mean (after Pelfini and Smiraglia, 1997), areal mean of deviations and NAO_{JJA}.

The cumulative net balance of Sarennes and Hintereisferner continues to decline after the mid-1980s to the end of the measurement period, while from 1988 onwards, the cumulative net balances of the Scandinavian glaciers have increased.

4.3.2 The relationship between long-term variations in mass balance and climate

Figure 4.3.3 illustrates the contrasting response evident in glacier mass balance between the Alps and Scandinavia to the large-scale atmospheric circulation. A positive NAO is positively correlated with the net balance of the Scandinavian glaciers, while it is negatively correlated with that of Alpine glaciers. There is however a marked seasonal bias in these relationships (Table 4.3.1). There are also occasions when this relationship weakens or breaks down, such as in the early part of the 1950s. Hoinkes (1968) found a similar inconsistency in his analysis of Alpine and Scandinavian glaciers during the ablation period. He found years in which a positive summer balance in the Alps occurred with both a high and low

index circulation. He suggested that the determining factor was due to the location of the zero deviation of the mean 500 hPa surface.

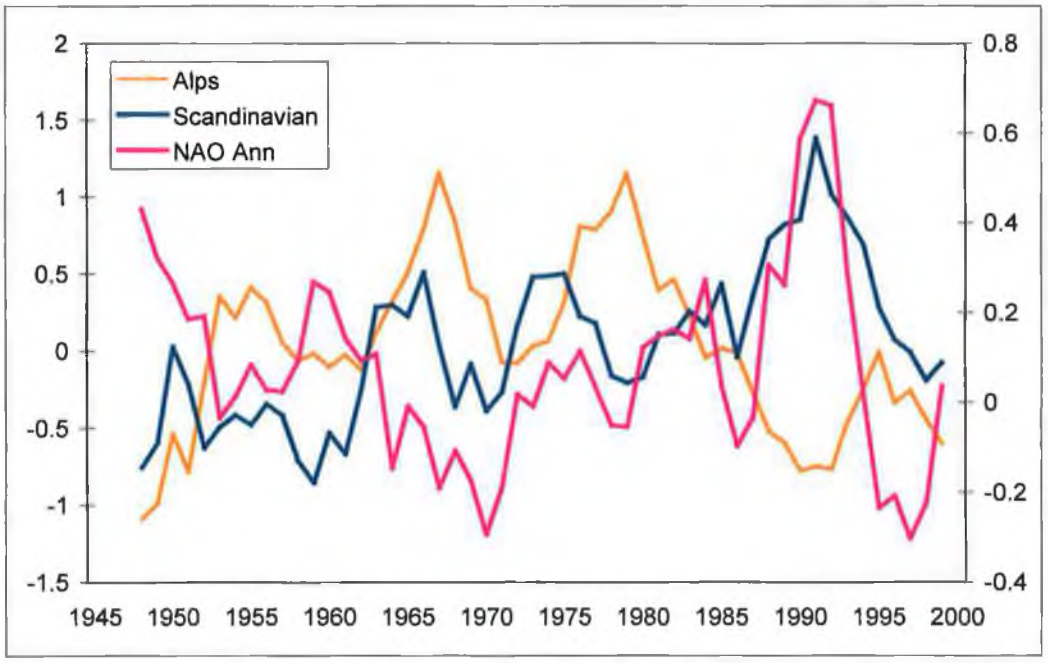

Figure 4.3.3 5-year centred moving average of the standardised mean net balance of eleven Alpine glaciers (Alps) and ten Scandinavian glaciers (Scandinavian) from 1948-2000. The annual NAO is also plotted (After Six *et al.*, 2001)

Previous findings have demonstrated that variations in the NAO were significantly related to the European temperature and precipitation series examined. These relationships were found to have a marked spatial component at the regional scale. An analysis of the long-term characteristics of both series indicated significant regional variations in these variables: variations which were found to be primarily a response to long-term fluctuations in the large-scale modes of atmospheric circulation.

Early century decreases evident in the Alpine summer temperatures series are in contrast to the Scandinavian series. The Scandinavian temperature series indicate an increasing trend around 1910, which is followed by slight decreases at a number of stations. After low temperatures recorded around the 1920s, after which overall increases are apparent until the late 1930s. After a local maximum recorded during the 1930s, temperatures decrease rapidly, particularly during the early 1940s. Significant increases in winter precipitation are evident at three of the

Scandinavian stations, while Bergen indicates a decline in precipitation over the 1920-1940s. Winter temperatures gradually increase until the mid 1930s, after which there is a rapid decline, with a slight recovery in the late 1940s, until the mid to late 1960s.

Glacier	DJF/Bw	JJA/Bs	DJF/Bn
Sarennes	-0.17	-0.46**	-0.47**
Hintereisferner	0.02	-0.45**	-0.28
Storbreen	0.65**	0.30*	0.55**
Storglaciaren	0.60**	-0.03	0.55**

** (*) Correlation is significant at the 0.01 (0.05) level (2-tailed).

Table 4.3.1 Relationship between the NAO (DJF) and EA-JP (JJA) and winter (Bw), summer (Bs) and net (Bn) mass balance from the four long term European glaciers.

The increasingly negative phase of the NAO during the 1940s – 1970s with consequent increases in winter precipitation, coupled with decreases in summer temperature during this period (Figure 4.3.2), should have produced more favourable conditions for positive glacier mass balances in southern Europe. However, the decreases in summer temperature would still have remained above the threshold required for melting. While in northern Europe from 1910-1970, southern Norway was experiencing decreasing winter precipitation (Hanssen-Bauer and Førland, 1998b) associated with a low index NAO. This decrease in winter precipitation was primarily due to a reduction in the moisture supply which would have been effectively cut off during these low index years. In spite of the decreasing trend apparent in winter temperature, particularly during the 1940s, net balances would have continued to decline (Figure 4.3.1).

Station	1900-2000 (°C)	Pre-1970 (°C)	Post-1970 (°C)
Bologna	3.9	3.5	4.5
Lugano	3.2	2.8	3.9
Sonnblick	-12.3	-12.7	-11.4
Innsbruck	-0.6	-1.3	0.7
Saentis	-8.0	-8.5	-6.9

Table 4.3.2 Mean of the Alpine winter temperature series 1900-2000 and values pre- and post-1970.

During the 1960s and 1970s, both the Alpine winter temperature and precipitation series display an increasing trend at a number of stations, which coupled with the summer decreases in temperature, would result in very favourable conditions for accumulation and contributed significantly to the 10 positive net balances being recorded on Hintereisferner between 1965-1984 (Figure 4.2.3). However, Innsbruck and Saentis prove to be the exception by demonstrating decreasing winter precipitation during the 1970s.

After the initial period of decline up to the 1970s, a divergent signal becomes apparent in the cumulative mass balance of the four glaciers. The timing of this change corresponds to similar findings from other studies (Bardossy and Caspary, 1990; Smith, 1995; McCabe and Fountain, 1995; Vincent and Vallon, 1997; Weber, 1997; Hoppe and Kiely, 1999; Kiely, 1999; Werner *et al.*, 2000; Brunetti *et al.* 2001).

Summer temperatures across all the Alpine stations start to recover after the mid to late 1970s and display a trend towards increasing temperatures (Table 4.3.2). While the mid 1980s marks a return to increasing winter temperatures, which had started to decline after a peak around 1975. Alpine winter precipitation also starts to display a decreasing trend during this period, Saentis again proving to be the exception. This period also marks a point after which, glacier net balances on Hintereisferner have been consistently and strongly negative.

The delayed response evident in the cumulative net balance between Storglaciaren, and Storbreen appears to be primarily due to regional differences in precipitation receipts. Winter precipitation at Tromsoe, illustrative of conditions at Storglaciaren, begins to increase after 1970, while a decreasing trend evident in precipitation at Bergen, near Storbreen, continues until the end of the 1980s, after which increases are evident. Precipitation alone appears to largely reflect the differences in cumulative net balance between both these glaciers.

The recent trend towards more positive cumulative net balances apparent in the Scandinavian glacier series can be explained by a number of factors. The

increasing trend evident in the Alpine summer temperature series over the closing three decades of the last century does not appear to occur to the same degree in the Scandinavian temperature series. Only two Scandinavian stations demonstrate a positive and significant trend in summer temperatures, as compared to all of the Alpine stations. A second contributory factor is winter precipitation, which has been increasing in Scandinavia since the 1960s (Hanssen-Bauer and Førland, 1998b), unlike Alpine winter precipitation which has been decreasing over the same period, with the exception of Saentis.

Little if any increase in summer ablation coupled with increased winter accumulation largely resulted in the recent positive net balances being recorded in northern Europe. While in southern Europe, increased summer ablation coupled with decreased winter accumulation produced an increased tendency for more negative net balances, evident in recent decades.

4.4 Conclusion

In spite of the relatively small contribution of glaciers to the total terrestrial storage of ice, their sensitivity to changes in climate means that they are important contributors to decadal and longer timescale variations in sea level (Oerlemans and Fortuin, 1992). The current worldwide reduction apparent in the volume of glaciers is estimated to have already made a significant contribution to global sea level rise over the last 100 years. The rate of volume loss appears to have increased since the end of the 1980s and predictions of global warming suggest that these trends are likely to continue (Dyurgerov, 2003).

Dyurgerov (2003), in an analysis of the sensitivity of mountain and subpolar glaciers to climate warming, estimated that between 1961-1976, the glacier melt contribution to sea level rise was 0.15 mm/yr or 10% of total sea level rise. However, this contribution increased to 0.41 mm/yr or 27% of total sea level rise between 1988-1998 suggesting that glacier sensitivity to climate warming may be increasing.

Synchronicity in the timing of changes in the atmospheric modes of circulation, regional climate and glacier mass balance were examined in the present chapter to establish if fluctuations in mass balance could be explained by variations in the regional climate and hence large-scale circulation. In findings similar to Dyurgerov (2003), the rate of decrease of the cumulative net balance of the Alpine glaciers was found to have increased since the 1980s. In contrast, the rate of decline of the cumulative net balances of the Scandinavian glaciers evident prior to 1988 has ceased. Since this time, they have displayed evidence of positive cumulative net balances, primarily due to positive mass balances being recorded during the late 1990s. The regional climate response to the atmospheric circulation plays a crucial role in explaining these differences between southern and northern Europe.

Subsequent chapters will seek to build on the findings to date which have established linkages between both regional and temporal variations in climate and glacier mass balance. These regional differences in mass balance in Scandinavia and in particular, Norway will also be examined in greater detail. A more comprehensive assessment of these glaciers is warranted on the basis that they are currently responding to climate in a manner that is considered inconsistent with current global glacier trends.

Chapter V

Regional climate indices and Scandinavian glacier mass balance

5.1 Introduction

Previous chapters have demonstrated that linkages exist between large-scale atmospheric variability in the North Atlantic, regional climate and European glacier mass balance via two key climatic parameters, temperature and precipitation. This relationship was found to be most pronounced with Scandinavian glaciers. As a consequence of the largely positive phase of the NAO since the 1970s, a number of Scandinavian glaciers, particularly the maritime glaciers, have demonstrated a tendency towards positive net balances over the last thirty years. These increases are being manifested in volume increases and advancing front positions, in contrast to the current mass glacier recession evident in nearly all glaciated regions outside of Scandinavia.

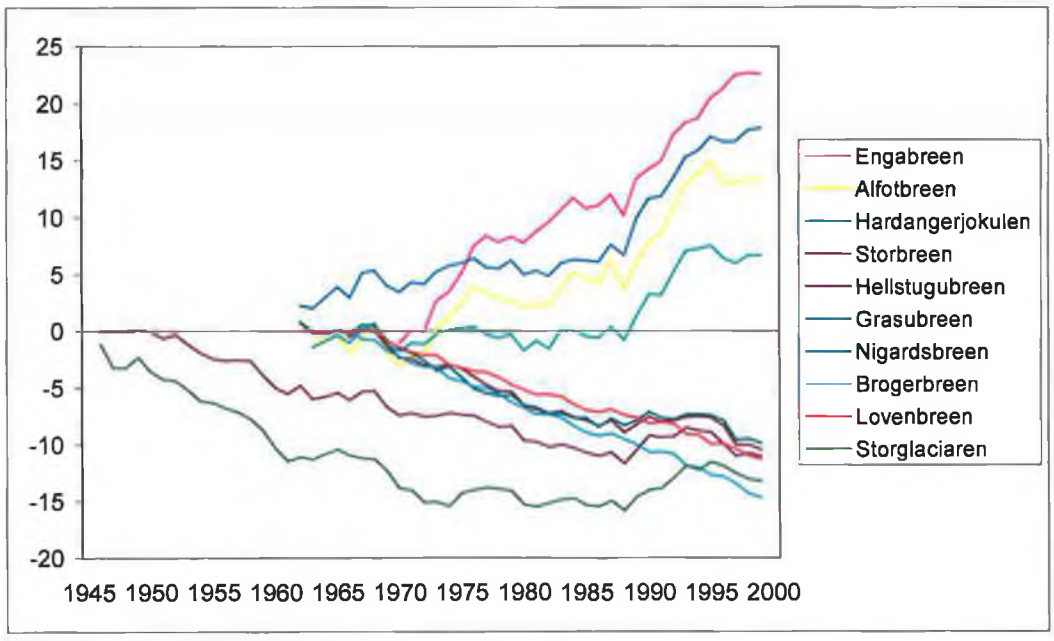

Figure 5.1.1 Cumulative net balance of selected Norwegian glaciers (including Storglaciaren). (Data from The Norwegian Water Resources and Energy Directorate).

In light of these increases, the remainder of this research will focus on examining the relationship between atmospheric variability and Scandinavian mass balance in

order to further our understanding of the links, as suggested by Meier (1965) between climate, the general meteorological environment and glacier behaviour.

5.2 Regional climate and mass balance

5.2.1 Circulation Indices

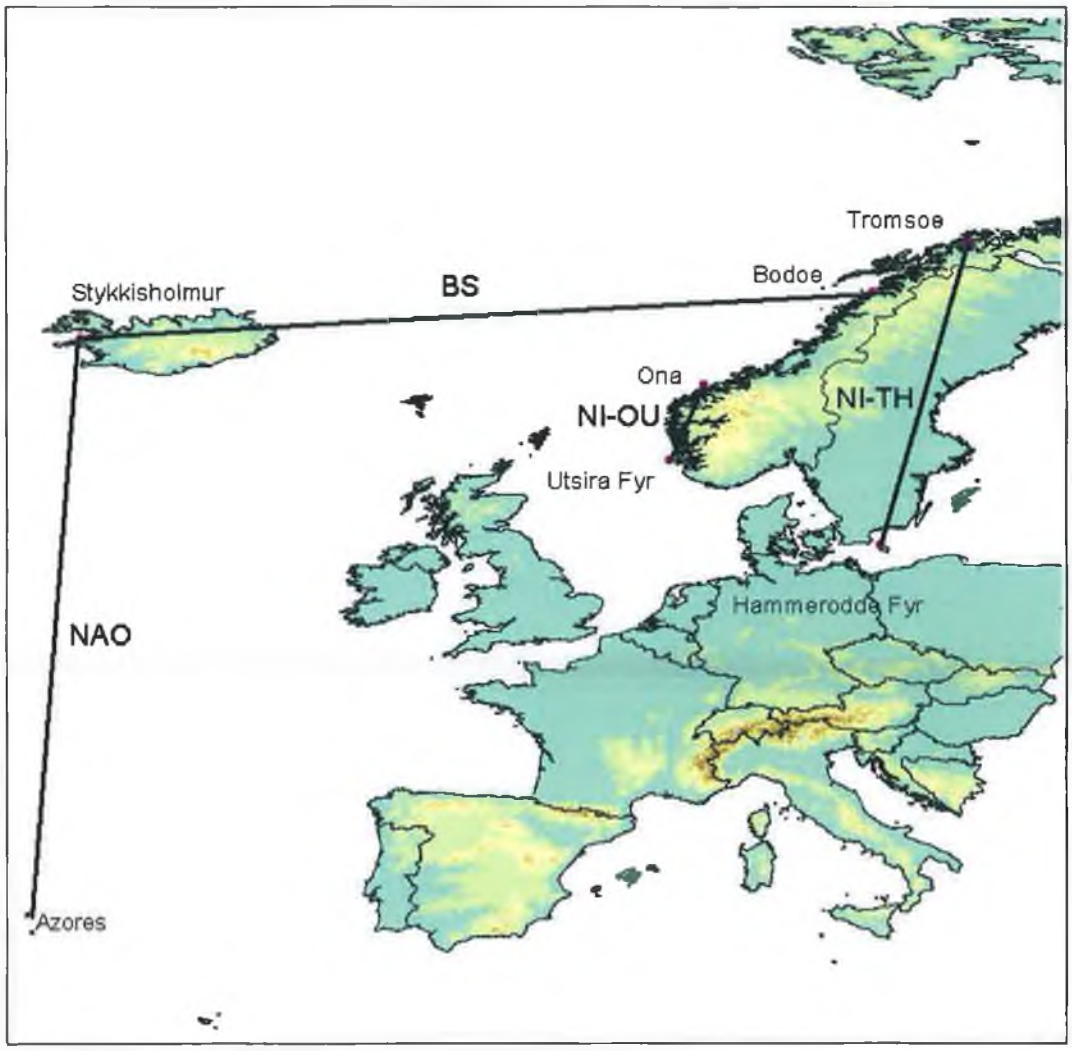

Figure 5.2.1 Location of Indices and glaciers

Figure 5.1.1 shows the cumulative net balance curves for selected Scandinavian glaciers, including Brogerbreen and Lovenbreen on Svalbard and Storglaciaren in Sweden. Positive cumulative net balances are associated with the more maritime glaciers of Ålfotbreen, Hardangerjøkulen, Engabreen and Nigardsbreen, while the more continental glaciers of Storbreen, Hellstugubreen, Gråsubreen and

Storglaciaren all indicate decreasing cumulative net balances. The two glaciers from Svalbard also show decreasing cumulative net balances. However, after 1988, the rate of increase of mass balance on the maritime glaciers is shown to significantly increase, while the decreasing trend evident on the more continental glaciers ceases and becomes positive. Cumulative net balances of the glaciers on Svalbard have continued to decline over the same period. To examine these differences, the next sections will assess mass balance in the context of both zonal and meridional air flows over Scandinavia. These have contrasting seasonal effects on the regional climate due to ocean and land responses to received solar radiation and relative location of a body of water.

5.2.1.1 Zonal air flow

When the seasonally averaged winter NAO index (December-March) is related to net and winter glacier mass balance (Table 5.2.1) the strength of the correlations is shown to decrease with increasing distance from the coast and increasing continentality (Figure 5.2.2). The seasonally averaged summer NAO index (June-August) displays only one significant correlation when related to summer mass balance, from Gråsubreen. This is not unexpected considering that, while present, the NAO is greatly diminished during the summer months. The EA-JP, which is the dominant summer mode of atmospheric circulation, proved to be more influential when related to summer mass balance. However, while correlations between the EA-JP and summer mass balance are significant, they remain quite weak. In contrast to southern Europe, a positive EA-JP would act to suppress summer ablation by suppressing temperatures, particularly during the month of June.

Table 5.2.1 also displays correlations between winter balance (bn), summer balance (bs) and net balance (bn). The high correlations between winter balance and net balance for the maritime glaciers indicates the importance of winter accumulation and hence winter precipitation on the net balance of the maritime glaciers; while the net balance of the more continental regime glaciers tends to be dominated more by the summer balance reflecting the importance of summer

temperatures. The lack of any significant relationship between the NAO and the glaciers on Svalbard is not unexpected based on the results from previous sections indicating a latitudinal boundary to the influence of the NAO.

Glacier	Bw/NAO	Bn/NAO	Bs/EA-JP	Bw/Bn	Bs/Bn
1 Ålfotbreen	0.78**	0.71**		0.86	0.08
2 Nigardsbreen	0.71**	0.60**	0.45**	0.77	-0.07
3 Hardangerjøkulen	0.74**	0.70**	0.37*	0.85	0.70
4 Storbreen	0.62**	0.51**	0.30*	0.71	0.81
5 Hellstugubreen	0.65**	0.47**	0.46**	0.35	0.10
6 Gråsubreen	0.61**	0.34*	0.45**+	0.53	0.24
7 Engabreen	0.34	0.47**		0.75	0.69
8 Storglaciaren++	0.47**	0.39*		0.74	0.83
9 Md. Lovenbreen	0.06	-0.03		0.39	0.83
10 Au. Brogerbreen	-0.13	-0.03		0.38	0.86

** (*) Correlation is significant at the 0.01 (0.05) level (2-tailed).

Table 5.2.1 Glacier Mass Balance for a selected number of Scandinavian glaciers and the NAO (seasonal average between Dec-Mar) and the East Atlantic Jet Pattern (++Storglaciaren included due to record length; +Gråsubreen was the only glacier in which the summer balance was significantly correlated with the NAO averaged over June-August). The ratio of winter balance to net balance (bw/bn) and summer balance to net balance (bs/bn) are also included.

As mass wastage of the maritime glaciers during the summer ablation season is largely compensated for by winter accumulation (Figure 5.2.3), these glaciers tend to be characterised by large variability in both their winter and summer mass balances. The maritime glaciers also survive at much lower altitudes in comparison to the continental regime glaciers. The continental glaciers display much lower rates of ablation during the summer than that of their maritime counterparts, however their potential for accumulation during the winter is also much reduced due to their location relative to a moisture source. Figure 5.2.3 illustrates the importance of winter precipitation as a controlling influence on the maritime glaciers, while summer temperature tends to be the dominant control on the continental regime glaciers.

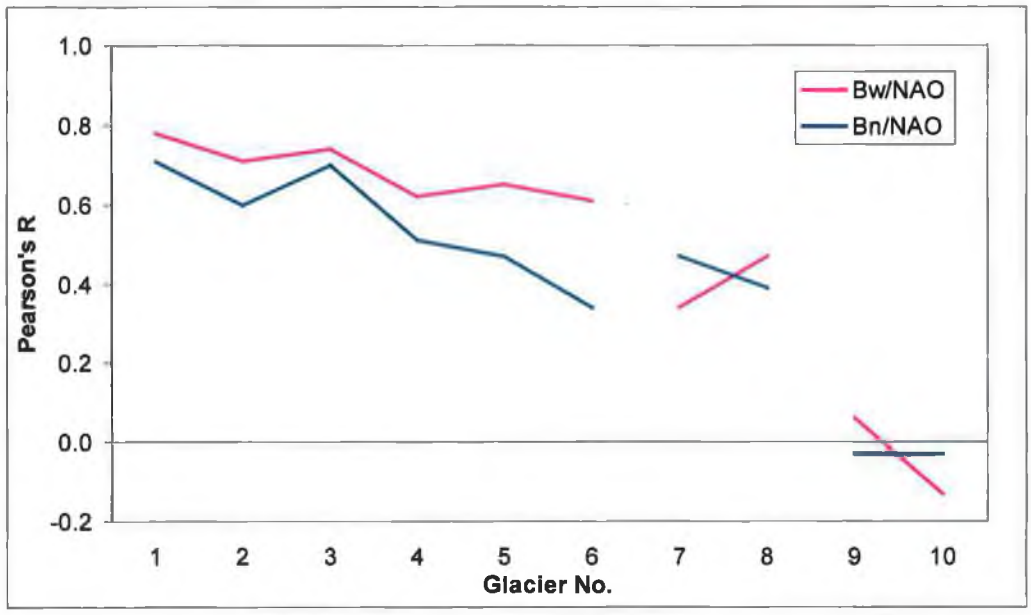

Figure 5.2.2 Correlation between glacier mass balance and the NAO indicating a decreasing relationship with increasing continentality of glacier location (1-6 Southern Norway; 7-8 Northern Scandinavia; 9-10 Svalbard).

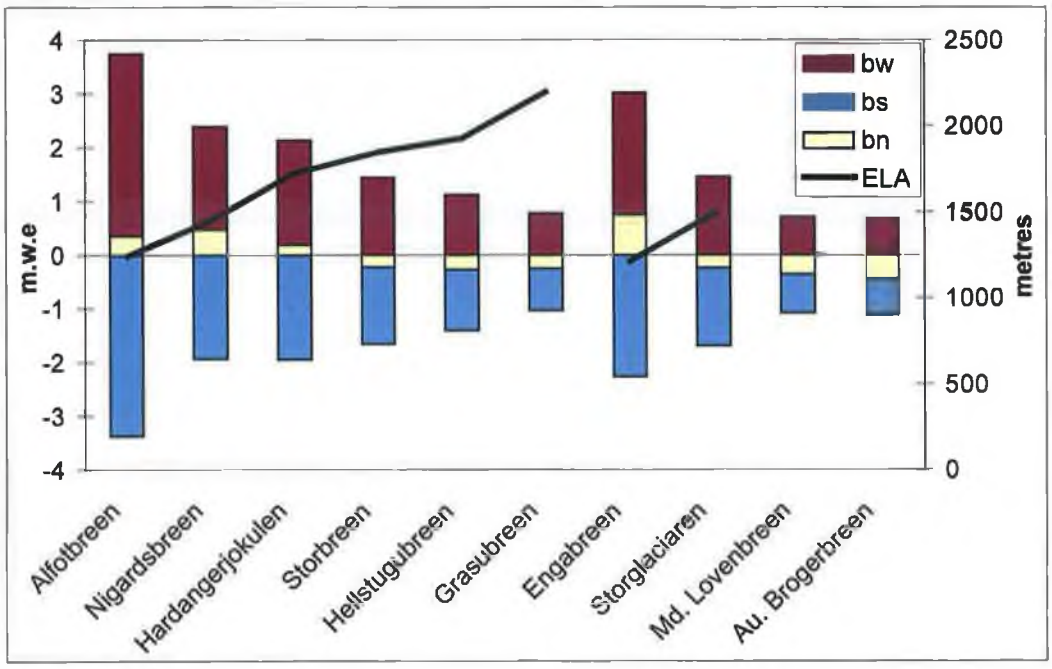

Figure 5.2.3 Mean winter, summer and net balance of the Norwegian glaciers (1968-1999). ELA of the glaciers is displayed on the right hand axis.

The NAO, which moderates the advection of warm, moist air onto the Scandinavian landmass, plays an important role in the winter and annual net balance of Norwegian glaciers, particularly the maritime glaciers. During the summer months, when the NAO is greatly diminished and in some cases absent,

which results in a reduction in westerly airflow, it is likely that the advection of continental air off the European landmass is an important feature in terms of glacier mass balance.

5.2.1.2 Meridional air flow

To assess the potential impact of meridional flow on glacier mass balance during the summer months, a circulation index between Bodo and Stykkisholmur (Iceland) was derived; calculations were based on the standardised pressure difference between stations from both these locations. The Bodo-Stykkisholmur index, or BS index, was derived in the same way as the NAO index between Iceland and Gibraltar, except that the BS index measures the strength of meridional (north-south) flows as oppose to zonal (west-east) air flows. The index was also derived for the winter period from December to March. The relationship between the BS index and net balance and summer balance are displayed in Table 5.2.2. The effects of the BS index on summer balance are weak, but it is more significant and its effects are more widespread than the EA-JP (Table 5.2.1).

	Glacier	**BS_{DJFM}/bw**	**BS_{JJA}/bs**
1	Ålfotbreen	-0.16	-0.46**
2	Nigardsbreen	-0.28	-0.36*
3	Hardangerjøkulen	-0.25	-0.43**
4	Storbreen	-0.24	-0.46**
5	Hellstugubreen	-0.35*	-0.47**
6	Gråsubreen	-0.32	-0.64**
7	Engabreen	0.01	-0.01
8	Storglaciaren	-0.03	-0.34*
9	MD. Lovenbreen	0.55**	0.19
10	Au. Brogerbreen	0.57**	0.11

** (*) Correlation is significant at the 0.01 (0.05) level (2-tailed).

Table 5.2.2 Bodo- Stykkisholmur (Meridional) Index (normal 1890-1999)

	Glacier	NI_{DJFM}/bw	NI_{JJA}/bs	NI_{DJFM}/bn
1	Ålfotbreen	0.69**	0.13	0.67**
2	Nigardsbreen	0.58**	0.39*	0.50**
3	Hardangerjøkulen	0.66**	0.37*	0.62**
4	Storbreen	0.57**	0.35*	0.41*
5	Hellstugubreen	0.36*	0.31	0.27
6	Gråsubreen	0.15	0.03	0.01
7	Engabreen	0.68**	0.42*	0.68**
8	Storglaciaren	0.74**	0.38*	0.55**

** (*) Correlation is significant at the 0.01 (0.05) level (2-tailed).

Table 5.2.3 Norwegian Index between Tromsoe and Hammerodde Fyr

The BS index for the winter months demonstrates significant, but weak correlations with both glaciers from Svalbard, namely Austre Brogerbreen and Midtre Lovenbreen. These relationships are likely to be reflecting the influence of moister air, associated with meridional airflows, as a consequence of the passage of air over the Norwegian Sea, between the Norwegian mainland and the island of Svalbard, collecting moisture on route.

5.2.1.3 Localised atmospheric circulation index

Tveito (1996), in a study on trends and variability in European pressure data, related the pressure gradient between Utsira and Ona to precipitation from Samnanger, a station located in southern Norway. He found that while variability existed within the month to month correlations, which ranged from 0.93 in March to 0.68 in August, the annual correlation was high, (r = 0.85). Based on these findings, it is likely that glacier mass balance and in particular, winter balance, should be sensitive to a more regionalised index of atmospheric variability. To investigate this, a refined index of atmospheric variability was derived, initially between Tromsoe and Hammerodde-Fyr, but also between Ona and Utsira-Fyr (Figure 5.2.1).

The correlations between the Norwegian Index, between Tromsoe and Hammerodde-Fyr, and glacier mass balance do not represent an improvement on previous indices (Table 5.2.3), suggesting that the NAO and EA-JP adequately capture variability at this scale (Table 5.2.1). However, both the central Scandinavian glaciers of Engabreen and Storglaciaren indicate a substantial improvement in Pearson's r when related to this zonal Norwegian Index, in winter, summer and net balance (Table 5.2.3), which may partly reflect a latitudinal constraint of the NAO.

Deriving a similar regionalised pressure gradient index for southern Norway, between Ona and Utsira Fyr, appears to improve upon the relationships established with the NAO and mass balance (Table 5.2.1), particularly winter balance (Table 5.2.4). The likely reason for this is the high degree of association between this index and precipitation, as reported by Tveito (1996), outlined above.

All of the indices appear to capture a large degree of variability in both the winter and annual net balances, particularly those of the maritime glaciers. The tendency towards a more positive index since the 1970s is positively associated with the increasing cumulative net balances being recorded on the maritime glaciers in Norway. This tendency produces an increase in the rate of advection of moist, maritime air during the winter months resulting in a surplus in accumulation for these glaciers. The positive correlation between Storglaciaren and zonal airflow has also resulted in a positive response being recorded in its cumulative net balance since the 1970s. The lagged response to the increase in zonal airflow evident in the cumulative net balances of Storbreen, Hellstugubreen and Gråsubreen is likely to be a function of their more continental location and hence, distance from a moisture source. The importance of wind direction, as represented by the pressure gradient, and a water body as a source of moisture to glacier mass balance is evident in the correlation between meridional airflow during the winter months and winter balance on Svalbard. The relative surface temperature of the ocean would enable moisture uptake to be feasible despite the fact that meridional air flowing off the continent during the winter months is likely to be cold. A possible

indication of this can be seen in the positive correlation between winter balance and meridional airflow on both Austre Brogerbreen and Midtre Lovenbreen.

	Glacier	NI_{DJFM}/bw	NI_{JJA}/bs	NI_{DJFM}/bn
1	Ålfotbreen	0.84**	0.43**	0.78**
2	Nigardsbreen	0.74**	0.48**	0.69**
3	Hardangerjøkulen	0.80**	0.51**	0.75**
4	Storbreen	0.72**	0.35*	0.58**
5	Hellstugubreen	0.55**	0.37*	0.40*
6	Gråsubreen	0.35*	0.16	0.17
7	Storglaciaren	0.76**	0.26	0.61**

** (*) Correlation is significant at the 0.01 (0.05) level (2-tailed).

Table 5.2.4 Norwegian Index between Ona and Utsira Fyr

The role of atmospheric variability on summer balance would appear to be less influential than on winter and net balance. Meridional airflow is suggested as having a control on summer balance, particularly on the continental regime glaciers. During the summer months, warm, dry air flowing off the continent would result in increased ablation. Gråsubreen appears to be most sensitive to the influence of a positive meridional pressure gradient, with just over 40% (r = -0.64, sig. 0.01) of variability in summer balance being accounted for by the meridional index alone (Table 5.2.2).

Over 52% (r = 0.746) of the variability on Hardangerjøkulen can be explained when both the Bodo-Stykkisholmur index and reduced Norwegian Index, between Ona and Utsira-Fyr, are regressed on the summer balance. This is a positive outcome as no significant correlation was found with the NAO, while the EA-JP only accounted for 13% (0.37, sig. 0.05) of the summer balance. When these indices were regressed on summer balances from the other Scandinavian glaciers, results ranged from 38% (r = 0.647) for Ålfotbreen to 43% (r = 0.676) for Storbreen. The Norwegian Index between Tromsoe and Hammerodde-Fyr was used in conjunction with the Bodo-Stykkisholmur index for Storglaciaren which

resulted in just over 30% (r = 0.578) of variability in summer balance being accounted for.

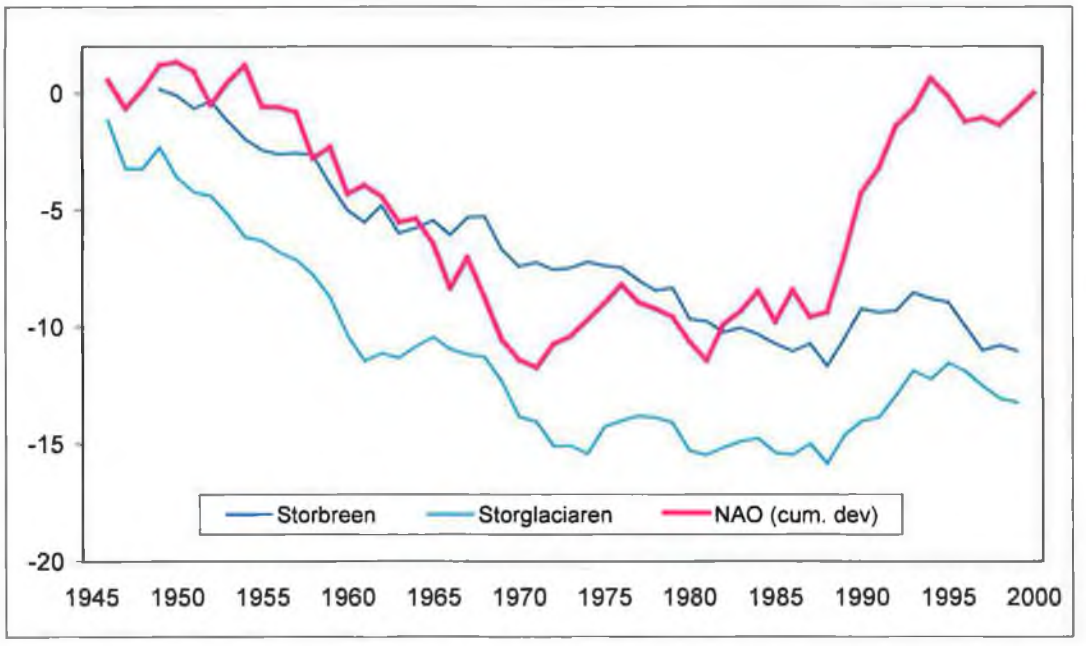

Figure 5.2.4 Cumulative net balance of both long-term monitored Scandinavian glaciers. Also plotted are the cumulative deviations of the annual NAO derived from the 1st principal component of pressure.

Since the 1970s, a number of Scandinavian glaciers have been displaying positive cumulative net balances. While these net increases have been confined to the more maritime glaciers, the decreasing net balances evident on the continental glaciers have largely diminished over a similar period, especially since 1988/1989. As a consequence of these positive cumulative net balances being recorded in recent decades, many front positions of the maritime glaciers responded to this mass balance forcing by advancing, thereby halting the decline that was evident up to the 1960s.

Large variations in the summed cumulative deviations of the atmospheric indices are also evident since the 1970s, particularly since 1988 (Figure 5.2.4); fluctuations which are consistent with the changes found in glacier mass balance in Scandinavia. When the various indices of atmospheric variability are related to glacier mass balance (Table 5.2.1, Table 5.2.3, Table 5.2.4), a strong association is

evident with winter balance and hence net balance for the maritime glaciers. It was also established that meridional airflow was an important contributor to summer balance on mainland Scandinavia, while on Svalbard, it was important for winter balance suggesting the importance of glacier location in relation to a water body (Table 5.2.2). The effects of increasing continentality are also evident in Figure 5.2.2, which demonstrates the decreasing relationship between the NAO and increasing distance from the coast.

As a consequence of reduced levels of precipitation penetrating inland, ELAs, which are sensitive indicators of the regional climate (Benn and Evans, 1998), increase in elevation with increasing distance from the coast (Figure 5.2.3). The mass balance gradient, which reflects the throughput of a glacier, also decreases with increasing continentality. Maritime glaciers tend to have a large throughput of mass and have a high winter balance to net balance ratio (Bw/Bn), symptomatic of their dependence on winter precipitation. High summer balance to net balance ratios (Bs/Bn) are consistent with more continental regime glaciers, where summer temperatures play a more dominant role in determining the annual net balance.

5.2.2 The local climate dimension

Tveito (1996) demonstrated the link between a regionalised atmospheric circulation index and precipitation for southern Norway. As expected, the relationship between this regionalised index and winter mass balance was high for all maritime glaciers. The relationship between the circulation indices and summer ablation diminishes, primarily due to more complex and more locally determined interactions, such as, temperature, cloudiness, rainfall, wind and energy fluxes at or near the glacier surface (Hodge *et al.*, 1998).

Figure 5.2.5-Figure 5.2.10 demonstrate the relationship between winter balance for two maritime glaciers of Ålfotbreen and Nigardsbreen and winter temperature, winter precipitation and the reduced circulation index. All three variables are positively correlated with winter balance (Ålfotbreen ~ 0.70, 0.68, 0.84; Nigardsbreen ~ 0.61, 0.69, 0.74 respectively). The positive correlations between

temperature and winter balance initially appears contradictory, as increased temperatures should produce an increase in melting. However, above average winter temperatures have an increased moisture carrying capacity, which, if they remain below a certain threshold, will produce an increase in solid precipitation falling during the winter months.

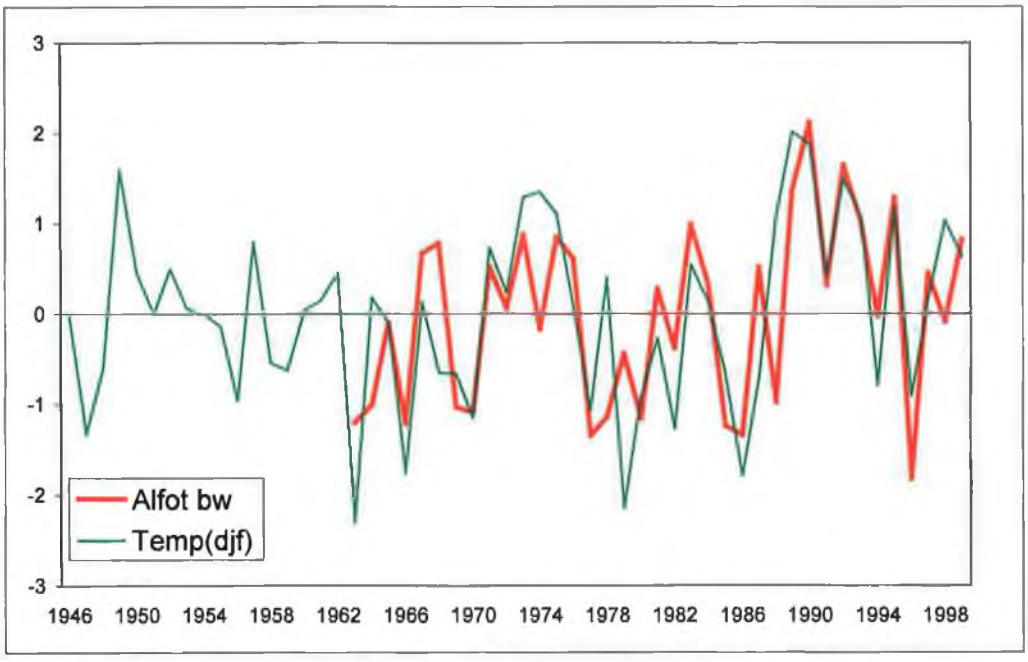

Figure 5.2.5 Winter temperature from Laerdal (54120) and winter balance from Ålfotbreen.

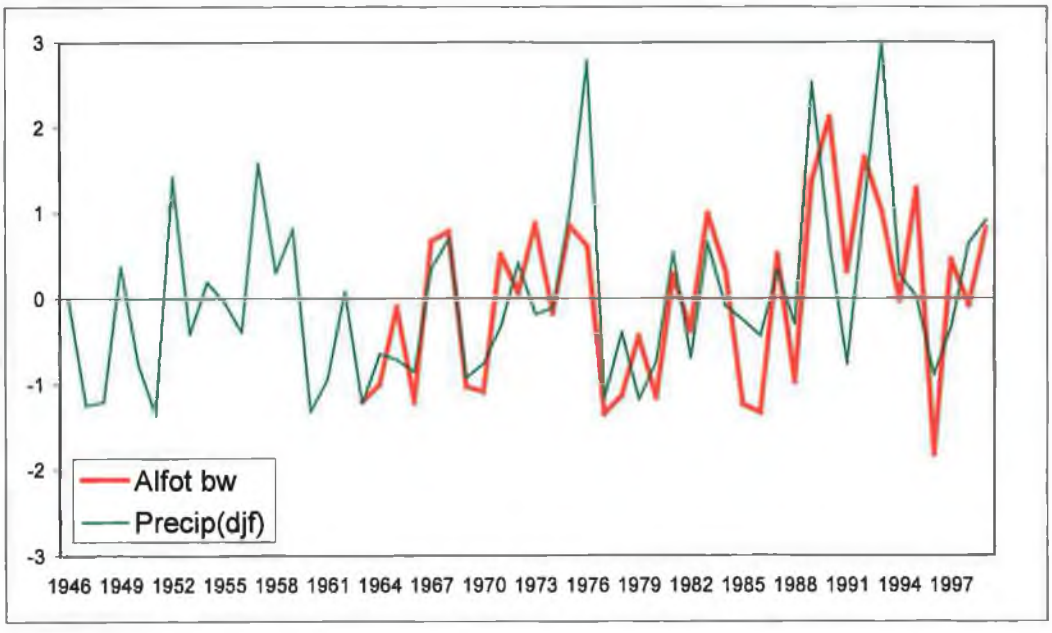

Figure 5.2.6 Winter precipitation from Skjaak (15600) and winter balance from Ålfotbreen.

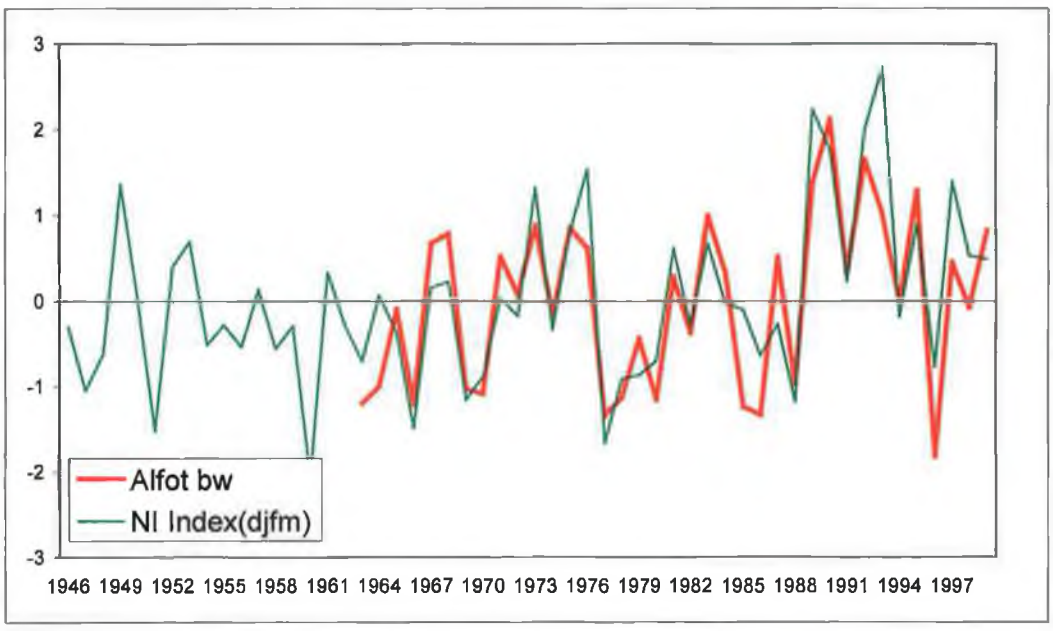

Figure 5.2.7 NI Index, between, Ona and Utsira-Fyr, and winter balance from Ålfotbreen.

A positive correlation between winter precipitation and winter balance is expected as increased moisture will result in increased accumulation on the glacier surface. Similarly, a positive correlation between the atmospheric variability index and winter balance is expected, as it is a measure of the influx of maritime westerly air, which during the winter months is warm and moist. These results are consistent with those from previous sections, in relation to temperature and precipitation and glacier mass balance.

A higher correlation was also found between winter balance and the circulation index than that found with either temperature or precipitation or both regressed together (adj. $r = 0.76$), suggesting that additional factors are being accounted for in the index that are not explicitly due to either of the climate variables.

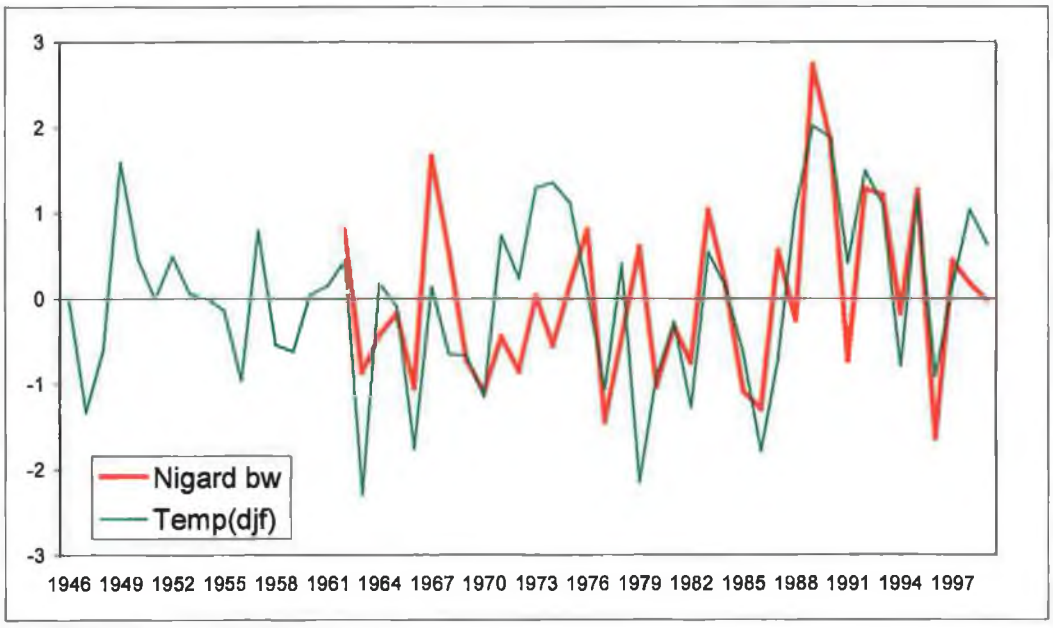

Figure 5.2.8 Winter temperature from Laerdal (54120) and winter balance from Nigardsbreen.

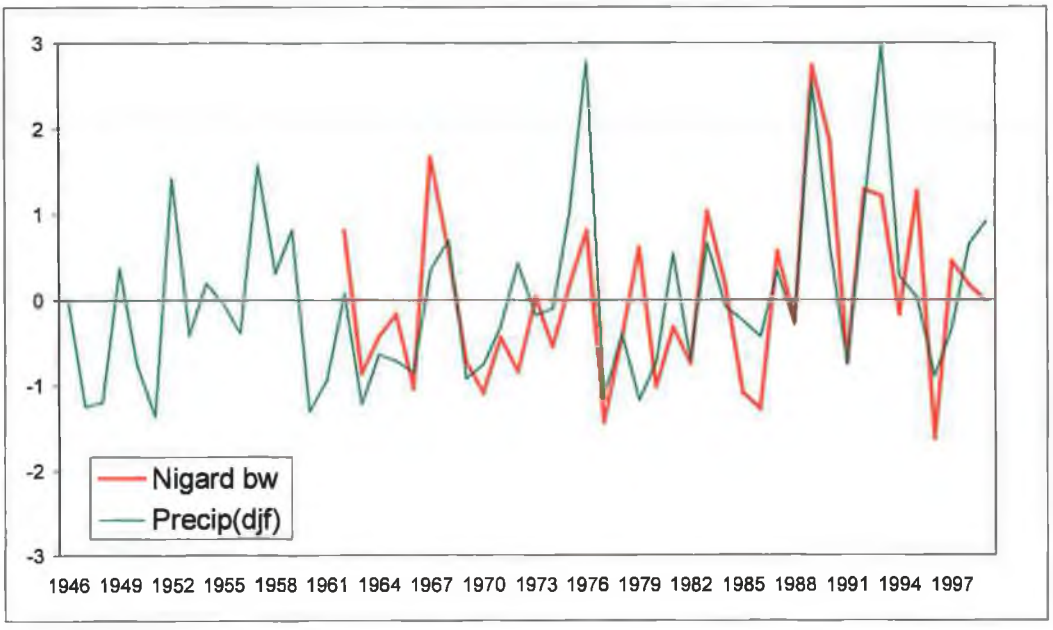

Figure 5.2.9 Winter precipitation from Skjaak (15600) and winter balance from Nigardsbreen.

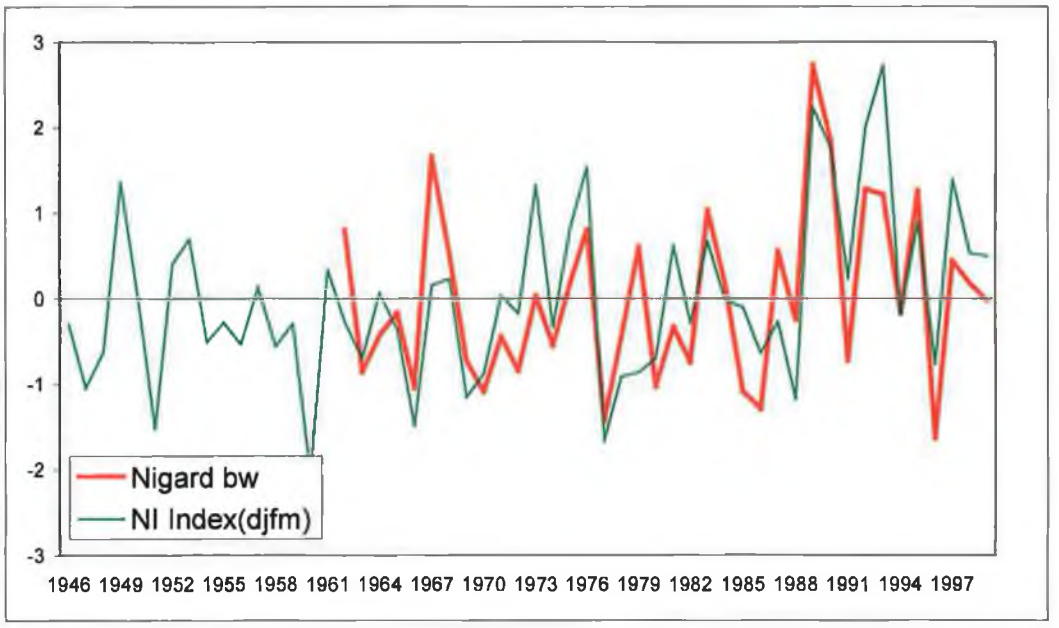

Figure 5.2.10 NI Index, between, Ona and Utsira-Fyr, and winter balance from Nigardsbreen.

Figure 5.2.11-Figure 5.2.13 illustrate the relationship between summer temperature and both zonal and meridional flows on the glacier summer balance of Ålfotbreen. High temperatures during the summer months are positively correlated with ablation resulting in high summer ablation values ($r = 0.53$). However, the response of glacier mass balance to increasing temperatures is not consistent (Figure 5.2.11), which is reflected in the moderate strength of the correlation. In 1980, above average temperatures coincide with a year in which summer balance was less than average. While in 1988, temperatures were also above average, but lower than those recorded in 1980, coinciding with the largest summer losses evident over the period of record.

The influence of maritime air during the summer months, despite being warm, would act to reduce ablation ($r = 0.43$) in comparison to warmer continental air flowing off the European continent which acts to enhance ablation ($r = -0.46$) (Figure 5.2.12-Figure 5.2.13).

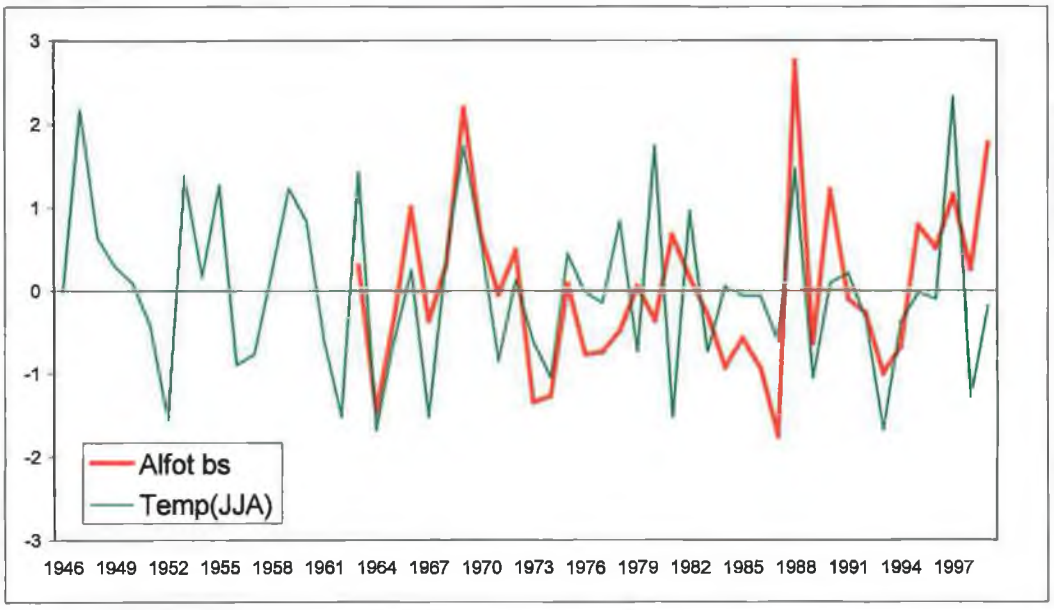

Figure 5.2.11 Summer temperature from Laerdal (54120) and summer balance from Ålfotbreen.

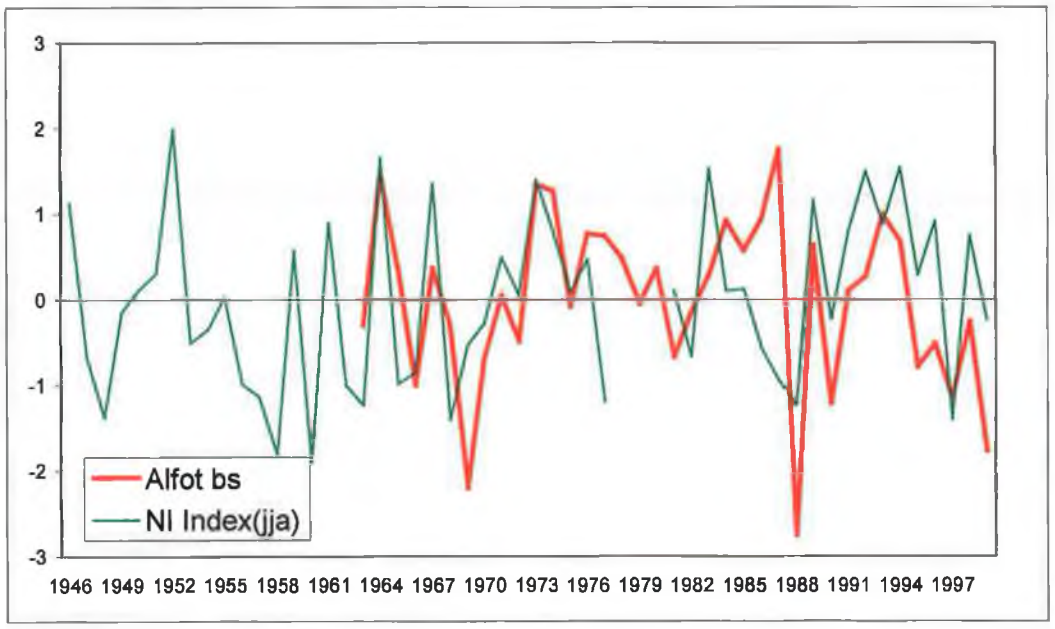

Figure 5.2.12 NI Index, between, Ona and Utsira-Fyr, and summer balance from Ålfotbreen.

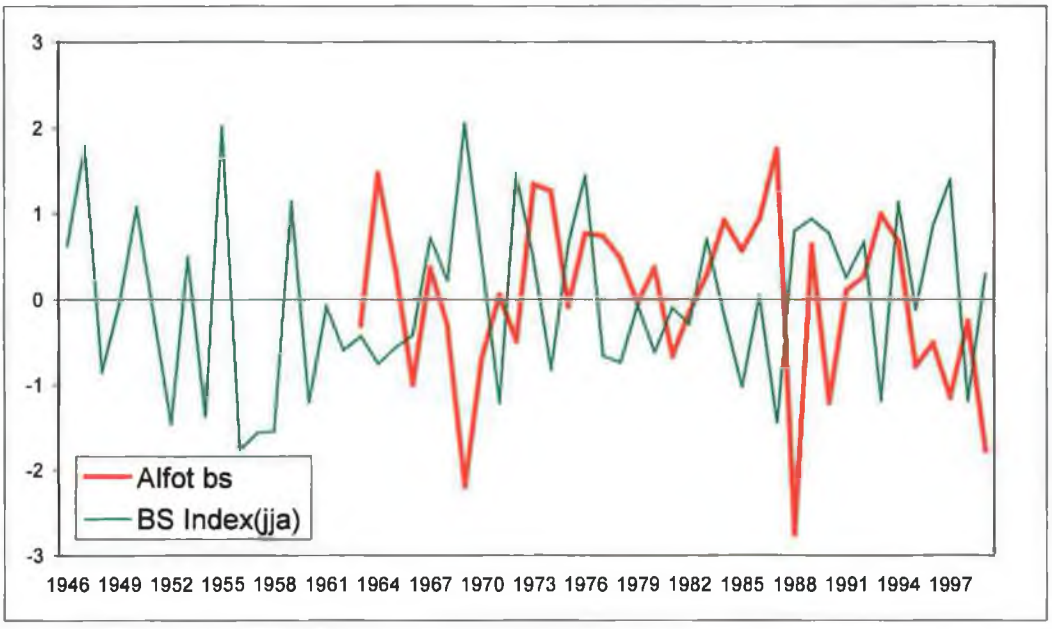

Figure 5.2.13 BS Index and summer balance from Ålfotbreen.

5.3 Discussion

Understanding the various links between large-scale atmospheric variability and glacier mass balance is crucial if we are to understand the process that affect glacier mass balance and hence, glacier behaviour, as a consequence of climate. Meier (1965) outlined the linkages between climate and glaciers but there still exists large gaps in our understanding of the various levels of interaction which are producing the changes we are currently witnessing in glaciers worldwide.

A number of researchers have focused on the impact of specific levels on individual glaciers, but very few have approached this topic in a holistic manner that is required to better understand the underlying climate process that affect glaciers. This approach is necessary if we are to link global changes to the local scale and may prove beneficial if we are to understand and accommodate future potential changes in glaciers as a consequence of climate change.

Incorporating this approach into an analysis of the links between climate and glaciers requires looking at large scale atmospheric variability and its influence on climatic parameters, such as temperature and precipitation, which in turn will have

an influence on glacier mass balance and behaviour. The dominant mode of atmospheric variability in the North Atlantic is the NAO and it was shown to have a strong influence, both temporally and spatially, on temperature and precipitation across the European landmass. While winter temperatures were shown to increase with a positive NAO, as a consequence of the advection of warm maritime air into Europe, there existed large regional differences in precipitation receipt. The consequences of these regional differences in temperature and particularly, precipitation are evident in the divergent mass balance trends between Alpine and Scandinavian glaciers since the 1970s. The tendency for a more positive NAO since this period coincides with a number of changes evident in a suite of atmospheric and climatic parameters (Bardossy and Caspary, 1990; McCabe and Fountain, 1995; Smith, 1995; Vincent and Vallon 1997; Weber, 1997; Hoppe and Kiely, 1999; Kiely, 1999; Werner *et al.*, 2000; Brunetti *et al.*, 2001). These results are consistent with findings from other authors on a hemispherical scale and are not just confined to Europe. Findings from previous chapters suggested that a number of change points had occurred in the European climate series over the course of the 20th century. These change points appeared to be primarily driven by changes in atmospheric variability, however, there exists a large degree of local variability which makes conclusions difficult.

Hodge *et al.* (1998), in an analysis of climate variations and mass balance of three glaciers in western North America, also established that the year 1989 was a significant point after which there was a change in the relationship between climate and mass balance. Their research suggested that after this time, the glaciers under study not only started to display a coherent signal, but also demonstrated the highest rates of net mass loss over their entire records. They suggested a breakdown of the large-scale teleconnection between the Pacific Northwest and the tropical Pacific since 1989 to the degree that it is no longer statistically significant as the probable cause of the changes they found in mass balance (Hodge *et al.*, 1998). They also suggest that this breakdown may prove to be more important than the regime shift that occurred in the Pacific during 1976-1977 (Hodge *et al.*, 1998).

5.3.1 Evidence of a non-stationary response to climate? A note of caution

To investigate if similar changes in climate-glacier interactions have occurred in the Scandinavian series, correlations were derived based on an "increasing length of time series" (Hodge *et al.*, 1998) of the mass balance and atmospheric data for both the winter accumulation and summer ablation period. This initially involved taking a minimum period of time, which amounted to approximately 18 years for the majority of the Norwegian glaciers (~1963-1980), 32 years for Storbreen (1949-1980) and 35 years for Storglaciaren (1946-1980); deriving a correlation, then incrementing the series by one year until all available years have been included in the analysis. The subsequent correlations, based on the incremented time series, can then be plotted over time to assess years in which obvious changes have occurred (Figure 5.3.1-Figure 5.3.3).

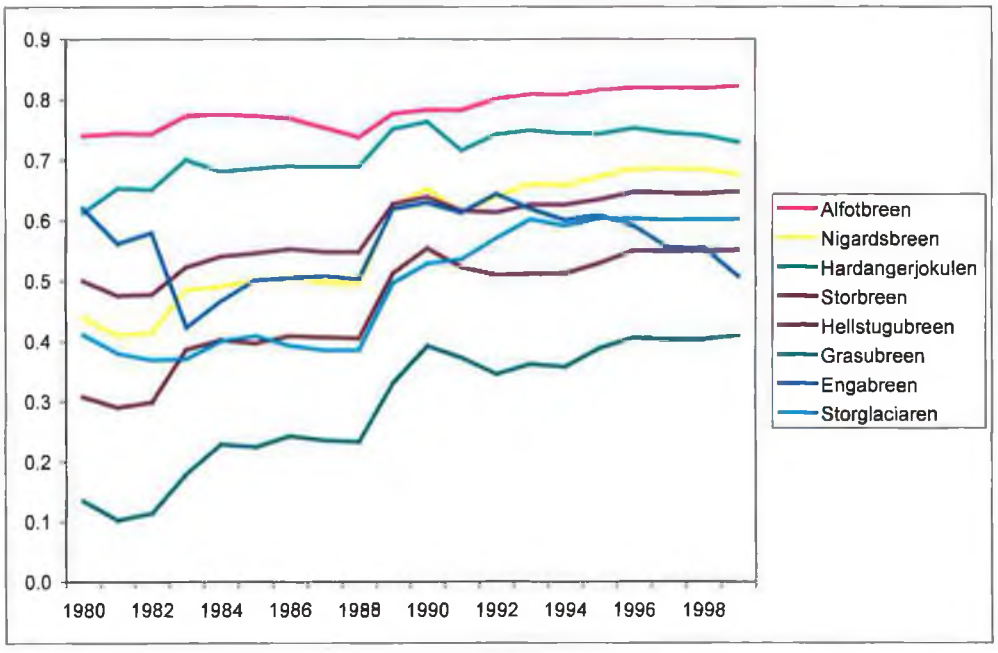

Figure 5.3.1 DJF NAO correlations (Pearson's r) with "increasing length of time series" 1980-1999 and winter balance.

A change in the relationship between circulation and mass balance appears to have occurred between 1988 and 1989, with an additional increase between 1989 and 1990. Six of the eight glaciers show the largest winter balances on record as having occurred during either 1989 or 1990 which coincides with the change in the relationship between climate and glaciers as suggested by Figure 5.3.1. The

maritime glaciers of Ålfotbreen and Hardangerjøkulen display a more subdued change in Pearson's 'r' in comparison to the more continental glaciers of Gråsubreen and Hellstugubreen. However, continentality does not appear to be an overly important factor in the change in the relationship as it is apparent at both maritime and continental glaciers in northern and southern Scandinavia

Figure 5.3.2 and Figure 5.3.3 display the change in correlations between the East Atlantic Jet Pattern (zonal) and the Bodo-Stykkisholmur index (meridional) which indicates that the change in climate-glacier relationships are consistent in both the accumulation and ablation seasons of 1988-1989. Five of the eight glaciers recorded net ablation values that were the highest or second highest on record during this year. 1997 was the next year in which large ablation figures were recorded, mainly on the more continental glaciers. However, the response is varied during the change point evident in the ablation season of 1988, with some glaciers indicating a decreasing relationship after this point while others indicate an increasing relationship. Storglaciaren displays a gradual increase over time and does not display the step like change of the other glaciers during 1988.

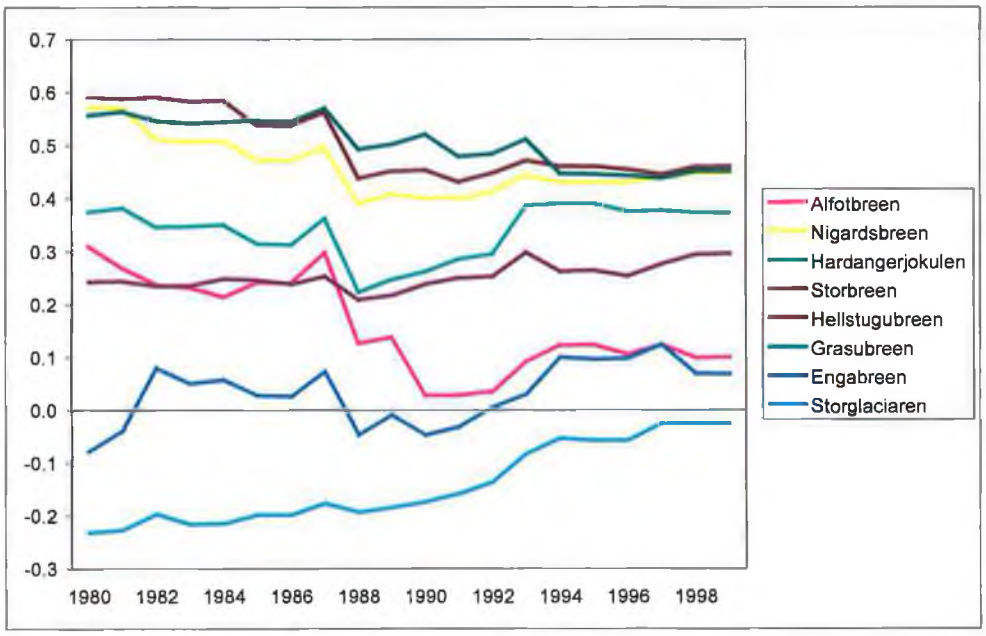

Figure 5.3.2 EA-JP correlations (Pearson's r) with "increasing length of time series" 1980-1999 and summer balance.

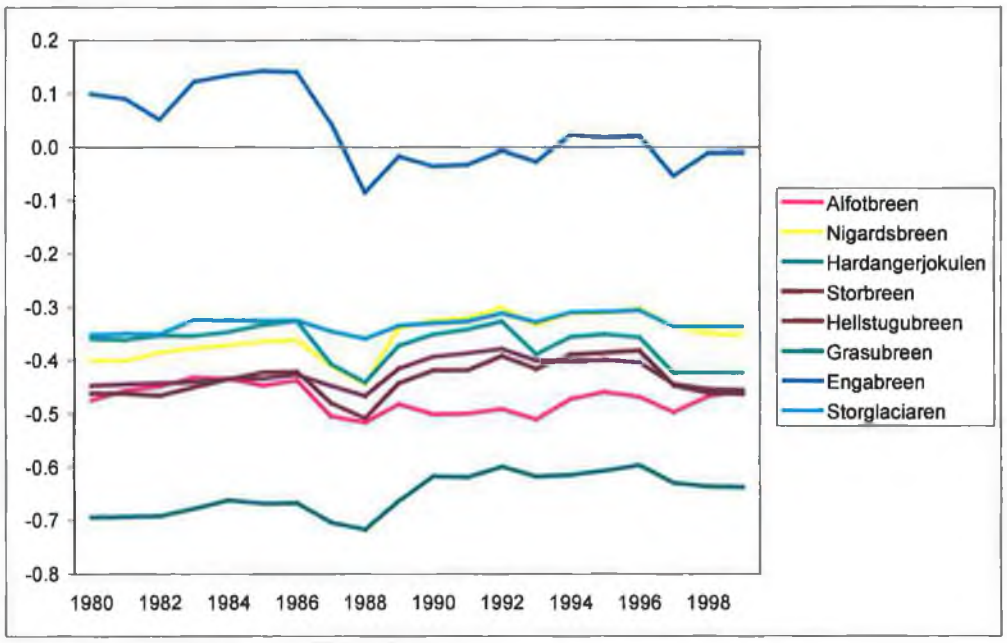

Figure 5.3.3 BS Index correlations (Pearson's r) with "increasing length of time series" 1980-1999 and summer balance.

Engabreen is the only glacier to show a change from a weakly positive to weakly negative response to meridional forcing. While the remaining glaciers do indicate a change in the relationship during 1988, the correlations recover quickly and remain relatively stable over the period of record.

The timing of these step like changes in the climate-glacier correlations are consistent with the change evident in the summed cumulative deviations of the annual NAO during 1988 (Figure 5.2.4) after which it strengthened for a number of years, to levels not previously exceed during the course of the 20th century.

These findings, if not coincidental, suggest a hemispherical scale linkage or teleconnection between the Pacific and Atlantic producing the changes in glaciers in both regions during 1988-1989. The timing of the change point in the NAO would seem to imply that it is part of the explanation while the timing of the changes would appear to lead the pacific glaciers by one year.

5.4 Conclusion

Scandinavian glaciers and in particular, Norwegian maritime glaciers, were examined further due to their current response to climate which is counter to that of glaciers on a global scale, with few minor exceptions. Positive cumulative net balances have resulted in glacier advances of a number of the maritime glaciers since the 1970s, halting the recession that was evident up to this period. The positive net balances being recorded on the maritime glaciers appear to be largely due to increases in winter precipitation, resulting in an accumulation surplus at the end of the balance year. These increases in precipitation, which Hanssen-Bauer and Førland (1998b) showed were statistically significant over south-western regions of Norway from 1960-1997, are likely the result of increased zonal airflow (Førland *et al.*, 1996) consistent with an increasing intensity of the NAO.

The present analysis has also highlighted 1988/1989 as a glaciological year that warrants further investigation, particularly for maritime glaciers which show accelerated rates of increase in their cumulative net balance since 1988/1989.

Globally, there is evidence to suggest that mass balance variability has been increasing, especially since the 1980s, which is likely attributable to climatic variability (Dyurgerov and Meier, 1999; Dyurgerov, 2002). Between 1982 and 1995, Storglaciären recorded eight of its thirteen highest values of winter accumulation, while six of its summertime ablation values were amongst the lowest recorded, indicating an increase in the frequency of extremes (Pohjola and Rodgers, 1997b). These findings are corroborated by those of Hurrell (1995) who suggests that the moisture flux over the North Atlantic has increased since the 1980s.

Findings to date have firmly established linkages between semi-hemispherical scale circulation, regional climate and glacier mass balance in Europe and in particular the mass balance of Scandinavian glaciers. These relationships have been shown to vary seasonally, with large-scale climate accounting for a large proportion of winter accumulation, while more regional- or local- scale climate

factors need to be included to account for variations in the summer balance. The relationship between climate and glaciers was also found to be dependant on location factors; continental glaciers have a greater dependence on summer temperatures, while maritime glaciers, which can exist at lower elevations, predominantly rely on winter precipitation.

In order to link the various scales of interaction highlighted and keeping in focus the two key objectives of this research - to further our understanding of climate-glacier interactions employing a methodology that is cost effective, transferable and utilises remote meteorological parameters - the central theme of the next chapter will concentrate on the application of a tested synoptic climatological methodology applied to a selection of Norwegian synoptic stations. The resulting synoptic classification will then be related to mass balance to determine linkages between the synoptic scale climate forcing and accumulation and ablation for a number of Norwegian glaciers. The methodology employed will include a broad range of meteorological parameters which link both the large- and local- scale climate in order that as many relevant climatic factors can be accounted for as possible.

Chapter VI

Temporal synoptic classification methodology

6.1 Introduction

The primary objective of this research is to fill some of the gaps that presently exist in our understanding of the linkages between climate and glacier mass balance. To date few systematic analyses have examined the interactions between the various scales at which these linkages occur. In an attempt to redress this deficiency, this chapter presents a methodology, which has previously been applied successfully to a number of circulation to environment studies (Kalkstein and Corrigan, 1986; Kalkstein *et al.*, 1990; Cheng and Lam, 2000) or in modified form (Kalkstein *et al.*, 1996), which explicitly takes account of a range of climate variables. The variables included are all considered important in determining the effects of climate on glacier mass balance.

The approach employed involves a synoptic climatological study in that it seeks to group or classify combinations of weather elements, characteristic of air masses, displaying similar properties (Yarnal, 1993). The benefit of this is that, while it is synoptic in scale, thermal and moisture variables are directly taken account of in the analysis. These variables are not explicitly included in many other synoptic classification studies.

Synoptic climatology is primarily concerned with understanding the local or regional scale climate through an examination of the links between local climate elements and atmospheric circulation (Yarnal, 1984). This is achieved through the establishment of relationships between the atmospheric circulation and the surface environment, thereby linking processes that operate at the large-scale to those at a regional or local-scale. Classification of the atmospheric circulation is of primary concern when performing synoptic climatological research as it enables the key elements of variability within the atmospheric circulation to be extracted and provides a means by which the surface environmental responses can be assessed.

The methodology employed, entitled 'Temporal Synoptic Index' (TSI) (Kalkstein *et al.*, 1990), is an automated and objective synoptic classification procedure, which classifies individual days into homogenous air mass categories based on the similarity of weather elements indicative of regional-scale climate. The procedure will be used to classify daily data for a 30 year period, between 1968-1997, for both winter and summer, from five Norwegian synoptic weather stations. The selected stations are on a north-south transect and were selected based on data availability and their proximity relative to a number of long-term monitored Norwegian glaciers.

Due to the inclusion of local weather elements, this methodology also facilitates an assessment of possible within airmass type changes, such as temperature or humidity changes, which may occur as a consequence of climate change but may be too subtle to be detected in mean annual or monthly temperature series, which take no account of the synoptic situation (Kalkstein *et al.*, 1990). Crucially, this approach directly facilitates an analysis of frequency changes of the different air mass types, which in the absence of any internal changes, may also result from a change in climate.

6.2 Synoptic climatological literature: A review of relevant classification techniques

A number of techniques have been developed in order to classify or categorise circulation patterns that are then assessed in terms of the surface environment. These techniques, based on either manual classification, correlation based, empirical orthogonal functions, principal components analysis, indexing or compositing (Yarnal *et al.*, 2001) broadly fall into two distinct categories, that of manual and automated classification procedures. Manual techniques have also been referred to as subjective techniques while automated techniques are termed objective. However, this distinction is not a constructive one, as automated techniques also require a number of subjective decisions to be made, which questions their implied objectivity.

Manual classification techniques, such as the Lamb classification of daily circulation patterns over the British Isles (Lamb, 1972) or *Grosswetterlagen* for central Europe (Hess and Brezowsky, 1977) and the Muller classification (1977) for the southern United States have a long and distinguished history in synoptic climatology. However, the subjective nature of these techniques, based on a manual classification of synoptic weather charts according to arbitrary criteria, is difficult to replicate, is labour intensive (Barry and Perry, 1973) and is totally dependant on the investigator's level of knowledge and judgement (Yarnal, 1993).

Application of manual classifications to diverse problems are often greatly limited due to their being tailored for specific purposes, such as an analysis of regional airflow patterns by Mayes (1991), who assessed daily and monthly airflow types for four specific regions in the British Isles and their effect on local precipitation. Despite some of these limitations, the more generic classifications (Yarnal, 1993), such as the Lamb and *Grosswetterlagen* classification have found widespread application in a range of environmental analyses (Yarnal, 1993).

Utilising Lamb's primary circulation categories, Sweeney (1985;1987) assessed the influence of airflow over Ireland on precipitation receipts. Changes in frequency of occurrence of synoptic types, in particular, an increase in cyclonic types at the expense of westerlies since the 1950s, were shown to have implications on the spatial distribution of precipitation and on annual receipts (Sweeney, 1985). Similar findings are outlined by O'Hare and Sweeney (1993) and Briffa *et al.* (1990) in their analysis of Lamb circulation types and weather characteristics over the British Isles.

An analysis of *Grosswetterlagen* by Werner *et al.* (2000) to assess climate variability in the European sector of the North Atlantic suggested that residence times of these weather states changed around the decade of 1981-1990, particularly evident with zonal flow. This time period also coincides with simultaneous increases in Northern Hemisphere temperature anomalies (Werner *et al.*, 2000).

Wilby (1992) utilised the Lamb weather types to determine event probabilities and magnitudes of daily precipitation for dominant synoptic classes. These probabilities and amounts were then used to condition a stochastic rainfall model used as input to a hydrological model. Using an amended version of the Baur *et al.* (1944) classification by Hess and Brezowsky (after Bardossy and Plate, 1991), Bardossy and Plate (1991) also simulated stochastic series of daily precipitation based on circulation pattern occurrence.

The potential for more automated and seemingly objective techniques has become increasingly feasible with the advent of increasing computing power. The Lamb classification for the British Isles, which was discontinued after Hubert Lamb's death in 1997, was replaced by an 'automated' technique, the Jenkinson and Collison daily catalogue of UK weather types, based on an objective scheme developed by Jenkinson and Collison (1977). The Jenkinson and Collison classification derives numerical indices of mean pressure, meridional and zonal flow and vorticity and total vorticity from a regularized 16-point grid of mean sea level pressure data using a domain centred on the UK. As daily gridded sea level pressure data for the Northern Hemisphere is available from 1880 onwards, is updated daily and due to the ease of applicability of the classification technique, a number of studies have been based on, or application of, the Jenkinson and Collison classification technique.

Jones *et al.* (1993) performed a comparison between the manual classification of Lamb's circulation types with those derived from the automated objective classification of Jenkinson and Collison and found negligible differences between the correlations of counts of circulation types and regional temperature and precipitation. However, a major discrepancy between both classifications was evident: the decline in westerlies since the 1940s in the manual classification procedure was less apparent in the objective classification. They attributed these differences to the different objectives behind the manual and automated techniques. Kyselý and Huth (2003) also compared a manual and automated atmospheric classification method and observed similar results to Werner *et al.* (2000) with the

objective classification, with less pronounced changes evident with the *Grosswetterlagen* catalogue of Hess-Brezowsky (1977).

An application of the Jenkinson and Collison catalogue was also developed for Egypt by Dessouky and Jenkinson (1979) who derived daily pressure, wind flow and vorticity indices from a modified nine-point grid configuration of sea level pressure from 1899 onwards. The catalogue was used to describe daily, monthly and seasonal weather features and to assess its potential for monthly and seasonal weather forecasts. Similar catalogues have been developed to evaluate the extent to which weather types determine local precipitation and temperature (Linderson, 2001) and winter temperature (Chen, 2000) in Scandinavia, temperature and precipitation in the Netherlands (Buishand and Brandsma, 1997) and precipitation in Portugal (Trigo and DaCamara, 2000) and Spain (Goodess and Palutikof, 1998).

Correlation-based map pattern classifications, which were first introduced by Lund (1963) to classify sea level pressure patterns, have also found widespread application in assessing circulation to surface environment relationships, due to ease of application and interpretation of results. This technique establishes the degree of similarity between map pairs (Yarnal, 1993), comprised of standardised variables, namely of sea level pressure, using Pearson product-moment correlations between points. Kirchhofer (1973) suggested a modification to the Lund classification by applying a sum-of-squares technique to calculate the correspondence between map pairs of weather maps, with key groups defined by the selection of a threshold and minimum group size. Blair (1998) proposed a subsequent modification, due to the discovery of errors when using the Kirchhofer technique to classify weather maps.

Frakes and Yarnal (1997) developed a procedure for blending both manual and correlation–based classifications to overcome significant shortcomings associated with both techniques, the labour intensive and subjective nature of the manual technique and the arbitrary selection of keydays by the automated correlation-based technique. Manual classification is first performed, over a short time period, to generate composite pressure surfaces, taking advantage of the researchers'

knowledge of synoptic circulation. These manually classified composite pressure surfaces are then used as seeds in a long-term correlation-based classification (Frakes and Yarnal, 1997). Over time periods of a month or greater the hybrid scheme displayed little difference to a manual classification of the same data and produced less within type variation, an important requirement to ensure homogeneity of classified groups. Comparison of both techniques over shorter time periods demonstrated substantial differences, which they attributed to errors associated with the subjective manual classification (Frakes and Yarnal, 1997). Their findings suggested that the hybrid classification technique was vastly superior to both the manual and correlation-based techniques; consequently, they suggest that correlation-based or manual classification techniques should not be used in isolation.

Brinkmann (1999) employed a correlation-based technique to classify daily 700 hPa heights for 25 summer seasons, over Lake Superior basin, which were then related to surface temperature to identify and remove sources of within-type variability of temperature. It was determined that the source of this within-type variability, which was considerable, was comprised of a climate change component and a component due to small-scale circulation features, which were not captured by the classification technique, but were identified using composite difference maps (Brinkmann, 1999). The regression models which related the map pattern frequencies to temperature produced poor results due to the large variability, as was previously suggested by Frakes and Yarnal (1997).

Brinkmann (2000) proposed a modification to the correlation-based classification employed previously in the Brinkmann (1999) study to reduce the large within type variability for both temperature and precipitation. Two approaches were compared, of which the modified, by changing the thresholds of classification, correlation based technique, produced superior results (Brinkmann, 2000). However, Kaufmann *et al.* (1999) added a note of caution when using the Kirchhofer technique and suggested a method by which the statistical significance of groups produced by the Kirchhofer technique should be evaluated, due to the possible

identification of groups purely due to random chance, and therefore not related, if a threshold based on minimum group size is specified incorrectly.

Map pattern classification using S-mode empirical orthogonal function analysis, which can also be used for regionalisation, and cluster analysis to classify days based on similar factor scores has also been used to determine synoptic types for New Zealand (Kidson, 1997; 2000). These synoptic types can then be related to surface variables, such as, temperature, precipitation, duration of bright sunshine and daily wind run to examine climate variability.

However, this method is not widely utilised due to difficulties in interpreting the loading maps which do not directly relate to any single keyday pattern (Yarnal, 1993). Findings by Kidson (1997) reaffirm these difficulties. Also, synoptic classes may disguise embedded features, such as, fronts (Kidson, 1997) that will have obvious impacts on precipitation occurrence. Wilby (1998) incorporated additional parameters to capture some of these embedded features, such as, weather patterns and frontal frequencies, into an analysis of low frequency rainfall events and airflow indices, and while the results captured a significant proportion of variation in rainfall, deficiencies were also highlighted.

A number of eigenvector-based techniques have become increasingly popular in classification studies, with large data sets being processed in a matter of minutes or less on a standard desktop computer. The tailoring of statistical packages, which were once the domain of the mainframe, for desktops has also facilitated the proliferation of these techniques. Yarnal (1993) suggested that these eigenvector-based techniques could be classified into two techniques: empirical orthogonal functions and principal components analysis on the basis of subtle differences in approaches. Empirical orthogonal functions are the unit-length eigenvector whereas principal components analysis weights this value with the square root of the eigenvalue and these weights represent the correlation between the original variable and each principal component analysed (Yarnal, 1993).

Utilising empirical orthogonal functions, Slonosky *et al.* (2000) analysed long series of monthly surface pressure observations from 1774-1995 to assess the variability of atmospheric circulation over Europe. While not strictly a synoptic climatological assessment, this work formed the basis for further work which related atmospheric circulation and surface temperature over Europe from the 18th century to 1995 (Slonosky *et al.,* 2001). In addition to the three leading principal components of the empirical orthogonal function, which represented the central tendency of European pressure (EOF1), a zonal circulation pattern (EOF2) and a meridional pattern (EOF3), they also incorporated additional circulation indices. This work demonstrated the importance of atmospheric circulation as a control on surface temperature over Europe. However, they also draw attention to the fact that a decadal variability existed in the correlations between circulation and climate that indicates non-stationarity in the relationship between both series. They also suggest that cycles of approximately 50-60 years in length exist in the strength of the correlations, a periodicity also outlined by Lamb (1982), which may be related to the convective overturning of the thermohaline circulation in the northern North Atlantic (after Delworth *et al.,* 1993).

The second eigenvector based technique, that of principal components analysis, has had widespread application in the study of climatology, where large and potentially noisy data can obscure the signal being sought; it offers the potential to greatly reduce the data size while extracting a maximum of information. Wibig (1999) employed rotated principal components of the 500 hPa heights to classify circulation patterns over the Euro-Atlantic sector which were then related to precipitation distributions over Europe during the winter months. In each month, a number of patterns were distinguished: the North Atlantic Oscillation, Scandinavian, Central European, East European and the East Atlantic pattern. Distribution maps were then generated, based on the correlations between precipitation from a large number of sites across Europe and the circulation patterns as defined by the principal components analysis, to illustrate the regions that were influenced by particular pattern types.

Galambosi *et al.* (1996) performed a principal components analysis on 500 hPa heights and then utilising a K-means clustering procedure classified daily atmospheric circulation patterns over the southwestern USA. The circulation patterns defined were subjected to further subjective classifying criteria, to produce three different cluster classifications. Based on the original procedure which produced 8 or 9 types depending on season, clustering fewer types to produce five or six classes and an aggregation of types according to precipitation producing mechanisms which produced 3 types in any season (Galambosi *et al.,* 1996). The different clustering mechanisms were then compared from the point of view of information content for precipitation modelling (Galambosi *et al.,* 1996) which could then be applied to global climate model (GCM) data. Their results suggested that the greater information content was with the larger the number of circulation types.

Bonell and Sumner (1992), in an analysis of precipitation over Wales, used a hybrid of both manual and an automated classification technique, in order to establish affinity areas for daily precipitation. They manually subset precipitation data into categories according to surface airflow direction and derived Pearson product-moment correlation matrices for each of these subsets that were then subjected to principal components analysis. The resultant factor scores were then clustered to produce precipitation affinity areas.

Romero *et al.* (1999b) classified atmospheric circulation patterns that were then related to spatial patterns or pattern groups of significant rainfall days for Mediterranean Spain derived in previous work by the authors (Romero *et al.*, 1999a). Using output from a T-mode principal components analysis, cluster analysis was performed to cluster days with similar loadings on the extracted components. This resulted in days in which the precipitation distributions were similar, irrespective of amounts, to be clustered together (Romero *et al.*, 1999a). Using gridded 925 and 500 hPa heights, 19 circulation types emerged for the period 1984-1993 (Romero *et al.*, 1999b). These patterns displayed a clear distinction between Atlantic and western Mediterranean types, with distinct

seasonal variations also being observed. Associations between the circulation types and the rainfall spatial patterns were then established.

Huth (2001) examined the occurrence frequencies of circulation types over Europe for the period 1949-1980 in an analysis of trends of surface climate elements in the Czech Republic. K-means clustering, a non-hierarchical clustering technique, was performed on output from a T-mode principal components analysis of daily 500 hPa heights in a separate analysis for both winter and summer months. The procedure, modified for the purposes of this study (Huth, 2001), classified 60% of days producing 13 types for the summer months and 12 types for the winter months, each containing more than 50 days. Inclusion of the remaining 40% of the data was not considered desirable (Huth, 2001) due to their effect on cluster means and hence cluster homogeneity and within type variance. Changes in winter circulation type frequency occurrences were found to be related to trends in the surface climate elements. However, a similar relationship was not found for surface elements during the summer months. The trends in surface elements were also shown to vary with circulation type.

Synoptic typing, an eigenvector based technique, is more concerned with changes in type and frequencies of atmospheric circulation over time (Yarnal, 1993), rather than spatial variation as in some of the previous examples, and is a technique that has had many applications over the last decade and a half. As opposed to classifying one variable over a large spatial area, synoptic typing classifies multiple surface elements over time from a specific location. These surface elements all measure aspects of airmass characteristics and hence the nature of any changes which may occur in circulation can be examined more closely. The technique has been extended to incorporate clusters that are spatially coherent and correspond closely to weather map features (Davis and Kalkstein, 1990; Kalkstein *et al.* 1996; Green and Kalkstein, 1996; Sheridan, 2002).

Synoptic typing has found a particular application in assessments of pollution concentration episodes as raw weather elements on an individual basis may have no obvious impact on concentration levels, but when included in a more holistic

approach combinations of elements that affect concentration levels can be exposed. This technique has also been used to identify distinctive synoptic or air mass categories in which high concentration levels would be expected (Kalkstein and Corrigan, 1986; Cheng and Lam, 2000) and thus, facilitate early warning systems to be enabled. Airmass classification has also been employed to investigate urban heat islands, using just a K-means clustering technique (Bejarán and Camilloni, 2003).

An obvious application of the synoptic typing classification is an assessment of circulation type and glacier mass balance, as the key surface elements that affect glacier mass balance, temperature and moisture, are included as variables in the typing procedure. To examine this assertion, the rest of this chapter will focus on the application of this methodology to derive a temporally based synoptic typing classification for Norway. The application of the resulting circulation classifications to glacier mass balance will be presented in a subsequent chapter.

6.3 Methodology

6.3.1 Data

Originally, data from six synoptic weather stations, Skabu, Takle, Flesland, Orlandet, Bodo and Nordstraum (Figure 6.3.1) were obtained from the Norwegian meteorological institute (DMNI). Daily data, measured at 0hr, 6hr, 12hr and 18hr, were acquired for all stations except Skabu, Takle and Nordstraum which only recorded data three times daily. Takle was subsequently excluded from further analysis due to missing data. Sub daily data were obtained in order to evaluate for any diurnal effects (Kalkstein *et al.*, 1990). All stations covered the measuring period 1968-1997 which coincides with the long-term measurements of glacier mass balance in Norway. This period also encompasses part of the 1961-1990 baseline period against which any future change in climate will be referenced from.

The data for each station comprised of a number of meteorological elements:

- mean sea-level pressure (hPa),
- minimum temperature (^{0}C),
- maximum temperature (^{0}C),
- relative humidity (%),
- wind direction (degrees),
- wind speed (ms^{-1}),
- cloud amount (oktas) and
- visibility (km)

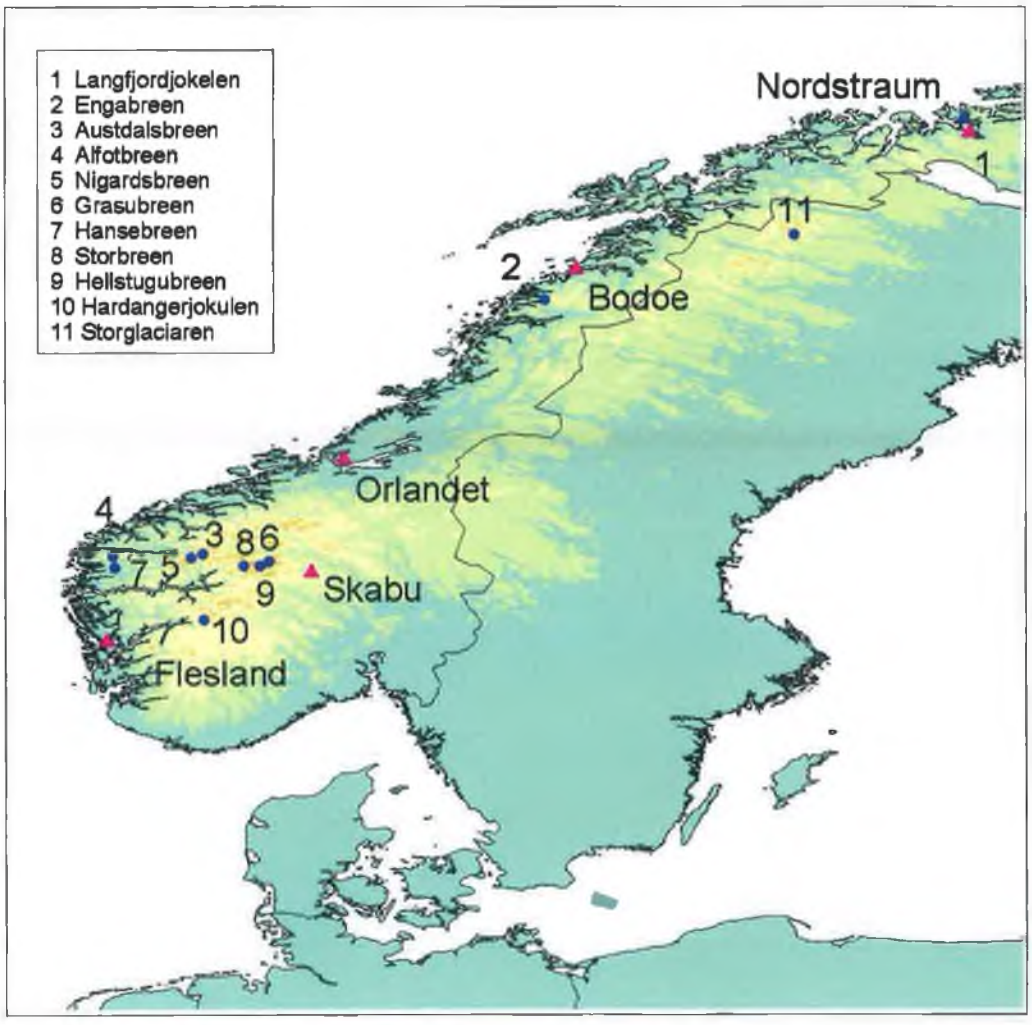

Figure 6.3.1 Stations locations and their position relative to monitored Norwegian glaciers.

These meteorological elements were selected, due to their availability and because these elements represent the key properties that distinguish air mass types. A

combination of these meteorological elements have also been successfully used for synoptic typing in previous studies (Kalkstein and Corrigan, 1986; Kalkstein *et al.*, 1990; Davis and Kalkstein, 1990; Kalkstein *et al.,* 1996; Green and Kalkstein, 1996; Cheng and Lam, 2000; Sheridan, 2002; Bejarán and Camilloni, 2003)

As mean sea level pressure for Skabu was not available, averaged data from three surrounding stations that were approximately equidistant from Skabu was used as substitute data for this variable. The effects of using this averaged data are considered to be minimal as sea level pressure is largely homogeneous over large areas.

Some prior processing had to be performed on the data before any analysis could be performed. The minimum and maximum temperatures were used to calculate mean temperature, resulting in a mean temperature recording for each 6 hourly interval. Relative humidity was converted to specific humidity according to the following formula:

$$rho = \frac{R_L}{R_V} \frac{e}{p + e\left(R_L/R_V - 1\right)}$$

$$R_L/R_V = 0.62197$$

$$es \text{ (saturation pressure)} = 6.1078 * 10^{((T * A^*)/(T + B^*))}$$

p = air pressure

T = temperature (^{0}C)

rH = relative humidity (%)

*A = 7.5
*B = 237.3 (^{0}K)
for use in vapour pressure with respect to water;

A = 9.5
B = 265.5 (^{0}K)
for use in vapour pressure with respect to ice;

$$e = es * rH$$

(source: http://www.agsci.kvl.dk/~bek/relhum.htm)

The two wind variables, wind direction and wind speed, were converted to a south scalar (*vv*) and a west scalar (*uu*), according to the formula,

$$vv = -((\cos(\text{wind direction})) * \text{wind speed})$$
$$uu = -((\sin(\text{wind direction})) * \text{wind speed})$$

Finally, visibility, recorded as a coded value, was converted to distance in kilometres according to the table in Appendix I-1. Cloud amount, despite being recorded as a categorical value, octas, was not recoded.

This processing resulted in a dataset with each day being defined by a total of seven elements measured four times daily. The data were then filtered to produce two subsets for each station, the first comprised of the winter months of December, January and February, while the second comprised of data for the summer months of June, July and August. These months were selected as it was felt that if any changes in climate were occurring it should be most apparent during these seasons.

6.3.2 Synoptic typing

6.3.2.1 Principal Components Analysis

Derivation of the Temporal Synoptic Index (TSI) was carried out as a two-step procedure. Firstly, the daily data was analysed using a principal components analysis and secondly, the loading scores from the principal components analysis were then clustered using a hierarchical and agglomerative clustering algorithm.

The daily data, which comprised of 28 variables for each day (7 elements measured four times daily) produced a data matrix of 28 by approximately 2700 cases (daily data for three months by 30 years) for each station and season. The configuration of the data, consisting of parameters as columns and time as cases, is a P-mode of decomposition resulting in an analysis of variables over time as required by the temporal component of the synoptic index. Due to the various units of measurement of each meteorological element, (hPa, degress, kilometres) each

element was standardised to have a mean of 0 and standard deviation of 1, according to the following,

$$\text{z - score} = \frac{\left(x - \bar{x}\right)}{\delta}$$

$x = \text{variable}_{i,j}$

$\bar{x} = mean$

δ = standard deviation

A correlation matrix (Table 6.3.1) was then derived and used as input to the principal components analysis (Yarnal, 1993).

Principal components analysis is primarily used to reduce a large number of intercorrelated variables to a smaller number of orthogonal and uncorrelated principal components that explain a large proportion of the variance of the original dataset (Kalkstein *et al.*, 1990; Jolliffe, 1990). Although the principal components analysis produces as many components as original variables, much of the variation in the data is explained in the first number of components (Yarnal, 1993), thus, principal components analysis is largely a variable reduction technique. This is achieved through a linear transformation of the original standardised and correlated data onto orthogonal axes (Kalkstein *et al.*, 1990).

Linear transformation of standardised variables onto orthogonal axes is carried out according to the following –

$$Z_1 = a_{11}x_1 + a_{12}x_2 + ... + a_{1p}x_p$$

Z_1 = first principal component

p variables, x_1, x_2, x_3, …,x_p, for n individuals

a_{11}, a_{12},…,a_{1p} coefficients such that the variance of Z_1 is maximised

such that, a^2_{11}, a^2_{12},…,a^2_{1p}= 1

$$Z_2 = a_{21}x_1 + a_{22}x_2 + ... + a_{2p}x_p$$

that the variance of Z_2 is maximised subject to constraint
that $a^2_{21}, a^2_{22},\ldots,a^2_{2p} = 1$ and,
Z_1 and Z_2 are uncorrelated

$$Z_3 = a_{31}x_1 + a_{32}x_2 + ... + a_{3p}x_p$$

that the variance of Z_3 is maximised subject to constraint
that $a^2_{31}, a^2_{32},\ldots,a^2_{3p} = 1$ and,
Z_3 is uncorrelated with Z_1 and Z_2

(Jolliffe, 1990)

These orthogonal axes describe the same amount of variability on a similar number of axes as the original data but in a way that the largest variance possible is accounted for by the first axis (Daultrey, 1976). The second axis then accounts for as much of the remaining variance possible while remaining uncorrelated to the first. This continues until 100% of the variation in the original data set is accounted for.

Rotation of the components was not performed as the principal components analysis served primarily as a data reduction technique in this analysis. Therefore rotation was not considered important. Orthogonal rotation can aid interpretability of the resultant components, but this is mainly a consideration for mapping procedures that utilise an eigenvector technique. Oblique rotation also removes the orthogonal nature of the principal components. Orthogonality of components also fulfils the requirements of the clustering procedure which requires that input variables are not related (Johnston, 1978).

	pres 00	pres 06	pres 12	pres 18	tmp 00	tmp 06	tmp 12	tmp 18	rho 00	rho 06	rho 12	rho 18	cld 00	cld 06	cld 12	cld 18	vis 00	vis 06	vis 12	vis 18	*vv* 00	*vv* 06	*vv* 12	*vv* 18	*uu* 00	*uu* 06	*uu* 12	*uu* 18
pres 00	1.00																											
pres 06	0.98	1.00																										
pres 12	0.92	0.98	1.00																									
pres 18	0.87	0.92	0.98	1.00																								
tmp 00	-0.20	-0.21	-0.21	-0.20	1.00																							
tmp 06	-0.18	-0.22	-0.22	-0.22	0.93	1.00																						
tmp 12	-0.07	-0.11	-0.13	-0.14	0.84	0.90	1.00																					
tmp 18	-0.06	-0.10	-0.14	-0.16	0.80	0.85	0.92	1.00																				
rho 00	-0.18	-0.18	-0.18	-0.17	0.79	0.76	0.70	0.65	1.00																			
rho 06	-0.15	-0.18	-0.19	-0.18	0.76	0.79	0.75	0.71	0.90	1.00																		
rho 12	-0.10	-0.14	-0.16	-0.17	0.69	0.74	0.74	0.73	0.79	0.90	1.00																	
rho 18	-0.07	-0.11	-0.14	-0.17	0.66	0.71	0.72	0.77	0.71	0.80	0.89	1.00																
cld 00	-0.24	-0.26	-0.26	-0.25	0.61	0.63	0.52	0.50	0.57	0.60	0.54	0.51	1.00															
cld 06	-0.18	-0.23	-0.25	-0.26	0.54	0.62	0.53	0.54	0.47	0.56	0.56	0.54	0.70	1.00														
cld 12	-0.16	-0.21	-0.25	-0.28	0.44	0.51	0.46	0.55	0.37	0.44	0.50	0.55	0.50	0.65	1.00													
cld 18	-0.10	-0.13	-0.17	-0.21	0.41	0.46	0.44	0.57	0.37	0.42	0.47	0.57	0.42	0.50	0.69	1.00												
vis 00	0.04	0.06	0.06	0.05	-0.20	-0.25	-0.22	-0.21	-0.42	-0.40	-0.35	-0.30	-0.45	-0.29	-0.19	-0.16	1.00											
vis 06	0.05	0.10	0.11	0.12	-0.28	-0.31	-0.29	-0.31	-0.40	-0.50	-0.47	-0.41	-0.46	-0.49	-0.34	-0.27	0.62	1.00										
vis 12	-0.02	0.02	0.05	0.07	-0.22	-0.25	-0.20	-0.28	-0.30	-0.38	-0.48	-0.46	-0.28	-0.37	-0.42	-0.32	0.36	0.51	1.00									
vis 18	-0.04	-0.02	0.02	0.06	-0.16	-0.19	-0.15	-0.19	-0.22	-0.29	-0.37	-0.46	-0.20	-0.27	-0.36	-0.42	0.26	0.34	0.59	1.00								
vv 00	-0.06	-0.14	-0.17	-0.17	0.31	0.38	0.37	0.37	0.27	0.36	0.35	0.34	0.33	0.37	0.32	0.26	-0.19	-0.26	-0.24	-0.19	1.00							
vv 06	0.06	-0.03	-0.11	-0.15	0.25	0.32	0.35	0.39	0.18	0.29	0.36	0.37	0.23	0.33	0.36	0.32	-0.08	-0.20	-0.28	-0.24	0.64	1.00						
vv 12	0.08	0.04	-0.05	-0.13	0.18	0.25	0.28	0.37	0.11	0.16	0.24	0.34	0.15	0.24	0.34	0.35	-0.03	-0.08	-0.21	-0.23	0.44	0.67	1.00					
vv 18	0.06	0.07	0.03	-0.06	0.11	0.14	0.18	0.27	0.04	0.07	0.11	0.24	0.06	0.13	0.23	0.33	0.02	-0.01	-0.09	-0.20	0.27	0.43	0.65	1.00				
uu 00	0.07	0.13	0.16	0.15	-0.10	-0.15	-0.15	-0.13	0.09	-0.02	-0.03	-0.04	-0.12	-0.17	-0.16	-0.09	-0.07	-0.01	0.00	0.01	-0.53	-0.41	-0.28	-0.16	1.00			
uu 06	-0.03	0.04	0.11	0.13	-0.05	-0.11	-0.15	-0.17	0.13	0.07	-0.01	-0.04	-0.04	-0.14	-0.18	-0.12	-0.10	-0.05	0.01	0.00	-0.32	-0.54	-0.42	-0.25	0.54	1.00		
uu 12	-0.03	-0.01	0.07	0.13	0.00	-0.03	-0.05	-0.12	0.18	0.18	0.13	0.02	0.03	-0.04	-0.16	-0.13	-0.14	-0.15	-0.07	-0.02	-0.16	-0.33	-0.54	-0.41	0.35	0.55	1.00	
uu 18	-0.03	-0.05	-0.03	0.05	0.05	0.03	0.01	-0.05	0.19	0.20	0.20	0.11	0.09	0.05	-0.04	-0.08	-0.15	-0.17	-0.15	-0.08	-0.05	-0.16	-0.33	-0.52	0.21	0.32	0.56	1.00

Table 6.3.1 Correlation Matrix used as input to Principal Components Analysis for Bergen-Florida DJF

	Component					
	1	2	3	4	5	6
pres 00	-0.32	0.68	0.61			
pres 06	-0.37	0.65	0.65			
pres 12	-0.40	0.59	0.68			
pres 18	-0.42	0.52	0.70			
tmp 00	0.85		0.13	0.23		-0.29
tmp 06	0.89		0.11	0.21		-0.24
tmp 12	0.81	0.11	0.16	0.35	0.12	-0.19
tmp 18	0.85	0.18	0.08	0.19	0.23	-0.11
rho 00	0.83	-0.15	0.24	0.20		-0.15
rho 06	0.88		0.23	0.17		
rho 12	0.88		0.19	0.13		
rho 18	0.86	0.11	0.13		0.19	
cld 00	0.74			-0.19	-0.26	-0.28
cld 06	0.75			-0.27	-0.15	-0.11
cld 12	0.69	0.19	-0.16	-0.36	0.18	
cld 18	0.62	0.23	-0.14	-0.35	0.37	0.14
vis 00	-0.69	0.11	-0.15	0.24	0.33	0.18
vis 06	-0.72		-0.12	0.34	0.34	
vis 12	-0.76			0.42	0.09	-0.13
vis 18	-0.71	-0.15		0.45	-0.13	-0.19
vv 00	0.56	0.31	-0.22	0.28	-0.40	0.25
vv 06	0.54	0.49	-0.28	0.26	-0.26	0.32
vv 12	0.45	0.60	-0.33	0.17		0.31
vv 18	0.34	0.58	-0.31	0.11	0.29	0.17
uu 00	0.16	-0.50	0.45		0.42	0.13
uu 06	0.24	-0.59	0.48		0.15	0.25
uu 12	0.28	-0.54	0.50		-0.16	0.38
uu 18	0.37	-0.42	0.37		-0.19	0.45

Table 6.3.2 Component matrix for Flesland with six extracted components. Values less than 0.1 are not displayed. Pres-pressure; tmp-temperature; rho-specific humidity; cld-cloud amount; vis-visibility; *vv*-south scalar; *uu*-west scalar

Components accounting for less than the variation in the original variable, that is any component with an eigenvalue < 1.0, are generally discarded (Table 6.3.3). A number of methods can be used to determine the correct number of components to retain, such as the scree plot (Figure 6.3.2), which plots the eigenvalue against the eigennumber to indicate any breaks in slope and hence number of components to retain (Yarnal, 1993). Natural breaks in slope can also be used to indicate the number of components to retain. As no one individual test will give the 'correct' number of components, a combination of techniques should be employed.

However, Yarnal (1993) points out that the correct specification of components to retain is not as critical to the synoptic typing procedure as to studies whose goal is regionalisation due to the robustness of the synoptic typing procedure.

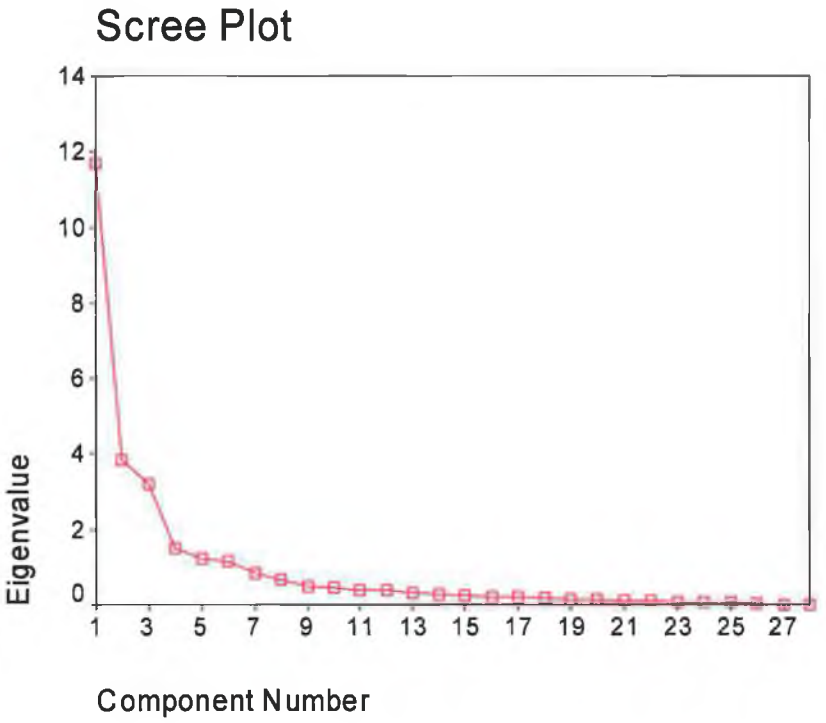

Figure 6.3.2 Scree Plot for Flesland DJF

The relationship between the original variable and each component is then described by the components loading matrix (Table 6.3.2) (Yarnal, 1993). Principal component scores, for each day, are derived from multiplication of the original standardised data matrix by the components loading matrix (Table 6.3.2). The resultant values of the component scores should exhibit proximate scores for days in which a similar combination of weather elements has occurred (Kalkstein *et al.*, 1990).

$$\text{Scores} = -0.32 * z_{press00} + -0.37 * z_{press06} + -0.40 * z_{press12} + -0.42 * z_{press18} \ldots 0.37 * z_{uu18}$$

Values from Table 6.3.2

z_{var} = standardised variable (Table 6.3.1)

The loadings for each component were similar for all stations (Table 6.3.2 and Appendix II-1) with the temperature and moisture variables loading the highest on component one. Cloud cover and the west scalar also load highly and positively on

component one, with visibility loading negatively. The pressure variable tended to load highly on either component two or three or both.

The component scores matrix, comprised of daily values for each retained component, which in the case of Flesland (Table 6.3.3) accounted for 80.7% of the variance of the original data matrix of 28 variables in just 6 components, all with an eigenvalue of greater than 1.0. This represents a significant reduction in 'noise' and the removal of any collinearity that may have existed in the original data matrix.

Total Variance Explained

	Initial Eigenvalues			Extraction Sums of Squared Loadings		
Component	Total	% Variance	Cumulative %	Total	% Variance	Cumulative %
1	**11.69**	**41.74**	**41.74**	11.688	41.744	41.744
2	**3.84**	**13.71**	**55.45**	3.838	13.708	55.452
3	**3.22**	**11.50**	**66.95**	3.220	11.501	66.953
4	**1.49**	**5.32**	**72.27**	1.489	5.318	72.271
5	**1.22**	**4.35**	**76.62**	1.218	4.351	76.623
6	**1.16**	**4.13**	**80.75**	1.155	4.125	80.748
7	0.85	3.03	83.78			
8	0.65	2.32	86.10			
9	0.49	1.76	87.86			
10	0.44	1.57	89.44			
11	0.38	1.36	90.80			
12	0.37	1.31	92.11			
13	0.33	1.17	93.28			
14	0.29	1.04	94.31			
15	0.26	0.92	95.23			
16	0.21	0.75	95.97			
17	0.19	0.69	96.67			
18	0.18	0.64	97.30			
19	0.15	0.54	97.85			
20	0.14	0.50	98.35			
21	0.11	0.40	98.75			
22	0.10	0.34	99.10			
23	0.08	0.29	99.39			
24	0.06	0.23	99.62			
25	0.05	0.19	99.81			
26	0.04	0.14	99.95			
27	0.01	0.04	99.99			
28	0.00	0.01	100.00			

Extraction Method: Principal Component Analysis.

Table 6.3.3 % Explained variance of each extracted component

6.3.2.2 Normalisation Constraints

An additional step was performed on the resultant component scores prior to clustering. The software package used to perform the PCA, SPSS (Statistical Package for the Social Sciencies), normalised the component matrix for each component by dividing by the relevant eigenvalue ie. component 1 in the component matrix for Flesland is divided by 11.69 from Table 6.3.3. The normalisation of component scores is based on the following -

$$\sum_{i=1}^{p} \alpha_{ki}^{2} = 1/\lambda_k ,$$

which gives var(z_k) = 1, for all k = 1,2,...p. (Jolliffe, 1990)

A second normalisation procedure is also possible, based on the following-

$$\sum_{i=1}^{p} \alpha_{ki}^{2} = 1 .$$

However, this constraint is normally employed in empirical orthogonal functions, a technique commonly applied in meteorology, but has the effect of distorting the relationship between components (Jolliffe, 1990).

For the purposes of this study, the normalisation constraint employed by SPSS was not considered appropriate and therefore a more appropriate normalisation constraint was adopted based on -

$$\sum_{i=1}^{p} \alpha_{ki}^{2} = \lambda_k ,$$

λ_k is the variance of z_k

The use of this normalisation constraint has the effect of increasing the loadings on the primary or leading Principal Components (PC) while decreasing those of the

latter, according to the components eigenvalue. The relative loadings of each variable remain unchanged (Jolliffe, 1990). This technique can be justified for use in this research as variables that are considered key determinants of air mass characterisation, such as temperature and moisture, load on the leading PCs and therefore their influence is weighted as more important than variables that load on the latter PCs.

6.3.2.3 Clustering Procedure

In order to classify days with similar component scores and hence, with similar characteristics, an automated, agglomerative and hierarchical clustering technique is performed on the normalised component scores matrix. A number of hierarchical clustering techniques are available to determine cluster membership employing methods such as, between-groups linkage, within-groups linkage, nearest neighbour, furthest neighbour, centroid clustering, median clustering, and Ward's method. Ultimately, the aim of any clustering procedure is to minimise within group variation while maximising the between group variation, producing a number of clusters comprised of homogenous data that are distinguishable from neighbouring clusters.

In the first step of an agglomerative hierarchical cluster analysis, each case represents an initial cluster. The second step results in the two most similar cases being grouped together. Successive grouping of similar cases and clusters continues until all cases eventually form one cluster. Once a cluster is formed, or a case has been assigned to a particular cluster, it cannot be split from that cluster, it can only be combined with another cluster. Various methods are used to determine similarity or dissimilarity between cases, the most common being the squared Euclidean Distance. The use of a particular cluster method then determines cluster membership based on the similarity/dissimilarity measure.

The most suitable clustering method selected for this study was the between-group average linkage method or unweighted pair-group method using arithmetic averages (UPGMA). The similarity statistic ($L_{1,2}$) for two clusters, 1 and 2 is as follows-

$$L_{1,2} = \frac{1}{N_1 N_2} \sum_{p=1}^{N_1} \sum_{q=1}^{N_2} D_{pq}^2,$$

p, q order of observations in 1 and 2,

D^2_{pq} squared Euclidean distance.

(Kalkstein *et al.*, 1987)

The between-group average linkage clustering method attempts to minimise the within-group variance while maximising the between group variance (Kalkstein *et al.*, 1987) by assessing the average squared Euclidean distance between all possible pairs of observations between two clusters and joining those that have the minimum average distance between them (Kalkstein *et al.*, 1987).

Ultimately the number of synoptic types identified and their characteristics will depend on the specification of the clustering algorithm and selection of a cut-off point in the clustering procedure (Yarnal, 1993). The clustering algorithm can have far reaching impacts in the derivation of homogenous synoptic types. Kalkstein *et al.* (1987) evaluated a number of algorithms commonly used in climatological research to determine which procedure yielded the most meaningful synoptic classification. They evaluated the Ward's, average linkage and centroid method utilising a similar methodology to the one employed in this research. They found that the Ward's method tended to produce clusters of similar size, thus, days on which extreme weather conditions were experienced were forced into clusters comprising of days on which less extreme weather occurred. This acted to increase the within group variance of clusters, thereby producing clusters that were less homogenous. The second method evaluated, that of the centroid method, produced one large group with many single day groups, again an unsatisfactory result when synoptic typing. The third method evaluated, that of the average linkage procedure was considered the most appropriate, as it minimised within group variances and maximised between group variances, producing distinctive and homogenous synoptic types while combining extreme weather days into distinct clusters (Kalkstein *et al.*, 1987).

Selection of the truncation point of the clustering procedure will also determine the number of clusters to retain and hence, number of synoptic types identified. Again, there are a number of tests that can be applied, none of which will give the 'correct' cut off point. A scree plot of the coefficient of determination against the cluster number can be produced to assess for breaks in slope (Figure 6.3.3). These breaks indicate that two dissimilar clusters are being grouped together, thus, changing the within and between group variances. This is a subjective technique as several breaks may occur.

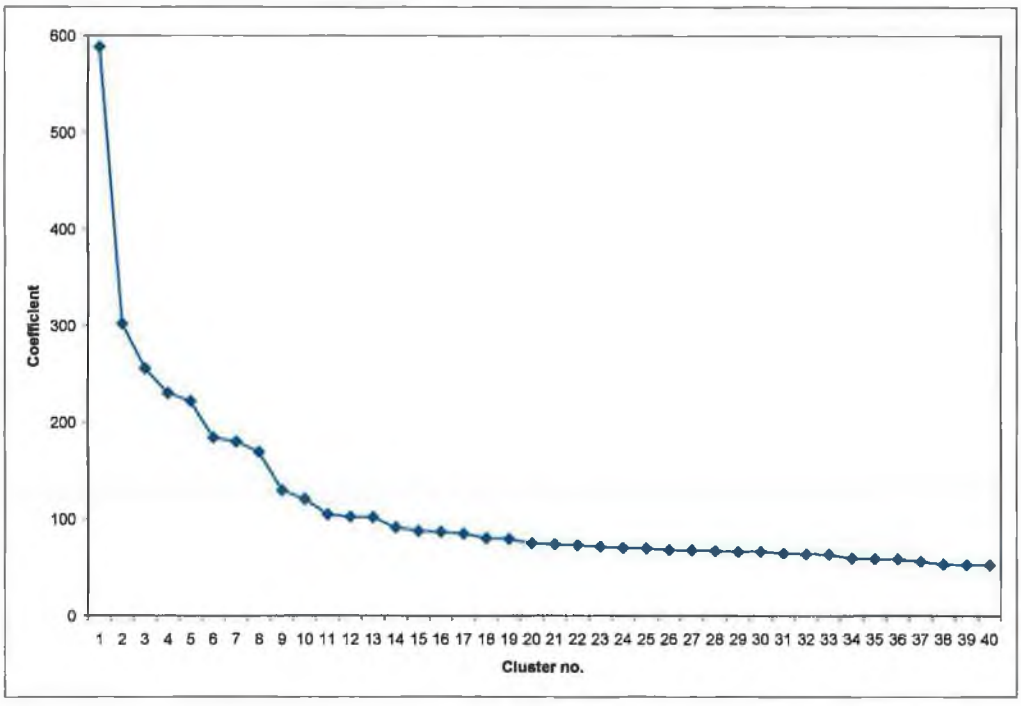

Figure 6.3.3 Scree plot of cluster centres for Flesland

Once the number of clusters to retain has been determined, each case representing a particular day can then be assigned to a cluster or homogenous synoptic type which can be assessed in terms of its meteorological elements. In a similar manner to the methodology employed by Kalkstein *et al.* (1990), any cluster or synoptic category that contained more than 15% of the total number of days was further subdivided by passing it through a second average-linkage clustering procedure, using the original normalised component scores for those days.

Mean characteristics for each synoptic type can be identified and days from each cluster can be compared to weather maps as an aid to interpretation. Changes in frequencies of air mass types can also be assessed. In addition, and a major advantage of using this particular methodology, within type changes in air mass characteristics can be assessed. This is a crucial part of the methodology of the 'Temporal Synoptic Index' as air mass frequencies may remain constant, while they may still be undergoing modification as a consequence of climate change. Thus, any study, which analyses air mass frequency changes as an indicator of climate change could, incorrectly conclude that, in the absence of a noticeable or significant change in frequencies, climate change may not be occurring.

6.4 Conclusion

This chapter applied a synoptic-climatological methodology, which has been successfully used in a number of other studies, to five synoptic stations in Norway. The methodology was selected primarily because it incorporated key climate variables which characterise airmass types into an automated classification procedure. Analysis of climate at the synoptic scale also fulfils two requirements of this study - establishing links between the large-scale atmospheric circulation, local weather elements and glacier mass balance, which provided the focus of research for previous chapters and secondly, the utilisation of readily available meteorological data remotely measured from the glacier.

The use of such an automated technique results in a methodology which, aside from being reproducible, is readily transferable. While the technique is reasonably robust, a number of subjective decisions, some of which are more critical than others, are required. However, these are not considered detrimental to the analysis.

Chapter VII

Temporal Synoptic Index results

7.1 Introduction

This chapter will concentrate on an analysis of the results from the synoptic scale classification, presented in the previous chapter, and glacier mass balance. This analysis will initially involve an assessment of air mass types and characteristics to determine if changes have occurred in the frequency of occurrence or in the characteristics of particular air mass types. The principal objective of this chapter however will be an examination of the relationship between the synoptic classification and glacier mass balance.

It is also intended to conduct a more detailed analysis on one particular glacier, that of Rembesdalskåka, an outlet glacier from Hardangerjøkulen in southern Norway, assuming linkages exist between the synoptic classification and glacier mass balance. This case study will try to establish if recent changes evident in its mass balance can be attributed to any recent changes in climate that may have occurred and which are reflected in the air mass frequencies. These results will then provide the basis for the remainder of the thesis, which proposes to assess likely future changes in air mass frequencies and the consequent effect on glacier mass balance. Likely changes in the future glacier behaviour of Rembesdalskåka, as a consequence of climate change, will also be examined.

7.2 Results from temporal synoptic index

7.2.1 Principal Components

While the number of components extracted from each station for winter varied between four for Nordstraum to six for Flesland and Skabu, the first principal component for all stations was dominated by the thermal and moisture variables, indicating their relative importance in the air mass classification (Appendix II). Cloud amount and its related variable, visibility, also loaded highly on the first

component. The primary component at all stations accounted for a minimum of 30% of total variance at Skabu to a maximum of 41% of total variance at Flesland.

The second component tended to comprise of the *uu* and *vv* wind scalars for the majority of stations indicating a strong directional component. Pressure also exerted an influence on this component for Flesland, Orlandet and Skabu, while for Nordstraum, pressure loaded highest on the third component. Pressure is the dominant variable for all stations, except Bodo, on component three. The wind scalars also have a contribution to this component again suggesting a directional component. Component four, appears to comprise of cloud, visibility and the wind scalars, but in contrast to component one, cloud amount loads negatively while visibility is positive for all stations, except Skabu. Component five and beyond are more difficult to interpret.

In all, extracted components, with eigenvalues greater than 1.0, accounted for a minimum of 73% of total variance at Skabu to a maximum of 82% at Bodo. This represents a substantial reduction in noise and in the data size with very little loss of data for all stations.

The component loadings for the extracted components for the summer months differ from those of the winter loadings. The dominance of the thermal and moisture variables on the first component, evident during the winter months, are less apparent. Moisture, cloud amount, visibility and the wind scalars are the dominant variables for the southern station of Flesland. While pressure, which loads negatively, also contributes to this component for the southern stations of Flesland and Bergen. The central and northern stations have a large thermal loading for component one, unlike their southern counterparts. While for the more continental station of Skabu, the influence of the thermal variable appears to have a diurnal influence and the component is dominated by the pressure variables. Orlandet, Bodo and Skabu show a diurnal strengthening of the thermal variable indicating increased variability possibly due to the warming of the landmass during the day. While no such influence for the southern, maritime influenced stations is obvious, possibly indicating a moderating influence of the ocean on daytime temperature variation during the summer months at these locations.

Component two is essentially a thermal and moisture component, for all but the northern most station, Nordstraum. The influence of pressure also plays an important contribution to this component, especially for the southern, maritime stations. Again there is little consistency across stations for component three. For the southern stations, moisture and the wind scalars appear most important, while for the central stations of Orlandet and Bodo, the component is dominated by pressure. At Skabu, visibility and the *vv* scalar, with a negative pressure component are the key influences on this component. While humidity, visibility and the scalars, all interrelated variables, are most important for Nordstraum.

Interestingly, pressure is again a key ingredient for component four at the southern stations and Nordstraum. The *vv* scalar dominates for the central stations. After component four, interpretation again becomes increasingly difficult.

7.2.2 Cluster characteristics

Having determined the number of clusters to retain from an examination of break points in the scree plots, each cluster type was then characterised in terms of the mean of its seven weather elements. These clusters were classified according to the similarity of their weather elements and therefore should represent homogenous air mass types. Any cluster that comprised of more than 15% of the total number of days were sub-clustered. Mean characteristics for the sub-clusters were also derived (Table 7.2.1-Table 7.2.10).

To determine what circulation types the resultant air masses were associated with, gridded daily mean sea level pressure for a domain over Europe (Long 20^0 W-30^0 E, Lat 30^0 N-80^0 N) was extracted from the National Centres for Environmental Prediction (NCEP/NCAR) reanalysis data. This data, which exists on a 2.5^o x 2.5^o grid, was then averaged to produce a composite mean pressure surface for each cluster, at each station (Appendix III). Each composite surface, representing daily averaged mean sea level pressure, was then mapped in order to infer the large-scale circulation types associated with each cluster type and station location. Only composite surfaces for the primary air mass types were mapped. Due to differences in scale between both datasets, some discrepancies arose with regards

to the large-scale circulation and station level wind directions. However, these differences do not present any inconsistency due to the different nature of the datasets being compared.

7.2.2.1 Winter

Nine major synoptic air mass categories, defined as containing 20 or more days, were identified for Flesland; three of which contained more than 15% of the total number of days and were sub-clustered (Table 7.2.1). Nine categories were also identified for Orlandet and Skabu (Table 7.2.2, Table 7.2.3), with two categories in each requiring further sub-clustering. Eleven synoptic categories were identified for Bodo, one of which contained days greater than 15% of total (Table 7.2.4). Nordstraum produced the least number of categories, eight, with two requiring sub-clustering (Table 7.2.5). An element common to all stations was that one of the categories requiring sub-clustering tended to be associated with an easterly wind direction recorded at the station level.

The coldest synoptic categories at all stations during winter were associated with an easterly circulation type. Humidity for these categories was also very low, resulting from cold dry air being advected off the continental land mass. While the warmest synoptic categories were all associated with westerly circulation types. These westerly associated air mass types also produced some of the highest humidity values, associated with warm, moist air advected off the ocean. This maritime-continental divide is evident at all stations during the winter season.

To investigate any changes that may have occurred in the frequencies of the synoptic categories over the observed period, yearly frequencies of the coldest and warmest air mass types were examined. The coldest and warmest categories were selected as it is expected that these categories are likely to be more sensitive to any changes that may have occurred in climate as a consequence of global warming.

	Number of days	Pressure (hPa)	Temperature (°C)	Specific Humidity	Cloud Cover	Visibility (km)	Wind Direction and Speed	Circ Type
1								SW
1a	98	1006	0.6-1.9	0.35-0.38	6-7	29-32	ESE, Light Air	
1b	17	1015-1013↓	-1.3- 1.0	0.28-0.33↑	5-7	27-33	SE-SSE, Light	
1c	105	1021	-1.2- 0.9	0.32-0.33	4-6↑	31-35	ESE-SE, Light Air	
1d	107	1027	0.9-2.1	0.42-0.47↑	7	25-18↓	SE, Light Air	
1e	16	1035	0.0-2.3	0.42-0.46	4-6↑	26-35	E/ESE, Light Air	
1f	34	1017-1024↑	1.8-3.2	0.51-0.43↓	3-6	26-41	SW-SSE, Light Air	
1g	14	1024-1027↑	3.0-5.4	0.63-0.51↓	7-3↓	17-36	ESE-SSW, Light Air	
2	173	998-1001	-1.7-0	0.33-030↓	4-5	33-43	SSE-SE, Light Air	NW
3								AE
3a	199	1012-1014↑	-3.1– -1.0	0.24-0.26	3-4	40-52	E, Light Air	
3b	170	1024-1025	-5.0– -1.5	0.19-0.20	1-2	53-61	E, Light Air	
3c	64	1002-1004↑	-7.3– -3.5	0.17-0.19	1-2	55-64	E, Light Air	
3d	80	1031	-1.8- 1.6	0.30-0.33	2-3	38-47↑	ESE-SE, Light Air	
3e	19	1022-1026	-2.6- 1.2	0.23-0.27↑	2-7↑	51-39↓	SE, Light	
3f	9	1030-1027↓	-5.0- 0.0	0.21-0.28↑	0-8↑	70-35↓	E-SSE, Light	
4								SW
4a	230	1020-1018↓	3.4-4.4	0.55-0.61↑	7	17-15↓	S/SSE, Light	
4b	127	1007-1003↓	2.9-4.0	0.42-0.48↑	7	28-23↓	SE/SSE, Gentle	
4c	25	990-989	1.4-2.7	0.34-0.37↑	7	24-28	ESE/SE, Light	
4d	9	1029-1024↓	2.9-3.9	0.41-0.46↑	6-8↑	18-29	SSE, Gentle	
5	145	988-984↓	4.4-4.8	0.62-0.64	7-8	17-19	SSE/S, Gentle	SW
6	296	993-997↑	2.7-1.9↓	0.52-0.47↓	6-7	22-27	S, Light	CS
7	171	1013-1008↓	5.7-6.5	0.72-0.80	8	11-14	S, Gentle	ASW
8	189	1001-1003	5.1-5.9	0.73-0.64↓	7-8	13-18↑	SW/WSW, Light	AW
9	15	1004-1010↑	5.0-3.4↓	0.65-0.47↓	5-7	18-25↑	WSW/WNW, Gentle	ANW
10	20	1025-1027	-11.2– -6.8	0.10	0-1	63-68	E/SE, Light Air	SE
11	5	967-971	5.4-3.5	0.78-0.53↓	6-8	11-20	SW-WNW, Gentle	CW
12	14	989-991	6.6-7.8	0.92-1.0	8	10-15	S-SSW, Gentle	CSW

Table 7.2.1 Flesland mean winter diurnal range of meteorological variables (↓ indicates increasing or decreasing diurnal trend)

	Number of days	Pressure (hPa)	Temperature (°C)	Specific Humidity	Cloud Cover	Visibility (km)	Wind Direction and Speed	Circ Type
1								CSE
1a	58	997-995↓	-2.0– -1.3	0.26-0.27	2-3	51-58	ESE, Gentle	
1b	73	1007-1005↓	-4.8 – -4.0	0.24-0.25	4-5	39-45	ESE, Light	
1c	158	1018-1017	-0.8 – -0.3	0.35-0.32↓	3-4	46-53	SE, Light	
1d	18	1018-1012↓	-1.3 – -0.2↑	0.25-0.23↓	2-3	59-65	SE, Moderate	
1e	39	1010-1006	0.8-2.0	0.29-0.30	4-6	51-58	SE, Moderate	
1f	24	989-996↑	-6.4 – -1.8↓	0.32-0.21↓	5-3↓	41-56	ENE-ESE, Light	
2	40	1023-1024	-11.4 – -10.3	0.12-0.14	1-2	46-47	E/ESE, Gentle	SE
3	320	995-991↓	2.0-2.9	0.38-0.42	5-6	46-53	SE, Gentle	CSW
4	341	1011-1012	-0.9 – -0.8	0.38-0.36↓	5-6	33-38	SSE, Light	SW
5	274	1021-1020	-5.4 – -4.4	0.21	1-2	52-54	ESE, Gentle	SE
6								W
6a	214	1005-1006	3.5-3.8	0.58-0.60	7	23-26	SW, Gentle	
6b	175	1007-1005↓	1.9-2.6	0.47-0.51↑	6-7	33-37	S, Light	
6c	92	1025-1026	3.4-3.9	0.56-0.58	6-7	29-36	SSW, Light	
6d	81	991-988↓	3.1-3.8	0.51-0.58↑	7	36-28↓	S-SSW, Gentle	
6e	35	975-982↑	2.6-2.2↓	0.51-0.55	6-7	22-23	SW-WSW, Gentle	
6f	15	987-983↓	4.7-6.5	0.60-0.74	8-7↓	37-24↓	SE-SSW, Gentle↑	
7	162	1003-1010↑	1.3-0.7↓	0.46-0.42	7	23-25	W, Gentle	ANW
8	125	1013-1014	5.8-6.2	0.75-0.80	7-8	19-21	WSW, Moderate	AW
9	43	996-999↓	-10.1 – -9.3	0.15-0.16	3-4	37-36↓	E, Light	E
10	8	992-987	5.6-6.4	0.82-0.90	8	9-14	SW-W, Moderate	AW

Table 7.2.2 Orlandet mean winter diurnal range of meteorological variables (↓ indicates increasing or decreasing diurnal trend)

	Number of days	Pressure (hPa)	Temperature (°C)	Specific Humidity	Cloud Cover	Visibility (km)	Wind Direction and Speed	Circ Type
1								SW
1a	121	1030-1031	-12.4--8.3	0.11-0.13	0-1	22-34	NE-SSE, Light Air	
1b	87	1020-1021	-8.7--6.7	0.17-0.19	5-6	11-17	E-ESE, Light Air	
1c	87	1028-1029	-7.5--3.9	0.17-0.2	1-2	19-27	ESE-SSW, Light Air	
1d	169	1014-1015↑	-11.7--8.9	0.12-0.13	2	15-29	ESE-S, Light Air	
1e	44	1006	-16.8--15.2	0.08-0.09	3	10-17	ENE-ESE, Light Air	
1f	17	1001-1006↑	-11.1--8.4	0.11-0.14↓	1-4	12-29	SW-NNW, Light	
1g	92	999-1000	-13.9--12.2	0.11-0.12	4	11-15	E-ESE, Light Air	
1h	12	1030-1032↑	-14.4--12.2	0.11-0.13	6-7	7-12	NNE-E, Light Air	
1i	12	1019-1025↑	-6.1--2.7	0.17-0.2	1-2	27-38	SE-NNW, Light	
1j	6	1003-1008↑	-7--5.1	0.16-0.18↓	3-5	11-38	WNW-NNW, Gentle	
2								W
2a	85	1023	-3.1--0.5	0.27-0.29	3-3	21-29	SE-S, Light Air	
2b	22	1002-1008↑	-8.8--6.3	0.13-0.16↓	1-2	13-32	WSW-W, Light	
2c	140	997-998	-9.3--8	0.19-0.21	7	6	E-ESE, Light Air	
2d	184	1000-1002↑	-7--5	0.20-0.21	3-4	18-32	SSE-S, Light Air	
2e	14	978-982↑	-11.8--9.4	0.14-0.16	3-4	24-30	SSE-S, Light Air	
2f	12	1021-1022↑	0.3-2.4	0.29-0.31	3-4	30-36	SSW-WNW, Light	
2g	37	1002-1003	-2.3--0.4	0.30-0.31	3-4	26-37	SSE-S, Light Air	
2h	64	1016-1017↑	-4.9--3.4	0.26-0.27	6-7	7-10	ESE, Light Air	
2i	15	989-993	-6.3--4.2	0.16-0.22↓	2-3	17-36	WSW, Light	
2j	8	996-1003↑	-3.4--3.2	0.25-0.28	5-6	6-21	SSE-W, Light	
3	33	1023-1025↑	1.3-3.0	0.39-0.43↓	3-4	35-45	SE-S, Light Air	AW
4	149	1018-1019↑	-18.3--15.5	0.07-0.08	0-1	36-43	NE-ESE, Light Air	AE
5	5	974-982↑	-7.2--5.7	0.16-0.20↓	5-6	10-24	NW-NNW, Gentle	CNW
6	146	1014-1015	-7.6--5.2	0.18-0.20	1-2	72-74	E-ESE, Light Air	AW
7	157	990-988↓	-3.4--2.1	0.32-0.35	6-7	13-14	ESE-SSE, Light Air	CSW
8	20	998	-0.7-0	0.32-0.34	4	75-79	SE-S, Light	CW
9	56	1000-1001	-1.3-0.4	0.28-0.33↓	3-4	16-29	SSW-SW, Light	CW
10	29	1000-998↓	1.8-2.8↑	0.44-0.47	5-6	19-23	SSE-SSW, Light	CSW
11	5	1028-1033↑	-4.3--2.4	0.18-0.18	1-2	24-35	SSW-WNW, Gentle	ANW

Table 7.2.3 Skabu mean winter diurnal range of meteorological variables (↓ indicates increasing or decreasing diurnal trend)

	Number of days	Pressure (hPa)	Temperature (°C)	Specific Humidity	Cloud Cover	Visibility (km)	Wind Direction and Speed	Circ Type
1	206	995	-3.5 – -3.0	0.25	5-6	55-49↓	ESE, Gentle	CS
2	263	1010-1011	2-2.5	0.46	7	31-36	SSW, Gentle	ASW
3								S/SE
3a	50	1007-1004↓	-3.8 – -2.9	0.21-0.22	3-6↑	75-65↓	ESE, Moderate	
3b	138	1009	-6.8 – -6.1	0.18	2-4	65-70	E, Gentle	
3c	56	1013	-5.5 – -4.7	0.19-0.22↑	5-7	64-40↓	ESE/E, Gentle	
3d	84	991-993	-5.4 – -6.8↓	0.21-0.18↓	3-4	61-72↑	E, Gentle	
3e	14	1009-1013↑	-3.6 – -7.3↓	0.27-0.17↓	7-2↓	22-75↑	SSE-E, Light	
3f	81	1028	-2.3 – -2.9	0.22-0.24	2-3	68-70	ESE/E, Gentle	
3g	7	1028-1025↓	0.5-1.2	0.23-0.26	1-4↑	80-64↓	ESE, Moderate	
3h	13	1016-1014↓	-6.8 – -7.4	0.13	4-5	75-78	SE, Moderate	
4	217	1014-1015	-8.5 – -8.0	0.15	1-2	75	E, Gentle	CE
5	125	1007-1004↓	5.5	0.67-0.70	8	19-19	SW-WSW, Moderate	SW
6	114	987	3.1-3.7	0.54-0.56	7	24-26	SSW-SW, Gentle	AW
7	218	1002-1005↑	-0.5 – -1.6	0.35-0.30↓	6-7	27-37↑	SW-SSW, Light	SW
8	210	995-922↓	1-1.6	0.34-0.37↑	6-7	58-50↓	ESE, Gentle	CSW
9	132	1021-1022	-0.7 – -1.1	0.30-0.28↓	5	59-66	ESE, Light	AS
10	142	1019	3.6-4.4	0.56-0.60	7-8	24-27	SSW-SW, Gentle	AW
11	82	984	1.5-1.8	0.44-0.46	7	35-38	SSE, Light	W
12	6	989-985	-12.6 – -11.9	0.11-0.13↑	3-6↑	63-29↓	ENE-E, Gentle	CSE
13	10	1012-1024↑	1.8-0.9↓	0.45-0.33	6-8	22-28	WNW, Moderate	NW
14	8	963-961	-0.5 – -1.0	0.30-0.32	5-8	70-60	ESE, Gentle	CSE

Table 7.2.4 Bodo mean winter diurnal range of meteorological variables (↓ indicates increasing or decreasing diurnal trend)

	Number of days	Pressure (hPa)	Temperature (°C)	Specific Humidity	Cloud Cover	Visibility (km)	Wind Direction and Speed	Circ Type
1								S
1a	176	1001	-9.8 – -9.3↓	0.15	2-3	48-50	SSE, Light	
1b	236	1021-1022	-6.8 – -6.3	0.17-0.18	2	53-56	SSE, Light	
1c	140	1014-1015	-12.1 – -11.7	0.11	1	51-55	SE/SSE, Light	
1d	29	981-982	-8.3 – -7.37↓	0.18	2-4	51-54	SSE, Light	
1e	20	1023-1024	-9.5 – -9.3	0.14	3-4	34-40	SSE-SE, Light	
1f	19	1001-995↓	-7.9 – -7.3↓	0.18-0.19	5-7	48-40↓	SSE, Gentle	
1g	29	998	-10.0 – -10.8↑	0.13-0.15↑	5-6	17-38	SE, Light	
1h	9	995-993↓	-16.9 – -15.7↑	0.08-0.09	2-5↑	18-41	SSE, Light	
2								SE
2a	156	1006-1007	-7.9 – -7.4↑	0.18-0.20	5-6	29-31	SE/SSE, Light	
2b	88	1024-1025	-3.6 – -2.8 ↓	0.28-0.25↓	5-3↓	46-52	SSE, Light	
2c	242	1003-1001↓	-4.0 – -3.4	0.24-0.25	4-5	50-51	SSE, Light	
2d	24	1007-1005↓	-3.9 – -3.1	0.23-0.24	1-2	60-65	SSE/S, Gentle	
2e	30	989-985↓	-7.0 – -6.7	0.19-0.21	5-7	37-26↓	SSE, Gentle	
2f	129	1015-1016	-1.8 – -1.2	0.31-0.32	5-6	43-45	SSE, Light Air	
2g	101	992-993	-4.4 – -3.6↑	0.25-0.29	6-7	39-30↓	SSE/S, Light	
2h	8	1028-1029	-0.2- 2.76↓	0.46-0.34↓	4-2↓	53-56	SSW-SE, Light	
3	294	1000-1003↑	-4.0 – -3.7	0.26-0.28	6-7	18-24	WSW, Light	NW
4	199	985-986	0.5-0.9	0.41-0.45↑	6-7	39-29↓	S/SSW, Light	W
5	196	998-1003↑	-1.1 – -0.5	0.38-0.40	7	12-16	WNW, Gentle	ANW
6	193	1014-1015	1.4-2.0	0.45-0.47	6-7	35-40↑	SSW, Light Air	AW
7	71	1003-1006↑	3.4-4.4	0.58-0.60	7	21-25	SW-W, Light	AW
8	241	993-991↓	0.4-0.9	0.37-0.38	5-6	50-51	S, Light	CS
10	8	970-965↓	-5.0 – -4.3↓	0.23-0.26↑	6	45-56	S/SSE, Gentle	CS

Table 7.2.5 Nordstraum mean winter diurnal range of meteorological variables (↓ indicates increasing or decreasing diurnal trend)

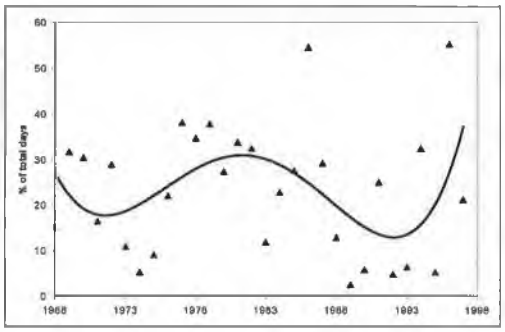

Figure 7.2.1 Flesland cold (TSI 3)

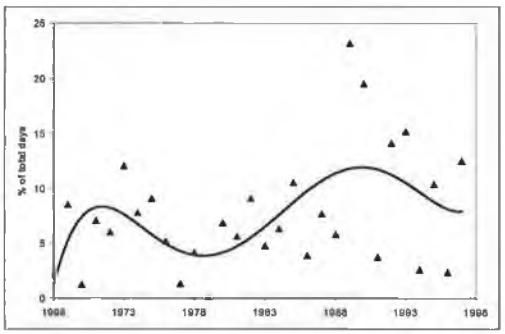

Figure 7.2.4 Flesland warm (TSI 7 +12)

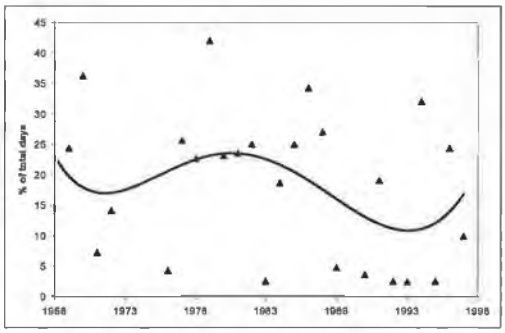

Figure 7.2.2 Orlandet cold (TSI 2 +5+9)

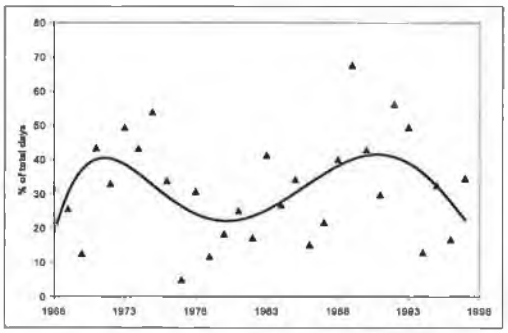

Figure 7.2.5 Orlandet warm (TSI 6+8)

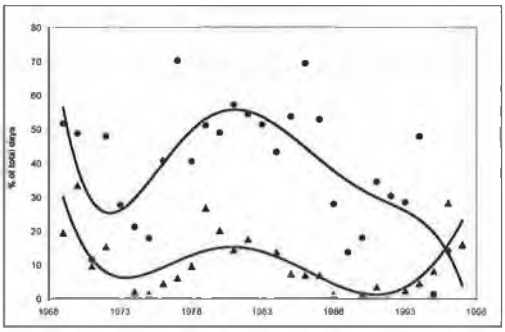

Figure 7.2.3 Skabu cold (TSI4-coldest (▲) and TSI1-second coldest(●))

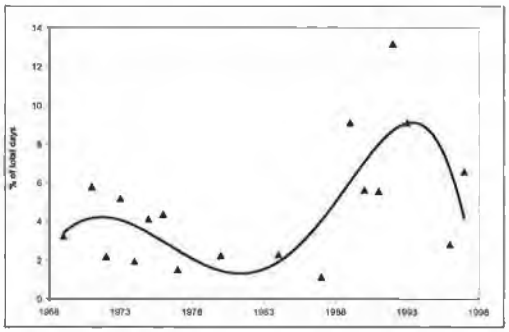

Figure 7.2.6 Skabu djf warm (TSI 3 +10)

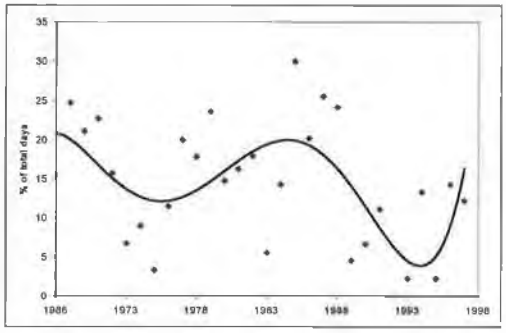

Figure 7.2.7 Nordstraum cold (TSI 1b+1c)

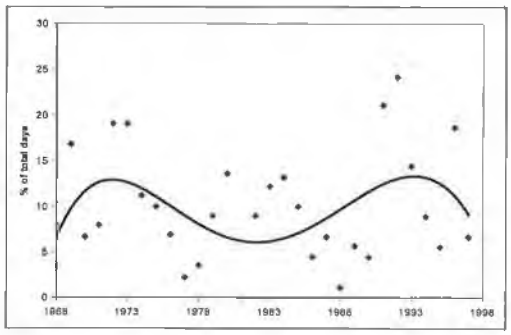

Figure 7.2.9 Nordstraum warm (TSI 6+7)

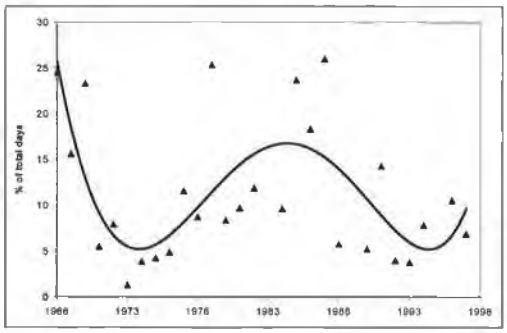

Figure 7.2.8 Bodo cold (TSI 4)

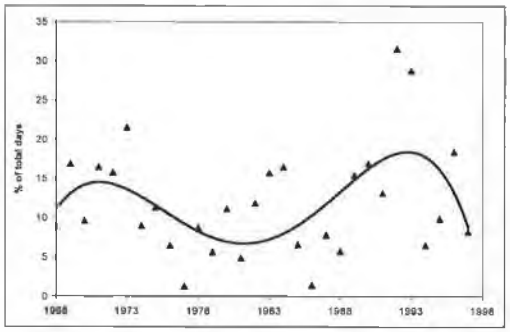

Figure 7.2.10 Bodo warm (TSI 5 + 10)

Figure 7.2.1-Figure 7.2.10 display the frequencies of both the coldest and warmest air mass types for all stations for winter. There appears to be a marginal decrease in the frequencies of the coldest air mass types up until the early 1990s. After 1993/1994, the frequencies of the coldest types start to show an increasing trend that is marked at all stations. The second coldest cluster from Skabu, a continental station, was included as the number of occurrences of cold days was considered low and this does however show a decreasing overall trend from the late 1970s. There is a marked comparison in the frequencies of the coldest type with an increase evident in the late 1970s to early 1980s and a decline afterwards until the 1990s. This increase occurs with a slight lag at the two more northern stations of Bodo and Nordstraum.

An analysis of frequencies of the warmest synoptic categories for winter suggests slight increases in occurrence at Flesland, Skabu and Bodo, with frequencies at Orlandet and Nordstraum remaining fairly constant. The increase in frequency starts in the late 1970s and early 1980s. The largest occurrences for all stations occurs in

the late 1980s and early 1990s, with some stations showing an increase for some years more than double their average during this period, with a decreasing trend after this. The similarity in the timing of this increase would suggest that a circulation scale as oppose to a regional scale driver was in operation.

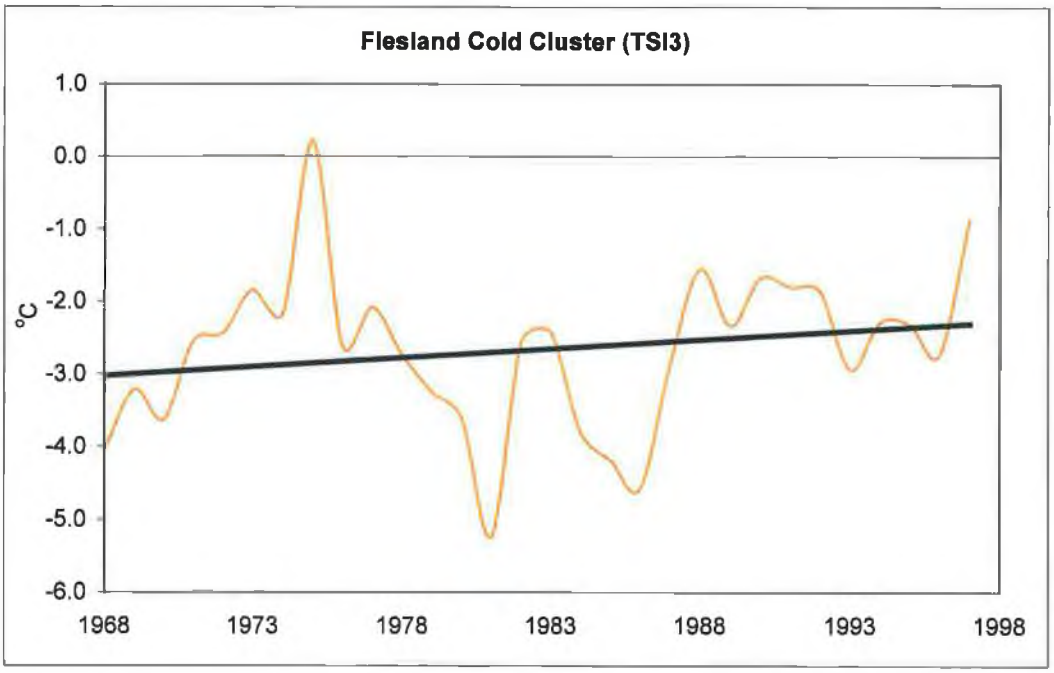

Figure 7.2.11 Mean temperature of cold cluster (TSI3) from Flesland

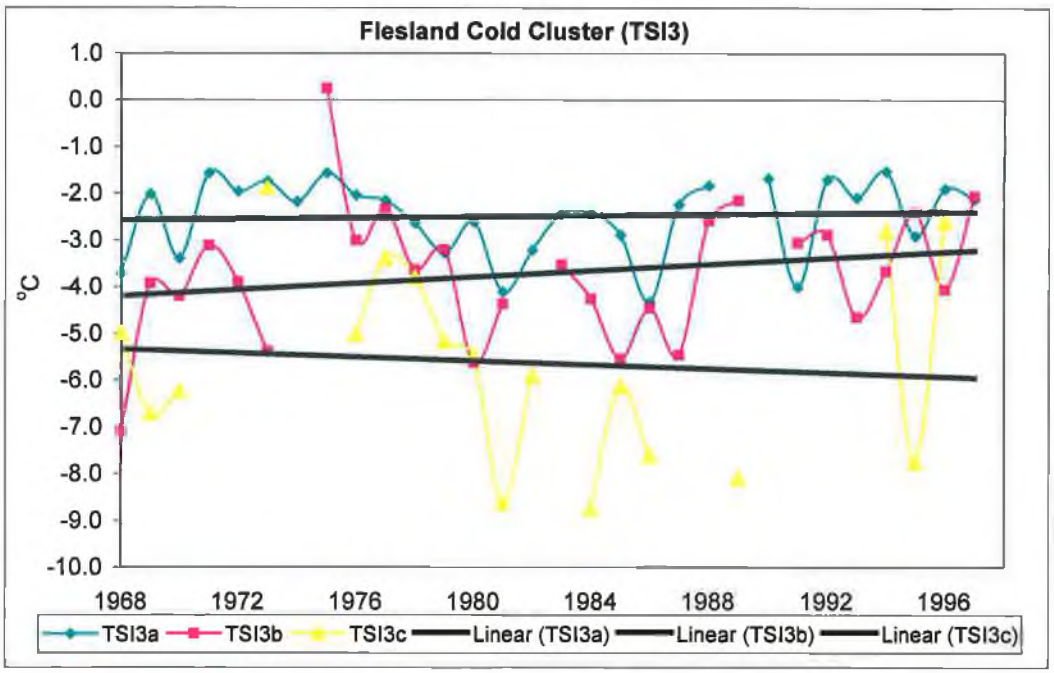

Figure 7.2.12 Mean temperature of cold cluster (TSI3a, TSI3b and TSI 3c) from Flesland

An analysis of within category temperatures suggests that some degree of modification of the coldest and warmest air mass types has occurred over the period of analysis. The coldest cluster from Flesland (in the case of Flesland all TSI 3 was included in this category), Bodo and Nordstraum appear to have warmed slightly over the 1968-1997 period (Figure 7.2.11, Figure 7.2.13, Figure 7.2.14). However, contradictory results are suggested when within category temperatures are assessed for sub-cluster 3 (TSI3) from Flesland (Figure 7.2.12). The temperature of the coldest sub cluster, TSI 3c, appears to be getting increasingly colder. Slight warming in the remaining sub clusters within this category is compensating for this decrease in temperature in TSI 3c.

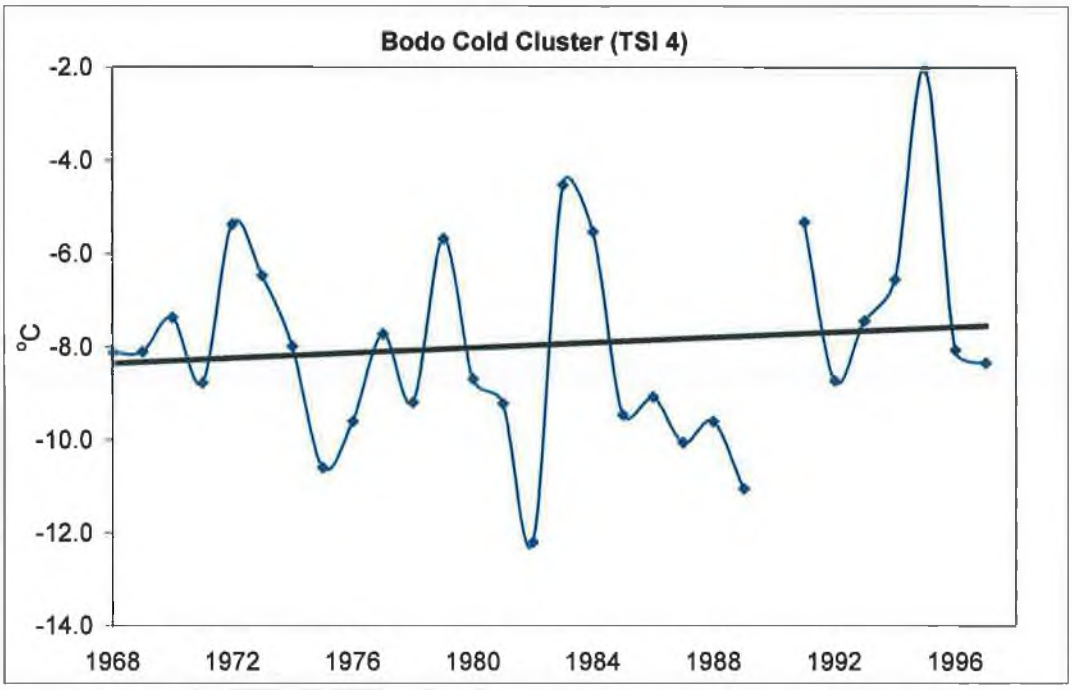

Figure 7.2.13 Mean temperature of cold cluster (TSI4) from Bodo

In contrast, no obvious trend was detected in the warm cluster types with the exception of Nordstraum, which was the only station to display an increasing trend in the average temperature of its warm cluster types during the winter season (Figure 7.2.15).

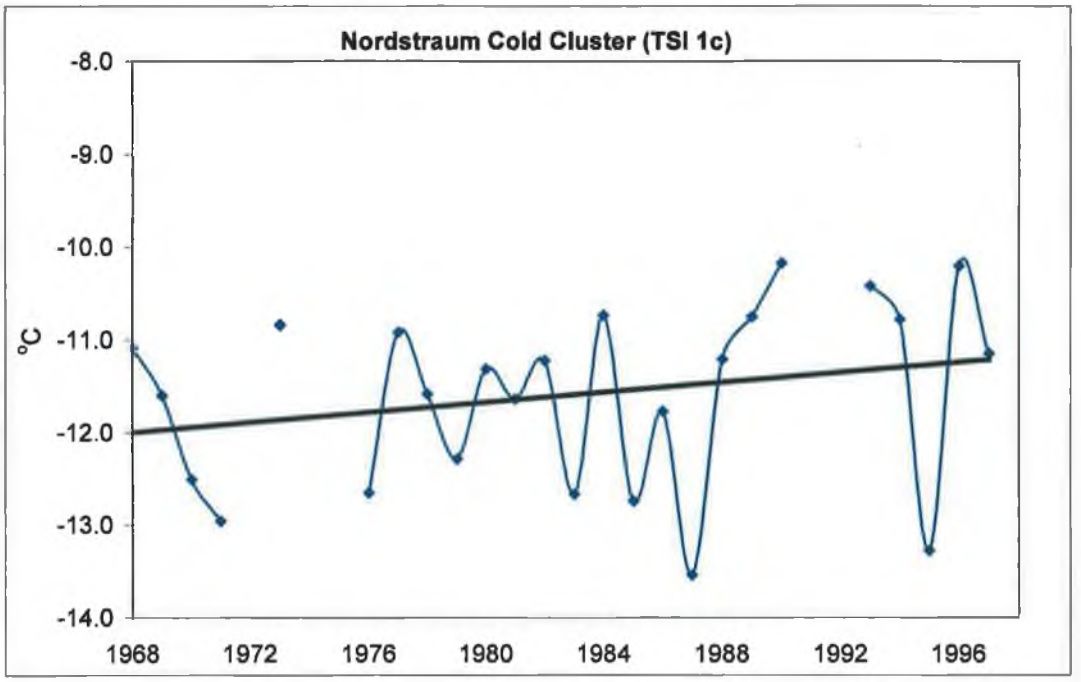

Figure 7.2.14 Mean temperature of cold cluster (TSI 1c) from Nordstraum

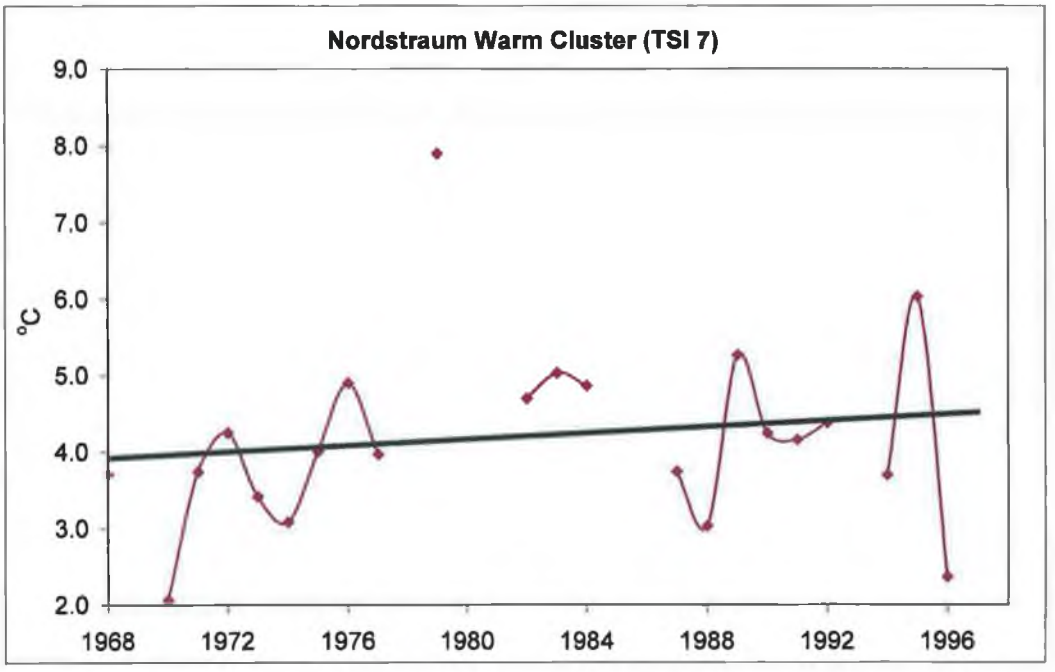

Figure 7.2.15 Mean temperature of warm cluster (TSI 7) from Nordstraum

7.2.2.2 Summer

	Number of days	Pressure (hPa)	Temperature (°C)	Specific Humidity	Cloud Cover	Visibility (km)	Wind Direction and Speed	Circ Type
1	271	1021-1020	11.4-18.9	1.23-1.40	3	42-54	SE-W, Light Air	SW
2								CW
2a	479	1009-1010	11.6-13.9↑	1.34-1.38	7	22-25	SSE-SW, Light	
2b	69	1002-1000↓	11.3-12.6↑	1.23-1.31↑	7	20-25	SSE-S, Light	
2c	32	994-997	10.6-11.8↑	1.17-1.35↓	7-8	15-20	S-SW, Light	
2d	30	1004-1000↓	9.6-13.4↑	0.92-0.97	5-7	33-46	E-SSE, Light	
2e	7	997-1000	7.2-8.7↑	0.72-0.9↑	7-8	18-27	SE-SW, Light	
2f	30	1004-1009↑	12.7-14.2↑	1.47-1.87↓	6-7	15-32	WSW-WNW, Light	
3								NW
3a	180	1009-1010↑	9.9-12.6↑	1.00-1.15↓	6-7	21-38	SW-WNW, Light	
3b	189	1016-1017	9.9-14.5↑	1.02-1.15	5-6	32-46	S-WNW, Light Air	
3c	69	1000-1002	9.4-11.5↑	0.98-1.07↓	7	20-32	SW-WNW, Light	
3d	71	1006-1007	10.7-16.2↑	1.10-1.26	5-6	41-58	ESE-W, Light Air	
3e	93	1012-1013	12.2-17.3↑	1.39-1.65↓	4-6	23-43	SSE-WNW, Light Air	
3f	73	1022-1023	11.3-14.8↑	1.26-1.37	5-7	26-31	SSE-W, Light Air	
4								CNW
4a	77	1014-1017↑	9.3-12.1↑	0.80-0.99↓	5-6	25-54	WNW-NW, Light	
4b	208	1018	9.6-15.5↑	0.96-1.07↓	2-3	44-62	SW-NW, Light	
4c	78	1005-1006	7.6-13.2↑	0.81-0.92	4-5	46-56	SE-WNW, Light Air	
4d	86	1010	7.6-13.5↑	0.75-0.80	2-4	55-68	SW-NW, Light	
4e	44	1015-1017↑	7.8-12.5↑	0.68-0.71	2	57-71	WNW-NW, Light	
4f	12	1026-1027	6.5-13.5↑	0.63-0.74	1-4	64-73	WSW-NW, Light Air	
4g	12	1004-1012↑	8.6-10.5↑	0.74-1.14↓	5-8	13-43	WNW-NNW, Light	
4h	10	1004-1006↑	7.9-11↑	0.66-0.76↓	4-6	41-63	NNW, Light	
5	13	1020-1021	6.6-12.3↑	0.69-0.88	2-7↑	37-66↓	SE-S, Light Air	SW
6	113	1016-1014↓	14.6-20.6↑	1.66-1.79	4-5↑	33-39↓	ESE-SW, Light	ASE
7	51	1017-1014↓	10.6-14.4↑	0.98-1.39↑	5-8↑	21-40↓	SE-SSE, Light	S
8	165	1011-1010	14.6-16↑	1.87-2.01↑	7	17-19↑	SSE-SSW, Light	CSW
9	104	1021-1020↓	14.8-23.7↑	1.68-2.14	2	40-52↑	E-WNW, Light Air	E
10	10	1021	16.7-23.7↑	3.01-3.90	3-5↑	27-34↑	ESE-WSW, Light Air	SE
11	26	1017-1016	16.4-19.5↑	2.53-2.91	6-7	13-19↑	SSE-SSW, Light	ASE

Table 7.2.6 Flesland mean summer diurnal range of meteorological variables (↓ indicates increasing or decreasing diurnal trend)

Nine major categories were also identified for Flesland during the summer months, three of which were sub clustered due to their size (Table 7.2.6). Eleven synoptic categories were uncovered for Orlandet, two requiring further clustering (Table 7.2.7). The continental station of Skabu (Table 7.2.8) and more northern station of Bodo (Table 7.2.9), both produced seven synoptic categories, again with two requiring sub-clustering for Skabu and three for Bodo. The northern most station, Nordstraum, produced the least amount of synoptic categories, six, three of which required further sub-clustering (Table 7.2.10).

	Number of days	Pressure (hPa)	Temperature (°C)	Specific Humidity	Cloud Cover	Visibility (km)	Wind Direction and Speed	Circ Type
1								SW
1a	158	1020	9.9-14.0↑	1.20-1.28	6-4↓	39-57↑	S-WSW, Light Air	
1b	87	1006	7.5-11.3↑	0.88-0.91	5-6	46-62↑	SSE-W, Light	
1c	114	1016	8.9-11.8↑	1.05-1.02↓	6	38-53↑	SSW-W, Light	
1d	47	1024-1026↑	9.7-11.9↑	1.09-1.00↓	7-4↓	30-57↑	SW-WNW, Light	
1e	238	1009	9.8-13.5↑	1.19-1.33↑	6	42-50↑	SSE-SW, Light Air	
2	370	1015	12.3-15.9↑	1.67-1.89↑	5-6	31-38↑	S-WSW, Light Air	SW
3	199	1014-1011↓	10.9-18.4↑	1.24-1.62↑	2-4	54-67↑	ESE-SW, Light	S
4								CW
4a	46	1002-1005	10.6-10.9	1.40-1.26↓	8	14-19	WSW-W, Gentle	
4b	142	1016-1018	10.8-12.1↑	1.39-1.30↓	7-8	20-37↑	SW-W, Light	
4c	46	1000-1001	12.4-13.4↑	1.75-1.93	7-8	19-24	SSW-WNW, Light	
4d	194	1003-1005	10.4-12.0↑	1.29-1.36↑	7	31-36↑	SSW-WSW, Light	
4e	63	1018-1019	11.9-10.6↑	1.52-1.64↑	7-8	20-23	SW-WSW, Light	
5	169	1007-1010↑	8.6-9.7↑	1.05-0.98↓	7	24-34↑	WSW-W, Gentle	NW
6	131	1015-1018↑	7.3-9.5↑	0.83-0.77↓	6-7	33-52↑	W-WNW, Light	NW
7	219	1018-1016↓	7.2-13.7↑	0.86-1.03↑	3	56-71↑	ESE-W, Light Air	W
8	140	1001-999↓	10.6-15.0↑	1.29-1.46↑	6	42-54↑	SE-SW, Light	CS
9	123	1007-1009	14.4-18.0↑	1.93-2.42↑	5-7	33-38↑	ESE-SSW, Light	CSW
10	92	1019-1017↓	13.9-22.6↑	1.87-2.48↑	2-3	34-48↑	ESE-SW, Light Air	S
11	74	1006-1003↓	14.6-20.4↑	1.43-1.72↑	5	52-60↑	ESE-SSE, Light	SE
12	9	1019-1015↓	16.6-24.7↑	3.03-6.12↑	2-3	28-48↑	E-SSE, Light	
13	11	1010-1007↓	18.8-24.8↑	2.49-3.07↑	4-5	40-31↓	ESE-SSE, Light	
14	11	1017-1015↓	16.1-23.2↑	1.32-1.18↓	1-2	62-70↑	ESE-S, Gentle	

Table 7.2.7 Orlandet mean summer diurnal range of meteorological variables (↓ indicates increasing or decreasing diurnal trend)

The warmest air mass types at all stations were associated with an easterly circulation type again reflecting the heat capacity of the landmass, in this case for heat uptake, during the summer months. An analysis of the frequency occurrence of the warmest air mass types during the summer season suggests that the frequency of warm types have increased at all stations. The synchronicity in timing of these increases evident at all stations at the end of the 1980s, early 1990s, again indicates the influence of a large scale forcing mechanism.

	Number of days	Pressure (hPa)	Temperature (°C)	Specific Humidity	Cloud Cover	Visibility (km)	Wind Direction and Speed	Circ Type
1								CW
1a	224	1002-1003	5.4-8.3↑	0.69-0.71	7	13-17	SSE-S, Light Air	
1b	542	1010	7.3-11.8↑	0.75-0.81↓	6	23-27	ESE-S, Light Air	
1c	334	1014-1013↓	8-14.2↑	0.65-0.74↓	3-4	40-43	ESE-SSW, Light Air	
1d	171	1005	9.2-11.2↑	1.13-1.18↑	7-8	9-11	E-SE, Light Air	
1e	46	1002	6.7-10.6↑	0.54-0.66↓	4-5	33-38	SSE-SW, Light	
1f	28	1003	5.9-10.2↑	0.75-0.8	5-6	80-80	NE-S, Light	
1g	10	1006-1009↑	10.4-13.2↑	0.99-1.41↓	5-8↓	12-26	S-NW, Light	
2	265	1018	6.7-13.7↑	0.51-0.60↓	2	48-51	SSE-SSW, Light	NE
3								E
3a	251	1022-1020↓	11.8-19.5↑	0.82-0.98↓	2-3	31-37	ENE-SSW, Light Air	
3b	47	1024-1022↓	13.6-22.4↑	0.94-1.32↓	0-1	60-64	ENE-S, Light Air	
3c	99	1023-1021↓	10.2-19.1↑	0.70-0.91↓	1-2	66-68	ENE-SSW, Light Air	
3d	8	1020-1019↓	9.7-16.4↑	0.95-1.07↓	3-4	80-80	NE-SE, Light	
4	252	1015-1014↓	11.9-17↑	1.27-1.35↓	5-6	26-32	E-SSE, Light Air	SW
5	20	1009-1012↑	5.4-9.3↑	0.43-0.48↓	3-5	58-62	WSW-WNW, Gentle	NW
6	50	1020-1018↓	14.1-20.8↑	1.73-1.76	3-5	44-52	NE-SSE, Light Air	SE
7	53	1009-1011↑	4.8-9.1↑	0.43-0.50↓	4-5	29-34	W-NNW, Light	NW

Table 7.2.8 Skabu mean summer diurnal range of meteorological variables (↓ indicates increasing or decreasing diurnal trend)

An examination of within category temperatures reveals some intriguing results. Over the 1968-1997 period, it is suggested that summer temperatures have been decreasing for the warmest air mass types at all stations. The rate of decrease is marginal for some stations, namely Flesland, Bodo and Nordstraum (Figure 7.2.22,

Figure 7.2.25, Figure 7.2.26). While for Orlandet (TSI 10 and 11) and Skabu, the decrease over time is more obvious (Figure 7.2.23, Figure 7.2.24).

	Number of days	Pressure (hPa)	Temperature (°C)	Specific Humidity	Cloud Cover	Visibility (km)	Wind Direction and Speed	Circ Type
1								SW
1a	137	1009-1010	8.3-9.4↑	0.93-0.98	7	35-33↓	SSW-WSW, Light	
1b	25	1025-1027	9.2-12.6↑	1.01-1.05	5-6	51-56	S-WSW, Light	
1c	17	996-1002↑	6.8-7.5↑	0.88-0.78↓	7-8	17-38↑	WSW, Gentle	
1d	53	1001-1004	8.8-9.4↑	1.04-0.88↓	7-8	27-41	WSW-W, Light	
1e	192	1016-1018↑	8.0-9.0↑	0.90-0.87↓	7-8	30-44↑	WSW-W, Light	
1f	42	1017-1018	10.5-10.9	1.29-1.23	8	12-18↑	SW/WSW, Gentle	
1g	245	1016	9.1-11.4↑	1.00-1.04	7	47-56	S-SW, Light Air	
1h	154	1014-1015	11.1-11.7	1.37-1.32↓	7-8	25-28	SW-WSW, Light	
1i	34	1001-1003	10.2-10.6	1.24-1.20↓	7-8	23-19↓	SW, Gentle	
2	167	1019-1017↓	14.1-21.2	1.39-1.63	2-3	66-70	E-SSE, Light	SE
3								SE
3a	39	1020-1021	11.7-15.4↑	1.36-1.44↑	7-5↓	42-60	SE-S, Light Air	
3b	111	1010	12.9-15.8↑	1.42-1.69↑	6-7	60-49↓	SE-S, Light	
3c	234	1004-1006	11.5-12.7↑	1.36-1.43↑	7	39-42	SSE-WSW, Light Air	
3d	31	999-1001	8.4-10.9↑	0.83-0.98↑	5-7	70-44↓	ESE-SSW, Light	
3e	158	1005-1006	9.9-13.2↑	1.13-1.20	7-6↓	51-67	SSE-S, Light Air	
3f	91	999-1000	13.8-17.1↑	1.28-1.44↑	6-7	68-59↓	E-SE, Light	
3g	104	1005-1003↓	11.3-16.6↑	1.03-1.11↑	5-6	73-75	E-SE, Light	
3h	101	1010-1008↓	12.7-19.2↑	1.27-1.46↑	3-4	68-76	E-SSE, Light	
3i	28	1020-1017	13.2-19.1↑	1.63-1.97↑	3-5	45-54	SE-SSW, Light Air	
3j	13	997-994↓	9.9-11.6↑	0.82-0.93↑	6-7	72-78	E-SE, Gentle	
4	148	1014-1016↑	6.6-8.4↑	0.69-0.62↓	5-6	52-70↑	SW-WSW, Light	SW
5								E
5a	98	1016-1017	7.9-11.9↑	0.83-0.90	6-4↓	61-76	S-SE, Light Air	
5b	50	1003	6.4-9.8↑	0.67-0.72	5-6	61-72	SE-SSE, Light	
5c	32	1003-1001↓	7.3-13.1↑	0.87-0.97	2-3	75-70↓	ENE-ESE, Light	
5d	45	1019-1017↓	5.5-12.4↑	0.66-0.79	2	75-79↑	E-SSE, Light	
5e	174	1015-1014↓	9.04-15.4↑	0.93-1.07	3-4	72-76	ESE-SSE, Light	
5f	11	1028-1026↓	5.9-10.4↑	0.62-0.72	3-5	71-80↑	S-SSE, Light	
6	92	1011-1012	13.4-14.5↓	1.82-1.97↑	7-8	24-37	SSE-WSW, Light	CSW
7	43	1007-1005↓	16.7-19.6↑	1.91-2.38↑	6-7	53-43↓	E-SE, Light	SE
8	12	1006-1008↑	8.9-9.4	1.10-1.12	7-8	16-20	SW/WSW, Moderate	CW

Table 7.2.9 Bodo mean summer diurnal range of meteorological variables (↓ indicates increasing or decreasing diurnal trend)

	Number of days	Pressure (hPa)	Temperature (°C)	Specific Humidity	Cloud Cover	Visibility (km)	Wind Direction and Speed	Circ Type
1								NW
1a	13	1015-1012↓	5.2-6.2↑	0.68-0.77↑	8	20-24	ESE-SSW, Light Air	
1b	93	1016-1019↑	5.2-6.3↑	0.62-0.64↓	6-7	37-47	WNW, Light	
1c	48	997-999↑	7.3-8.5↑	0.90-1.05↓	7	26-31	WNW, Light	
1d	301	1010-1012↑	7.6-8.4↑	0.82-0.87	7	35-43	WNW-NW, Light	
1e	198	1004-1005↑	8.8-10↑	1.01-1.07	6-7	39-46	WSW-WNW, Light Air	
2								W
2a	413	1018-1019	8.7-11↑	0.91-0.96↑	4-5	53-59	WSW-WNW, Light Air	
2b	547	1009-1009	10.2-12.1↑	1.15-1.22↑	6	50-53	S-WSW, Light Air	
2c	66	1020-1022	11.8-12.7↑	1.45-1.51	6-7	32-39	WSW-WNW, Light	
2d	105	1006-1007	10.9-11.9↑	1.48-1.66	8	20-24	SSW-W, Light Air	
2e	130	1008-1009	13.4-14.8↑	1.83-2.03	6	36-43	S-SW, Light Air	
2f	8	991-992	10.7-13.5↑	1.19-1.32	6-7	43-53	S-SW,Light	
3								SE
3a	47	1014-1012↓	16.0-20.0↑	1.48-1.63	2-3	56-65	S/SE, Light	
3b	26	1021-1018↓	13.4-17.5↑	1.01-1.06	1-2	63-72	SE-S, Light	
3c	63	1020-1022	15.2-18.8↑	1.79-2.08	2	48-54	S-WSW, Light Air	
3d	222	1017-1015↓	12.9-16↑	1.42-1.56	3-4	53-60	S-W, light Air	
3e	34	1024-1021↓	8.9-12.7↑	0.82-0.87↑	1-2	63-71	SE-WSW, Light Air	
3f	89	1011-1013↑	10.7-14.4↑	0.94-0.97	3-4	59-65	SSE-S, Light	
3g	16	1018-1015↓	18.6-22.4↑	2.29-2.46	1-2	56-62	SW-WSW, Light Air	
4	52	1004-1008↑	6.4-7.2	0.77-0.84↓	7-8	21-27	SSW-WNW, Gentle	NW
5	213	1008-1006↓	14.6-17.5↑	1.81-1.95↑	5-6	45-50	SSE-S, Light	CS
6	36	1012-1010↓	19.4-22.5↑	3.05-3.50↓	3	42-45	S-SW, Light	CS

Table 7.2.10 Nordstraum mean summer diurnal range of meteorological variables (↓ indicates increasing or decreasing diurnal trend)

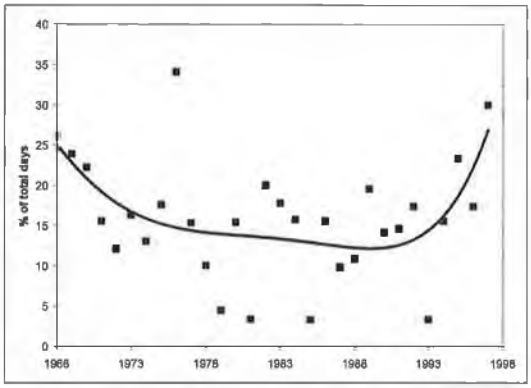

Figure 7.2.16 Bergen jja warm (TSI 1)

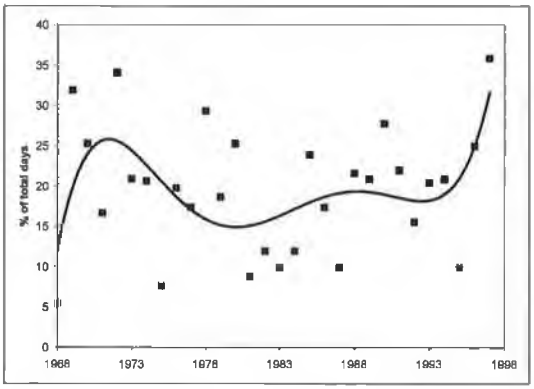

Figure 7.2.19 Nordstraum jja warm (TSI 3+6)

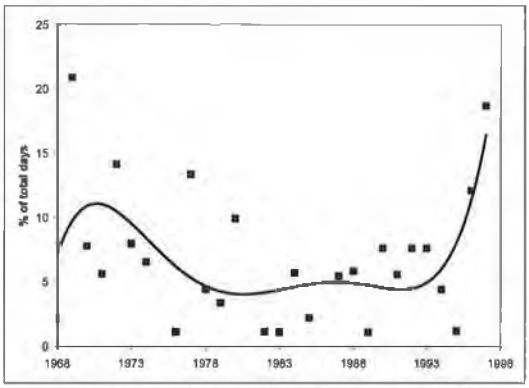

Figure 7.2.17 Bodo jja warm (TSI 2)

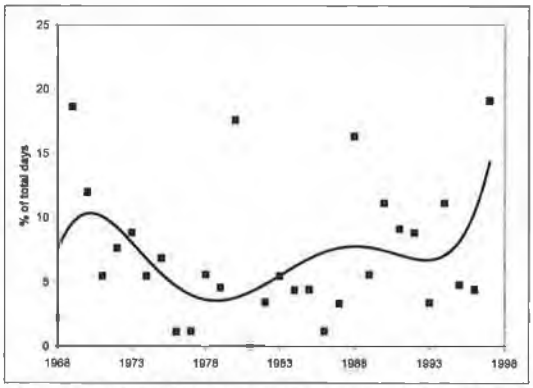

Figure 7.2.20 Orlandet jja warm (TSI 10-14)

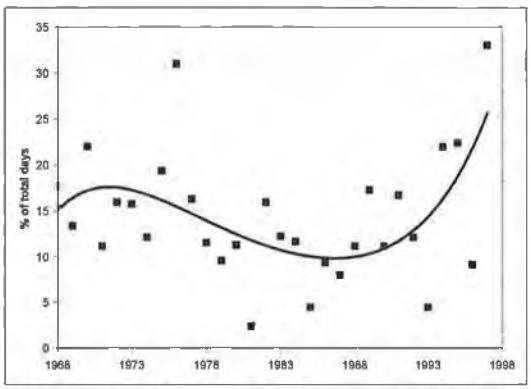

Figure 7.2.18 Flesland jja warm (TSI 1+9)

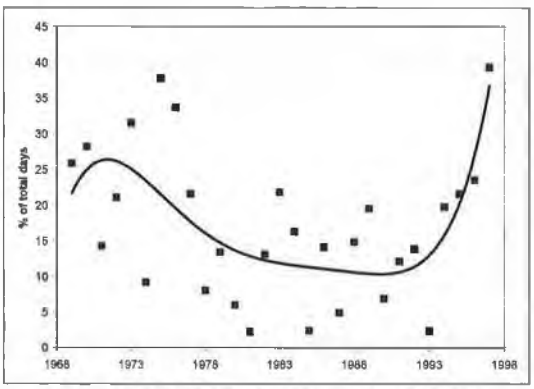

Figure 7.2.21 Skabu jja warm (TSI 3)

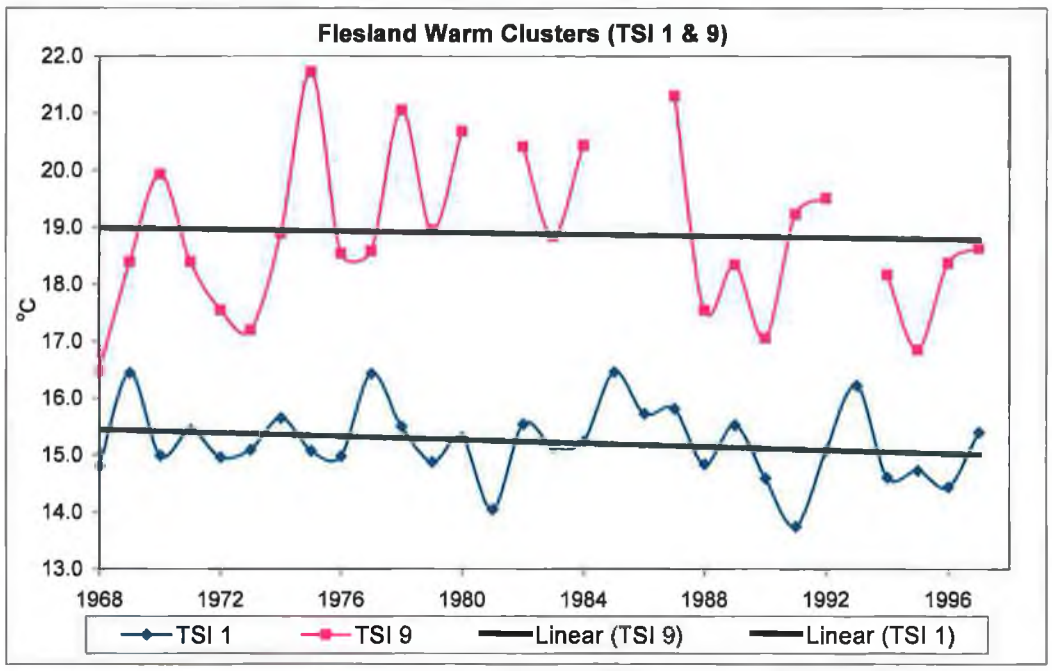

Figure 7.2.22 Mean temperature of warm clusters (TSI 1 & 9) from Flesland

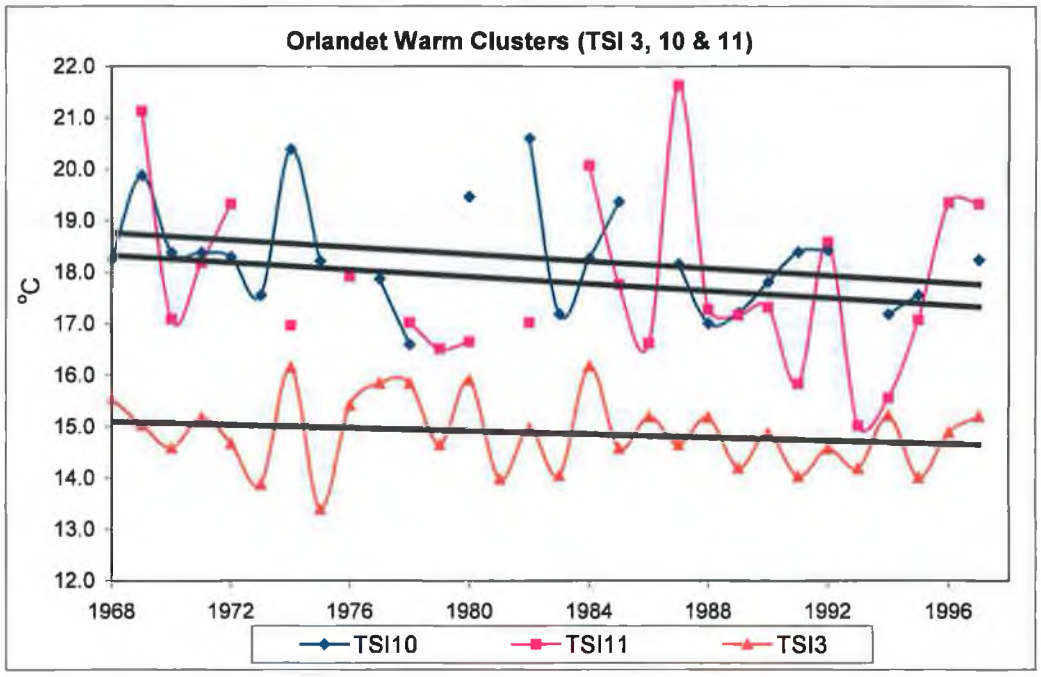

Figure 7.2.23 Mean temperature of warm clusters (TSI 3, 10 & 11) from Orlandet

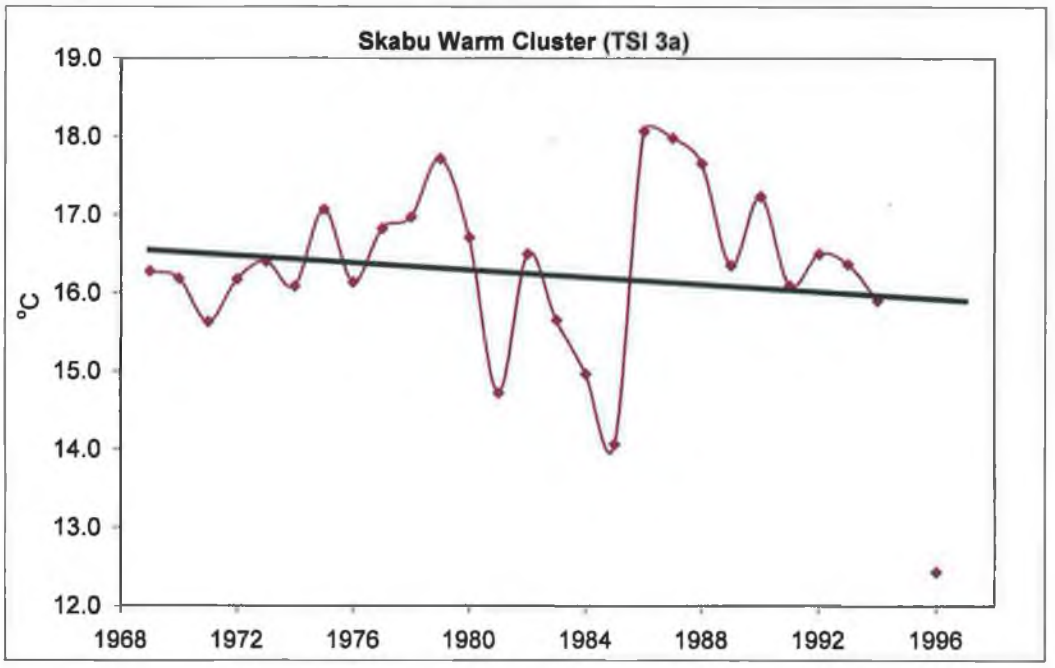

Figure 7.2.24 Mean temperature of warm clusters (TSI 3a) from Skabu (This cluster was chosen due to too few days in TSI 3b and TSI 6)

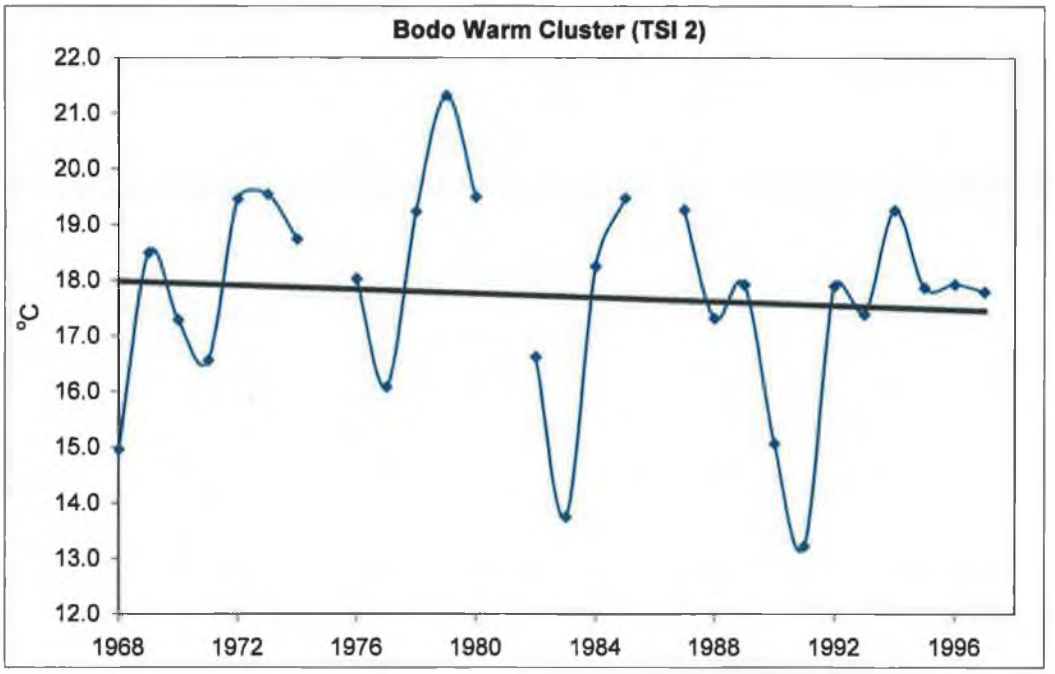

Figure 7.2.25 Mean temperature of warm clusters (TSI 2) from Bodo.

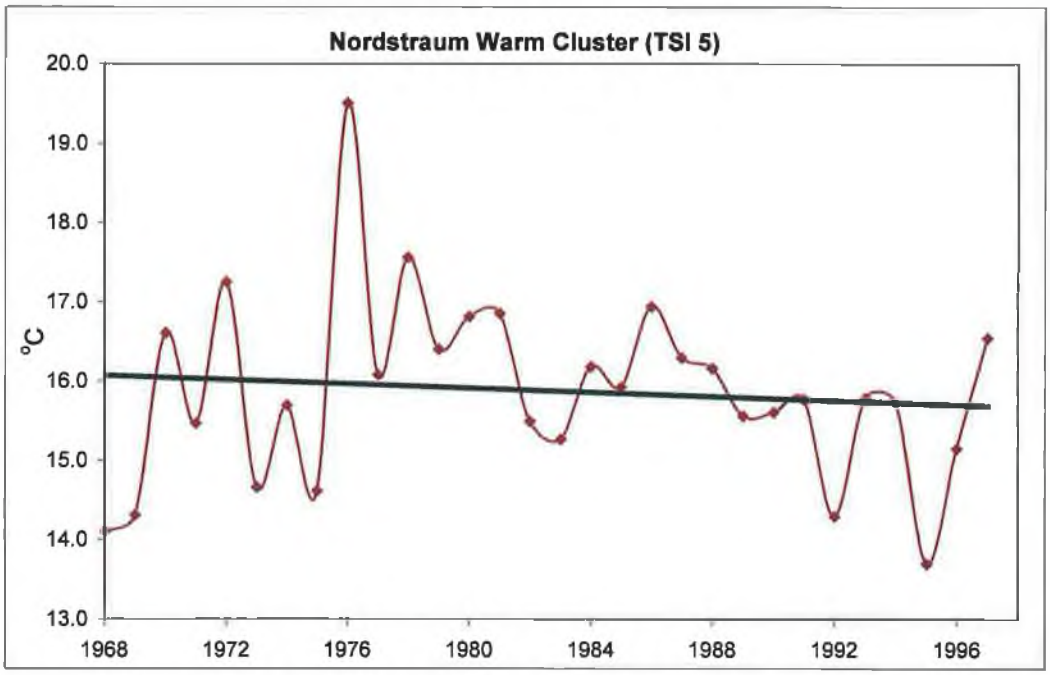

Figure 7.2.26 Mean temperature of warm clusters (TSI 5) from Nordstraum.

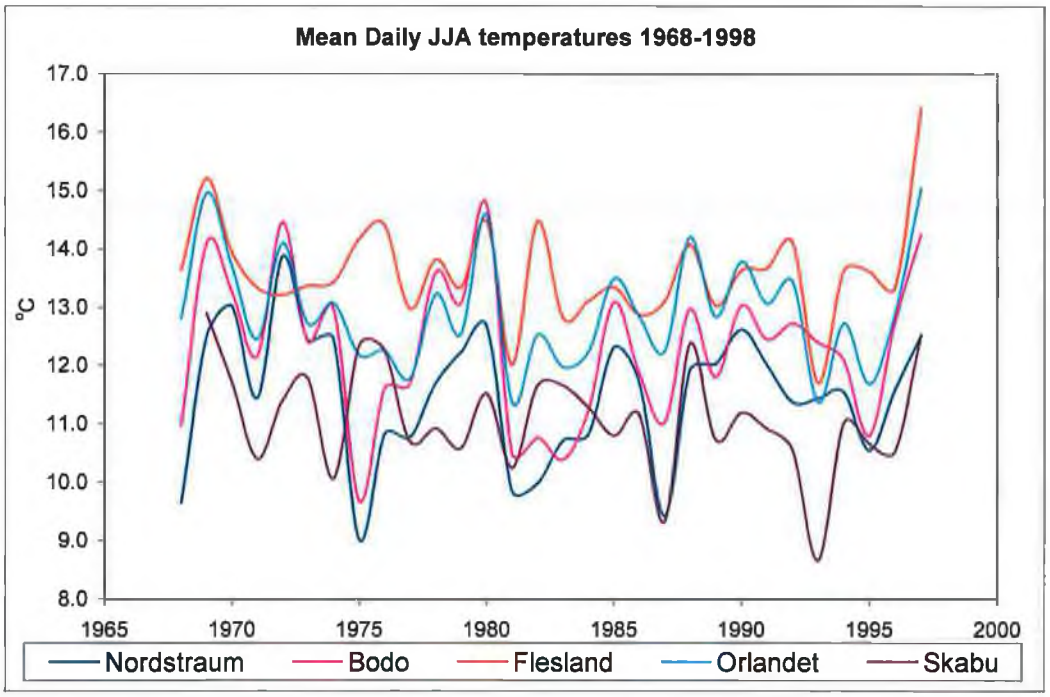

Figure 7.2.27 Mean daily temperatures for JJA for all stations (1968-1998).

Despite the decreasing trends found in the warm clusters, an examination of temperatures, independent of their air mass association, suggests no apparent trend. The increasing frequencies of the warm air mass types evident since the early

1990s are likely compensating for within category changes, which in the case of the warm categories are decreasing temperatures.

7.2.3 Conclusion

The Temporal Synoptic Index appears to produce results that are realistic and not purely an artefact of the methodology. There is also a large degree of consistency between the results from the synoptic stations, which is interpreted as an indication of the usefulness of the methodology as the technique is applied to each station independently. A synchronicity in timing between stations occurs during winter, when the frequencies of warm types increase, some dramatically, in the late 1980s early 1990s, consistent with findings from previous chapters. During the summer period, coherence between stations is evident with similar increases in warm air mass types occurring during the same period.

An analysis of within category temperature changes also indicated that the cold clusters, at some stations, were warming marginally during the winter period, while the warm clusters appeared to be cooling during the months of June, July and August, despite their increasing frequency of occurrence.

The effects of these within category temperature changes on glacier mass balance are likely to vary with season. Increases in the temperature of cold air mass types during winter are likely, at least initially, to have a positive effect on mass balance as warmer air can carry more moisture, and hence, an increase in precipitation, assuming an adequate moisture source. However, if the cold clusters warm above an absolute value of about 1°C (Laumann and Reeh, 1993), the point at which snow no longer falls, it has the potential to provide energy for melting during the winter. Any reductions in snow cover would also affect glacier albedo and would result in the surface of the glacier being more prone to further melting. However, decreases in the within category temperatures of the warm clusters during the summer period are likely to have very little effect, in the absence of any changes in frequency, on mass balance as the summer cluster temperatures are well above melting point.

7.3 Relationship between air mass frequencies and glacier mass balance

To examine the effectiveness of the air mass types determined by the methodology in chapter five and whether or not the derived classifications are useful in an examination of glacier mass balance, air mass frequencies produced from the Temporal Synoptic Index (TSI) were related to glacier mass balance. Results from four of the synoptic stations, namely Flesland, Skabu, Bodo and Nordstraum, were related to a selection of glaciers in relative proximity to the stations (Figure 7.3.1).

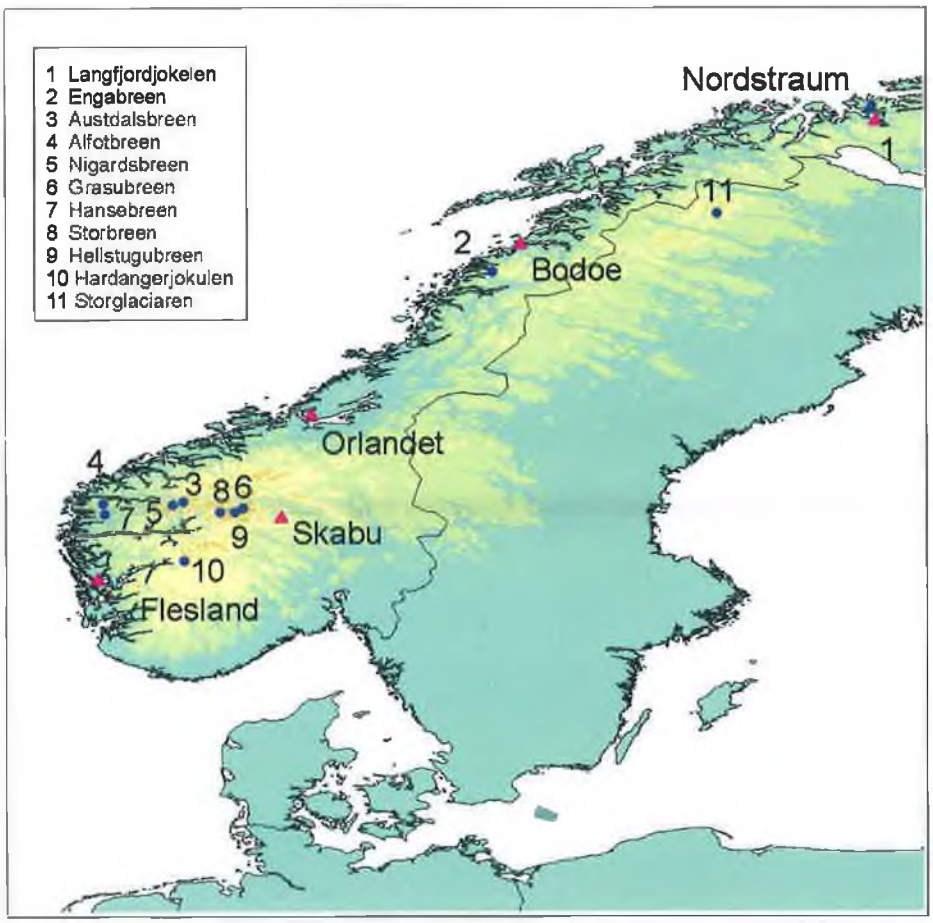

Figure 7.3.1 Location of synoptic stations (▲) and glaciers (●)

Obtaining significant correlations was found to be sensitive to the number of retained clusters but insensitive to the sub-classifications of the larger clusters. If a number of break points were suggested in the cluster scree plot, each of the cluster solutions was tested with regards to mass balance. However, it is envisaged that this step may not be a necessary requirement in all studies of this type as an

experienced climatological investigator could readily determine the 'correct' cluster solution as it generally occurred in the low teens, largely reflecting the key air mass types and variants of them.

Despite this, air mass type frequencies, from all four stations and both seasons, were found to be significantly correlated with glacier mass balance for a selection of glaciers in Norway (including Storglaciaren in Sweden). Zero order correlations from individual stations are shown to be consistent across a number of glaciers (Table 7.3.1-Table 7.3.8). Three glaciers, Hansebreen, Austdalsbreen and Langfjordjøkulen, appear to display very poor results, however, on investigation these glaciers also have the shortest period of measurements, approximately two-thirds less than the others, which is reflected in the poor correlations.

Correlations between mass balance and Flesland for the winter period indicates TSI 3 and TSI 8 as having the highest correlations. TSI 3 is essentially a cold and very dry synoptic type, reflecting its continental source. As a consequence of the low humidity values, this types negatively impacts or acts to suppress winter balance. TSI 8, on the other hand, is a 'warm' type, with relatively high temperatures and humidity, as a consequence of its more maritime source and has the effect of being positively associated with winter mass balance. TSI 6 and 7 also act to enhance winter balance, mainly due to high humidity values which would produce increased snowfall at elevation, due to the temperature lapse rate.

The major synoptic types associated with winter balance from Skabu are TSI 1,4,7 and 9. TSI 1 and 4 are both cold type clusters, TSI 4 having the lowest humidity values for all of the air mass types found at Skabu, and as such are negatively correlated to winter mass balance. While TSI 7 and 9 are associated with a westerly type circulation, resulting in moisture being advected in off the ocean and has the effect of enhancing the winter balance.

For the more northern stations of Bodo and Nordstraum, the maritime versus continental air mass types again reflect the key differentiation between enhanced and suppressed glacier mass balance during winter.

		TSI1	TSI2	TSI3	TSI4	TSI5	TSI6	TSI7	TSI8	TSI9	TSI10	TSI11	TSI12	TSI13	TSI14
Alfotbreen	r	-0.123	*-0.428*	*-0.784*	-0.030	*0.404*	*0.614*	*0.613*	*0.691*	*0.544*	-0.099	*0.372*	0.269	0.143	0.291
	sig	0.519	0.018	0.000	0.875	0.027	0.000	0.000	0.000	0.002	0.603	0.043	0.151	0.452	0.119
	n	30	30	30	30	30	30	30	30	30	30	30	30	30	30
Nigardsbreen	r	-0.253	-0.320	*-0.724*	-0.190	0.330	*0.640*	*0.638*	*0.771*	*0.513*	0.068	*0.390*	*0.371*	0.077	0.230
	sig	0.177	0.085	0.000	0.315	0.075	0.000	0.000	0.000	0.004	0.723	0.033	0.043	0.684	0.221
	n	30	30	30	30	30	30	30	30	30	30	30	30	30	30
Hardangerjøkulen	r	-0.098	-0.356	*-0.683*	-0.194	0.279	*0.525*	*0.582*	*0.760*	*0.536*	-0.027	*0.431*	0.277	0.347	0.328
	sig	0.608	0.054	0.000	0.305	0.135	0.003	0.001	0.000	0.002	0.889	0.018	0.139	0.061	0.077
	n	30	30	30	30	30	30	30	30	30	30	30	30	30	30
Storbreen	r	-0.245	-0.344	*-0.695*	-0.262	*0.441*	*0.692*	*0.642*	*0.698*	*0.517*	-0.016	0.337	*0.388*	0.068	0.065
	sig	0.191	0.063	0.000	0.161	0.015	0.000	0.000	0.000	0.003	0.931	0.069	0.034	0.721	0.735
	n	30	30	30	30	30	30	30	30	30	30	30	30	30	30
Hellstugubreen	r	-0.249	-0.156	*-0.689*	-0.256	*0.467*	*0.714*	*0.509*	*0.621*	*0.416*	0.082	0.197	0.278	0.113	0.026
	sig	0.184	0.410	0.000	0.172	0.009	0.000	0.004	0.000	0.022	0.666	0.297	0.137	0.551	0.893
	n	30	30	30	30	30	30	30	30	30	30	30	30	30	30
Grasubreen	r	-0.274	0.015	*-0.537*	-0.266	*0.499*	*0.668*	0.344	*0.406*	0.232	0.032	0.097	0.306	-0.015	-0.062
	sig	0.143	0.937	0.002	0.155	0.005	0.000	0.063	0.026	0.218	0.867	0.608	0.100	0.935	0.745
	n	30	30	30	30	30	30	30	30	30	30	30	30	30	30
Hansebreen	r	-0.124	-0.088	0.066	-0.446	-0.009	0.131	-0.068	0.356	0.285	-0.345	0.147	-0.030	.	0.249
	sig	0.687	0.775	0.830	0.127	0.976	0.669	0.825	0.232	0.345	0.248	0.632	0.923	.	0.412
	n	13	13	13	13	13	13	13	13	13	13	13	13	13	13
Austdalsbreen	r	-0.049	-0.411	*-0.826*	-0.072	0.358	0.381	*0.902*	*0.701*	*0.738*	.	0.190	0.402	.	0.175
	sig	0.892	0.238	0.003	0.844	0.309	0.278	0.000	0.024	0.015	.	0.599	0.250	.	0.628
	n	10	10	10	10	10	10	10	10	10	10	10	10	10	10

Table 7.3.1 Flesland 14 cluster solution for winter (Significant correlations are in italics)

		TSI3	TSI4	TSI5	TSI6	TSI7	TSI9	TSI11	TSI18
Engabreen	r	*-0.582*	*-0.470*	*0.561*	*0.582*	*0.447*	*-0.402*	0.345	*0.401*
	sig	0.001	0.012	0.002	0.001	0.017	0.034	0.072	0.034
	n	28	28	28	28	28	28	28	28
Storglaciaren	r	*-0.587*	*-0.467*	*0.606*	*0.676*	0.292	*-0.600*	*0.562*	0.229
	sig	0.001	0.009	0.000	0.000	0.117	0.000	0.001	0.225
	n	30	30	30	30	30	30	30	30

Table 7.3.2 Bodo 18 cluster solution for winter (Significant correlations are in italics). (Non-significant cluster types were removed for space purposes)

		TS1	TS2	TS3	TS4	TS5	TS6	TS7	TS8	TS9	TS10
Storglaciaren	r	*-0.527*	*-0.514*	0.057	*0.690*	*0.556*	-0.092	0.148	*0.492*	-0.783	-0.167
	sig	0.003	0.004	0.763	0.000	0.002	0.642	0.499	0.008	0.427	0.751
	n	30	30	30	30	29	28	23	28	3	6
Langfjordjokelen	r	-0.582	-0.547	0.390	0.530	0.648	-0.012	0.373	0.104	.	-0.936
	sig	0.100	0.128	0.299	0.142	0.059	0.975	0.363	0.790	.	0.228
	n	9	9	9	9	9	9	8	9	2	3

Table 7.3.3 Nordstraum 12 cluster solution for winter (Significant correlations are in italics)

		TSI1	TSI2	TSI3	TSI4	TSI5	TSI6	TSI7	TSI8	TSI9	TSI10	TSI11
Alfotbreen	r	*-0.494*	*0.360*	*0.376*	*-0.570*	0.011	0.071	*0.579*	0.186	*0.510*	0.088	*0.516*
	sig	0.007	0.055	0.044	0.001	0.954	0.716	0.001	0.335	0.005	0.648	0.004
	n	29	29	29	29	29	29	29	29	29	29	29
Nigardsbreen	r	*-0.460*	0.305	0.247	*-0.484*	0.027	0.016	*0.604*	0.183	*0.600*	-0.080	*0.573*
	sig	0.012	0.108	0.197	0.008	0.891	0.935	0.001	0.343	0.001	0.678	0.001
	n	29	29	29	29	29	29	29	29	29	29	29
Hardangerjøkulen	r	*-0.388*	0.290	0.340	*-0.509*	0.105	0.012	*0.488*	0.121	*0.582*	-0.029	*0.448*
	sig	0.038	0.127	0.071	0.005	0.589	0.951	0.007	0.531	0.001	0.882	0.015
	n	29	29	29	29	29	29	29	29	29	29	29
Storbreen	r	*-0.453*	0.350	0.135	*-0.513*	0.002	0.004	*0.662*	0.140	*0.513*	-0.007	*0.591*
	sig	0.014	0.063	0.487	0.004	0.991	0.984	0.000	0.469	0.004	0.973	0.001
	n	29	29	29	29	29	29	29	29	29	29	29
Hellstugubreen	r	*-0.428*	*0.441*	0.046	*-0.528*	0.087	-0.043	*0.647*	0.111	*0.433*	-0.003	*0.416*
	sig	0.021	0.017	0.813	0.003	0.653	0.824	0.000	0.566	0.019	0.989	0.025
	n	29	29	29	29	29	29	29	29	29	29	29
Grasubreen	r	-0.346	0.296	-0.125	*-0.395*	0.101	-0.002	*0.627*	0.179	0.225	-0.220	0.328
	sig	0.066	0.120	0.518	0.034	0.601	0.992	0.000	0.352	0.241	0.251	0.082
	n	29	29	29	29	29	29	29	29	29	29	29
Hansebreen	r	0.084	0.501	0.404	-0.220	-0.331	-0.451	0.232	-0.567	0.347	.	0.161
	sig	0.785	0.081	0.171	0.470	0.270	0.122	0.446	0.044	0.245	.	0.599
	n	13	13	13	13	13	13	13	13	13	13	13
Austdalsbreen	r	-0.368	0.245	0.145	-0.526	-0.045	-0.123	0.656	0.084	0.416	.	0.614
	sig	0.295	0.494	0.690	0.119	0.901	0.735	0.039	0.818	0.232	.	0.059
	n	10	10	10	10	10	10	10	10	10	10	10

Table 7.3.4 Skabu 18 cluster solution for winter (Significant correlations are in italics)

		TSI1	TSI2	TSI3	TSI4	TSI5	TSI6	TSI7	TSI8	TSI9	TSI10	TSI11	TSI12
Alfotbreen	r	-0.002	0.110	*-0.575*	-0.216	-0.124	*0.422*	0.090	*0.493*	0.245	0.284	*0.417*	0.131
	sig	0.993	0.564	0.001	0.251	0.514	0.020	0.635	0.006	0.193	0.128	0.022	0.490
	n	30	30	30	30	30	30	30	30	30	30	30	30
Nigardsbreen	r	0.173	-0.146	*-0.420*	-0.147	-0.032	*0.487*	0.068	0.251	0.265	0.236	*0.420*	0.002
	sig	0.360	0.443	0.021	0.438	0.868	0.006	0.723	0.181	0.157	0.210	0.021	0.990
	n	30	30	30	30	30	30	30	30	30	30	30	30
Hardangerjøkulen	r	0.213	-0.218	*-0.487*	-0.331	-0.157	*0.714*	-0.031	*0.375*	*0.417*	*0.495*	0.337	0.066
	sig	0.258	0.246	0.006	0.074	0.406	0.000	0.872	0.041	0.022	0.005	0.069	0.729
	n	30	30	30	30	30	30	30	30	30	30	30	30
Storbreen	r	0.213	-0.315	*-0.437*	-0.351	-0.174	*0.806*	-0.113	0.286	*0.485*	*0.553*	*0.427*	0.211
	sig	0.258	0.090	0.016	0.057	0.357	0.000	0.551	0.126	0.007	0.002	0.019	0.263
	n	30	30	30	30	30	30	30	30	30	30	30	30
Hellstugubreen	r	0.325	-0.211	*-0.531*	-0.335	-0.037	*0.694*	-0.010	0.303	*0.379*	*0.559*	0.317	-0.022
	sig	0.080	0.263	0.003	0.070	0.845	0.000	0.958	0.104	0.039	0.001	0.088	0.907
	n	30	30	30	30	30	30	30	30	30	30	30	30
Grasubreen	r	*0.447*	-0.344	*-0.572*	-0.297	0.048	*0.645*	0.122	0.170	*0.483*	*0.553*	0.355	0.091
	sig	0.013	0.062	0.001	0.111	0.799	0.000	0.520	0.368	0.007	0.002	0.054	0.633
	n	30	30	30	30	30	30	30	30	30	30	30	30
Hansebreen	r	0.216	0.140	*-0.616*	-0.131	-0.337	0.370	0.225	*0.710*	0.048	0.103	.	-0.103
	sig	0.500	0.664	0.033	0.685	0.284	0.237	0.482	0.010	0.883	0.751	.	0.750
	n	12	12	12	12	12	12	12	12	12	12	12	12
Austdalsbreen	r	0.209	0.043	*-0.799*	-0.505	-0.412	*0.731*	-0.240	0.626	0.245	0.456	.	-0.224
	sig	0.562	0.907	0.006	0.136	0.237	0.016	0.504	0.053	0.496	0.185	.	0.534
	n	10	10	10	10	10	10	10	10	10	10	10	10

Table 7.3.5 Flesland 19 cluster solution for summer (Significant correlations are in italics)

		TSI1	TSI2	TSI3	TSI4	TSI5	TSI6	TSI7	TSI8	TSI9	TSI10	TSI11	TSI12
Engabreen	r	*-0.531*	*0.375*	*0.517*	-0.372	-0.068	*0.511*	0.363	-0.230	-0.156	0.194	-0.381	*0.468*
	sig	0.004	0.049	0.005	0.051	0.730	0.005	0.058	0.240	0.427	0.321	0.045	0.012
	n	28	28	28	28	28	28	28	28	28	28	28	28
Storglaciaren	r	*-0.389*	*0.552*	0.314	*-0.510*	-0.158	*0.593*	*0.397*	-0.225	0.014	0.064	-0.374	0.285
	sig	0.034	0.002	0.091	0.004	0.404	0.001	0.030	0.231	0.942	0.737	0.042	0.127
	n	30	30	30	30	30	30	30	30	30	30	30	30

Table 7.3.6 Bodo 12 cluster solution for summer (Significant correlations are in italics)

		TSI1	TSI2	TSI3	TSI4	TSI5	TSI6
Storglaciaren	r	*-0.607*	0.025	*0.636*	*-0.500*	0.217	*0.442*
	sig	0.000	0.898	0.000	0.005	0.249	0.015
	n	30	30	30	30	30	30
Langfjordjokelen	r	-0.563	-0.093	*0.739*	*-0.672*	0.141	0.532
	sig	0.115	0.812	0.023	0.048	0.717	0.140
	n	9	9	9	9	9	9

Table 7.3.7 Nordstraum 9 cluster solution for summer (Significant correlations are in italics)

		TSI1	TSI2	TSI3	TSI4	TSI5	TSI6	TSI7
Alfotbreen	r	*-0.380*	0.012	0.193	*0.668*	0.015	0.103	*-0.382*
	sig	0.042	0.949	0.315	0.000	0.940	0.596	0.041
	n	29	29	29	29	29	29	29
Nigardsbreen	r	-0.336	-0.083	0.269	0.536	-0.148	0.111	-0.293
	sig	0.075	0.668	0.158	0.003	0.444	0.567	0.123
	n	29	29	29	29	29	29	29
Hardangerjøkulen	r	*-0.506*	-0.012	*0.426*	*0.606*	-0.065	0.193	*-0.398*
	sig	0.005	0.949	0.021	0.000	0.737	0.315	0.032
	n	29	29	29	29	29	29	29
Storbreen	r	*-0.612*	0.075	*0.452*	*0.627*	0.051	0.315	*-0.376*
	sig	0.000	0.699	0.014	0.000	0.793	0.096	0.044
	n	29	29	29	29	29	29	29
Hellstugubreen	r	*-0.562*	0.079	*0.508*	*0.546*	-0.044	0.101	-0.303
	sig	0.002	0.684	0.005	0.002	0.821	0.602	0.110
	n	29	29	29	29	29	29	29
Grasubreen	r	*-0.735*	0.240	*0.753*	*0.369*	0.102	0.233	*-0.413*
	sig	0.000	0.211	0.000	0.049	0.600	0.223	0.026
	n	29	29	29	29	29	29	29
Hansebreen	r	-0.163	0.077	0.142	0.037	0.146	0.181	-0.058
	sig	0.594	0.803	0.644	0.906	0.635	0.553	0.850
	n	13	13	13	13	13	13	13
Austdalsbreen	r	-0.300	-0.027	0.448	*0.647*	-0.224	-0.089	-0.422
	sig	0.399	0.941	0.194	0.043	0.533	0.807	0.225
	n	10	10	10	10	10	10	10

Table 7.3.8 Skabu 13 cluster solution for summer (Significant correlations are in italics)

Summer air mass frequencies from Flesland were shown to be correlated with summer balance from a number of glaciers. In particular, TSI 3 and 6, neither of which are considered to be the warmest, were indicated as being the most influential on summer balance. TSI 3 was associated with a north westerly circulation type and this air mass type would act to suppress summer melting by drawing down cooler polar air during the ablation season. While TSI 6 is associated with warm continental air during the ablation period and therefore produces enhanced melting during this period.

Air mass frequencies from Skabu again highlight the varying influences of maritime and continental air mass types, in this case, on summer balance. Wind direction associated with TSI 1 suggests a continental influence, but this type is embedded in a westerly circulation type and therefore indicative of cooler maritime air during the summer months. This is again evident at the more northern stations of Bodo and Nordstraum.

7.4 Case study of Rembesdalskåka, an outlet glacier from Hardangerjøkulen

Hardangerjøkulen glacier, situated in southern Norway, has an area of 73km^2 and is Norway's sixth largest glacier. It has been continuously monitored since 1963, initially by the Norwegian Polar Institute (NPI) and since 1985 to the present by the Norwegian Water Resources and Energy Directorate (NVE) (Figure 7.4.1). As part of the monitoring strategy, depth to bed and surface elevations were surveyed in 1961 and again in 1995, providing useful additional information on top of the bi-annual mass balance measurements recorded since 1963.

To investigate the relationship between synoptic scale climate and the glacier mass balance of Rembesdalskåka, the results from the previous section, which demonstrated that a relationship existed between the air mass frequencies and glacier mass balance for a selection of glaciers, are further investigated in order to determine the key air mass frequencies that influence its mass balance. Having established the key air mass types, empirical relationships will then be derived to statistically link these to glacier mass balance.

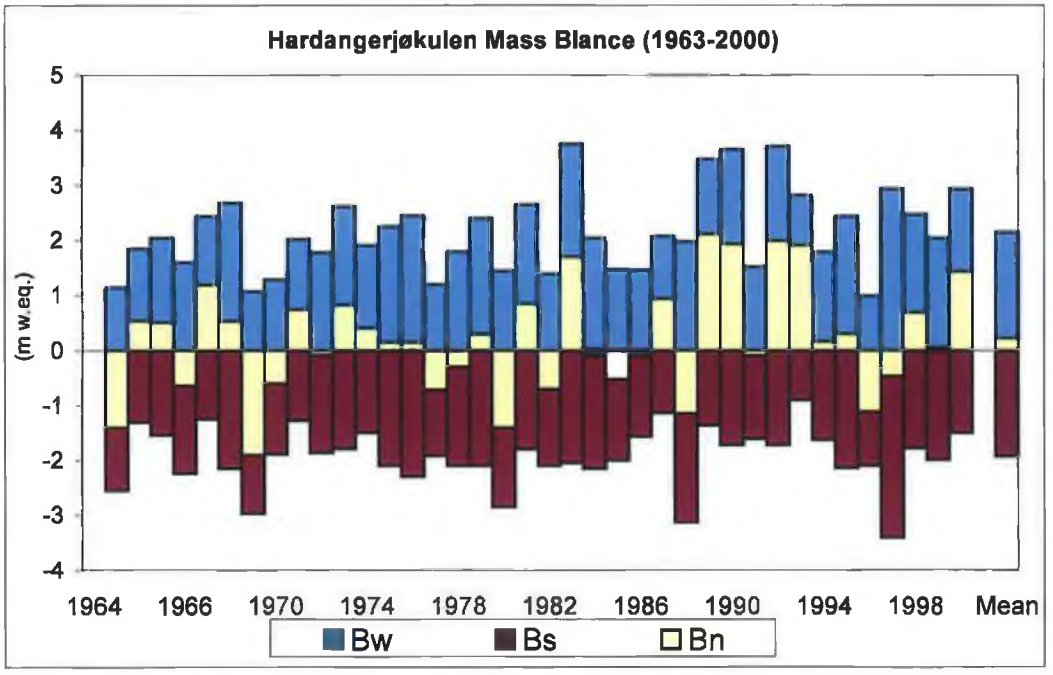

Figure 7.4.1 Mass balance for Hardangerjøkulen 1963-2000.

The influence of key air mass types from both the maritime station of Flesland and the continental station of Skabu were analysed to assess their influence on the mass balance of Rembesdalskåka. Results from which suggested that the synoptic classification from Flesland had the most significant influence on winter balance. For the summer balance, the summer synoptic classification from the more continental station of Skabu produced the most significant results (Table 7.4.1). Intuitively, these results make sense. The influence of maritime dominated air mass types during the winter accumulation period largely reflects the importance of winter precipitation, while during the summer ablation period, warm continental air is likely to be one of the dominant influences on summer mass balance.

A number of key synoptic types were initially identified as being influential on winter balance from Flesland, namely that of TSI 3 and 8. In addition to the zero order correlations, partial correlations were also examined. The partial correlations suggested that TSI 4, which was not identified in the original analysis (Table 7.4.1), was also significant to winter mass balance (Table 7.4.2). The inclusion of TSI 8 was also ruled out from further analysis, as when this variable was entered into a regression analysis, it resulted in the exclusion of important additional

synoptic types. Therefore, only TSI 3 and TSI 4 were considered for further analysis.

	Flesland DJF		**Skabu JJA**	
	R	*Sig.*	*R*	*Sig.*
TSI 1	-0.098	0.60	**-0.506**	0
TSI 2	**-0.356**	0.05	-0.012	0.94
TSI 3	**-0.683**	0	**0.426**	0.02
TSI 4	-0.194	0.30	**0.606**	0
TSI 5	0.279	0.13	-0.065	0.73
TSI 6	**0.525**	0.00	0.193	0.31
TSI 7	**0.582**	0.00	**-0.398**	0.03
TSI 8	**0.760**	0.00	**-0.375**	0.04
TSI 9	**0.536**	0.00	-0.165	0.39
TSI 10	-0.027	0.88	0.112	0.56
TSI 11	**0.431**	0.01	0.063	0.74
TSI 12	0.277	0.13	-0.258	0.17
TSI 13	**0.347**	0.06	-0.123	0.52
TSI 14	**0.328**	0.07		

Table 7.4.1 Correlations and significance levels (two-tailed) for Rembesdalskåka's winter balance and winter synoptic index for Flesland and summer balance and summer synoptic index for Skabu (n=30).

	TSI3	**TSI4**
Winter Balance	-0.804	-0.602
	P=0.000	P=0.001

Table 7.4.2 Partial correlations for TSI 3 and TSI4 and winter balance at Rembesdalskåka (27 degrees of freedom, n=30).

When both these variables were input into a stepwise regression analysis as predictors of winter mass balance, the percentage explained variance was 63.4%. For comparative purposes, winter seasonal precipitation and temperature from Bergen, located close to Flesland, were also entered as predictors into a separate stepwise multiple linear regression of winter mass balance. Only winter precipitation was considered significant with an explained variance of 26.5%. The

results of the air mass frequencies offer a significant improvement over these findings.

Winter mass balance =	3.977	+ (-0.0459 x TSI 3)	+ (-0.0463 x TSI 4)
	(0.295)	(0.007)	(0.012)

Standard errors in parenthesis

Equation 7.4.1 Regression equation relating air mass frequencies from Flesland and winter mass balance from Rembesdalskåka.

There key synoptic types, TSI 3, 4 and 5, were selected from Skabu as being the most influential on the summer mass balance of Rembesdalskåka. Again, zero order correlations of TSI 5 from Skabu and summer balance do not appear to be statistically significant, but when partial correlations are examined, its relevance becomes more apparent. When data for the whole period were included in the analysis, all three predictors enter the equation with a percentage explained variance of 63.9%.

	TSI3	**TSI4**	**TSI5**
Summer Balance	0.695	0.766	-0.394
	P=0.000	P=0.000	P=0.042

Table 7.4.3 Partial correlations for TSI 3 (with TSI 4 and TSI 5 held constant) and summer balance at Rembesdalskåka (25 degrees of freedom, n=29).

However, for validation purposes which results in a reduced number of cases available for calibration, the relevance of TSI 5 becomes insignificant and therefore drops out of the subsequent analysis. As a consequence, only TSI 3 and TSI 4 are considered for input into the subsequent regression analysis (Equation 7.4.2), which results in a slight drop of the original R^2 value to 58.9%.

Summer Mass balance =	0.934	+ (0.05465 x TSI 4)	+ (0.02751 x TSI 3)
	(0.177)	(0.010)	(0.007)

Standard errors in parenthesis

Equation 7.4.2 Regression equation relating air mass frequencies from Skabu and summer mass balance from Rembesdalskåka.

Again for comparative purposes, mean summer temperature from Skabu was input as a predictor into a separate regression analysis and was found to be negatively and strongly correlated to summer balance on Rembesdalskåka with an R^2 of 55%. While Skabu is located some distance from Rembesdalskåka, which may reduce the strength of the correlation with temperature, the results from the air mass frequencies are again shown to be comparative.

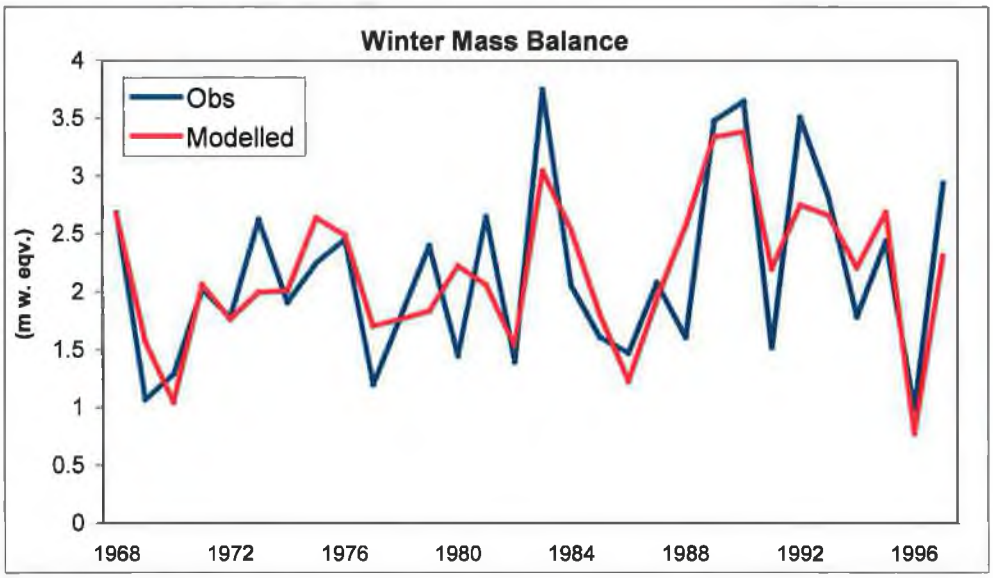

Figure 7.4.2 Observed and modelled mass balance for winter based on a split sample.

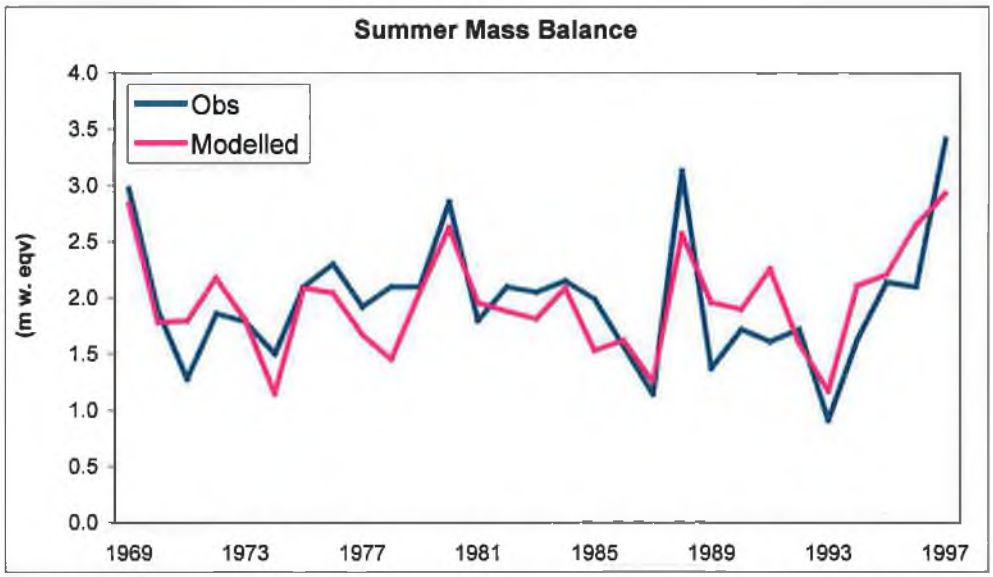

Figure 7.4.3 Observed and modelled mass balance for summer based on a split sample.

While it is problematical to validate with only thirty cases as input to a regression analysis, a split sample was used to test the validity of the derived empirical relationships. For this, the regression equations were calibrated over two thirds of the data with the predicted values for the remaining one third being compared with the observed data withheld from the analysis. Figure 7.4.2 displays the results from calibration including the reduced sample, after 1990, for winter balance, which are encouraging.

Verification of the regression equations for summer was found to be sensitive to selection of cases for calibration and verification. The best verification was found when the calibration period included the 1990s (Figure 7.4.3).

7.5 Conclusion

Analysis of glacier mass balance incorporating the regional scale climate is an area that has largely been neglected in the climate-glacier interaction literature. In an attempt to redress this deficiency, this chapter set out to bridge the gap by employing results from a synoptic scale climate classification, outlined in a preceding chapter. This classified daily weather elements into homogenous cluster types, derived using an objective and automated technique according to specific air mass types. The derived air mass types were assessed for their frequency of occurrence which were then related to glacier mass balance from a selection of glaciers in Norway. Having determined that an association existed, the relationship was further examined for a specific glacier, Rembesdalskåka, located in southern Norway.

Results from the synoptic analysis were found to be in line with findings from previous chapters. An increase in frequency of the warm cluster types during winter in the late 1980s and early 1990s is consistent with an intensification evident in the NAO, outlined previously, over the same time period. This period also marks the onset of positive net balances being recorded on the more continental glaciers, presumably resulting from a deeper penetration of moist air mass types on to the land mass.

Frequency changes evident during winter in the warm and cold air mass types are also in line with findings of previous research which applied a similar technique to detect climate changes in the western North American Arctic. Kalkstein *et al.* (1990) found that the frequencies of cold air masses appeared to be decreasing, while the warmest air mass frequencies were found to be increasing over the 40 year period examined, prior to 1990.

Chapter VIII

Statistical downscaling: a synoptic classification for the 21st century

8.1 Introduction

Large scale dynamical models of the climate system or global climate models (GCMs) suggest that mean global temperatures could rise significantly as a consequence of increasing anthropogenic emissions of greenhouse gases. Estimates from a selection of GCM models suggest that end of century increases in global temperatures could be in the range of between 1.4-5.8°C, depending on which emissions scenario is considered likely (Figure 8.1.1) (IPCC, 2001b). An increase in global temperatures of this magnitude is likely to have a significant impact on climate processes operating at various scales, from global and hemispherical scale processes to the regional and local scale surface environmental variables.

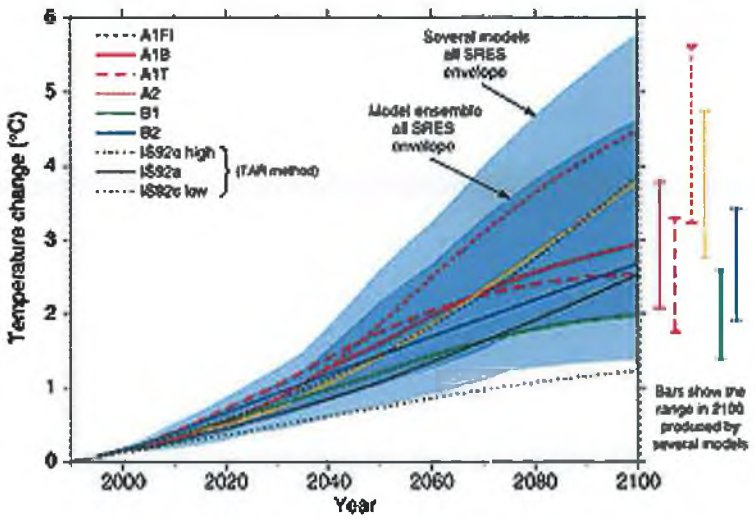

Figure 8.1.1 Temperature change by 2100 depending on emissions scenario (IPCC, 2001b)

Confidence in the simulations of these models is largely based on the assumptions and parameterisations used to develop them but also on the ability of these models to reproduce the observed climate (Karl *et al.*, 1990) (Figure 8.1.2 and Figure 8.1.3). In recent years increasing sophistication of these models has resulted from an improved understanding of the underlying climate process and ability to incorporate these advances into these numerical models. Complexity of the climate

system is also accounted for with the incorporation of horizontal and vertical exchanges of heat, moisture and momentum extending into the atmosphere and ocean (Figure 8.1.4). However, this increasing sophistication requires thousands of calculations for every model timestep, generally in the order of 30 minutes, and gridbox, generally in the order of ~2.5^0 x 3.75^0 resolution (Figure 8.1.5), resulting in the requirement of huge computational resources. The limiting factor, in terms of output scales of GCMs both temporally and spatially, is fundamentally dependent on the available computational power, restricting the set up and operation of these GCMs to a limited number of institutions.

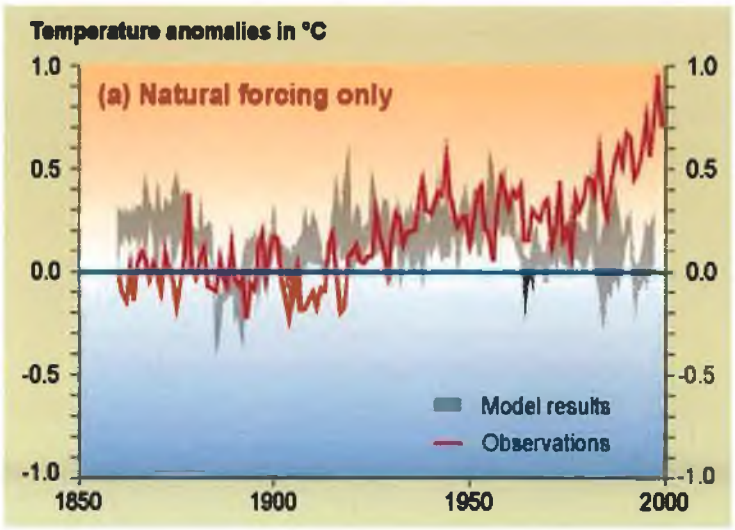

Figure 8.1.2 Modelled output with natural forcing only (IPCC, 2001a)

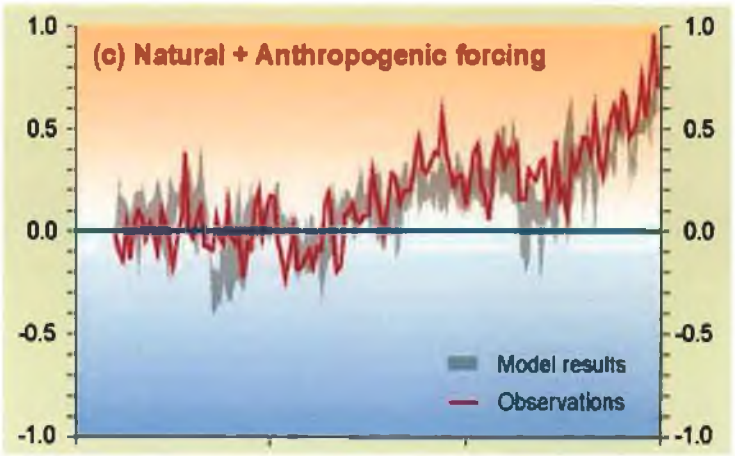

Figure 8.1.3 Modelled output with natural and anthropogenic forcing (IPCC, 2001a)

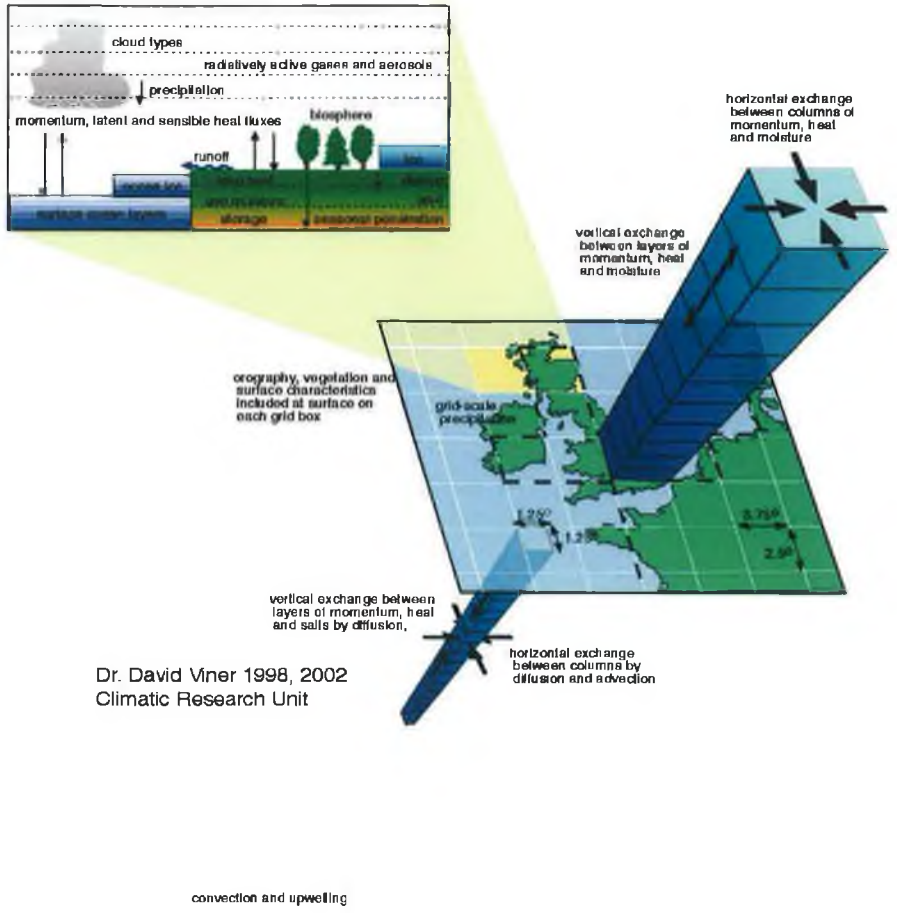

Figure 8.1.4 Conceptual 3-Dimensional structure of a GCM

Despite the high degree of sophistication of GCMs, their output is generally too coarse to be useful for regional or local scale impacts analysis, as important processes which occur at sub grid scale are not at present resolved by these models (Wilby *et al.,* 1999). Changes in both temporal and spatial variability, which may be just as important as the magnitude of change, are also masked at the sub grid scale (Wigley *et al.*, 1990), as it is unlikely that all locations will warm by the same amount and at the same rate (Figure 8.1.6). Global variations in the amount and rate of warming will also affect the distribution and rates of change of other meteorological variables, such as precipitation (Figure 8.1.7), a key variable for glacier mass balance.

Therefore a disparity of scales exists between the global scenarios, as output by GCMs, and changes that could occur at the regional or local level due to these

large-scale changes. In order to overcome some of these scale differences, a number of techniques have been developed in which large-scale GCM output can be translated or 'downscaled' into information about changes in the climate which can then be used for local scale impact analysis.

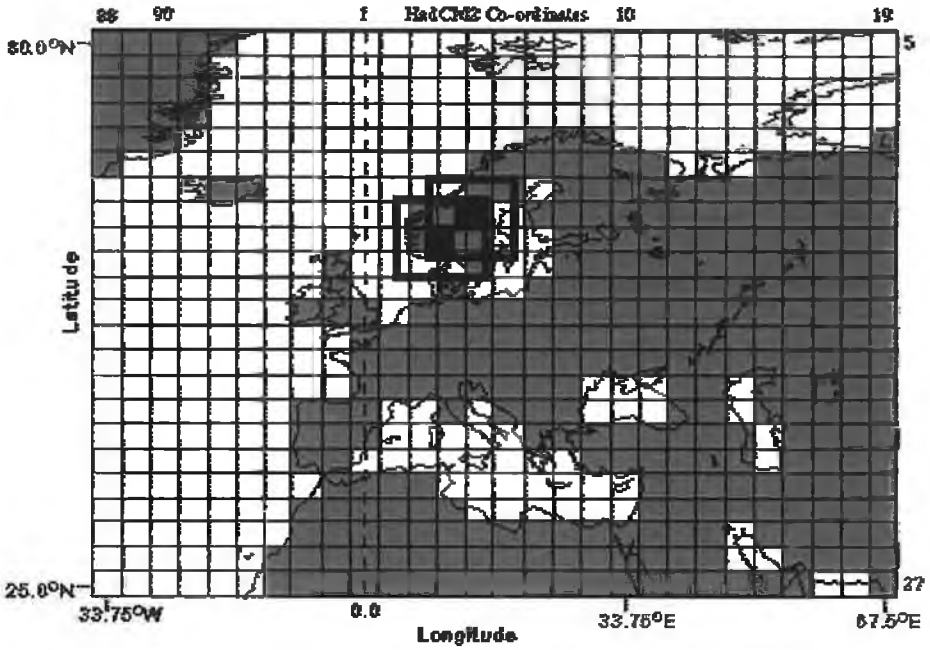

Figure 8.1.5 GCM land-sea mask and output resolution for the European domain. Grid box locations selected for downscaling are shown as black boxes. The selected sub-domain for each station is illustrated by the box outlines (Source: The Climate Impacts LINK Project).

Translating across scales or downscaling describes a set of techniques that fundamentally relate a surface environmental variable to the larger scale atmospheric forcing (Hewitson and Crane, 1996). Ultimately the aim is to describe the relationship between the various scales (Yarnal *et al.*, 2001) and the techniques were developed specifically so that these relationships could be used to develop more detailed regional and local climate information from GCMs (Hewitson and Crane, 1996).

The techniques involved in downscaling GCM output to the local-scale range from the simplistic to the complex. A widespread and readily applicable technique involves scaling an observed timeseries of a particular meteorological variable by the difference in the modelled variable between a scenario and control run of a GCM. For example, if a GCM suggests that the land area represented by a particular grid box will increase by 2°C between a control period, generally 1961-

1990, and a future time period, then this value is added to an observed temperature timeseries from a station geographically located within the gridbox to produce a climate scenario. While this technique offers a low cost and rapid assessment of possible change for a region, it is based on a number of simplifying assumptions, the crudest of which assumes that any change that occurs will be uniformly distributed over the area of interest. Despite its shortcomings, the change factor method has found widespread use due to its ease of application.

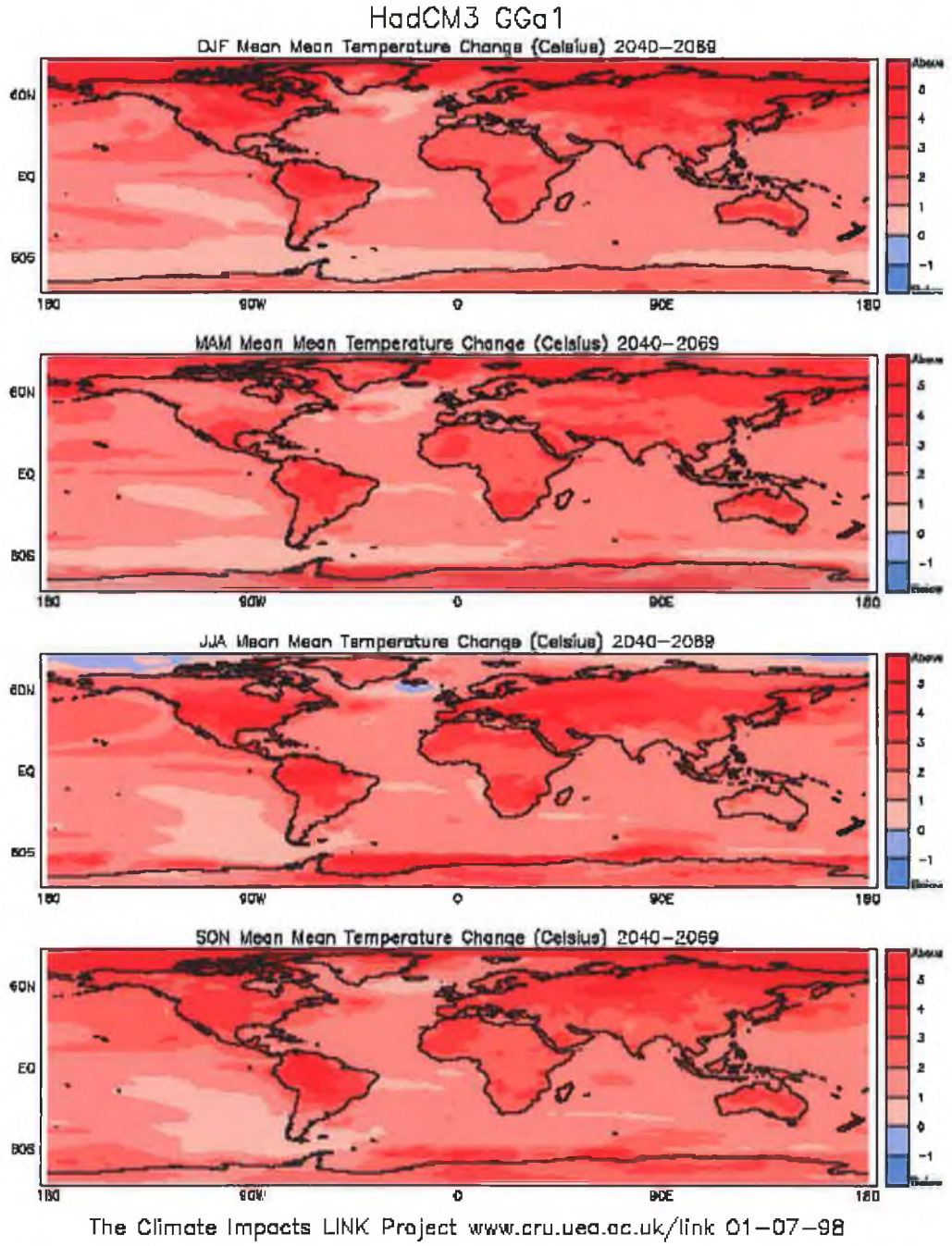

Figure 8.1.6 Temperature for the period 2040-2069 (Source: The Climate Impacts LINK Project).

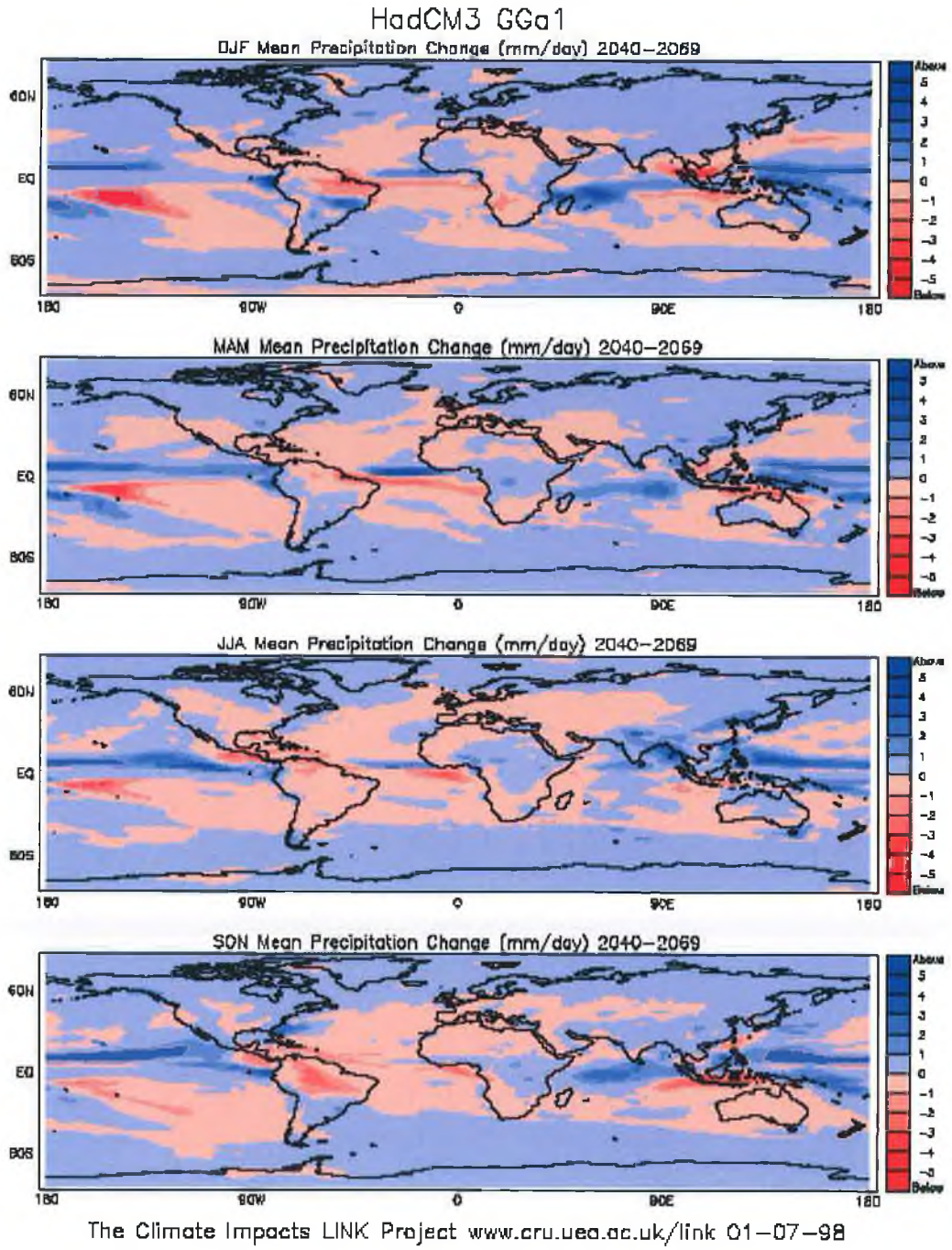

Figure 8.1.7 Precipitation for the period 2040-2069 (Source: The Climate Impacts LINK Project).

Stochastic weather generators have also found widespread application in bridging the gap between the GCM scale and that required by impacts modellers (Zorita *et al.*, 1995; Fowler *et al.*, 2000; Palutikof *et al.*, 2002) mainly in the engineering field. Weather generators are essentially random number generators conditioned to reproduce the statistical properties of the observed series being modelled, thus, they can generate long synthetic series useful for modelling. While the synthetic or

generated values will not match those of the observed series, the statistical properties of both series should be comparable. Comparisons of both the observed and modelled series on timescales of a month or less indicate the effectiveness of weather generators, but agreement tends to break down when interannual variability is assessed, with the weather generator producing less variability than that of the observed series (Wilks and Wilby, 1999). Despite these shortcomings, the synthetic time series can be scaled according to a GCM or the parameters that characterise an observed weather series can be related to circulation indices, which are then derived from a GCM in order to produce downscaled climate scenarios. Much recent development of weather generators has focused on multisite simulation of climate variables (Wilks, 1998; Palutikof *et al.*, 2002). For a more comprehensive review of stochastic weather models see Wilks and Wilby (1999).

The application of regional climate models (RCMs), which are dynamical in nature, to the downscaling problem have become more widespread in recent years due to the increase in available computational resources. RCMs are fundamentally similar to GCMs in that they utilise physical parameterisations that are either consistent to their respective resolutions or each other (Yarnal *et al.*, 2001). Their added value is derived from the fact that they operate on a much smaller domain and as such offer a much higher resolution than that of the parent GCM within which they are nested. The optimum resolution at which nested RCMs operate is in the tens of kilometres, which may still be too coarse for some impacts analysis needs.

Empirical statistical downscaling has become a viable alternative to that of RCMs where high spatial and temporal resolution climate scenarios are required. It requires substantially less computational resources and produces results that are comparable to that output from RCMs. The methodologies employed in statistical downscaling are largely in common with those of synoptic climatology, however, the goal of downscaling is to adequately describe the relationship between atmospheric circulation and the surface environment, with attention being focused more on model parsimony and accuracy, rather than understanding the relationship between them (Yarnal *et al.*, 2001). As a consequence of their relative ease of

implementation and comparability of output to RCMs, the use of statistical downscaling methodologies to produce climate scenarios from GCMs is now the favoured technique for many researchers.

The aim of this chapter is to employ a statistical downscaling technique to produce climate scenarios, using output from a Global Climate Model (GCM), for the two synoptic stations whose air mass frequencies were found to influence glacier mass balance on Rembesdalskåka, namely Flesland and Skabu. The statistical downscaling procedure will be carried out for each of the seven observed meteorological variables employed previously to derive the temporal synoptic index (TSI) in order to produce a TSI based on the downscaled and modelled data. The modelled TSI will then be used as input to the regression equations, which related the air mass frequencies to the glacier mass balance of Rembesdalskåka, to assess likely changes in glacier mass balance as a consequence of climate change over the course of the present century.

8.2 Statistical downscaling: a brief review and highlighting of some issues raised

Early work in this area described the mismatch in scales between GCMs and local surface variables as a climate inversion problem (Kim *et al.*, 1984) which was concerned with estimating the most probable distribution of a climate variable which corresponded with a given large scale gridpoint value. Kim *et al.* (1984) analysed monthly averaged surface temperature and total monthly precipitation in order to relate their most probable mesoscale distribution to large-scale monthly anomalies for a number of stations in Oregon using principal components and regression analysis. In a critique of the technique employed by Kim *et al.* (1984), Wigley *et al.* (1990) also employed a regression analysis using monthly data for temperature and precipitation for a number of stations in Oregon, but in contrast to Kim *et al.* (1984), employed a separate analysis for each month, to account for the effects of seasonality.

Karl *et al.* (1990) introduced a methodology that resulted from a generalisation of the procedures used in numerical weather forecasting, namely model output statistics (MOS) and perfect prog (PP) procedures, which they called climatological projection by model statistics (CPMS) to relate GCM grid point free-atmosphere statistics to surface environment variables of interest, such as, temperature, precipitation and cloud ceilings. Principal components analysis was used initially to reduce redundancy in the predictor set, then canonical correlation analysis is employed to relate a set of predictors to a number of predictands, namely the surface environment variables of interest. Canonical correlation is used to ensure that each day's projections are consistent among the variables (Karl *et al.*, 1990). As the final step, inflated regression analysis is then used to relate the significant canonical variables to each of the surface environment variables. Importantly, Karl *et al.* (1990) highlight the requirement for standardisation of the model output using the model means and variances as a crucial step as it helps overcome certain systematic biases that may occur in the GCM model output. Standardisation of model output using observed mean and variances was found to poorly reproduce the variability of the observed surface climate (Karl *et al.*, 1990).

The development and application of various statistical techniques (Kim *et al.*, 1984; Karl *et al.*, 1990; Wigley *et al.*, 1990; Von Storch *et al.*, 1993) and selection of an optimum predictor set of atmospheric variables have been the focus of much research. However, no one technique or predictor set has come to the fore and there has been little research in evaluating the skill of various atmospheric predictor sets between studies and regions. Cross comparisons between predictors and evaluation of skill has been complicated by the fact that different studies have utilised different techniques and atmospheric predictor combinations for different regions. A number of studies have shown that choice of technique (Wilby *et al.*, 1998; Huth, 2003) and predictors can have an impact on the resulting downscaled scenarios (Winkler *et al.*, 1997; Huth, 2003).

In one of the few studies in which a comparison between techniques was conducted, Wilby *et al.* (1998) employed a range of different statistical downscaling models to downscale daily precipitation in order to compare methods.

They used a standard set of observed and GCM derived predictors for a number of methods, two of which were based on weather generators, two employed grid point vorticity and two were based on artificial neural networks, to facilitate an evaluation of skill of the different methods. This study indicated that significant differences in the level of skill were evident between the observed and modelled data, depending on which technique was employed (Wilby *et al.*, 1998).

Zorita and Von Storch (1998) compared an analogue method to a number of more complicated methods, namely that of canonical correlation analysis (CCA), a linear method, a method based on classification and regression tree analysis (CART), a weather generator method and a neural network, to downscale daily and monthly winter precipitation for the Iberian Peninsula. Their results suggested that the analogue method performed as well as if not better than some of the more complicated methods. Based on their findings, the authors suggested that in the case of normally distributed variables, and where linear methods could be applied, that they provided a direct physical interpretation and were therefore the preferable option. However, in the case of non-linear variables, they indicated that the analogue method is preferable due to ease of implementation and simplicity of method (Zorita and Von Storch, 1998). As a comprehensive review of synoptic climatological techniques, which are also used for statistical downscaling, was carried out previously and will not be repeated here. Instead some issues arising out of the statistical downscaling literature will be discussed.

Cavazos and Hewitson (2002) try to address what they see as a lack of systematic study in the evaluation of the relative performance of predictors used in downscaling. In their analysis, they examined the skill and errors of a large number of individual atmospheric predictors of daily precipitation as applied to a range of different locations. They also tried to determine the best combination of predictors for examined locations for winter and summer. Their results indicated that a humidity variable and mid-tropospheric geopotential heights were two of the most relevant controls on daily precipitation for all locations and seasons analysed (Cavazos and Hewitson, 2002). The incorporation of an atmospheric moisture variable in downscaling precipitation has proved crucial, as changes are likely to

occur in the moisture capacity of warmed air which may not be reflected in circulation changes alone (Murphy, 2000). This was first highlighted by Karl *et al.* (1990) and Wigley *et al.* (1990) but it was common until recently to find studies that did not include some measure of atmospheric moisture content or humidity.

Additional effects on the resultant climate change estimates may arise as a consequence of the size of the domain used from which the predictors are selected (Benestad, 2001). Wilby and Wigley (2000) in an analysis of suitable GCM predictors for use in downscaling precipitation found that spatial offsets can occur in the relationship between predictors and predictands and that the use of atmospheric variables from the grid cell directly over the point of interest can fail to capture the strongest relationships. This spatial offset in the relationship between predictor and predictand was found to vary both seasonally and geographically indicating the importance of domain size when selecting predictors. Selection of domain size is also important from the point of view of GCM output as the predictive capability or skill of the model is expected to increase with increasing domain size (Goodess and Palutikof, 1998).

In order to overcome some of the issues associated with the skill level of various domain sizes, the use of mean sea-level pressure or variables derived from mean sea-level pressure have formed the centrepiece of many downscaling studies due to its relatively conservative variability and hence predictability (Wilby, 1997; Wilby, 1998; Goodess and Palutikof, 1998; Kilsby *et al.*, 1998; Trigo and DaCamara, 2000; Chen, 2000). Much of the circulation-based downscaling work has focused attention on the use of Lamb Weather Types (LWTs) or the derived objective classification technique of Jenkinson and Collison (1977) and Jones *et al.* (1993) in an extension of the methods used in synoptic climatology. Modelled mesoscale predictor variables, such as, mean sea-level pressure and geopotential heights, are also considered to have a much improved skill level in comparison to grid precipitation which depends on sub grid scale processes, such as, clouds being adequately modelled (Wilby and Wigley, 2000).

Huth (2003) in an examination of models and predictors used to downscale daily temperature found that change estimates varied widely depending on both the models and predictors used. In line with the results of Cavazos and Hewitson (2002), Huth's (2003) results also indicated that the use of circulation indices alone were not sufficient and that additional variables were required, such as a variable that described radiation-induced changes, otherwise the models predicted unrealistically low change estimates (Huth, 2003).

8.3 Methodology

Empirical statistical downscaling is based on the development of mathematical transfer functions or relationships between observed large-scale atmospheric variables and the surface environmental variable of interest. The transfer functions are generally regression based and are derived between a set of atmospheric grid scale predictors and a single predictand, however, some studies have utilised Canonical Correlation Analysis (CCA) to derive relationships between sets of predictors and predictands (Karl *et al.,* 1990: Zorita and Von Storch, 1998; Busuioc and Von Storch, 2003).

As suggested by Karl *et al.* (1990), prior standardisation of the predictor variables is recommended to ensure that the statistical properties between predictor datasets is maintained. Standardisation is normally undertaken by applying the standard z-score method using means and variances internal to the predictor variable (Karl *et al.*, 1990) which may help overcome some of the systematic biases that can occur in GCM output.

In order to ensure consistency between the developmental stage and production of scenarios from GCM data, gridded observed data, which are readily available from a number of reanalysis projects, are used to calibrate the transfer functions. Even though the reanalysis data are essentially modelled data, they are constrained by observed data from the global network and are a modelled, gridded replicate of the observed data. Relationships between grid box values from reanalysis data are highly correlated with that of the underlying observed network of stations.

The gridded reanalysis data, whose output resolution is approximately 2.5° x 2.5° degrees, are first interpolated to the output resolution of the GCM (in the case of the Hadley GCM-2.5° x 3.75° degrees) to overcome any mismatch in scales that may exist between predictor datasets.

Relationships between the predictors and predictand are derived for an observed time period with a portion of the data withheld from the calibration of the transfer functions in order that the derived relationships can be tested on the withheld or independent data, for verification purposes. Once satisfactory verification of the transfer functions for the independent time period have been completed, they can then be used to generate climate change estimates by substituting in the atmospheric variable from the GCM in place of the reanalysed atmospheric data.

The calibration period is normally undertaken for the 1961-1990 period or some portion of this, as this period is considered the baseline reference period against which future changes in climate will be assessed. This 30-year period, defined by the World Meteorological Organisation (WMO) as the 30-year normal period is considered representative of the present day climate and encompasses a range of natural variability (IPCC, 2001c). Also, prescribed increases in CO_2 emissions in the model simulations commence from the model year 1990.

The use of statistical downscaling requires that a number of additional assumptions are made by the researcher, in addition to those made when conducting synoptic climatological research. The most fundamental of which assumes that the derived relationships between the observed predictor and predictand will remain constant under conditions of climate change and that the relationships are time-invariant (Yarnal, 2001). It also assumes that the employed large-scale predictor variables are adequately modelled by the GCM for the resultant scenarios to be valid (Appendix III).

Von Storch *et al.* (1993) suggested that if statistical downscaling is to be useful, the relationship between predictor and predictand should explain a large part of the observed variability and that the expected changes in the mean climate should lie

within the range of its natural variability. Busuioc *et al.* (1998), in their verification of the validity of empirical downscaling techniques, found that in the case considered, GCMs were reliable at the regional scale with respect to precipitation in their study area and that the assumptions of validity of predictor-predictand relationship held up under changed climate conditions. However, much more work is required to test the assumptions that are implicit in statistical downscaling.

8.3.1 Data

Global climate model data was obtained from the Climate Impacts LINK project which warehouses data from the United Kingdom's Meteorological Office, Hadley Centre's climate model. The model data were from the most recent model, the HadCM3, which is a coupled ocean-atmosphere model. Flux adjustments, which were a standard requirement in previous generations of models to prevent model drift in simulated climate as a consequence of an in balance between modelled and actual heat transport in the ocean, were not required by the HadCM3 GCM (Gordon *et al.*, 2000). The ocean component used in the HadCM3 is also a substantial improvement on that used in previous Hadley models and comprises of 20 vertical levels, with exchanges of heat, momentum and salts occurring within these levels and modelled at a spatial resolution 1.25^{o} x 1.25^{o} degrees.

The scenario used from the HadCM3 GCM, HadCM3gga1, was forced using the historical increase in the individual greenhouse gases from 1860-1990 and then individual increases in greenhouse gases producing a compound rise in radiative forcing of 1% per annum starting from 1990 as described in the IS95a (Kattenburg *et al.*, 1996). Unlike the SRES (Special Report on Emissions Scenario) scenarios, tropospheric ozone is not included in this scenario, as its geographical distribution was not specified in the IS95a. However, this scenario was a precursor to the SRES scenarios and produces warming not dissimilar to the SRES A2 scenario.

The observed data comprised of the meteorological data used previously to derive the temporal synoptic index (TSI) for the two stations, Flesland and Skabu, whose air masses frequencies were found to have the largest influence on glacier mass

balance on Rembesdalskåka (Table 8.3.1). The data covered the period 1968/9-1996/7 and measurements were recorded four times daily for Flesland and three times daily for Skabu.

Station	Location	Latitude	Longitude
Flesland	Coast	60.3°N	5.2°E
Skabu	Interior	61.5°N	9.4°E

Table 8.3.1 Location of stations

Observed large-scale reanalysis data was extracted from the NCEP (National Centre for Environmental Prediction) reanalysis project for the period 1968-1997 for a domain centred over each of the stations (Figure 8.1.5). This data, which exists on a 2.5° x 2.5 ° grid resolution, was then spatially interpolated to conform to the output resolution of the Hadley Centre's GCM of 2.5° x 3.75 ° and a 3 x 3 grid box configuration, again centred over both stations, was extracted from the interpolated data (Figure 8.1.5). The extracted variables comprised of daily grid point mean sea-level pressure, 500 hPa, 700 hPa and 850 hPa geopotential heights, relative humidity from each of the geopotential heights, 2-metre specific humidity and 2-metre air temperature. A number of important secondary variables were then derived from each of the pressure surface levels for the central grid point of the extracted domain. These secondary variables, which convey important information about the state and stability of the circulation, consisted of daily vorticity (Z), westerly shear vorticity (ZW), southerly shear vorticity (ZS) geostrophic flow strength (FFF), westerly flow (W), southerly flow (S) (Table 8.3.2). These were derived according to the methods described by El Dessouky and Jenkinson (1979) and based on the pressure values of a nine-grid array centred over the area or station of interest.

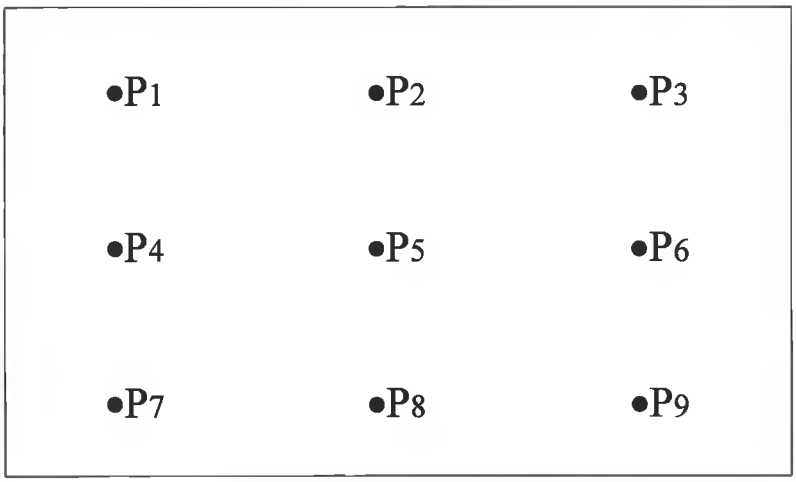

Figure 8.3.1 Organisation of grid points used in calculation. The grid P_5 represents the grid box containing the surface station.

The mean pressure for the area was calculated from the daily values of pressure at each of the grid points according to

$$\bar{P} = \frac{1}{16}\left[\left(P_1 + P_3 + P_7 + P_9\right) + 2\left(P_2 + P_4 + P_6 + P_8\right) + 4P_5\right]$$

P_1 =pressure at point P_1

The westerly flow component was calculated from the geostrophic wind equation

$$W = -\frac{1}{\rho f}\frac{\partial P}{\partial y}$$

$$W = \frac{1}{4}\left[\left(P_7 + 2P_8 + P_9\right) - \left(P_1 + 2P_2 + P_3\right)\right] \text{m/sec}$$

The southerly flow component was calculated from the geostrophic southerly flow

$$S = \left(\frac{\partial p}{\partial x}\right) = \frac{1}{\rho f}\left(\frac{\Delta p}{\Delta n}\right)$$

where Δn is 7.5° longitude at 62.5° N

360° longitude = $2\pi R \cos 62.5$

360° latitude = $2\pi R$

R= radius of earth

7.5° longitude/5° latitude = $1.5 \cos 62.5 = 0.6926$

$$S = \frac{1}{0.6926}\left[\frac{1}{4}(P_3 + 2P_6 + P_9) - \frac{1}{4}(P_1 + 2P_4 + P_7)\right]$$

Geostrophic flow (F) could then be obtained from W and S

$$F = \sqrt{W^2 + S^2} = \left(W^2 + S^2\right)^{\frac{1}{2}}$$

ZW and ZS, the westerly and southerly shear vorticity could then be calculated (for Flesland)

$$W_{north} = \left[\frac{1}{4}(P_4 + 2P_5 + P_6) - \frac{1}{4}(P_1 + 2P_2 + P_3)\right] x \frac{2\sin 60}{\sin 61.25}$$

$$W_{south} = \left[\frac{1}{4}(P_7 + 2P_8 + P_9) - \frac{1}{4}(P_4 + 2P_5 + P_6)\right] x \frac{2\sin 60}{\sin 58.75}$$

$$ZW = Z(W_{south} - W_{north})$$

$$S_{east} = \left[\frac{1}{4}(P_3 + 2P_6 + P_9) - \frac{1}{4}(P_1 + 2P_4 + P_7)\right]$$

$$S_{west} = \left[\frac{1}{4}(P_3 + 2P_6 + P_9) - \frac{1}{4}(P_1 + 2P_4 + P_7)\right]$$

$$ZS = (S_{east} - S_{west})$$

Total Shear Z= ZW + ZS

Z is positive for cyclonic and negative for anticyclonic

(El Dessouky and Jenkinson, 1979)

Two additional derived variables were calculated from relative humidity and mean sea-level pressure. These additional variables were calculated by taking the present value of the variable minus the previous days value to produce a rate of change value for the variable of interest which are often indicative of important atmospheric changes (Karl *et al.*, 1990). A similar set of indices were extracted from the GCM output for both of the domains used in this study.

Variables		**Derived Indices**
Mean sea-level pressure (hPa)	mslp	W, S, FFF, ZW, ZS, Z, SLP_{lag24}
500hPa geopotential height (m)	500	W_{500}, S_{500}, FFF_{500}, ZW_{500}, ZS_{500}, Z_{500}
700hPa geopotential height (m)	700	W_{700}, S_{700}, FFF_{700}, ZW_{700}, ZS_{700}, Z_{700}
850hPa geopotential height (m)	850	W_{850}, S_{850}, FFF_{850}, ZW_{850}, ZS_{850}, Z_{850}
*00-*00hPa geopotential (m)	thick	
500hPa Relative humidity (%)	R_{500}	$R_{500\text{-}lag24}$
700hPa Relative humidity (%)	R_{700}	$R_{700\text{-}lag24}$
850hPa Relative humidity (%)	R_{850}	$R_{850\text{-}lag24}$
2m Specific Humidity (g/kg)	Sph	
2m Air Temperature (^{o}C)	temp	

Table 8.3.2 Primary and derived predictor variables

The predictor variables from both NCEP and the GCM were standardised using their internal monthly means and variances according the z-score method for the period 1968-1996, as advocated by Karl *et al.* (1990).

8.3.2 Development of transfer functions

The development of the transfer functions which relate the large-scale atmospheric variables to the surface environmental variables, such as pressure, temperature, humidity, cloud amount, visibility and the wind scalars, measured at both Flesland and Skabu meteorological stations was carried out using a statistical downscaling modelling tool (SDSM). SDSM is a decision support tool that was developed to assess the regional impacts of climate change (Wilby *et al.*, 2002). SDSM allows the user to generate climate scenarios for point locations using a robust statistical

downscaling technique. Its ease of use facilitates the rapid development of scenarios and in addition provides a suite of diagnostic tools in which the data can be tested and compared to ensure adequate models are selected for downscaling purposes.

SDSM is a regression-based tool but, importantly, incorporates stochastic techniques which are used to inflate the variance of the downscaled data providing a better fit between modelled and observed data. Inflation of the variance is based on the assumption that local variability can be accounted for by large-scale variability (Von Storch, 1999).

The downscaling process is broken down into seven discrete tasks in SDSM (Wilby and Dawson, 2001) and they are as follows-

1. Quality control and data transformation
2. screening of predictor variables
3. model calibration
4. weather generation (observed predictors)
5. statistical analysis
6. graphing model output
7. scenario generation (using climate model predictors)

Quality control allows the user to check the input data for errors and missing values and the identification of outliers that may affect the analysis. In addition, the user can perform data transformations if required. As SDSM is regression based, assumptions of normality are required for the input data. Selection of important predictor variables, from the large-scale variables extracted from the NCEP reanalysis project, a crucial step in the downscaling process, is performed under the screening of predictor variables option. The relative importance of predictor variables may be seasonally variable which can be assessed as part of the selection process in SDSM. Partial correlation analysis can also be performed to assist in the selection of a parsimonious set of predictor variables and in the identification of problems associated with collinearity. Collinearity of predictor variables should be avoided as it affects the variance of the predictors in the model and can result in

model misspecification due to the exclusion of important predictor variables as a consequence of incorrect model standard errors.

Having selected a parsimonious set of predictor variables for the surface environmental variable and timeframe of interest, which in this case was winter and summer, model calibration was then carried out. Model calibration was conducted on a split sample of fifteen years from 1968-1982 for all variables, with the remaining data withheld for verification purposes.

The weather generator was then used to synthetically generate multiple ensembles of daily weather series given the observed NCEP reanalysis predictor variables. Depending on the degree of regional or large-scale forcing of the surface variable and the percentage of explained variance by the model, stochastic 'white noise' is generated based on the standard errors of the model (Wilby and Dawson, 2001). This 'white noise' was synthetically generated for each day and was added to the deterministic component resulting in an inflation of model output variances that correspond better with the observed series (Wilby *et al.*, 2002).

Statistical analysis of the observed and modelled output derived from either the NCEP or GCM predictors can then be performed, to test model adequacy. Results can also be graphically analysed.

The final step in the downscaling procedure in SDSM is scenario generation using the GCM atmospheric predictors in place of the observed NCEP reanalysis predictor set to produce climate change scenarios.

8.4 Results

8.4.1 Calibration and verification

Table 8.4.1 lists the selected predictors for each of the predictands. Only predictors that consistently entered the equations for each of the four daily measurements in the case of Flesland and three daily measurements in the case of Skabu were selected.

Variable	Flesland	Skabu
Cloud Amount (**00,06,12**,18)	Thick7_8	MSLP
	W_{850}	Z_{850}
	R_{850}	R_{700}
Mslp (**00,06,12**,18)	FFF	FFF
	SLP_{lag24}	Z
	Thick5_7	Thick5_7
	W_{850}	W_{850}
	Z_{850}	Z_{850}
	R_{700}	R_{700}
Specific Humidity (**00,06,12**,18)	Thick7_8	FFF
	W_{850}	Z
	R_{850}	Thick7_8
		S_{850}
		$R850_{lag24}$
Temperature (**00,06,12**,18)	SLP_{lag24}	FFF
	Thick7_8	Thick7_8
	FFF_{850}	S_{850}
	W_{850}	850
	R850	R850
uu-scalar (**00,06,12**,18)	MSLP	FFF
	S	S
	SLP_{lag24}	W
	ZS	ZS
	FFF_{850}	$R500_{lag24}$
	W_{850}	R850
	$R500_{lag24}$	
Visibility (**00,06,12**,18)	Z	Z
	Thick7_8	W_{850}
	FFF_{850}	ZS_{850}
	W_{850}	R700
	R850	Skabcl00**
	$R850_{lag24}$	
vv-scalar (**00,06,12**,18)	W	S
	Z	W
	SLPlag24	ZW
	500	F_{850}
	S_{850}	
	ZS_{850}	
	$R850_{lag24}$	

Table 8.4.1 List of selected predictors for Flesland (ns) and Skabu (nn) (Bold indicates the time of measurement for Skabu). (Skabcl00- Cloud Amounts from Skabu)**

While SDSM has a number of options for the time resolution of the model fit, namely, monthly, seasonal and annual, it is unlikely that predictors will be consistent across all the months or seasons of the year. In the case of this study, only the winter months of December, January and February were relevant for Flesland and in the case of Skabu only the summer months of June, July and August were relevant. Despite this, SDSM derives transfer functions for all months or seasons and the output below reflects this.

The percentage of explained variance also reflects the fact that all months are included in the analysis and not just the months or seasons of interest, for each of the predictands are shown in Table 8.4.2. The effect of this is likely to result in lower explained variance as a consequence of the predictor selection criteria that was focused on selecting the best predictors for the relevant winter or summer months from each station and not on selecting predictors suitable for all months of the year.

Predictand	**% explained variance (R^2)**	
	Flesland	*Skabu*
Mslp (**00,06,12**,18)	0.96-0.97	0.97
Temperature (**00,06,12**,18)	0.59-0.64	0.62-0.69
Specific Humidity (**00,06,12**,18)	0.51-0.59	0.47-0.52
Visibility (**00,06,12**,18)	0.33-0.39	0.26-0.28
Cloud Amount (**00,06,12**,18)	0.24-0.36	0.14-0.22
uu-scalar (**00,06,12**,18)	0.29-0.34	0.14-0.21
vv-scalar (**00,06,12**,18)	0.50-0.56	0.22-0.31

Table 8.4.2 % explained variance (R^2) for each variable and location (Bold indicates the time of measurement for Skabu)

Validation of the downscaling model for each variable was conducted on an independent timeseries withheld from the analysis, from 1983-1996. Results for some of the observed means and variances for a selection of variables are shown in Figure 8.4.1-Figure 8.4.12. Temperature means and variances, from both Skabu and Flesland, appear to have been modelled adequately, which is also reflected in their respective R^2 values from Table 8.4.2

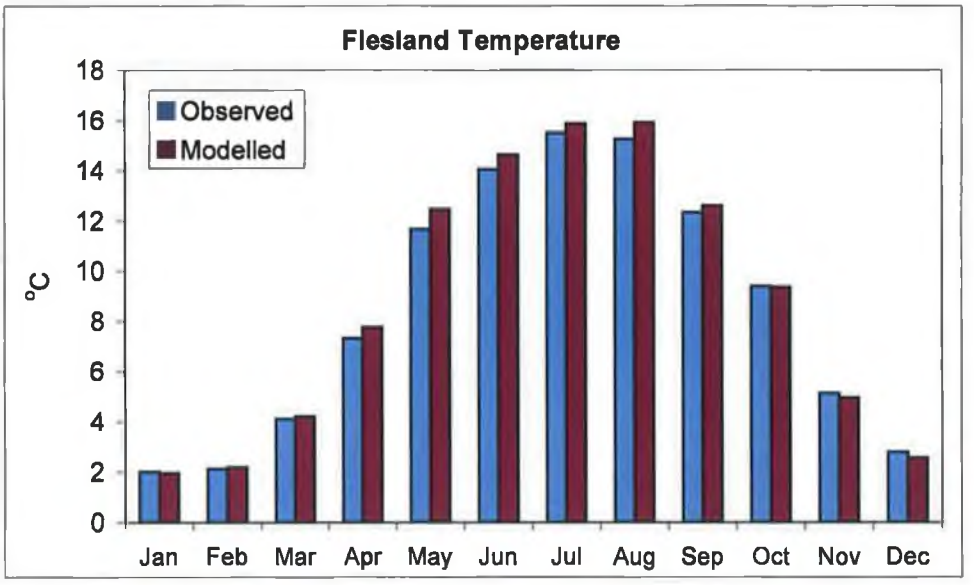

Figure 8.4.1 Verification for downscaled temperature-Flesland (1983-1996)

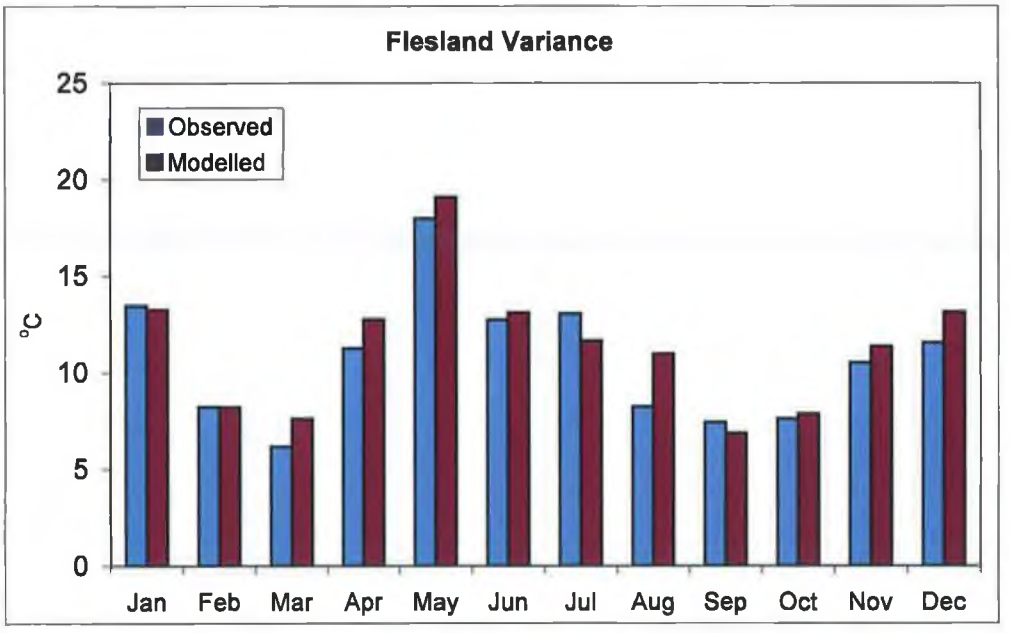

Figure 8.4.2 Verification for downscaled temperature variance-Flesland (1983-1996)

Modelled means of specific humidity were slightly underestimated for both stations. The variance is also underestimated for Flesland, but over estimated for Skabu. However, when just the months of interest are assessed, these discrepancies are much reduced, indicating much smaller differences between the modelled and observed data series.

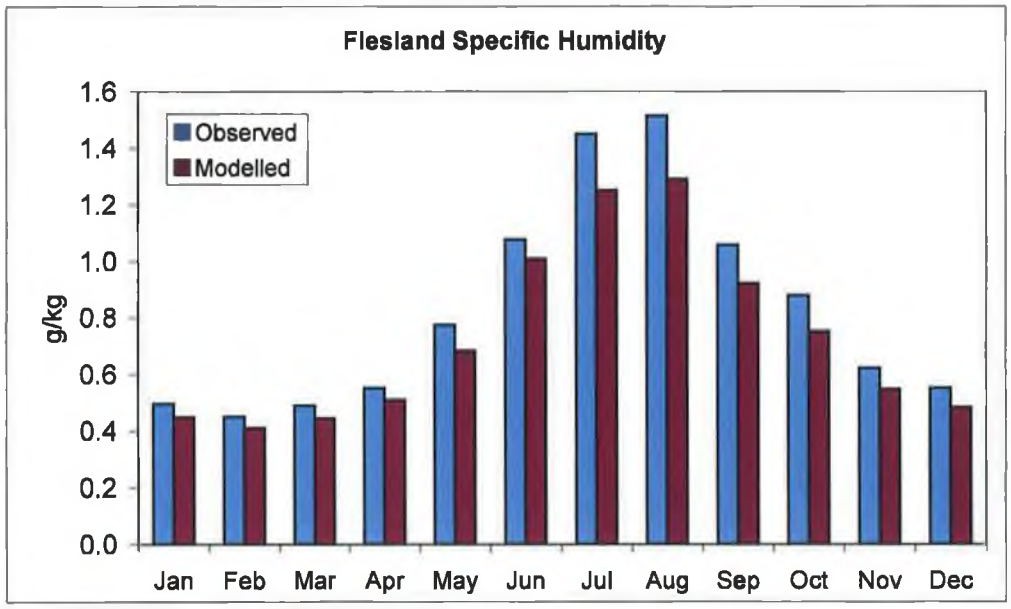

Figure 8.4.3 Verification of downscaled specific humidity-Flesland (1983-1996)

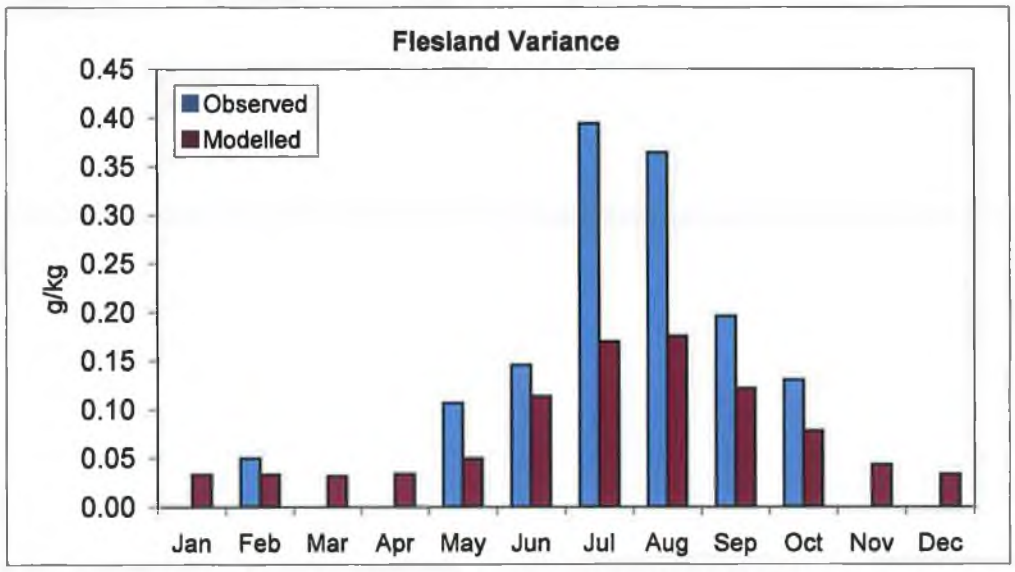

Figure 8.4.4 Verification of downscaled specific humidity variance-Flesland (1983-1996)

Despite the low explained variance for the *uu* scalar for Flesland (0.29-0.34), comparisons between observed and modelled means and variances suggest a reasonably good fit. The model fit for Skabu has a tendency to underestimate both the means and variances for the summer months of June, July and August. The explained variance for Skabu (0.14-0.21) is the lowest for all variables, indicating a poor fit.

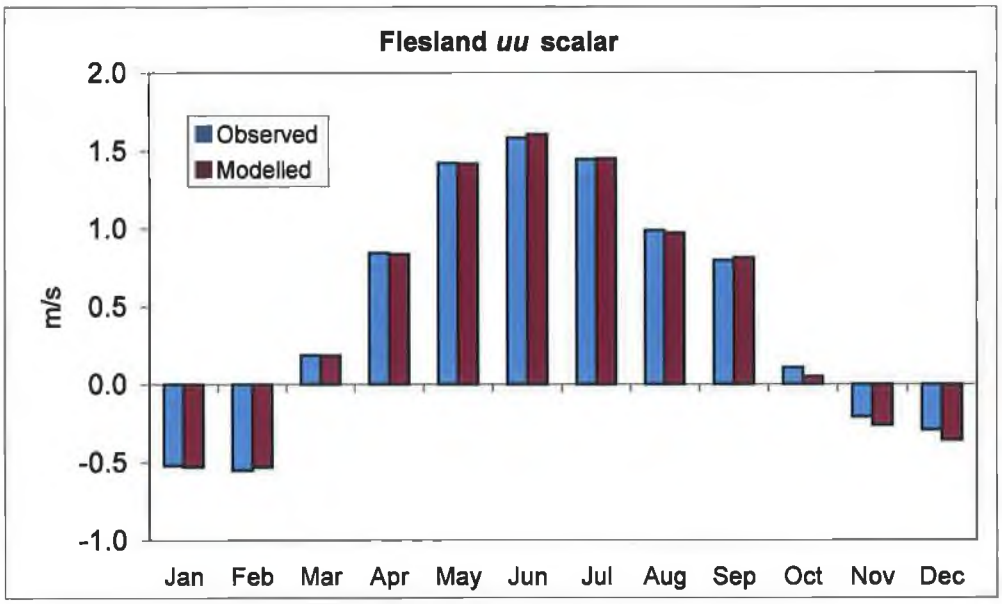

Figure 8.4.5 Verification of downscaled *uu* scalar - Flesland (1983-1996)

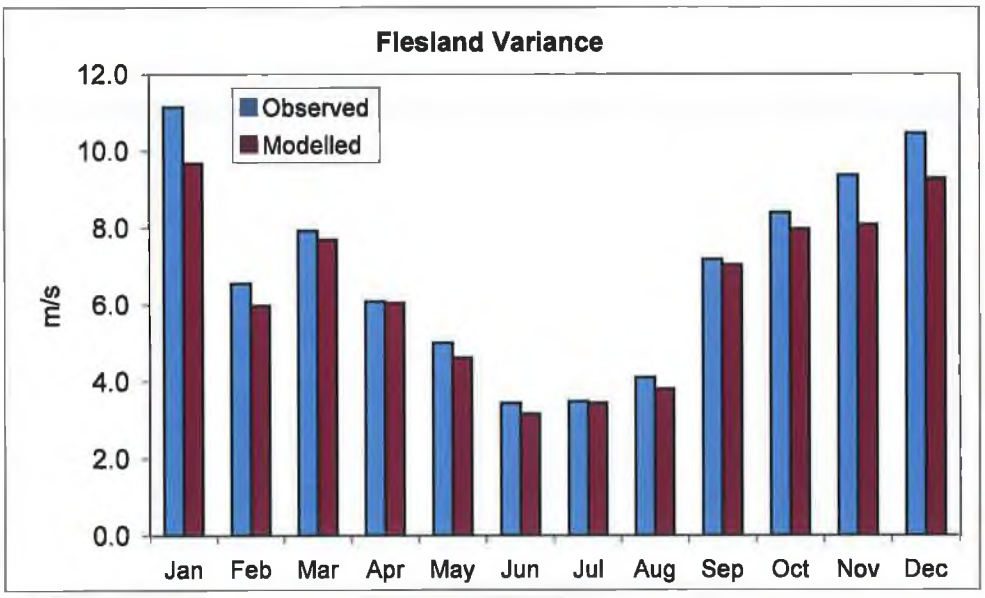

Figure 8.4.6 Verification of downscaled *uu* scalar variance-Flesland (1983-1996)

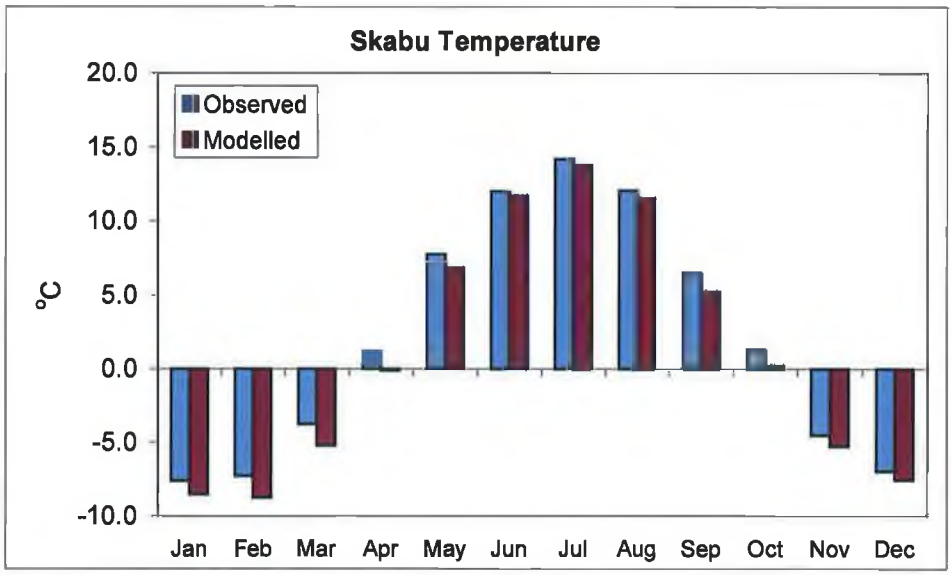

Figure 8.4.7 Verification of downscaled temperature-Skabu (1983-1996)

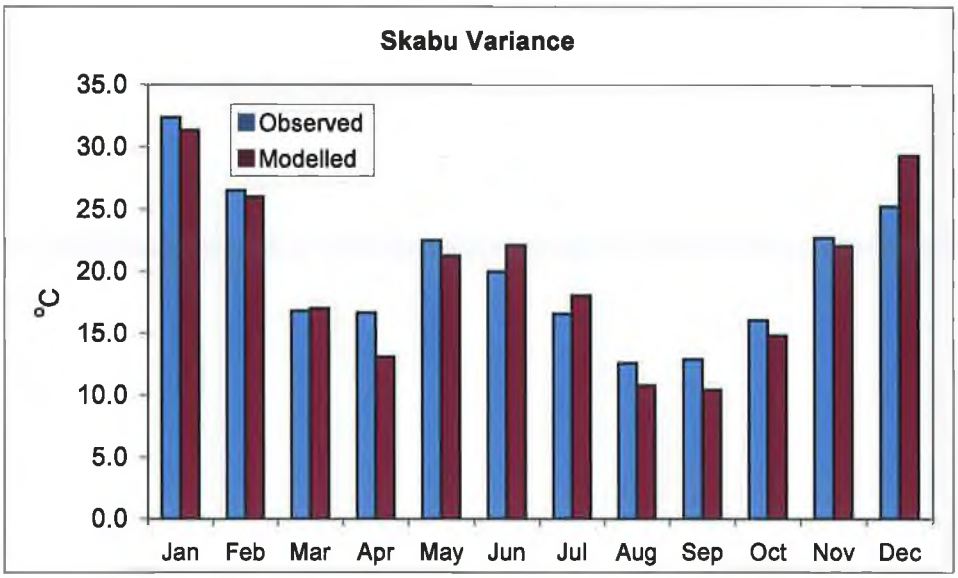

Figure 8.4.8 Verification of downscaled temperature variance-Skabu (1983-1996)

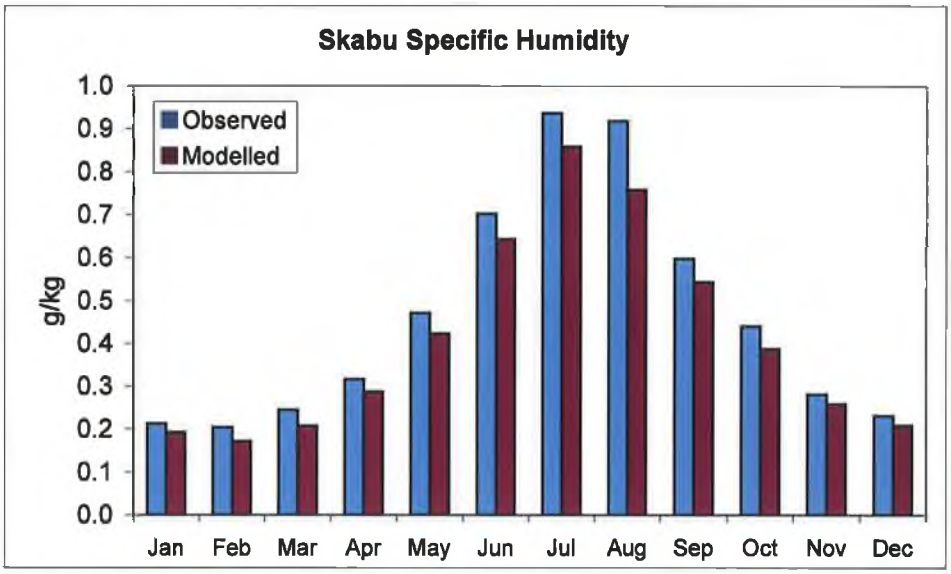

Figure 8.4.9 Verification of downscaled specific humidity-Skabu (1983-1996)

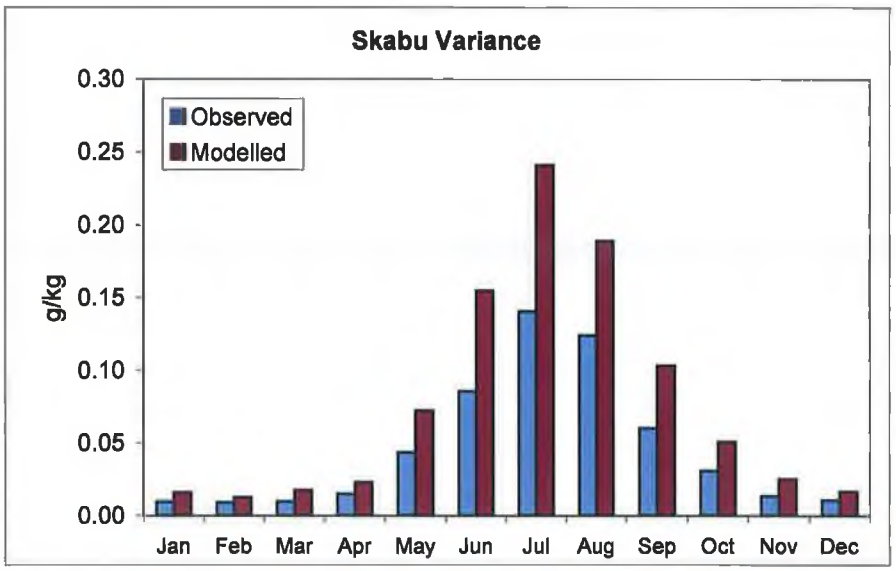

Figure 8.4.10 Verification of Skabu specific humidity variance (1983-1996)

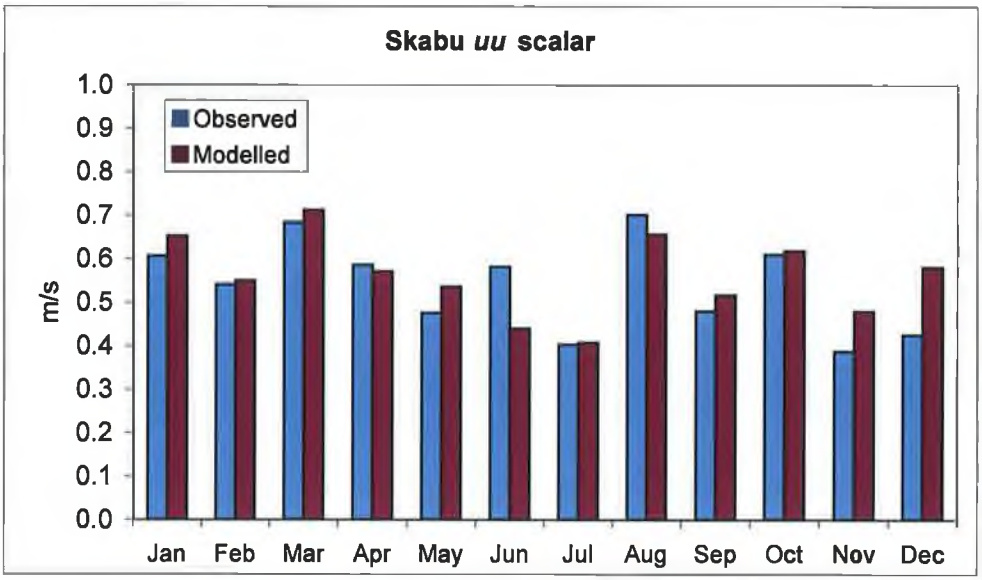

Figure 8.4.11 Verification of Skabu *uu* scalar (1983-1996)

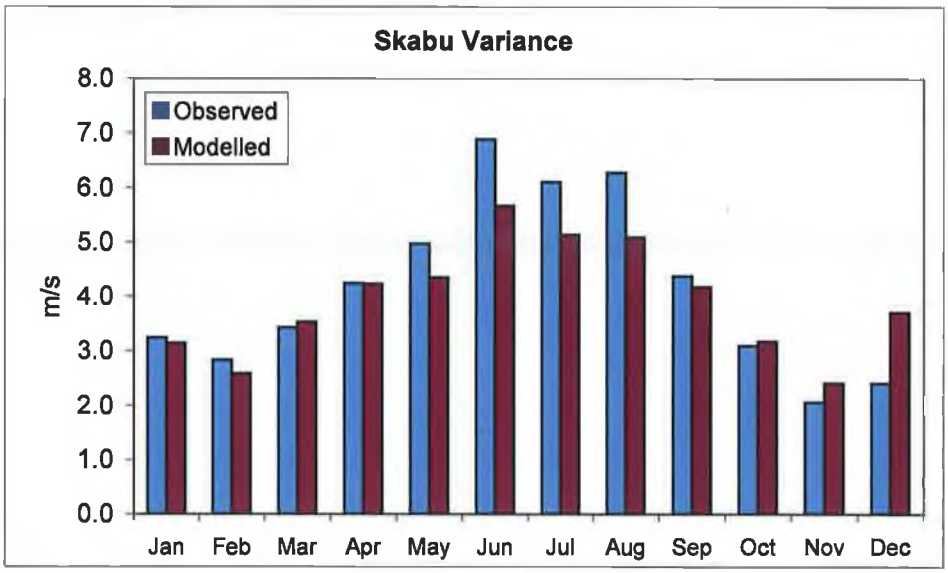

Figure 8.4.12 Verification of downscaled *uu* scalar variance-Skabu (1983-1996)

8.4.2 Scenario Generation

Having derived the transfer functions for each variable, measurement period and station for their respective seasons of interest based on the observed NCEP reanalysis data, a comparative set of large-scale predictors from the GCM are then used as input to the transfer functions to produce climate change scenarios. In order to assess the gradual influence of a changing climate on glacier mass balance,

continuous daily data from the HadCM3 model was used (Figure 8.4.13 and Figure 8.4.14) as opposed to selecting a future timeslice of data from the model (Figure 8.4.15-Figure 8.4.18). Selection of a timeslice is generally performed in order to assess the likely impacts of a changed climate on a particular surface environmental variable and largely ignores the effects that a gradual change in climate may have and which may be important, as in the case of glacier mass balance.

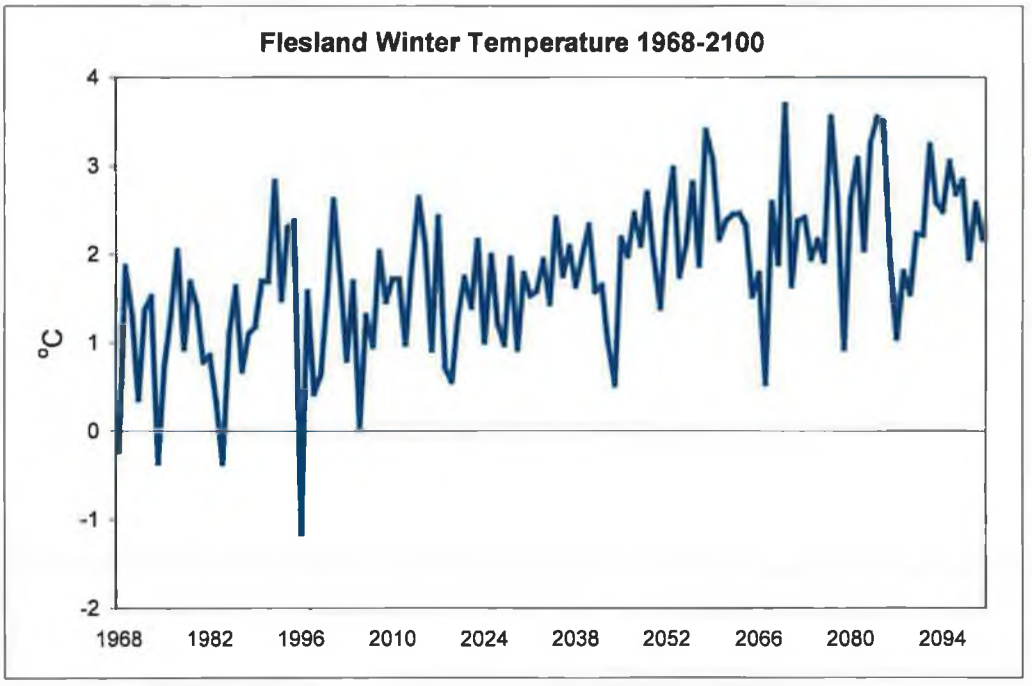

Figure 8.4.13 Winter temperature (December, January and February) for Flesland 1968-2100, downscaled from the HadCM3 GCM.

This section will only cover a discussion on the suggested likely changes in the two key parameters that affect glacier mass balance, that of temperature and moisture availability.

Downscaled data from the HadCM3 gga1 scenario suggest that mean winter temperatures will increase by ~1.25°C at Flesland by 2100, with the largest monthly increases occurring during December and January (Figure 8.4.15). Summer temperatures from Skabu are suggested to have larger increases, in the region of 2.5°C, by the end of the present century. The months of June and August are indicated to have the largest increases, of 2.6°C and 3.4°C respectively. The

mean July temperature increase is suggested to be less than that of the summer average, with an increase of 1.5°C (Figure 8.4.16).

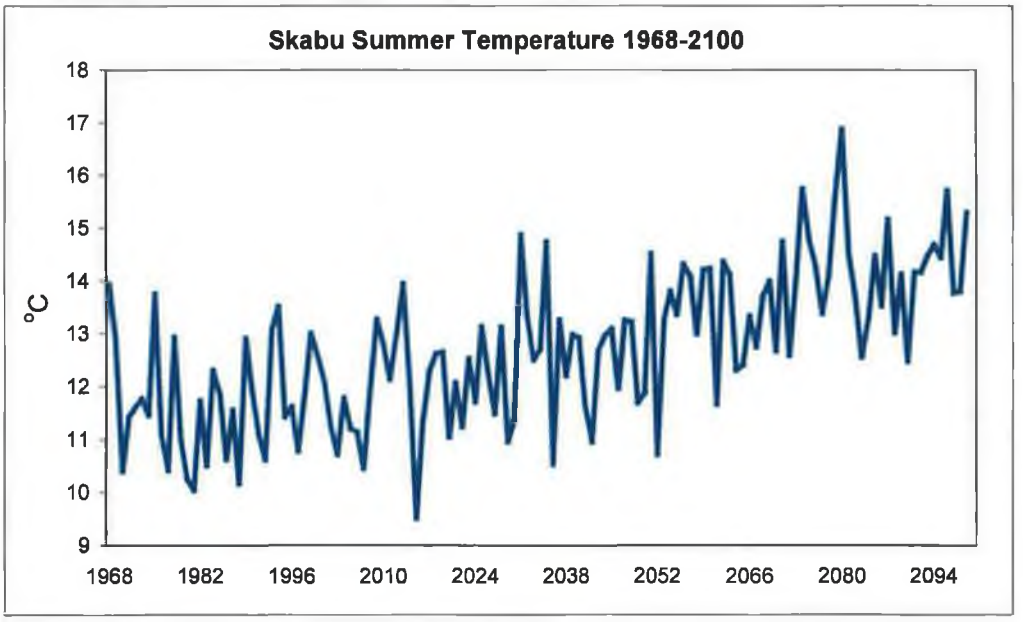

Figure 8.4.14 Mean Summer temperature (June, July and August) for Skabu 1968-2100, downscaled from the HadCM3 GCM.

While a comparison between a maritime and continentally located station are not directly comparative, the suggested seasonal increases in temperature, are found not to be consistent with findings from other research, which suggest that warming should be at a maximum during the winter and at a minimum during the summer (Jóhannesson *et al.*, 1995; Førland *et al.*, 2000; Hanssen-Bauer *et al.*, 2003;). Higher warming rates, particularly during the winter months, are expected for more northern latitudes due to a change in the sea-ice cover (IPCC, 2001a). However, there is a large degree of uncertainty in regards to the rates of increase for Nordic countries and regions around the northern North Atlantic as a reduction in warming rates may result as a consequence of vertical mixing in the ocean (Jóhannesson *et al.*, 1995).

The scenarios suggest that specific humidity in Flesland could increase slightly for all the winter months of December, January and February (Figure 8.4.17). These findings are consistent with what is expected under conditions of a warmer climate, as warmer air is likely to have an increased moisture carrying capacity.

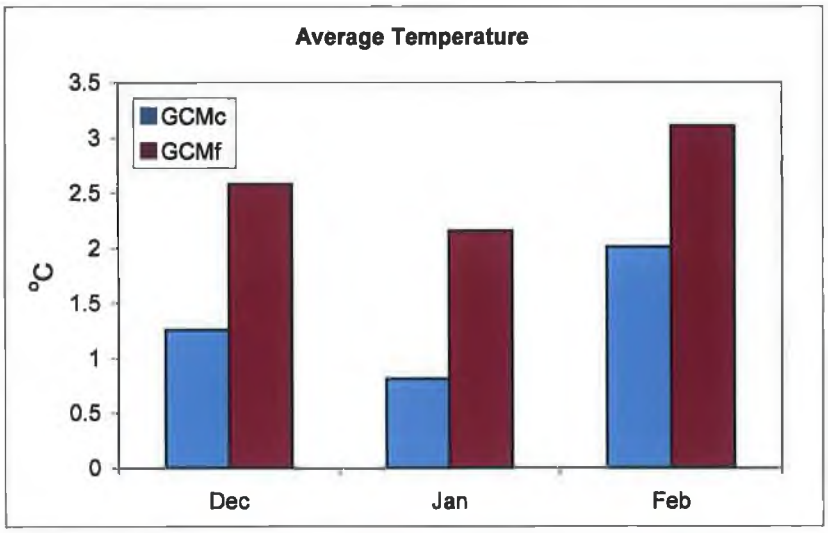

Figure 8.4.15 Flesland winter temperature-$GCM_{control}$ (1968-1996) and GCM_{future} (2068-2096)

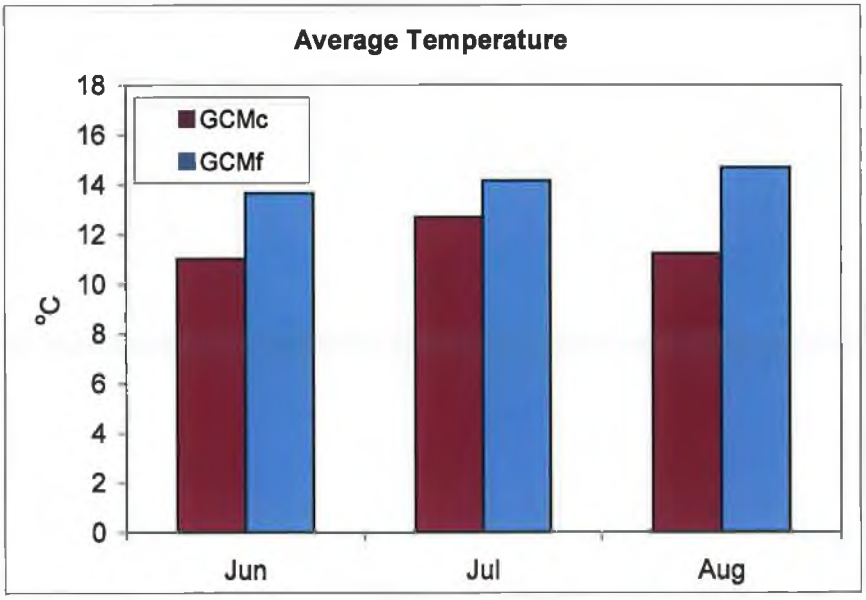

Figure 8.4.16 Skabu summer temperature-$GCM_{control}$ (1968-1996) and GCM_{future} (2068-2096)

Overall reductions in specific humidity during the summer months are suggested for Skabu, consistent with warmer continental air. However, an increase is indicated for the month of August.

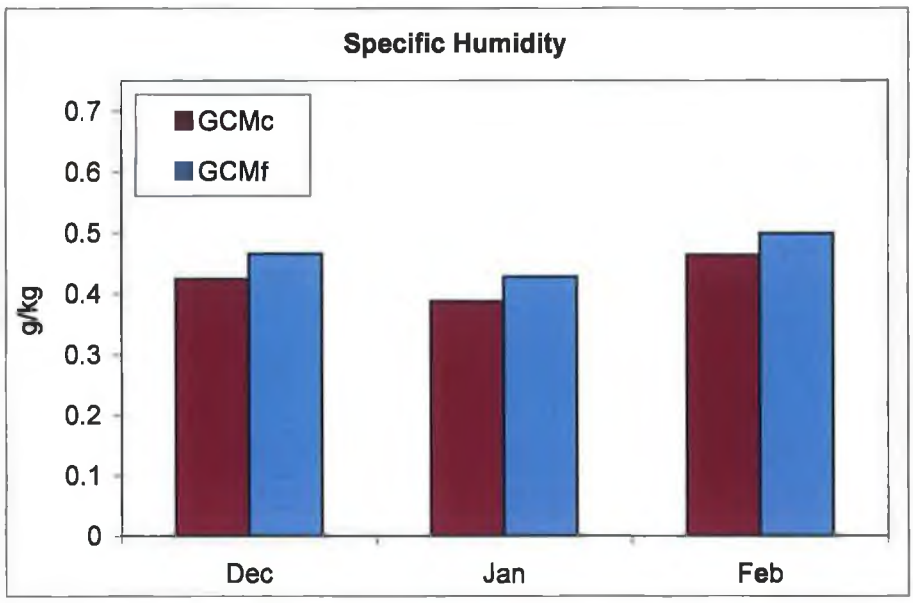

Figure 8.4.17 Flesland specific humidity-$GCM_{control}$ (1968-1996) and GCM_{future} (2068-2096)

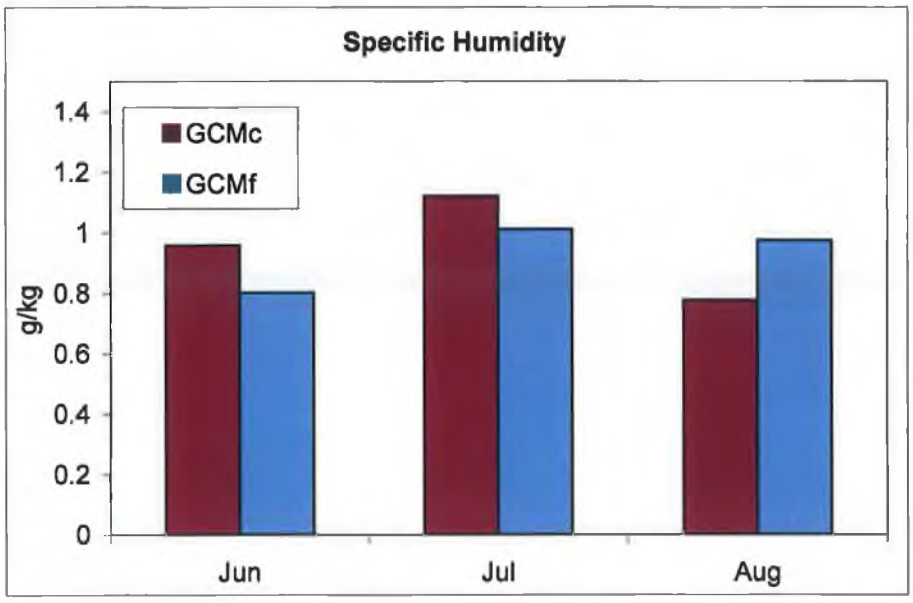

Figure 8.4.18 Skabu specific humidity-$GCM_{control}$ (1968-1996) and GCM_{future} (2068-2096)

8.4.3 Downscaled Temporal Synoptic Index 1968-2100

The downscaled variables for both stations, 28 for Flesland (7 variables by 4 daily measurements) and 21 for Skabu (7 variables by 3 daily measurements) were then used as input into separate principal components analysis for both winter and summer. A similar methodology to that employed for deriving the temporal synoptic index (TSI) in a previous chapter was used on both downscaled datasets.

	Component					
	1	**2**	**3**	**4**	**5**	**6**
pres 00	-0.35	0.71	0.46	0.24	-0.01	0.12
pres 06	-0.43	0.69	0.47	0.26	-0.07	0.07
pres 12	-0.47	0.65	0.48	0.28	-0.11	0.01
pres 18	-0.48	0.61	0.46	0.32	-0.14	-0.04
tmp 00	0.90	0.13	0.00	0.28	0.25	-0.04
tmp 06	0.92	0.11	0.02	0.22	0.25	-0.04
tmp 12	0.82	0.20	0.12	0.31	0.32	-0.15
tmp 18	0.90	0.16	0.10	0.23	0.23	-0.12
rho 00	0.95	0.06	0.18	-0.07	0.03	-0.09
rho 06	0.96	0.04	0.15	-0.03	0.04	-0.05
rho 12	0.97	0.06	0.15	-0.02	0.03	-0.06
rho 18	0.95	0.05	0.22	-0.07	0.03	-0.08
cld 00	0.82	0.05	-0.33	0.32	-0.04	0.20
cld 06	0.83	0.07	-0.30	0.32	-0.02	0.19
cld 12	0.85	0.06	-0.24	0.27	-0.02	0.22
cld 18	0.89	0.09	-0.12	0.21	-0.03	0.09
vis 00	-0.87	0.07	-0.05	0.07	0.35	0.21
vis 06	-0.87	0.02	-0.05	0.09	0.41	0.07
vis 12	-0.88	-0.09	0.00	0.01	0.37	-0.05
vis 18	-0.83	-0.15	-0.10	0.07	0.45	-0.02
vv 00	0.62	0.53	-0.06	-0.48	0.11	0.04
vv 06	0.50	0.67	0.01	-0.50	0.10	0.07
vv 12	0.32	0.77	0.03	-0.50	0.10	0.08
vv 18	0.21	0.81	0.01	-0.44	0.10	0.07
uu 00	0.20	-0.72	0.53	-0.12	0.08	0.18
uu 06	0.35	-0.74	0.47	-0.12	0.08	0.10
uu 12	0.38	-0.74	0.45	-0.11	-0.02	0.08
uu 18	0.53	-0.64	0.34	-0.20	0.11	0.06

Table 8.4.3 Component matrix for Flesland DJF (1968-1997) with six extracted components. Values less than 0.1 are not displayed. Pres-pressure; tmp-temperature; rho-specific humidity; cld-cloud amount; vis-visibility; *vv*-south scalar; *uu*-west scalar

Principal components for the modelled datasets were derived from the component scores based on the 1968/9-1996/7 period. The loading scores were then applied to the remainder of the dataset for the 1997-2100 period. This step was undertaken to ensure the correct standardisation of the modelled data prior to performing PCA, with variable means and variances reflecting the baseline period of 1968/9-1996/7.

	Component					
	1	2	3	4	5	6
pres 06	0.88	0.15	0.19	-0.09	-0.01	0.27
pres 12	0.87	0.11	0.15	0.02	-0.02	0.39
pres 18	0.85	0.05	0.12	0.06	-0.02	0.42
tmp 06	0.08	0.95	-0.02	0.14	-0.03	0.02
tmp 12	0.38	0.86	-0.21	0.04	-0.01	0.00
tmp 18	0.35	0.86	-0.19	0.04	-0.02	-0.02
rho 06	-0.16	0.95	-0.01	0.13	0.01	-0.04
rho 12	-0.18	0.94	0.03	0.13	0.01	-0.06
rho 18	-0.25	0.89	0.14	0.09	0.02	-0.07
cld 06	-0.89	0.03	0.01	0.21	-0.01	0.13
cld 12	-0.88	-0.02	0.05	0.21	-0.02	0.22
cld 18	-0.85	-0.06	0.10	0.21	-0.02	0.25
vis 06	0.80	-0.25	0.17	0.22	-0.01	-0.07
vis 12	0.82	-0.11	0.08	0.14	0.02	-0.26
vis 18	0.79	-0.13	0.10	0.20	0.00	-0.23
vv 06	-0.12	0.02	0.64	0.34	-0.01	-0.27
vv 12	-0.14	0.11	0.88	-0.15	0.03	0.04
vv 18	-0.17	0.11	0.87	-0.07	0.02	0.02
uu 06	0.03	-0.03	-0.05	0.18	0.98	0.05
uu 12	0.02	-0.24	-0.09	0.72	-0.16	0.11
uu 18	0.16	-0.26	-0.06	0.79	-0.05	-0.01

Table 8.4.4 Component matrix for Skabu JJA (1968-1997) with six extracted components. Values less than 0.1 are not displayed. Pres-pressure; tmp-temperature; rho-specific humidity; cld-cloud amount; vis-visibility; *vv*-south scalar; *uu*-west scalar

In the case of modelled Flesland, five components with eigenvalues greater than 1.0 were extracted using the downscaled data for the 1968-2100 period. Six components were extracted using the original observed dataset. In order to ensure consistency between both observed and modelled datasets and subsequent clustering procedure, it was decided to lower the eigenvalue extraction threshold below 1.0 in order that six components could be extracted from the PCA for the downscaled data. The eigenvalue threshold had also to be lowered for Skabu to ensure the required number of extracted components.

Normalisation of the principal components, using the eigenvalue for each component, was again conducted on the extracted principal components prior to clustering on both datasets.

When the component matrices between observed and modelled datasets are compared, the loading patterns display a good degree of consistency. In the case of Flesland, temperature, humidity and cloud amount load highly on component one, with pressure loading highly on component two. While in the case of Skabu, the pressure and cloud variables load highly on component one. However, there is a discrepancy in the loading pattern of temperature in the Skabu dataset. It loads highly in the observed dataset on both component one and two, while in the downscaled dataset, it loads weakly on component one and highly on component two. In general, the similarity of loading patterns, between both datasets, suggests that the downscaling techniques have at the very least captured some of the important interrelationships between variables at both stations, and that some of the underlying physical process have been captured, indicating a degree of confidence in the downscaled scenarios

Cluster centroids or means, from both stations, were extracted from the observed clusters discussed in chapter five. These were then input as seed cluster centres to a K-means clustering analysis performed on the modelled dataset. The K-means method, unlike the clustering technique previously employed, is a non-hierarchical technique but has an efficient clustering algorithm and is therefore suitable for large datasets. The primary reason for selecting this clustering method was that it allowed for the prior specification of cluster centres which is a requirement for this part of the study. Using the observed cluster centres constrains the modelled output and ensures that cluster characteristics are compatible between both observed and modelled datasets.

8.4.4 Results from the downscaled Temporal Synoptic Index

Figure 8.4.19 and Figure 8.4.21 show the comparison between observed and downscaled air mass frequencies for Flesland and Skabu. Results for Flesland indicate that the downscaled air mass clusters produce realistic frequencies when compared to the observed frequency occurrences. Eleven of the clusters are within ± 5%, with the remainder within ± 7% of the observed frequencies. A comparison of modelled current (Mod_c 1968-1996) and modelled future (Mod_f 2068-2096) suggest only minor changes in the winter airmass frequencies. Despite the relative small frequency changes, mean daily temperatures are suggested to increase across all clusters (Figure 8.4.20).

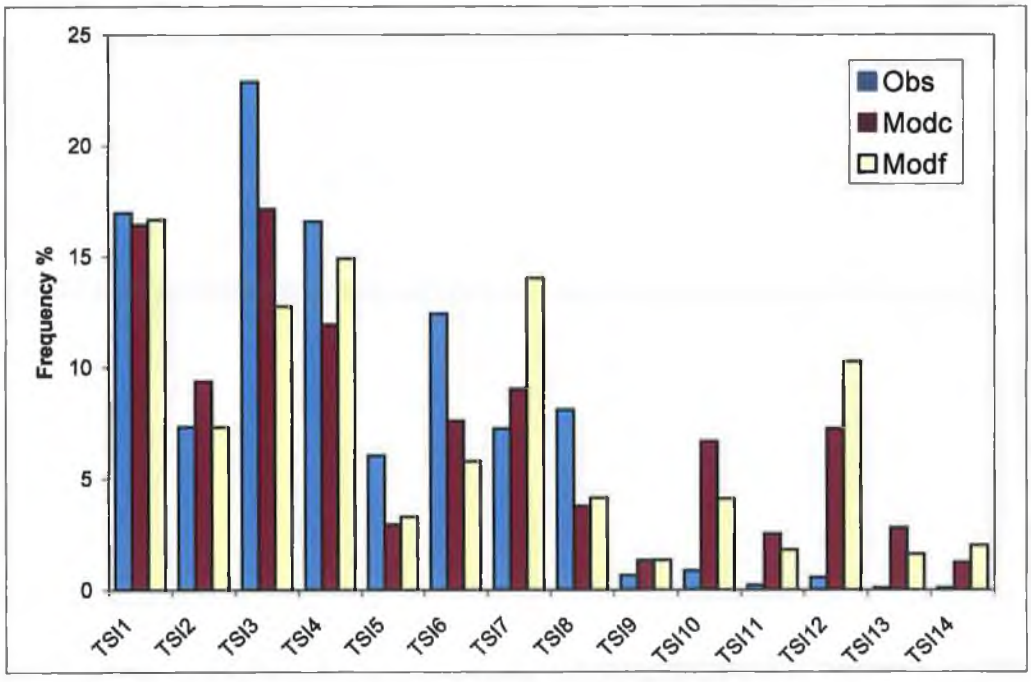

Figure 8.4.19 Comparison between winter air mass occurrence frequencies for Flesland. Observed (1968-1996), modelled current (1968-1996) and modelled future (2068-2096).

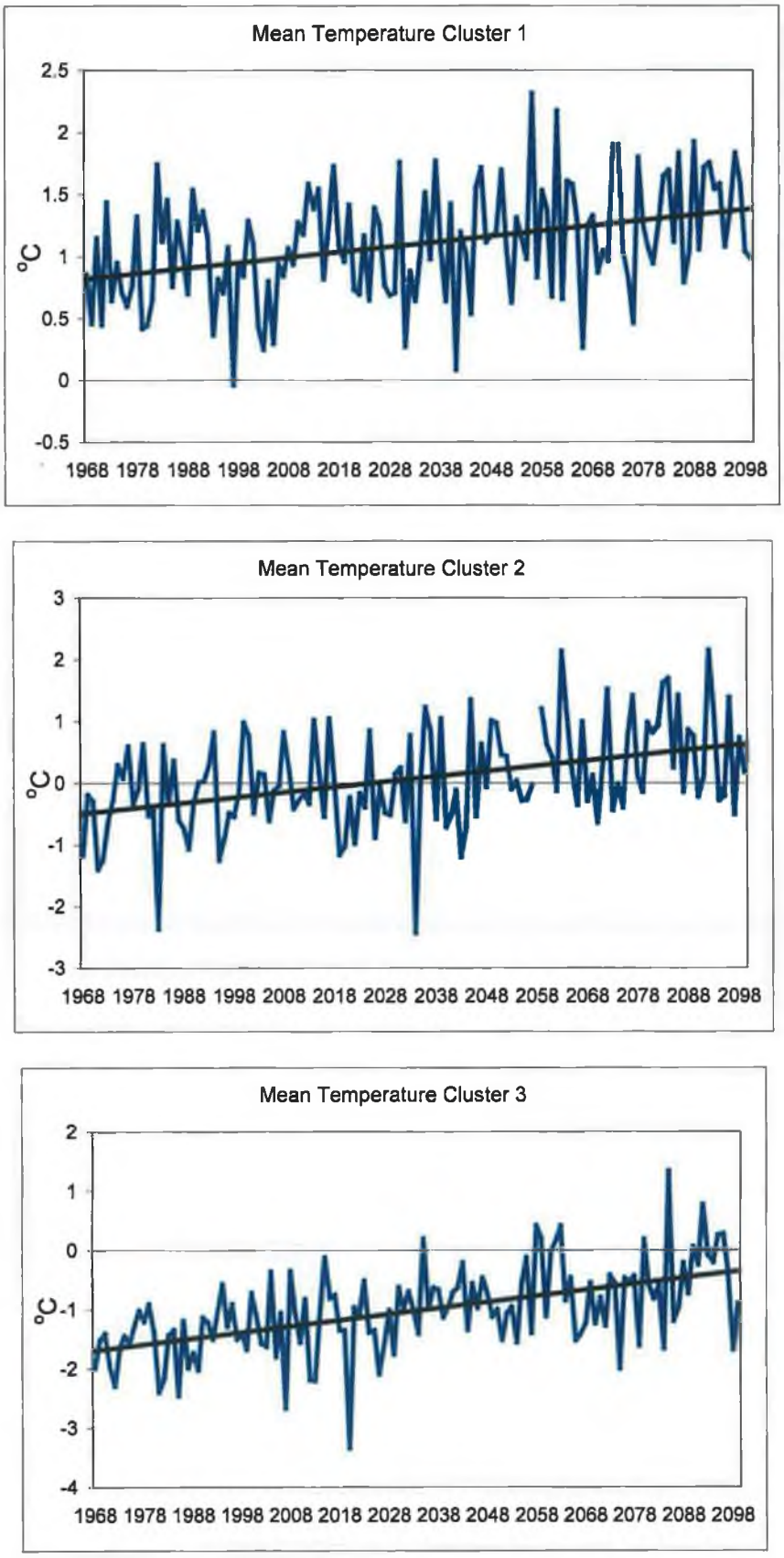

Figure 8.4.20 Mean daily winter temperature for clusters 1-3 for Flesland.

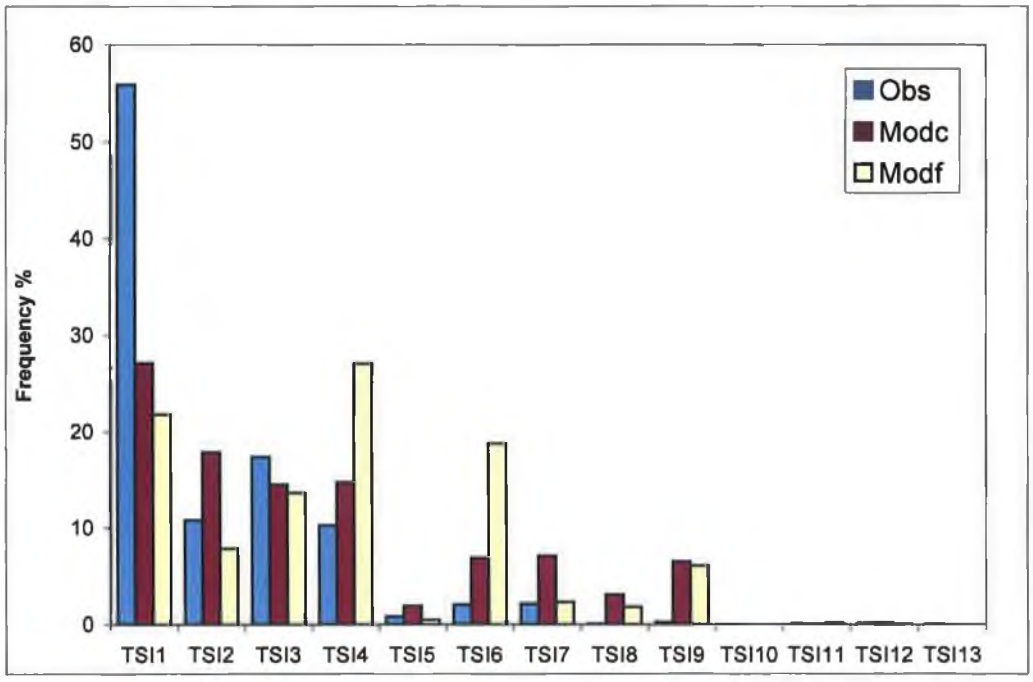

Figure 8.4.21 Comparison between summer air mass occurrence frequencies for Skabu. Observed (1968-1996), modelled current (1968-1996) and modelled future (2068-2096).

A comparison of observed and modelled air mass frequencies for Skabu indicates that the modelled frequencies for summer are less reliable, with cluster 1 being grossly underestimated, by as much as half. The remaining clusters are within ± 7% between observed and modelled frequency occurrence. There are a number of possible reasons for the underestimation in the modelled output for cluster 1, which is predominantly a westerly cluster. Errors in the downscaling technique, resulting from lower percentage explained variance during the summer months are a contributory factor. Evidence for this is suggested from the component scores in the principal component analysis, where the relationship between pressure and temperature in component one is weaker in the modelled data than that suggested by the component scores from the observed data.

It is also possible that systematic biases that may occur in the parent GCM are also being transmitted to the downscaled output. To test if this could be the case, wind direction, calculated from the geostrophic equations, was compared between the NCEP reanalysis data used in the calibration of the downscaling transfer functions and the HadCM3 GCM data for the observed period.

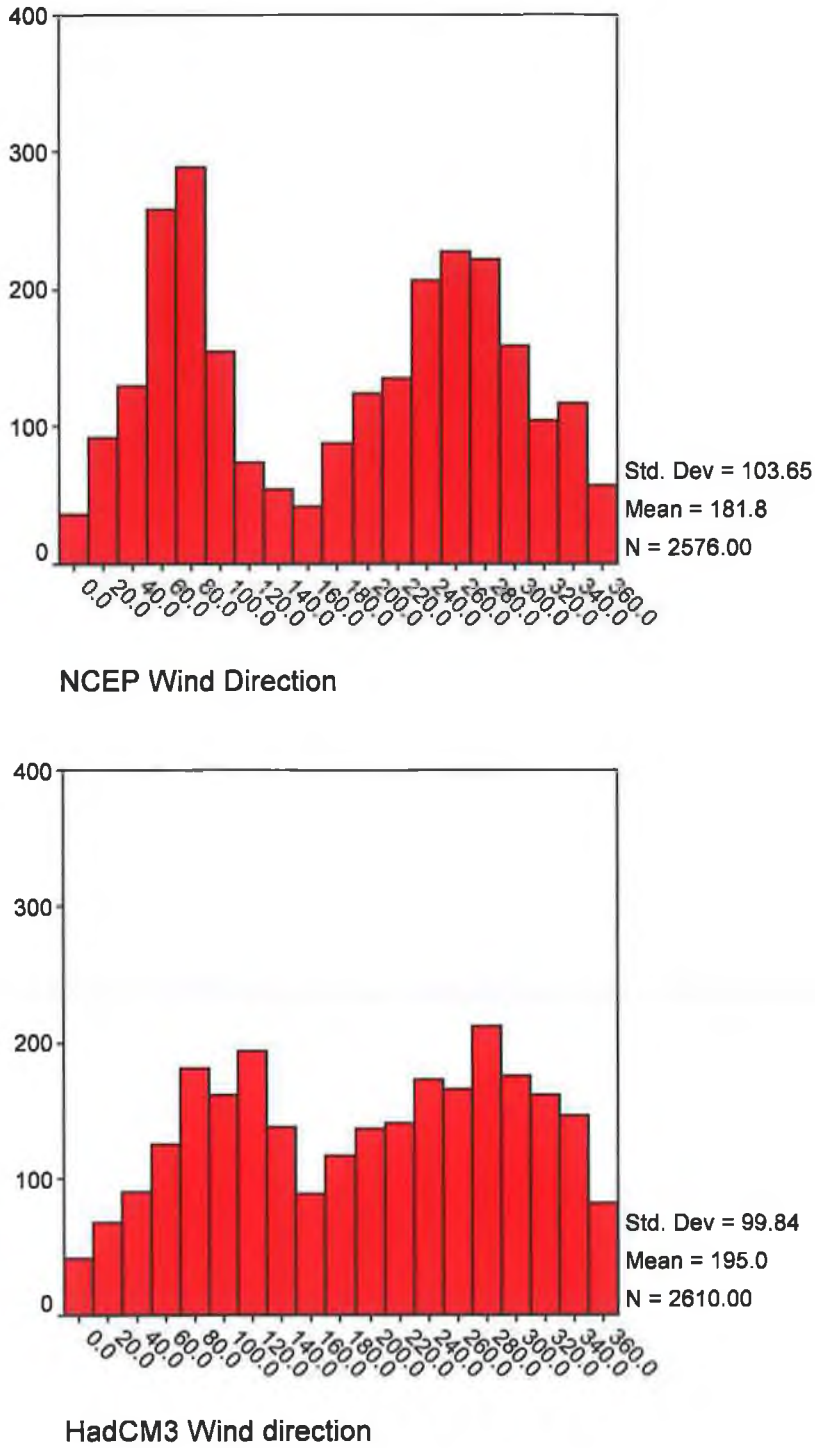

Figure 8.4.22 Histogram of wind direction from the observed NCEP Reanalysis data and HadCM3 GCM data.

A comparison of westerly wind direction between both histograms indicates that while the GCM is largely capturing the right frequency of occurrence, the shape of the probability distribution function (PDF) is flatter for wind directions between

180° to 300° (Figure 8.4.22). Thus, there is less definition between wind direction and inferred circulation types from the westerly segment (180° to 270°) that is likely to produce less defined frequencies of occurrence of westerly air mass types resulting in fewer westerly air mass types being classified as such. As cluster 1 from Skabu is associated with cyclonic westerly (CW) type circulation, the likely effect of this difference between the observed and modelled PDF are likely to impact this cluster the most severely.

As the frequency of cluster 1 is negatively correlated to that of clusters 2 and 3, in both observed and modelled air mass frequencies, the effect of underestimating modelled cluster 1 should result in increased occurrences of clusters 2 and 3. However, as the westerlies represented by the GCM are less defined, the effect of the error distribution between clusters may not be too critical.

Assuming that any bias being translated to the modelled air mass frequencies from the HadCM3 GCM data is consistent over time, then frequency changes between modelled current (1969-1997) and modelled future (2069-2097) should be reasonably robust. The frequency occurrence of cluster 4 and 6 show increases in the region of 12% and 11% respectively, while cluster 2 suggests a decrease in the order of 10%, between modelled current and modelled future.

Figure 8.4.23 shows mean daily summer temperature increasing for clusters 1 to 3; increases that are apparent across all the summer cluster types.

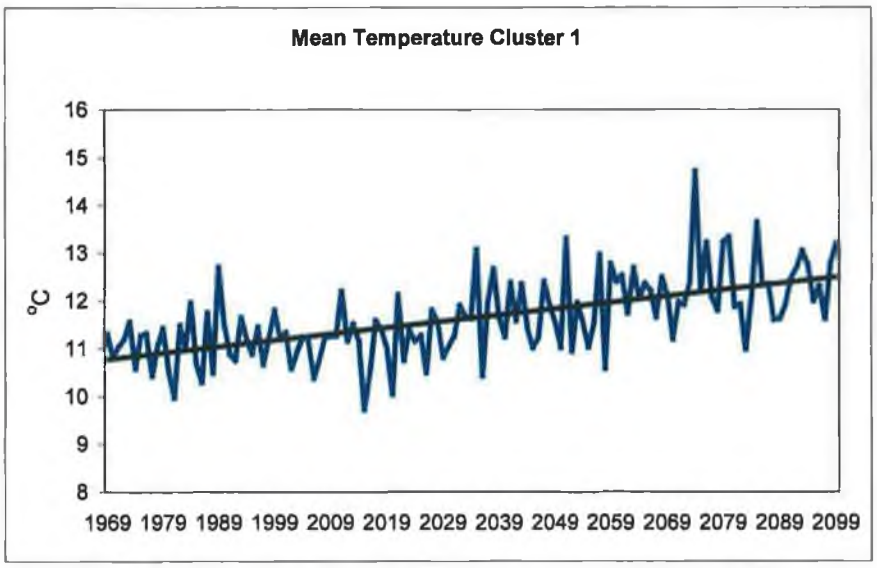

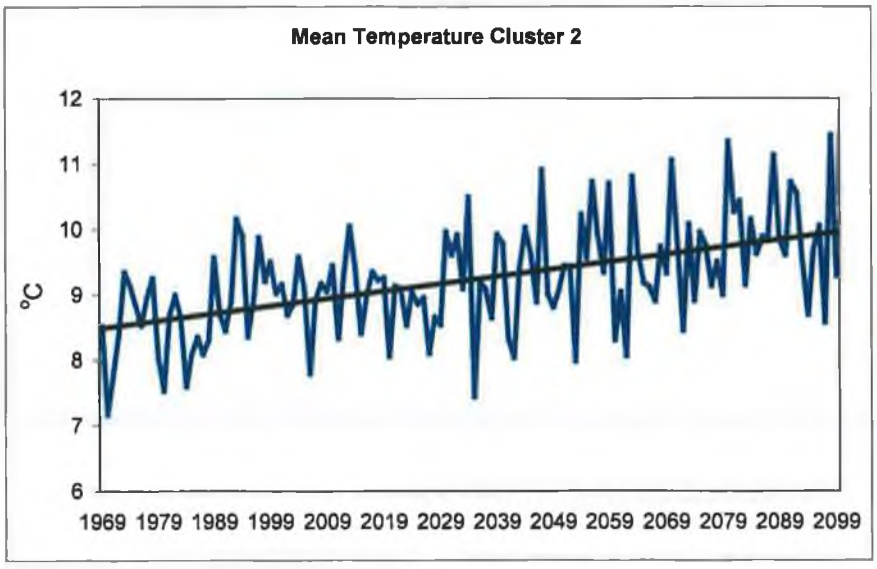

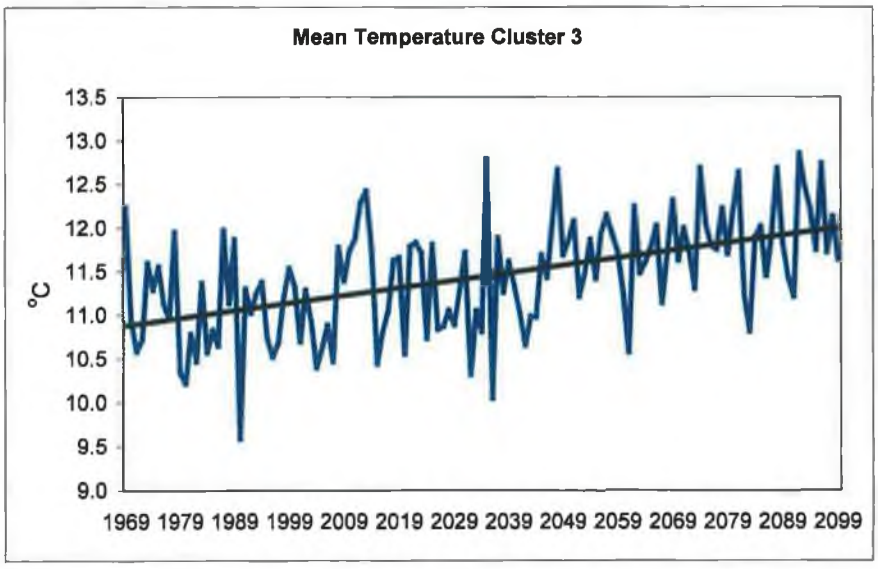

Figure 8.4.23 Mean daily summer temperature for clusters 1-4 for Skabu.

8.4.5 The effects of changing cluster frequency occurrence on glacier mass balance

As outlined previously, winter and summer air mass frequency occurrences based on the observed data from Flesland and Skabu were related to winter and summer glacier mass balance from Rembesdalskåka for the period 1968-1997. Having derived cluster frequencies for the period 1968-2100, for both of these stations, from downscaled output based on the HadCM3 GCM output, it should be possible to examine the effects of the suggested changes in frequencies of the air mass types on mass balance from Rembesdalskåka, based on the previously derived relationships.

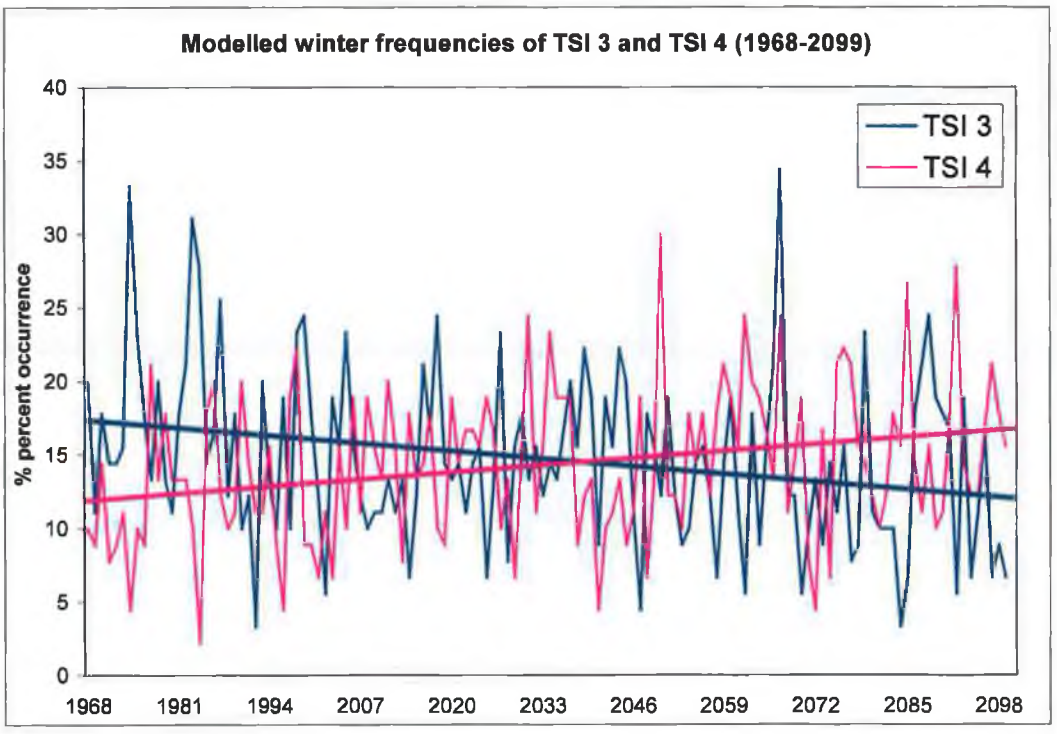

Figure 8.4.24 Modelled frequencies of TSI 3 and 4 for winter, based on downscaled data from Flesland.

In the regression equations based on the observed data from Flesland, TSI 4 enters the equation first indicating its relative importance to winter mass balance on Rembesdalskåka. Based on the downscaled air mass frequencies, the frequency of air mass type TSI 4 is likely to increase by 5-6% during the course of the present century from Figure 8.4.24. While the frequency of TSI 3 is suggested to decrease

from 18% to around 12%, by end of century. It is likely that, as both of these air mass types have a negative effect on winter mass balance, the increasing frequency of TSI 3 is likely to be compensated by a decrease in TSI 4 resulting in little change in winter balance.

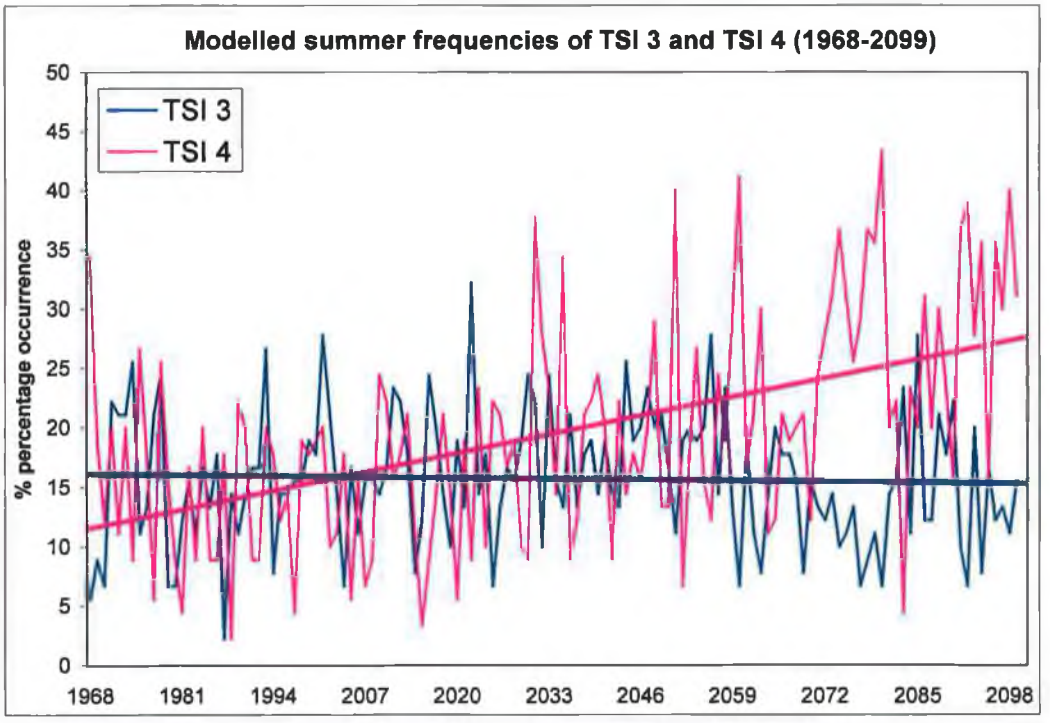

Figure 8.4.25 Modelled frequencies of TSI 3 and 4 for summer, based on downscaled data from Skabu.

Large changes in the frequency occurrence of the summer air mass type, TSI 4, from Skabu are suggested as occurring by end of century from Figure 8.4.25. The increase in frequency is almost threefold its current value of just over 10%. There is a marginal reduction suggested in the frequency of occurrence of TSI 3 during the summer months. Both TSI 3 and 4 from Skabu also have a negative effect on summer mass balance with any increases likely to result in increased ablation during the summer season.

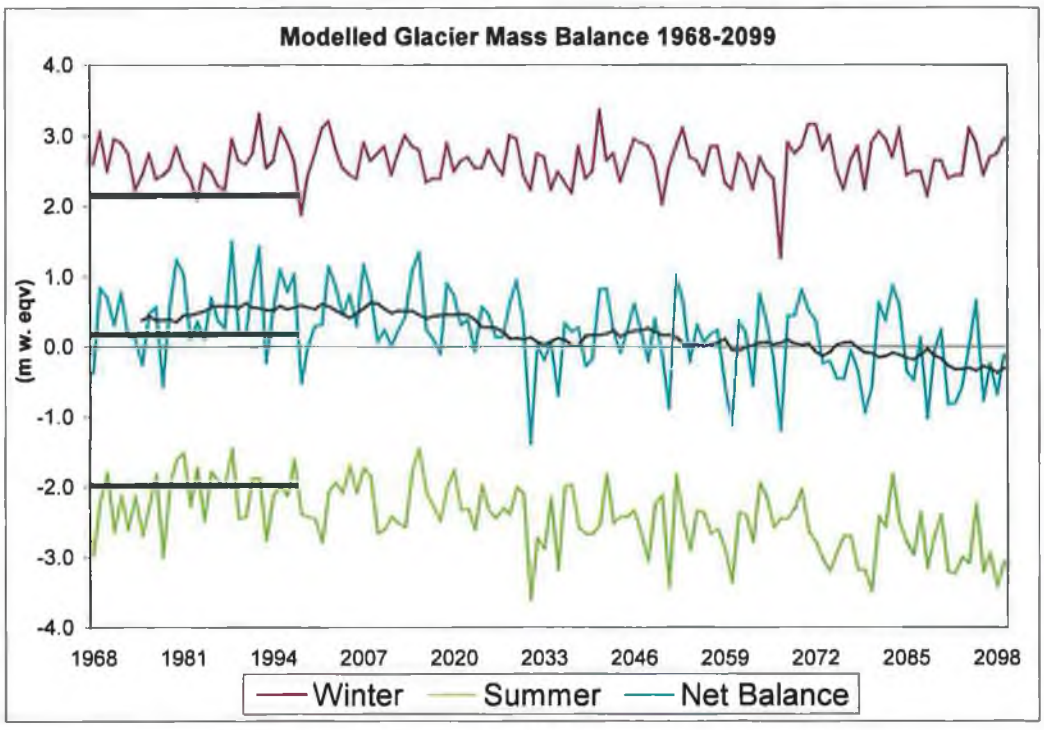

Figure 8.4.26 Modelled glacier mass balance for Rembesdalskåka based on relationships derived between the frequency occurrence of observed air mass types at Flesland and Skabu, 1968-2099 (Thick Lines-Observed mass balance for 1968-1997 included for comparative purposes; Thin line-15-year centred moving average).

Winter, summer and net balance were modelled for the period 1968-2099 using the modelled air mass frequencies from Flesland and Skabu as input into the equations relating airmass occurrences to mass balance (Figure 8.4.26). The modelled winter balance remains relatively constant over the course of the present century, while the summer balance, which remains constant to approximately 2010, begins to increase after this point resulting in increased ablation during the summer months. This increase in summer ablation is reflected in the net balance, which also starts to decline after 2010 until the 2030s. During the 2030s-2040s, net balance remains around zero or marginally positive. After 2050, net balance again starts to decline resulting in largely negative balances until the end of century.

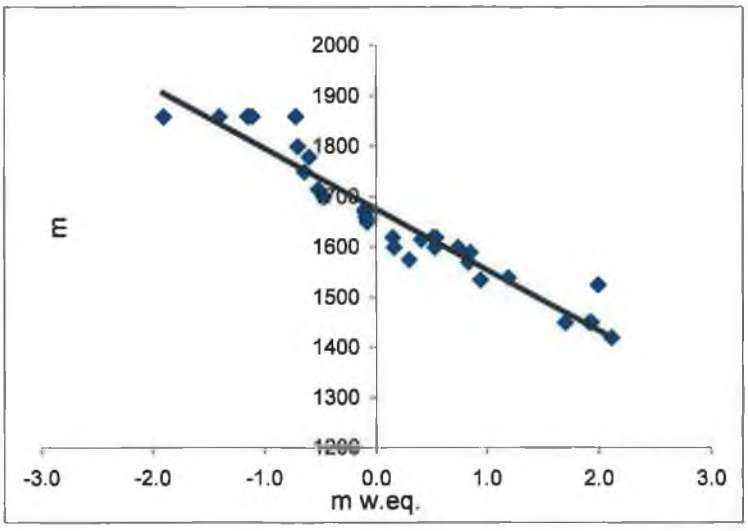

Figure 8.4.27 Observed relationship between the measured equilibrium line altitude (ELA) and net balance for Rembesdalskåka (1968-1997)

As a consequence of decreasing annual net balance and the dependence of the equilibrium line altitude (ELA) on net balance, it is likely that the ELA will increase in elevation by up to 100 metres as ablation begins to outpace accumulation over the course of the century (Figure 8.4.27, Figure 8.4.28). The effects of decreasing net balance, as a consequence of climate change, and its effects on the ELA of Rembesdalskåka (Figure 8.4.28) will be addressed in the next chapter where modelled net balance will be used as input to a 1-Dimensional ice flow model to determine the likely change in glacier behaviour of Rembesdalskåka.

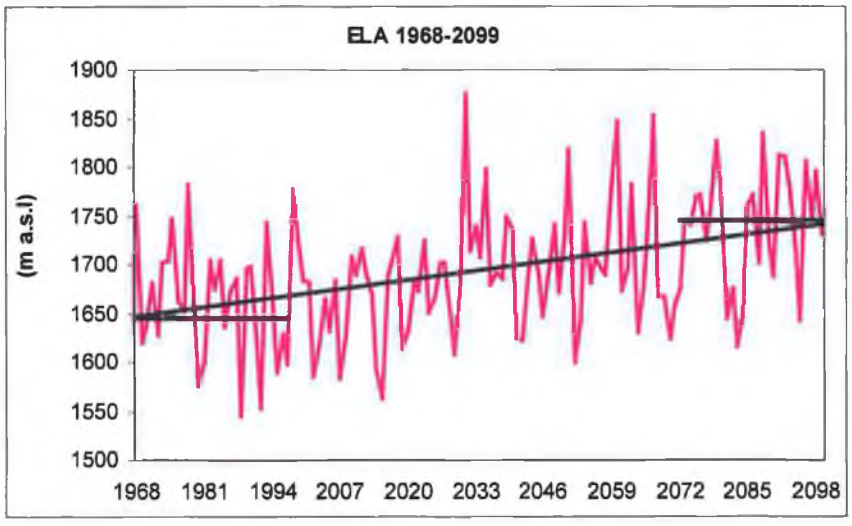

Figure 8.4.28 Effect of reducing net balance on the ELA of Rembesdalskåka 1968-2099 (the ELA has been adjusted to account for bias in the modelled net balance) (Horizontal lines represent means of the respective 30 year periods)

Chapter IX
Ice flow model

9.1 Introduction

Theoretically, if the mass balance of a glacier were to remain constant, the glacier would attain a position of equilibrium with the climate producing a steady state in which the size of the glacier would remain constant. However, accumulation and ablation rarely balance as a consequence of fluctuations in climate. These changes in accumulation and ablation, while having an immediate and short-term effect on the annual net balance, if sustained, will result in longer-term changes to the glacier front position (Nye, 1963b) and glacier behaviour. Changes in receipt on the glacier surface get propagated down the glacier as kinematic waves (Nye, 1963a) producing a lagged response to changes in accumulation and ablation (Paterson, 1981). The response time of a glacier to any perturbation varies depending primarily on its size (Bahr *et al.*, 1998) but also on a number of local and other factors. Front position changes therefore tend to lag changes in climate and this lag depends on the glacier's response time.

To investigate how climate change is likely to affect the glacier behaviour and front position of Rembesdalskåka, results from previous chapters were integrated in order to estimate mass balance changes over the course of this century. The aim of this chapter is to incorporate these suggested changes in net balance due to climate forcing, which produce changes in the equilibrium line altitude (ELA), as input to a 1-Dimensional glacier model. The model will consider the glacier as a one dimensional flow system. Despite obvious simplifying assumptions, the two-dimensional geometry or cross-sectional area of the glacier is also incorporated.

9.2 Review of mass balance and ice flow model literature

In an analysis of the influence of climate on glaciers, Nye (1960) assessed the mechanism of response time, treating the glacier as a one dimensional flow system, but incorporated kinematic wave theory. His results suggested that an important

interaction occurs between the direct response of the lower part of glacier to accumulation changes, resulting in compression, and the resultant kinematic wave. The interaction between both of these forces can produce large differences in glacier behaviour from one glacier to another (Nye, 1960). In later work, Nye (1963) calculated the response for any point on the glacier to supply and loss of mass, enabling a known history of glacier variation to be translated in to a history of gain and loss rates, response curves and budget history (Nye, 1965).

Oerlemans (1988) coupled a simple climate model, which calculates perturbations of surface radiation balance and temperature and forced using volcanic activity and greenhouse warming, to a schematic time dependant glacier model. The output from the simple climate model was first translated into changes in the equilibrium line altitude that were then used as input to the glacier model. Results from this study indicated good agreement with observed records of glacier front positions. However, it questions the assertion that the retreat of glaciers evident during the last century could all be attributed to global warming. Oerlemans (1998) suggested that only 50% of the retreat could be accounted for in this way.

Greuell (1989) in his comprehensive analysis of climate, mass balance and glacier front position of Hintereisferner, used a numerical flow model to model historical and future front positions, using both reconstructed climatic data and data based on a CO_2 concentration forcing. Greuell (1989) also incorporated a simulation with a climate forcing based on Oerlemans (1988). While model simulations compared well with the historical front position data allowing for some degree of confidence to be placed in the future simulations, the simulations were found to be sensitive to the parameterisation between mass balance and climate. High quality mass balance and climate data are therefore considered to be very important. Additional complications were also found to affect the simulated output, such as, the complexity of the glacier geometry.

Despite some of these complications, numerical modelling of glaciers has been undertaken by a number of researchers and in numerous locations, such as, the Nepal Himalaya (Kadota *et al.*, 1997), New Zealand (Oerlemans, 1997a), Africa

(Hastenrath, 1992), Austria (Greuell, 1989; Van De Wal and Orelemans, 1995; Schlosser, 1997; Zuo and Oerlemans, 1997), Sweden (Raper *et al.*, 1996; Brugger, 1997), Switzerland (Schmeits and Oerlemans, 1997; Wallinga and Van De Wal, 1998), Iceland (Jóhannesson, 1997) and Norway (Oerlemans, 1986; Laumann and Tvede, 1989; Oerlemans, 1997b).

Oerlemans (2000) suggests that the correct specification and hence, parameterisation, of mass balance is of crucial importance to any glacier modelling exercise. As mass balance is used to drive the ice flow model either directly or through perturbing the equilibrium line altitude, uncertainties that exist in the mass balance model are carried through the flow model and are reflected in the output. Kuhn (1989) assessed the response of the equilibrium line altitude to climate fluctuations of temperature, humidity and net radiation. Turbulent transfer coefficients were also used as input to the model.

The assumption that the mass balance gradient is conserved under conditions of climatic change was examined by Oerlemans and Hoogendoorn (1989). Observational data from a number of glaciers suggested that interannual changes in mass balance might in fact be independent of altitude. They also examined the assertion that interannual variations were transferable between various climatic states. To assess these assumptions, an altitude dependent mass balance model was developed which used altitude dependent values of precipitation, temperature and atmospheric transmissivity for solar radiation.

They also examined the effects of changes in temperature, cloudiness, albedo and precipitation on the derived mass balance profiles. Under typical climatic conditions for the Alps, they found that a $1^{o}K$ temperature change led to a change in the altitude of the ELA of 130m, the sensitivity of which was found to the significantly affected by albedo feedback. More importantly, their findings indicated that the mass balance profile cannot be expected to be independent of altitude and therefore they dismiss the linear balance model of Lliboutry (1974). However, their findings indicate support for the ELA profile approach in which the ELA curve is phase shifted up or down depending on the net balance.

Temperature and precipitation are two key climatic determinants of summer and winter balance and their importance is reflected in the fact that they form the most basic input into all mass balance modelling techniques. These variables are generally measured at numerous locations around a glacier, can be readily incorporated in to a simplistic mass balance model and produce satisfactory results.

The simplest way to incorporate these variables into a mass balance model is to derive regression equations relating them to winter balance, summer balance or net balance of a nearby glacier. This method was used by Laumann and Tvede (1989) in their analysis of the effects of climate change on Graubreen, a glacier located in western Norway. Using a slightly modified methodology, Brugger (1997) incorporated, in addition to temperature and precipitation, seasonal mass balance into the regression equations. Equilibrium line altitudes have also been calculated using temperature (Wallinga and Van De Wal, 1998) and precipitation anomalies in a multiple linear regression (Kerschner, 1997).

A number of studies have utilised the degree-day approach to modelling mass balance, which can incorporate annual, seasonal or daily temperature values, while snow accumulation is determined as the precipitation that falls when temperatures fall below $1^{\circ}C$ (Laumann and Reeh, 1993). Values for temperature and precipitation are taken from nearby climate stations. If the number of positive degree-days exceed the number of days needed to melt snow, then the remaining days are used to melt glacier ice but with a modified degree-day factor. The degree-day factors for snow melt and ice melt and lapse rates for temperature and precipitation are calibrated against observed mass balance data.

Having established a relationship between the climate parameters and mass balance, modifying the parameters can be used to assess the sensitivity of mass balance to climate change. Laumann and Reeh (1993) found that using this method, with an increase of $1\text{-}2^{\circ}K$ and an increase in precipitation of 10%, the low lying maritime glacier of Ålfotsbreen, despite being situated in a high precipitation

area, was more sensitive than the drier, but more elevated and inland glaciers of Nigardsbreen and Hellstugubreen.

Braithwaite and Zhang (1999) also found that maritime temperate glaciers had an increased sensitivity to warming in comparison to sub-polar glaciers which displayed much reduced sensitivities. These findings were part of a large-scale assessment of over 37 glaciers in different parts of the world. They used a degree-day modelling approach to simulate mass balance calibrated on temperature and precipitation extrapolated to altitude from nearby climate stations.

Jóhannesson *et al.* (1995) found that the degree-day parameters remained relatively stable over time in their application of the degree-day modelling approach to three glaciers, in Iceland, Greenland and Norway. However, findings by Vincent and Vallon (1997) which suggested a drift in the association between temperature and the summer balance of glacier de Sarennes, may require this assertion to be tested further. Adding a note of caution, the authors suggest that calibration of the model should be based on yearly mass balance data instead of mass balance data averaged over the measurement period, due to a wide range of possible model parameters that could be fit resulting in a similar solution (Jóhannesson *et al.*, 1995).

Oerlemans and Reichert (2000) quantify the climate sensitivity of the mean specific balance for a number of glaciers, utilising a model that incorporates temperature and precipitation anomalies to produce a seasonal sensitivity characteristic. Climatic sensitivity of the mass balance can then be determined from anomalies from the reference state for each month.

More sophisticated approaches, such as energy balance models, which try to account for energy passing into and out of a system, have also been used to model glacier mass balance. These models also address some of the deficiencies present in the simpler models. While they offer a much improved capability for modelling mass balance (Braithwaite and Zhang, 1999), their use to date has been restricted to a few glaciers due to a lack of glacier-specific meteorological data and have been of short duration.

The energy balance model is described as follows

$$Q_{AG} = R_S + R_l + H + S$$

Equation 9.1

Q_{AG} energy flux between Atmosphere and Glacier

R_S short wave radiation flux

R_l long wave radiation flux

H turbulent transfer of sensible heat

S turbulent transfer of latent heat

Fluxes from the atmosphere towards the glacier are regarded as positive

(Greuell and Oerlemans, 1986)

The mass balance equation

$$M = -\frac{F}{L_m} + \frac{H_{la}}{L_v}$$

Equation 9.2

M rate of change of mass

L_M latent heat of melting

L_V latent heat of vapourisation

H_{LA} latent heat flux

F energy flux at surface

(Oerlemans, 2000)

The correct specification of mass balance is of vital importance as uncertainties resulting from this process can get translated down to the final output of the glacier model (Oerlemans, 2000). As outlined above, there are numerous techniques in which mass balance can be modelled using a variety of climate parameters, from some of the simpler techniques that just include temperature to the more advanced techniques incorporating surface energy fluxes and turbulent fluxes. While the techniques that incorporate temperature and precipitation are widespread due to

readily available data, the same cannot be said for the energy balance based methods, which as a result are generally of short duration.

The synoptic based approach employed in this research, which incorporates key synoptic climate elements, such as temperature, humidity, wind direction and speed, cloudiness and visibility, does not require in-situ meteorological data from the surface of the glacier and offers a pragmatic solution to the energy balance technique while producing comparable results.

9.3 Glacier Model

9.3.1 Model Outline

The glacier model used to examine possible changes in the glacier behaviour of Rembesdalskåka is a 1-Dimensional ice flow model which assumes that the geometry of the selected glacier facilitates the selection of a flowline, x, an independent variable (Oerlemans, 1998) (Figure 9.3.1). Positioning of the flowline, while not too problematical in the lower areas of the glacier can present some problems in the upper regions. This was the case for Rembesdalskåka, mainly due to the presence of a nunatuk, which splits the flow that then rejoins the main body again (Figure 9.3.2). This feature was subsequently removed from calculations of bed width from the model.

Grid points along the flowline are selected at equal intervals and these locations define the points at which the numerical calculations are performed. Each point represents the area of the glacier for a specific elevational interval (Oerlemans, 1998) and therefore it is important that the area-elevation distribution relationships are preserved when positioning the flowline, particularly in the accumulation zone.

The dynamic behaviour of the glacier is described in terms of changes in ice thickness, calculated from a continuity equation integrated over the ice thickness and glacier width (Oerlemans, 1986; Oerlemans, 1998). Vertical mean velocity is determined by τ, the local driving stress, which is proportional to the ice thickness

and surface slope (Oerlemans, 1997). The density of the glacier is considered to be the same everywhere (Paterson, 1981) so a conservation equation for ice volume is

$$\frac{\delta S}{\delta t} = -\frac{\delta (US)}{\delta x} + \omega B$$

$$\omega = \omega_o + \lambda H$$

Equation 9.3

ω glacier width at the surface

λ slope of valley walls

H glacier thickness

$$S = H\left(\omega_o + \frac{1}{2}\lambda H\right)$$

area of glacier cross-section

Equation 9.4

$U = U_d + U_s$

Equation 9.5

mean ice velocity in cross section

$$= f_d H \tau^3 + \frac{f_s \tau^3}{H}$$

$$\tau = -\rho g H \frac{\delta h}{\delta x}$$

Equation 9.6

τ driving stress

ρ ice density

g acceleration due to gravity

$h = b + H$

h surface elevation

Equation 9.7

S cross sectional area, perpendicular to the flow line

b bed elevation

B specific balance

f_d velocity due to internal deformation

f_s velocity due to sliding

Substituting S, the cross sectional area, and ω, glacier width at the surface, into the continuity equation results in,

$$\frac{\delta H}{\delta t} = \frac{-1}{\omega_o + \lambda H}\frac{\delta}{\delta x}\left[\left(\omega_o + \frac{1}{2}\lambda H\right)UH\right] + \mathbf{B}$$

Equation 9.8

Incorporating driving stress, the mean ice velocity can be expressed in terms of thickness and surface slope

$$U = \left[f_d \gamma H^4 \left(\frac{\delta h}{\delta x}\right)^2 + f_s \gamma H^2 \left(\frac{\delta h}{\delta x}\right)^2\right]\frac{\delta h}{\delta x}$$

$$\gamma = (\rho g)^3$$

Equation 9.9

After substitution, gives

$$\frac{\delta H}{\delta t} = \frac{-1}{\omega_o + \lambda H}\frac{\delta}{\delta x}\left[D\frac{\delta(b+H)}{\delta x}\right] + B$$

Equation 9.10

where the ice thickness is governed by a non-linear diffusion equation, where the diffusivity, D, is

$$D = \left(\omega_o + \frac{1}{2}\lambda H\right)\left[f_d \gamma H^5 \left(\frac{\delta h}{\delta x}\right)^2 + f_s \gamma H^3 \left(\frac{\delta h}{\delta x}\right)^2\right]$$

Equation 9.11

(Oerlemans, 1997)

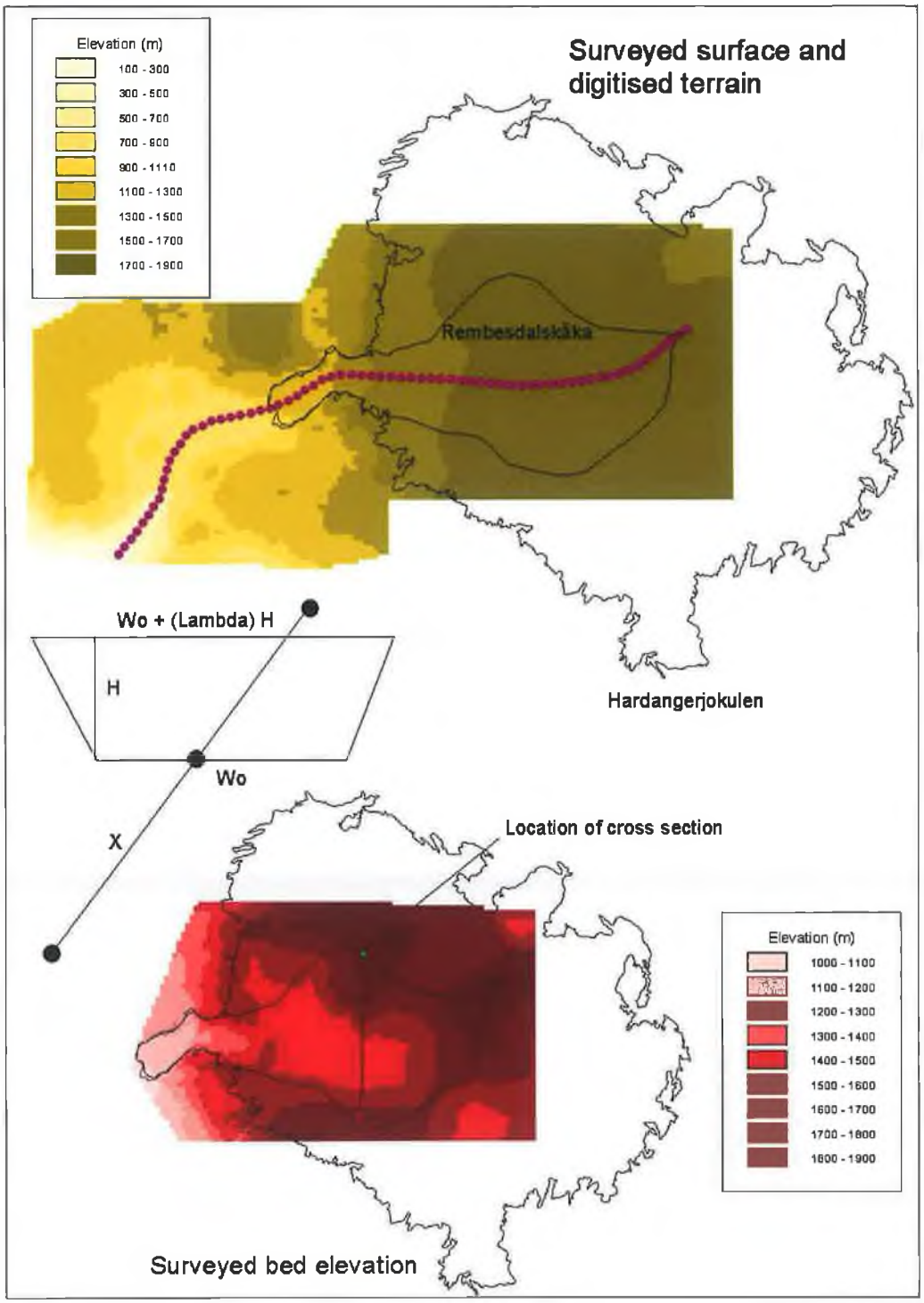

Figure 9.3.1 Surface and bed elevation data for Rembesdalskåka. Also, the flowline from which the data used as input to the glacier model was extracted from.

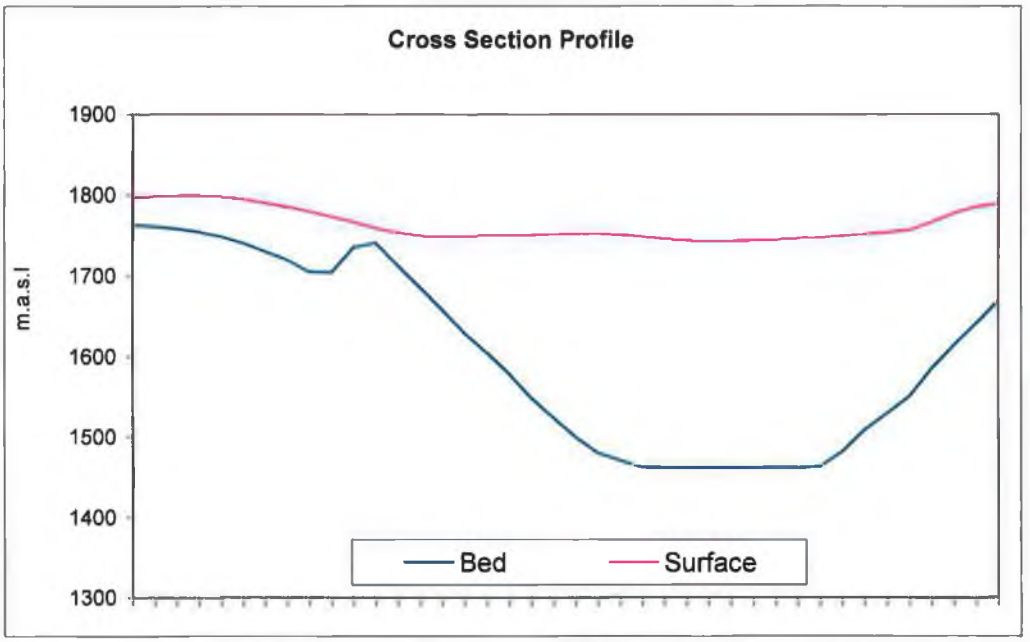

Figure 9.3.2 Cross section extracted from the profile line in Figure 9.3.1, displaying the bed elevation, glacier surface and nunatuk.

The correct calculation of U, the mean ice velocity, is dependent on f_d and f_s, the flow parameters, being approximated correctly. These parameters are in turn dependant on bed conditions, debris content and the crystal structure of the basal ice (Oerlemans, 1986). A range of values has been used previously for various different glaciers and these offer reasonable starting points to approximating more site specific values for a particular glacier being studied.

At the upper boundary, surface slope is set to zero and there is no ice flux, while conditions at the snout are more difficult to parameterise. However, the balance gradient dominates the glacier dynamics which will determine where the glacier ends (Oerlemans, unpublished).

9.3.2 Model Inputs

A number of inputs need to be specified prior to running the model. These inputs are extracted at each grid point whose spacing on the flowline was set at 200 metre intervals. Larger grid spacing can result in truncation errors in the model (Oerlemans, 1997). Truncation errors can also result as a consequence of large

timesteps, therefore the model timestep was set at a reasonably small value of 0.01 years (3.65 days).

In order to extract the required data, the bed and surface elevations, surveyed by the Norwegian Water Resources and Energy Directorate (NVE) in 1961 and again in 1995, were acquired. The data existed in the form of vector data, height contours, which were then imported into a geographic information systems (GIS) environment, ArcView 3.2, and converted to raster surfaces (Figure 9.3.1).

Elevation data only existed for the area bounded by the glacier, Hardangerjøkulen, and only the bed of Rembesdalskåka had been surveyed. In order to extend the flowline beyond the present extent of Rembesdalskåka, the area in front of the glacier was scanned in from the Norge 1:50000 map series of Myrdal (Statens Kartverk). The image was georeferenced and each 20-metre contour was then digitised on-screen using ERDAS Imagine software. The vector dataset was then imported into ArcView 3.2, converted to a raster surface and merged with the original data (top image Figure 9.3.1).

A flowline was then digitised over the surface of the glacier, which was then split into over 60 200-metre interval nodes or grid points. Perpendicular cross sections, which intersected the flow line at each grid point, were then constructed. These cross sections provided the profiles from which data were extracted from both the bed elevation and the glacier surface data (Figure 9.3.2).

Each extracted cross section, comprising of bed and surface elevation values for each profile, were then used to determine bed width (ω_o) and the slope of the glacier side walls (λ), from which the glacier width at the surface (ω) and glacier cross sectional area (S) could be determined.

While some of this information could have been extracted from glacier maps and other information, the ability to incorporate the digital data into a geographic information system allowed for the rapid acquisition of the necessary information, once the correct tools had been set up. It also facilitated rapid extraction and testing

of various grid configurations. Assuming that similar data exists for another glacier, the profiling and extraction techniques are also readily transferable within the GIS environment.

9.3.3 Glacier ice flow model

The numerical model, based on the differential equations outlined by Oerlemans (1997) was programmed in the PERL computer language (Appendix IV), which is a mathematically efficient scripting language and is cross platform compatible. The model was written so that it numerically calculates h over space, i, down the flowline, at i-½ and i+½, and over time, j, at j-½ and j+½. Initial conditions are known, either the model is initialised from bedrock or zero ice conditions, or it can be perturbed from an assumed steady state, with glacier ice. The pressure density of ice (ρ) was set to 910 kg m^{-3} and gravity (g), 9.81 ms^{-1}. The flow parameters were initially set to

$$f_d \ 1.9 \times 10^{-24} \ Pa^{-3} \ m^2 \ s^{-1}$$
$$f_s \ 5.7 \times 10^{-20} \ Pa^{-3} \ m^2 \ s^{-1}$$

(After Oerlemans, 1997).

However, these parameters were later modified during the initialisation runs, in order that the modelled and observed glacier profile matched.

9.3.4 Model initialisation

For initialisation and testing of the model and parameters, the mass balance (B) was prescribed based on an assumption of steady state. To obtain a steady state mass balance curve, the net balance was averaged for the period 1963-1997 (Figure 9.3.3). The forcing, B, was then based on fitting a piecewise linear fit to the observed mass balance expressed as a function of altitude. However, this method assumes that the shape of the curve will remain constant in a changed climate situation.

For elevation ≥ 1800 metres	B = 2.5395 + (-0.0081*(h-ELA))
For elevation ≥ 1750 metres	B = 1.1668 + (-0.0012*(h-ELA))
For elevation < 1700 metres	B = -0.1262 + (-0.0094*(h-ELA))

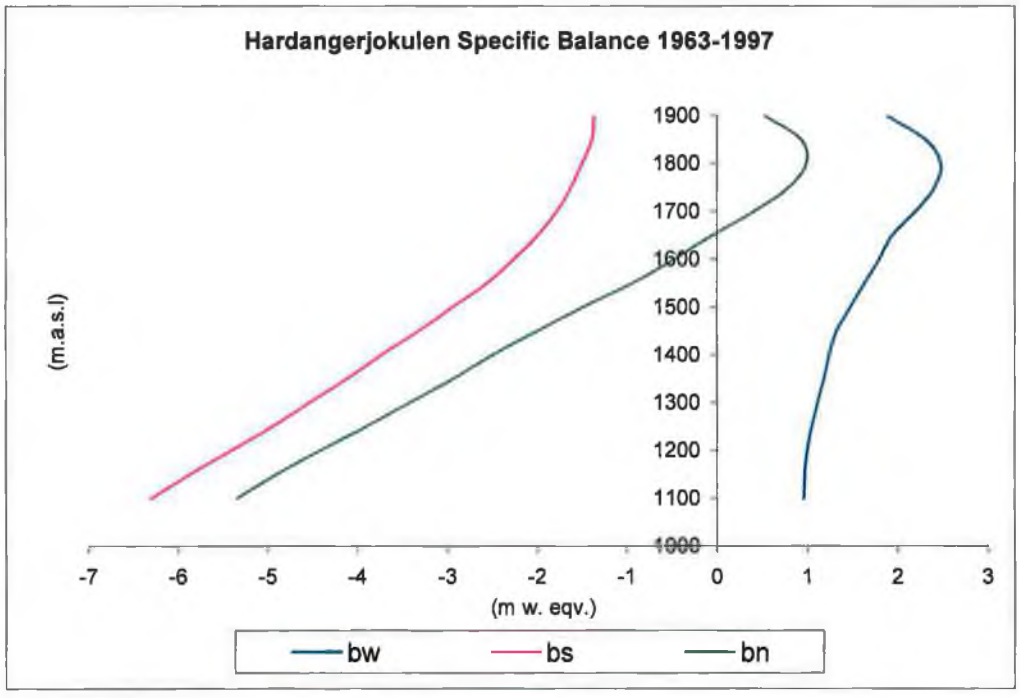

Figure 9.3.3 Altitudinal distribution of winter, summer and net balance for Hardangerjokulen averaged over the 1963-1997 period.

From Figure 9.3.3, mass balance reaches a maximum at approximately 1800 metres, 100 metres below the highest point of the glacier. From 1800 metres to the glacier front, there is a steep linear decrease in mass balance, which crosses from positive to negative at 1650 metres, the average ELA over the period of observation.

Initially, the model was run to a steady state starting with zero ice volume and the mass balance was input as outlined above, but adjusted so that B = 0. An ELA of 1650 metres, based on the average ELA for the observed period 1963-1997, was used in the piecewise linear equations. Figure 9.3.4-Figure 9.3.8 display the modelled glacier surface for various time intervals.

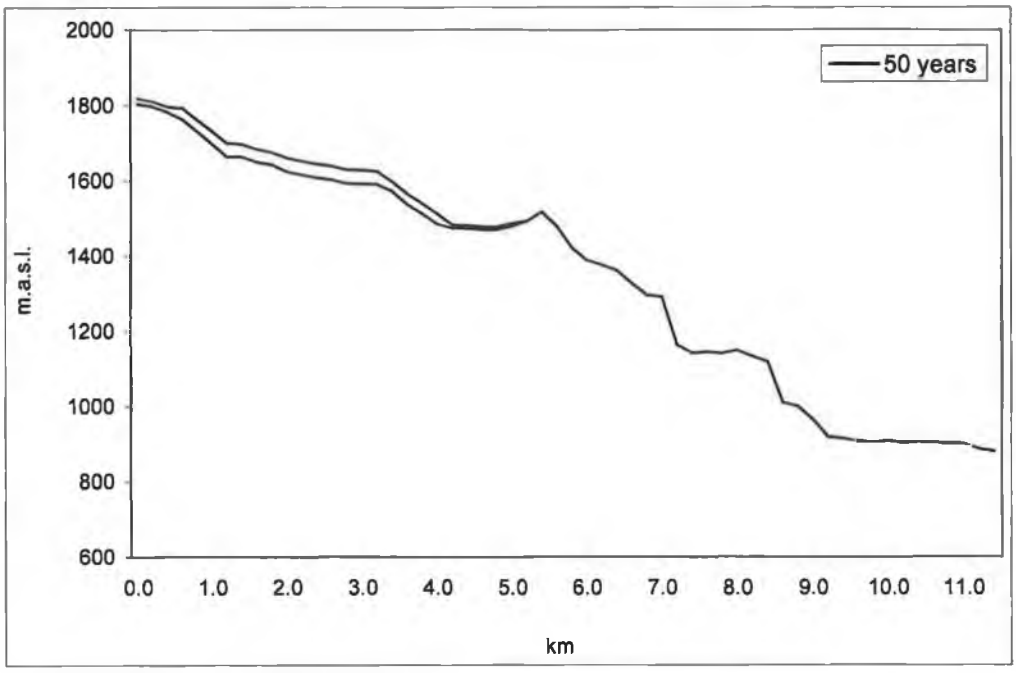

Figure 9.3.4 Modelled glacier surface after 50 years, starting from initial conditions of zero ice

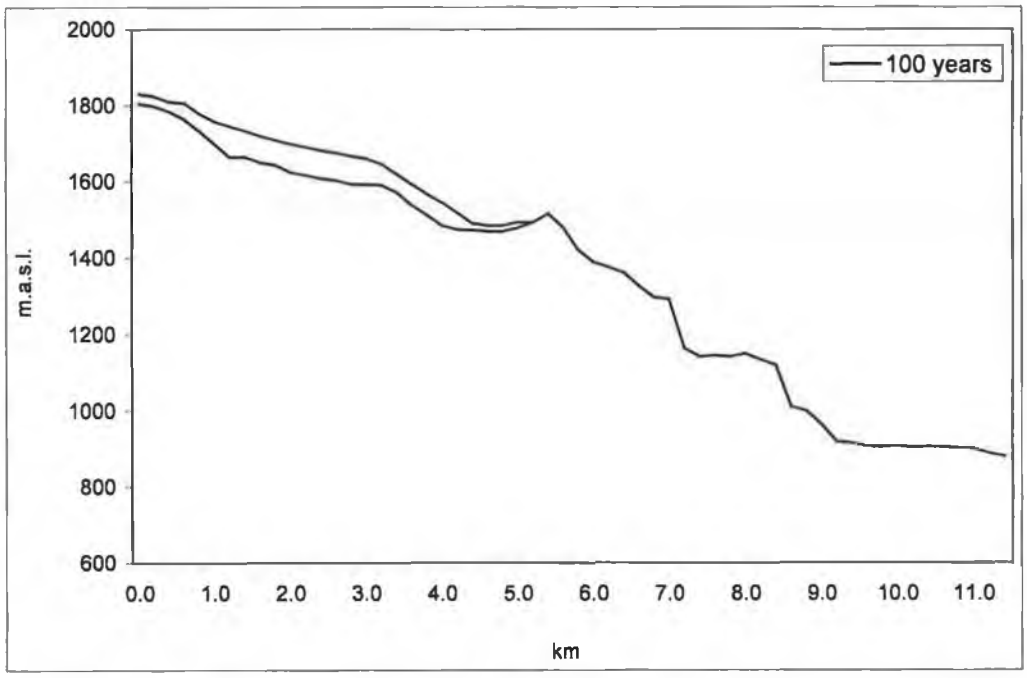

Figure 9.3.5 Modelled glacier surface after 100 years, starting from initial conditions of zero ice

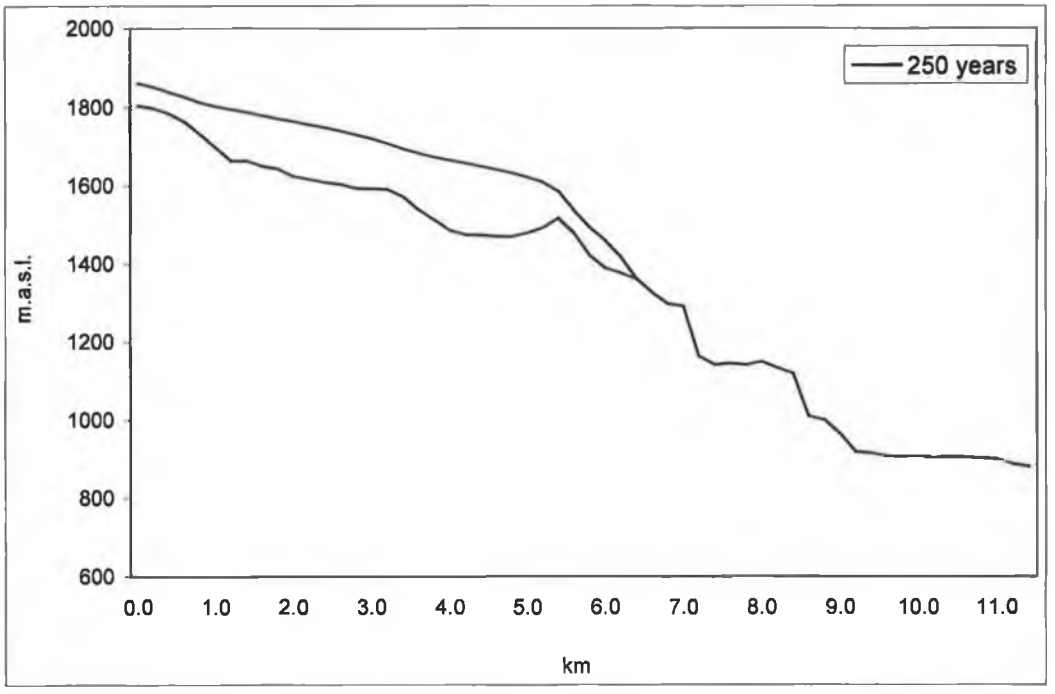

Figure 9.3.6 Modelled glacier surface after 250 years, starting from initial conditions of zero ice

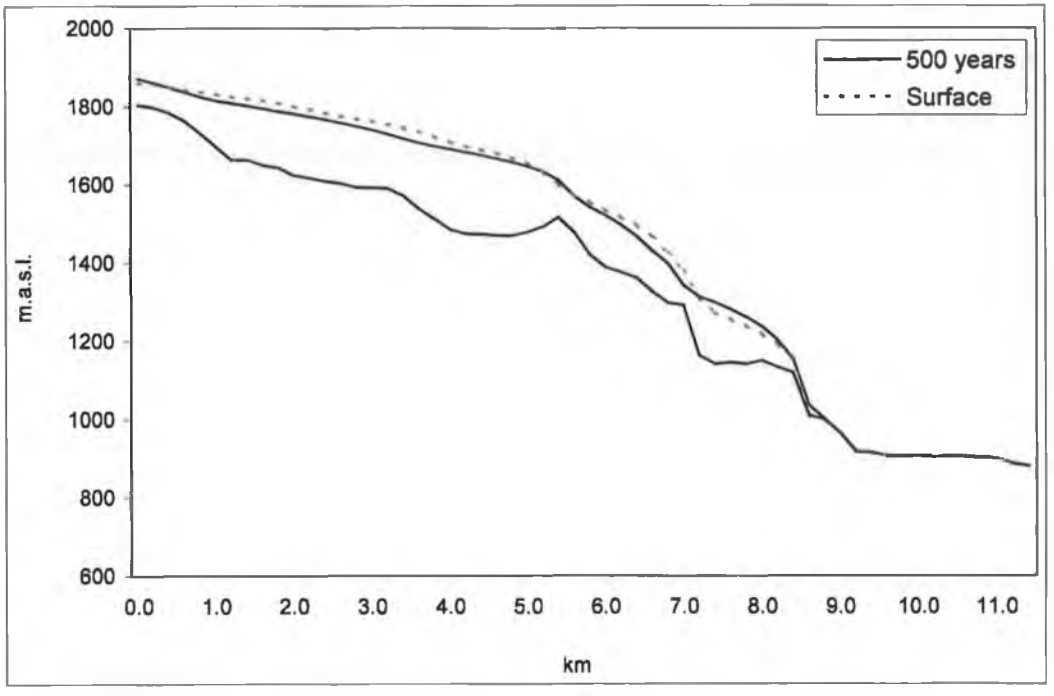

Figure 9.3.7 Present observed glacier surface (---) and modelled glacier surface (—) after 500 years, starting from initial conditions of zero ice

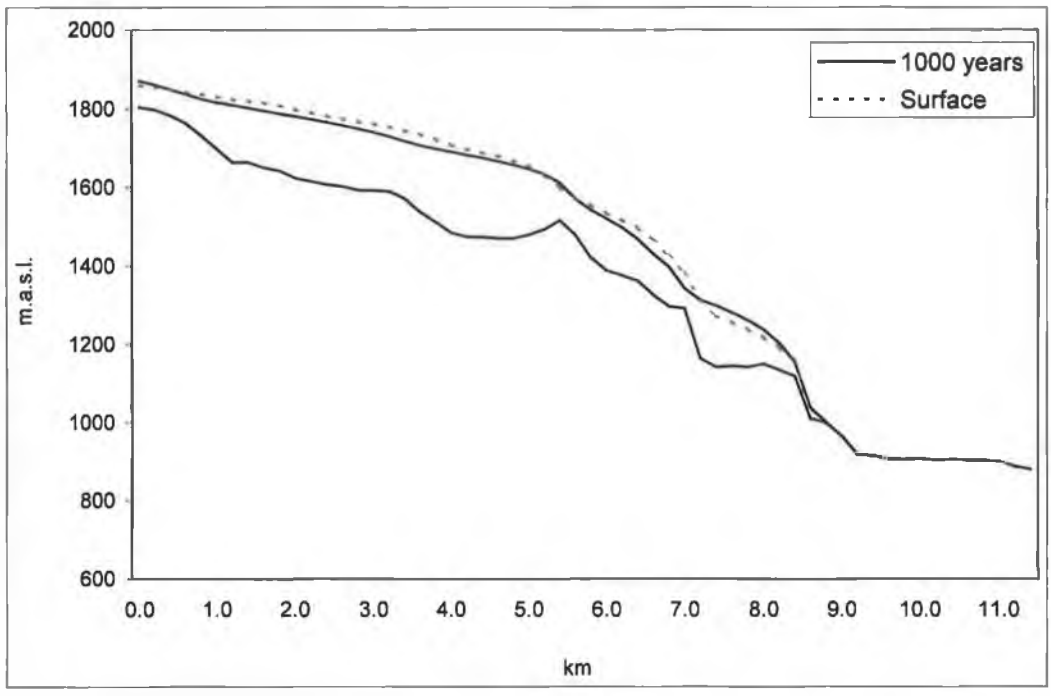

Figure 9.3.8 Present observed glacier surface and modelled glacier surface after 1000 years starting from initial conditions of zero ice

After 500 model years the glacier appears to reach equilibrium (Figure 9.3.7) and maintains its front position under the constant reference mass balance forcing. The agreement between model output and the observed glacier front position is very good, despite the coarse bed elevation.

A large range of flow parameters were also tested and the model was found to be very sensitive to adjustments in both these parameters, relative to each other; changes in either of these produced different steady state surfaces, findings similar to Oerlemans (1997). Eventually, the values selected were as follows-

$$f_d = 1.9 \times 10^{-16}$$
$$f_s = 5.7 \times 10^{-13}$$

While a combination of different parameter values may give similar results, the dependence of model sensitivity to the specific choice of values may be weak for non-surging glaciers (Oerlemans, 1998).

9.3.5 Implications for Rembesdalskåka

To investigate how the changes in mass balance suggested in the previous chapter may effect the behaviour of Rembesdalskåka, the ice flow model was run based on the climate scenario forcing from the HadCM3 GCM downscaled output. Model parameters determined during the initialisation runs were retained for the scenario run.

$$B = B(\text{steady state profile}) + \Delta B$$

The mass balance forcing, B, was based on perturbing the observed profile by a change in mass which would result in a raising or lowering of the ELA. Comparison of the observed and modelled winter and summer mass balances for the 1968-1997 period suggested that a bias existed in the modelled mass balance. The modelled series were adjusted so that their means compared with the observed data for the period 1968-1997 (Figure 9.3.9). The mass balance perturbations were then calculated from the resultant net balance, which, for ease of integration into the programme, were averaged for each decade.

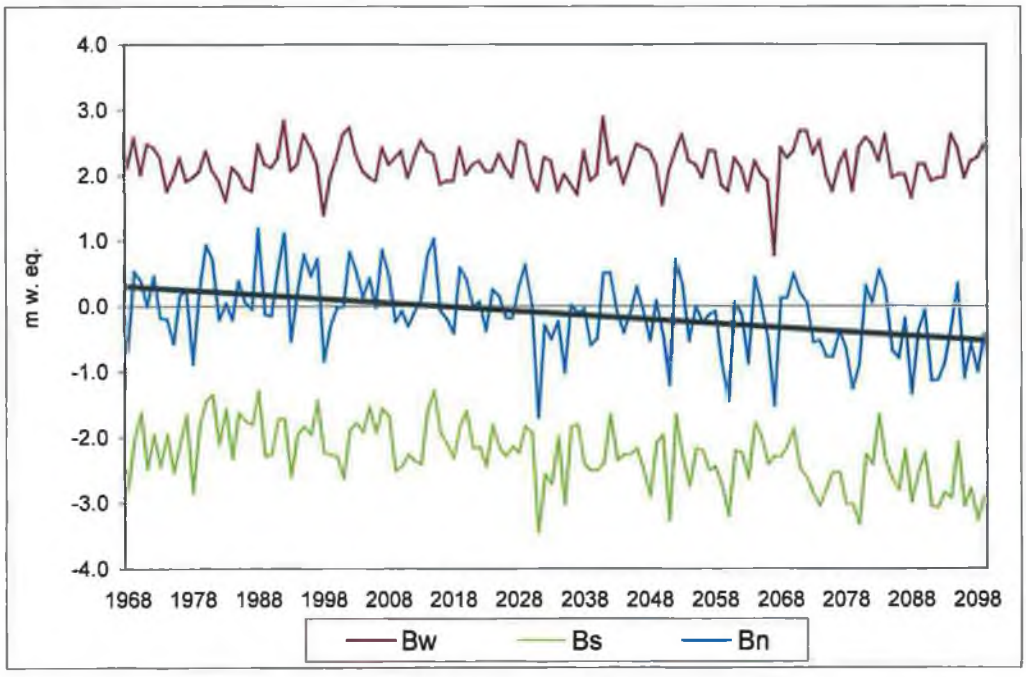

Figure 9.3.9 Adjusted mass balance series 1968-2099

From Figure 9.3.9, net balance shows a decreasing trend over the whole period. However, within this overall trend, it remains marginally positive until the early 2030s, after which the increasing influence of the summer over winter balance forces the net balance to become increasingly negative. The importance of the winter balance contribution to the net balance of Rembesdalskåka (Bw/Bn =0.85) is clearly evident for the first few decades of the century, after which summer balance (Bs) becomes a more important contributor to net balance.

A number of runs were undertaken to test the sensitivity of the model to the mass balance changes. These runs consisted of initialising the model from zero ice conditions or using the observed glacier surface prior to perturbing the mass balance. However, results were comparable for model runs irrespective of which initialisation method was used.

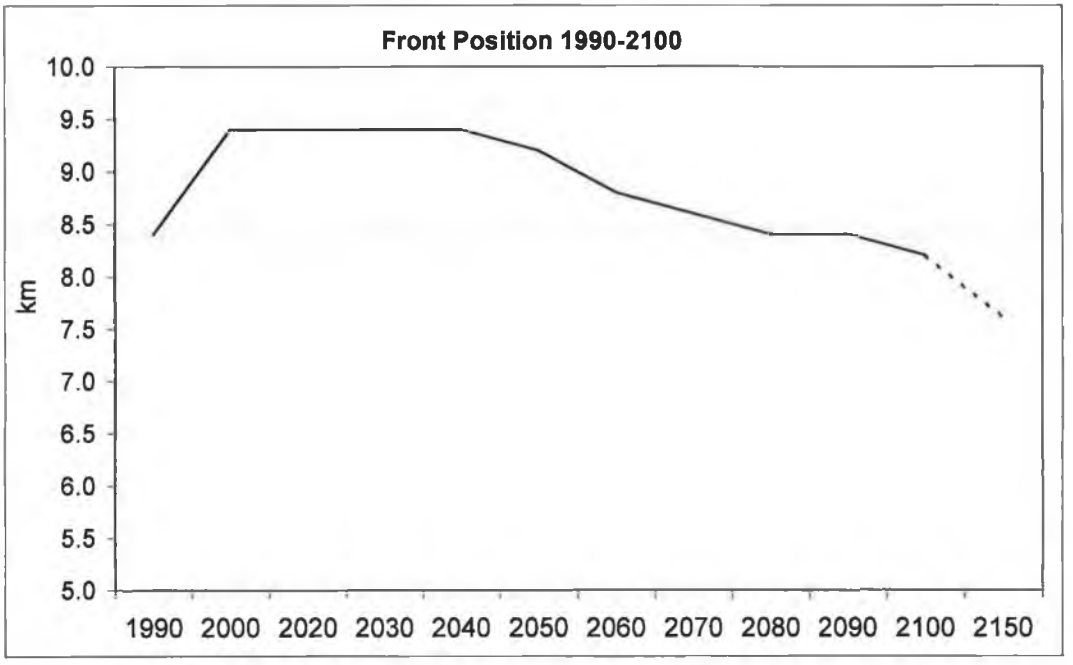

Figure 9.3.10 Modelled front position 1990-2100 (The model was run past 2100 to estimate likely front position after this period, assuming the 2100 decadal forcing does not change)

The modelled front position of Rembesdalskåka suggests that, as a consequence of the positive net balance during the early decades of the present century, the front position will initially advance by almost 1 km. It remains at this advanced position during the 2020s-2030s, after which, the negative net balances begin to have an

effect on the glacier front position. From the 2040s-2060s, the gains of the early century have been negated and the glacier front position returns to that of the 1990s. After 2070, the rate of retreat diminishes. However, the large negative net balances experienced during the 2090s gives rise to a much increased rate of retreat which becomes evident during the first half of the 22nd century.

A second mass balance forcing was also applied to the ice flow model, which uses the end of century ELA suggested to be 1750 metres. The model was initialised from zero ice conditions and allowed to reach equilibrium with Bn=0 mass. The change in net balance was then applied from 2000 onwards and results are shown (Figure 9.3.11). A persistent change in the ELA from its 30 year average position (1968-1997) of 1650 results in a retreat of the glacier front position of over 2.8 km from its steady state position and a lowering of the glacier surface throughout the whole elevational range.

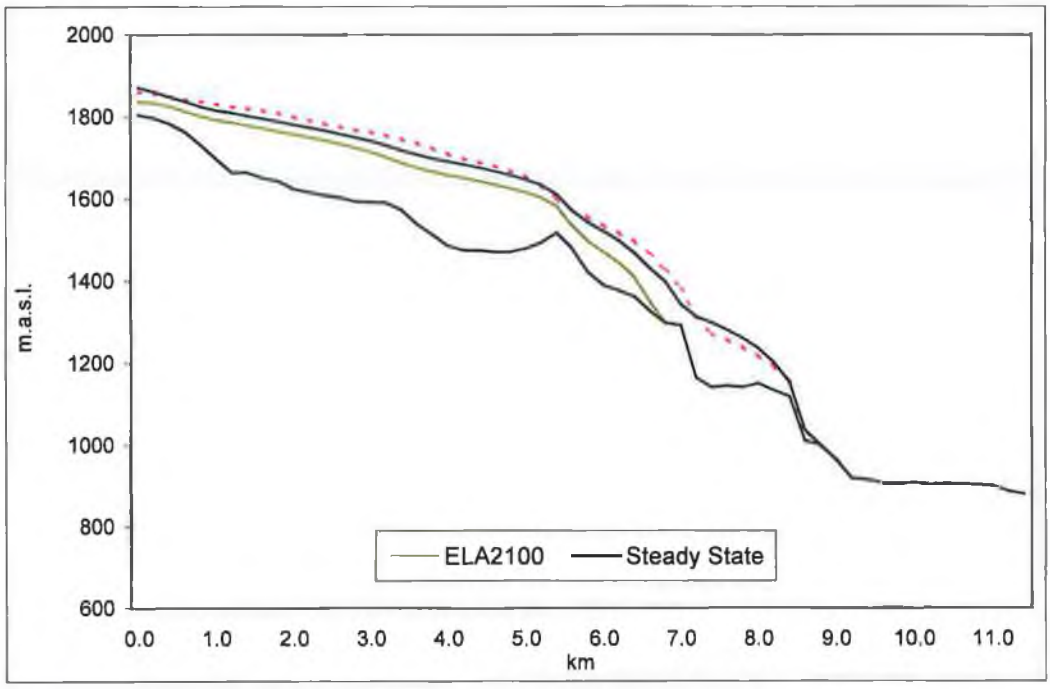

Figure 9.3.11 Ice flow model output for a steady state surface, based on the observed mass balance profile 1968-1997, and modelled scenario surface based on an ELA value of 1750 metres, representative of end of century conditions (The observed glacier surface of 1995 is included as a dashed line).

9.4 Discussion

Despite the simplifying assumptions in the ice flow model, the model more than adequately simulates the observed front position and longitudinal profile of the glacier. Long initialisation runs, of up to 2000 model years, were performed to test for instabilities in the model output, the results of which suggested that once the modelled profile attained equilibrium with constant mass balance forcing, it remained stable. While it would have been desirable to verify the capability of the model against historical front position changes, this was not possible due to lack of relevant information.

Results from the ice flow model are not entirely consistent with output from other modelling efforts. While comparisons are difficult, due to the various methodologies employed in calculating the mass balance component, the general trend from these studies suggests widespread glacier retreat during the course of the 21st century. However, results from the present study indicate that the front position of Rembesdalskåka could advance by up to 1 km, prior to any retreat occurring. Primarily due to the winter balance contributions to net balance, which remain high for the first few decades of the present century the glacier mass balance remains in marginally positive, producing an advance of the glacier front position.

In spite of the fact that Rembesdalskåka had a number of large positive mass balance years during the 1990s and has a small but positive net balance over the 1963-2000 measurement period, between 1998-1999 it retreated 20 metres and more recently during 2000-2001, a retreat of 46 metres in its front position has been recorded, while a further 16 metres retreat was recorded between 2001 and 2002 (Figure 9.4.1) (Andreassen and Kjøllmoen, 2000; Andreassen and Jackson, 2003).

Since 2000, the number of Norwegian glaciers in retreat has increased in contrast to the 1990s when the dominant signal was one of advancing front positions. This is marked in the cumulative net balance of Rembesdalskåka with the largest

cumulative balance being recorded in 2000, a value of 8.13 mass water equivalent, over the entire 40-year record. Since then, Rembesdalskåka's cumulative net balance, while still positive, is decreasing (Kjøllmoen, 2003).

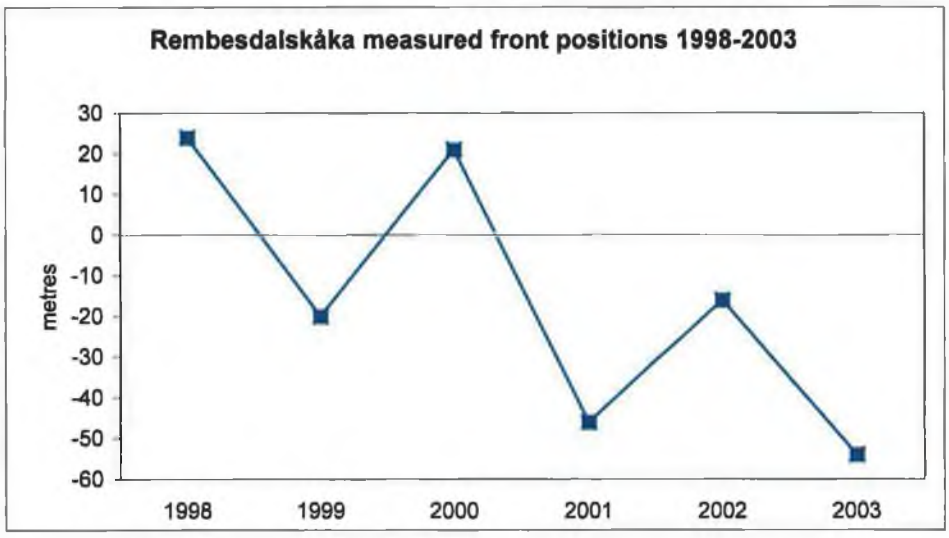

Figure 9.4.1 Measured front position changes for Rembesdalskåka 1998-2003 (Source: Norwegian Water Resources and Energy Directorate, Norway).

Chapter X

Conclusions: Summary of findings, research limitations and some future perspectives

10.1 Introduction

The primary objective of this research was an analysis of the relationship between climate and glaciers. It sought to build on previous research by progressing beyond a straightforward analysis of climate and glaciers through assessing various interactions that occur between the large-scale hemispherical forcing to those which occur at the regional and local scale. The main concern of this thesis then was to conduct a systematic analysis of climate-glacier interactions, through an examination of how climate fluctuations are reflected in glacier mass balance, the critical link between glaciers and climate.

The mass balance of a glacier is largely a response to climate forcing on a variety of scales from the large-scale planetary and hemispherical scales to that of localised, short duration events. While a number of previous studies have examined the relationship between climate and glaciers, these have concentrated on either small-scale interaction at the localised scale or with determining a relationship with large-scale atmospheric circulation. Few studies to date have approached this in a holistic manner, integrating the impact that various scales of climate forcing have on glacier mass balance, over both the short and long term. In attempting to fill this void this analysis employed the framework proposed by Meier (1965) (Table 10.1.1), placing an emphasis on interactions that occurred at the synoptic scale of climate and glacier mass balance.

Climate	→	General Meteorological Environment	→	Net Mass Balance of Glacier	→	Dynamic response of glacier	→	Lasting evidence of glacier margin position

Table 10.1.1 Relationship between climate-glacier interactions (after Meier, 1965)

In addition to the systematic analysis of the linkages between climate and glaciers, this thesis was also concerned with deriving a methodology that attempted to bridge the various scales at which climate and glaciers interact. The development and application of such a methodology also facilitated in realising the second objective of this thesis, which sought to assess the likely future implications of climate change, as prescribed by a GCM, on the mass balance of a particular glacier, that of Rembesdalskåka, in western Norway.

10.2 A brief overview and discussion of findings

A systematic analysis was presented which examined both the spatial and temporal components of climate and glacier mass balance. This analysis concentrated initially on large-scale climate variability, which in the North Atlantic is predominantly due to the North Atlantic Oscillation. Variations in the NAO, which account for a large proportion of variance in both the European temperature and precipitation series examined, were found to largely explain the divergent mass balance signal evident between southern and northern European glaciers. While local variability was evident in the climate series, long-term variations in both these variables could largely be accounted for by the NAO, resulting in short term trends superimposed on the long term increases or decreases recorded at these stations.

Temperature was found to be increasing significantly during both winter and summer at the southern European stations, while only two stations from Scandinavia displayed evidence of significant increases, restricted to the summer months. Increases in precipitation were also found to have occurred, particularly in Scandinavia. Synchronicity in the timing of changes in both the climate and mass balance series were also examined and were shown to largely reflect changes occurring in the large scale forcing mechanisms in the North Atlantic, which are in turn responsible for the large-scale transfer of heat and moisture from the equator to the pole through an integration of the ocean and atmosphere.

In an attempt to incorporate the various climate scales and variables which were found to be important for glacier mass balance, a synoptic-climatological methodology was developed which linked the atmospheric scale circulation and surface weather elements into a unified approach through classifying circulation types based on daily surface weather elements. This approach also facilitates an improved understanding of the climate controls, which operate at various scales and exert an influence on glacier mass balance.

An examination of the frequencies of occurrence of the air mass types indicated that they were highly correlated with both winter and summer mass balance. Changes in frequencies were also found to be linked to larger scale atmospheric changes. Marginal decreases in the occurrence of the cold cluster types, during the winter months, were suggested to have occurred up until the early 1990s. An analysis of the frequencies of the warm clusters, with an increased moisture capacity, indicated an increase in frequency from the late 1970s and early 1980s, with the highest frequencies occurring during the late 1980s and early 1990s. These increases resulted in largely positive net balances being recorded on maritime glaciers throughout this period, while positive net balances on the continental glaciers were evident after the late 1980s, coinciding with the increased frequencies of the warm types after this period. Increases in the frequencies of the warm types during the summer months were also evident after the late 1980s.

In addition to an assessment of the frequencies of occurrence of particular air mass types, physical changes, if any, which may have occurred over time within the individual synoptic types can be examined due to the inclusion of surface weather elements. Internal modification of both winter and summer air mass types was found to have occurred over the period examined. An analysis of the cold cluster types suggested that they were warming during the winter months. However, the effects are likely to small on winter balance as the average temperature of these clusters remains below zero degrees. In contrast, temperatures of the warm cluster types during the summer months were found to be decreasing. These decreases in temperature are unlikely to result in decreases in ablation as the frequency of occurrence of these air mass types was also found to be increasing.

In attempting to fulfil the second objective of the research, global climate model output was used to derive climate scenarios for two locations in southern Norway, one maritime and one continental. These scenarios were subsequently used to assess likely changes in glacier mass balance as a consequence of climate change. Changes in glacier mass balance, which reflect short-term variations in climate, will over time produce changes in glacier behaviour, reflective of longer-term variations in climate.

The effects of a changing climate on the glacier behaviour of a maritime glacier were also examined. The long-term findings were consistent with that of other similar studies; that glacier volume will significantly decrease as a consequence of global warming. However, early century increases evident in the glacier front position suggested by the ice flow model, reflecting the continued importance of the winter balance contribution to net balance, are in contrast to previous findings and may reflect weaknesses inherent in the methodology.

Despite some of the potential weaknesses of the various techniques employed in this thesis, it does present an important methodology that can be readily used in glacier modelling studies, especially in areas where on-site glacier specific meteorological data is unavailable. While degree-day models present a useful methodology for mass balance modelling, a changing climate may change the nature of the relationship between temperature and precipitation and glacier mass balance, as suggested in findings from this research. Also, degree-day models take no account of additional factors which may be influential on glacier mass balance.

Energy balance models, while taking account of a range of parameters, are also limited in their applicability due to the cost of data collection and the short duration of measurements. While a number of studies have highlighted the importance of the synoptic situation to glacier ablation, it is has also been found to be extremely important for accumulation. The synoptic methodology presented as part of this research represents an improvement over the degree-day method due to the inclusion of additional parameters and produces results comparable to that of energy-balance models. In addition, the meteorological data required for the

Temporal Synoptic Index classification represent standard variables measured at all synoptic stations and are likely to be measured from station inception, providing long term climate data, an important factor when trying to determine the influence of interannual or decadal scale variations in climate on mass balance. Due to the technique being synoptic in scale, results from one station can readily be applied to a number of glaciers in proximity to a synoptic station, making it a cost effective technique for glacier mass balance modelling.

This research examined the spatial and temporal components of climate variability that affect glacier mass balance. Variations in both of these components were found to largely explain mass balance differences both within and between the regions examined. Diminishing net balances over recent years in the Alpine region resulting primarily from significant increases in seasonal temperatures in both winter and summer, coupled with suppressed winter precipitation due to an increasingly positive and persistent phase of the NAO, particularly since the 1970s. Increasing net balances of maritime glaciers in Scandinavia experienced over the same period, halting the retreat evident up to this point and in direct contrast to the diminishing balances of Alpine glaciers, can be directly attributed to an increase in westerlies during the winter months resulting in significant increases in winter precipitation, consistent with a positive phase of the NAO. The seasonal increases in temperature apparent in the stations examined in southern Europe do not occur to the same extent in Scandinavia; coupled with increasing winter precipitation has resulted in increasingly positive net balances being recorded on these glaciers, particularly during the 1990s coinciding with a period of intensified westerly airflow onto northern Europe.

The more continentally located glaciers in Scandinavia also respond to this intensification of westerlies during the 1990s. The declining cumulative mass balances evident on these glaciers up until the late 1980s comes to a standstill due to more positive net balances being recorded after this period. A strengthening of the pressure gradient, which produced the intensification of the westerlies during the 1990s, resulted in a deeper penetration of maritime airflow into northern Europe with consequent increases in winter accumulation.

In attempting to uncover the linkages between climate and glaciers, variations in scale cannot be ignored. Any methodology that incorporates these various scales of interaction is more likely to succeed in the pursuit to further our understanding of the interconnections between climate and glaciers.

10.3 Limitations of Research

A number of limitations became apparent during the course of conducting this research; the majority of which were methodological in nature. While the methodology employed to classify the meteorological data is considered an objective technique, in comparison to manual techniques, a number of subjective decisions were required to be made at various steps in the methodology. While a number of techniques exist to aid with some of the decision making process, none are entirely conclusive. The effects of these decisions had varying impacts on the results. The selection of the required number of principal components to retain is not likely to bear too heavily on the outcome while specification of the required number of clusters to retain was problematical, particularly for the inexperienced, and was potentially detrimental to the establishment of linkages to glacier mass balance. Applying the methodology to more than one station facilitated, at the minimum, a subjective comparison of the results in terms of the number of cluster to retain.

Issues arising as a consequence of the downscaling presented some of the more serious limitations to achieving the second objective of this study. Despite the physical realism displayed between the statistically downscaled variables in the loading patterns of the principal components analysis, the resultant modelled air mass frequencies for Skabu were very poor when compared to the observed frequencies. While some of the differences may be attributable to biases within the GCM, errors within the methodology almost certainly contributed.

A second serious limitation to this objective was that model output was based on only one emissions scenario run, namely the GGa1 scenario. In order to have any

confidence in the resulting climate scenarios, a minimum of two emissions scenarios from a GCM should be used as input to the downscaling process. In addition to the incorporation of multiple scenarios, ideally, model output from more than just one GCM should be incorporated in order to address issues of model reliability. Due to the limitations imposed by the use of just one scenario, no measure of uncertainty can be associated with the resultant downscaled scenarios, other than those accrued in the methodology. However, these limitations are restricted to the second objective of the thesis which sought to derive a predictive model of glacier mass balance as a consequence of possible future climate change and do not affect the results based on the observed data.

10.4 Directions for further research

In pursuing this research, more questions have been raised than answered. Decreasing temperatures in the warm air mass types found during the summer period require further analysis. As more northern latitudes are expected to have an increased sensitivity to global warming, due to sea ice-albedo feedback processes, a decreasing trend was not *a priori* expected. However, increasing evidence of a freshening of sub arctic waters, linked to persistent phases of the NAO, may play a part in the explanation.

Detection and impacts of a possible change point in 1988/1989, with consequential effects on mass balances in Scandinavia and North America, also warrants further research. Changes in other climatically influenced variables, such as, fish stocks levels in the North Atlantic, have also been uncovered during this period. The impact of the event suggests that it was hemispherical in scale and of significance, climatically.

As GCMs become increasingly sophisticated, an improved coupling between the methodologies used for the synoptic classification and the downscaled output from the GCM should be possible. Further examination of this should result in improved output from the modelled synoptic index classification.

Additional areas highlighted for investigation are associated with the modelling of glacier mass balance. As uncertainties in the specification of mass balance can be transmitted through to the ice flow model and reflected in the output. Uncertainties associated with both components need to be quantified to establish the degree to which errors are transmitted and reduce noise in the output.

10.5 Future perspectives

A greater understanding of the interactions between climate and glaciers is crucial if we are to predict the likely impacts of climate change on society, from the local scale, being able to predict the occurrence of glacier outburst floods to that of the global scale with the impact of a rising sea-level on coastlines and island nations. A limiting factor to date in conducting this type of research is linked to the availability of long-term glacier data. However, this situation is changing.

Since 2000, a number of Norwegian glaciers have started to display diminishing net mass balances resulting in the retreat of a number of glaciers. In 2003, 21 of 25 glaciers measured recorded a retreat in their front positions, 17 of which recorded a retreat of more than 10 metres. The strength of the NAO has also diminished since 2000, recording only its third negative value since 1988 in 2001. Both 2002 and 2003 were characterised by a return to positive values, despite being very weak. That these linkages existed were highlighted throughout the course of this research.

Are glacier fluctuations solely a response to natural fluctuations inherent in the climate system? Glaciers respond to natural variations that occur in climate as they have done since their inception, however, over recent decades the synchronicity and similarity of glacier responses globally, would suggest a global driver of change in the form of increasing temperatures. An increasing body of evidence suggests that these increases in the global temperature record are directly attributable to the influence of increasing anthropogenic emissions, particularly since the post-Industrial Revolution era.

The complication when assessing surface environmental variables for an anthropogenic signal or trend in the North Atlantic region occurs due to the presence of the North Atlantic Oscillation as it is both a driver of and response to global fluctuations in climate, both natural and anthropogenic. Any increase in sea-surface temperatures (SSTs) is likely to be reflected in the strength and persistence of NAO phases transmitted via the Tropical Atlantic Variability (TAV). Additional feedbacks within the system add a further complication. Increased freshwater run-off from northern Europe during persistent high index phases of the NAO, will act to freshen the Norwegian Sea affecting its temperature and salinity which is likely to affect the deep water formation of the Meridional Overturning Circulation, which in turn will be reflected in changes in the NAO.

If we accept that anthropogenic climate change is occurring and that GCMs adequately represent these changes, then the future survival of mountain and valley glaciers look increasingly bleak over the course of the present century. Rates of wastage will be determined by the impact of climate change regionally but also by the response time or sensitivity of a particular glacier to change. While specific glaciers may initially respond positively due to potential increases in moisture, ultimately, the temperature threshold for melting will occur earlier in the season and last longer resulting in their demise over the long term. Specific glacier responses will also be constrained by local factors, such as, aspect, elevation and slope.

As a consequence of the suggested changes, the hydro-electric power generation industry in Norway is likely to benefit from climate change on both the short and medium term. Projected increases in winter storage coupled with increasing summer temperatures are likely to result in an increase in glacier runoff during the melt season. This situation is likely to continue throughout the century due to increasing summer ablation ultimately resulting in volume reductions and retreat of the front position. Over the longer term these benefits are likely to decrease as the glacier receeds and reaches equilibrium with future climate. Thus, initial infrastructure costs of new hydroelectric plants will have to be assessed in the

context of a reduced future potential of rivers which currently depend on seasonal meltwater contributions from glaciers.

As climate change is likely to be non-linear, the possibility of catastrophic failures of glacier damned lakes must also be considered, not just in Norway but globally. However, to assess the likelihood of these events occurring there is a real need for further research along the lines of the present study. Establishing the various scales at which climate and glaciers interact, as attempted in this study for a selection of glaciers in Europe, is hopefully the first step towards achieving this end.

Bibliography

Ahlmann, H.W. (1953) *Glacier variations and climatic fluctuations*, George Grady Press, New York.

Alt, B.T. (1987) Developing synoptic analogs for extreme mass balance conditions on Queen Elizabeth Island ice caps, *Journal of Climate and Applied Meteorology*, 26 (12), 1605 – 1623.

Andreassen, L.M. and Jackson, M. (2003) Glacier monitoring in Kjøllmoen, B (Ed) *Glaciological investigations in Norway in 2001*. Norwegian Water Resources and Energy Directorate, Norway.

Andreassen, L.M. and Jackson,M. (2003) Glacier monitoring in Kjøllmoen, B. (Ed) *Glaciological investigations in Norway in 2002*. Norwegian Water Resources and Energy Directorate, Norway.

Andreassen, L.M. and Kjollmoen, B. (2000) Breovervaking in Kjøllmoen, B. (Ed) *Glaciological investigations in Norway in 1999*. Norwegian Water Resources and Energy Directorate, Norway.

Appenzeller, C. (1997) Draft Fact-sheet Thermohaline Circulation, http://www.climate.unibe.ch/~christof/div/fact4thc.html

Bahr, D.B., Tad Pfeffer, W., Sassolas, C. and Meier, M.F. (1998) Response time of glaciers as a function of size and mass balance: 1. Theory, *Journal of Geophysical Research*, 103, B5, 9777-9782.

Bardossy, A and Caspary, H.J. (1990) Detection of climate change in Europe by analyzing European Atmospheric Circulation Patterns from 1881 to 1989, *Theoretical and Applied Climatology*, 42, 155-167.

Bardossy, A. and Plate, E.J. (1991) Modeling daily rainfall using a semi-Markov representation of circulation pattern occurrence, *Journal of Hydrology*, 122, 33-47.

Barry, R.G. and Perry, A.H. (1973) *Synoptic Climatology: Methods and Applications*, Methuen & Co Ltd, London.

Baur, F., Hess, P. and Nagel, H. (1944) *Kalender der Großwetterlagen Europas 1881-1939*, Bad Homburg.

Beaugrand, G., Brander, K.M., Lindley, J.A., Souissi, S. and Reid, P.C. (2003) Plankton effect on cod recruitment in the North Sea, *Nature*, 426, 661-664.

Bejarán, R.A. and Camilloni, I.A. (2003) Objective method for classifying air masses: an application to the analysis of Buenos Aires' (Argentina) urban heat island intensity, *Theoretical Applied Climatology*, 74, 93-103.

Benestad, R.E. (2001) A comparison between two empirical downscaling strategies, *International Journal of Climatology*, 21, 1645-1668.

Benn, D.I. and Evans, D.J.A. (1998) *Glaciers and Glaciation*. Arnold, London.

Bitz, C.M. and Battisti, D.S. (1999) Interannual to Decadal Variability in Climate and the Glacier Mass Balance in Washington, Western Canada, and Alaska, *Journal of Climate*, 12, 3181-3196

Blair, D. (1998) The Kirchhofer technique of synoptic typing revisited, *International Journal of Climatology*, 18, 1625-1635.

Böhm, R., Auer, I., Brunetti, M., Maugeri, M., Nanni, T. and Schoner, W. (2001) Regional temperature variability in the European Alps: 1760-1998 from homogenised instrumental time series, *International Journal of Climatology*, 21, 1779-1801.

Bonell, M. and Sumner, G. (1992) Atmospheric circulation and daily precipitation in Wales, *Theoretical Applied Climatology*, 46, 3-25.

Braithwaite, R.J. and Zhang, Y. (1999) Modelling changes in glacier mass balance that may occur as a result of climate change, *Geografiska Annaler*, 81A, 489-496.

Brazel, A.J., Chambers, F.B. and Kalkstein, L.S. (1992) Summer energy balance on West Gulkana Glacier, Alaska, and linkages to a temporal synoptic index, *Zeitschrift Für Geomorphologie*, 86, 15-34.

Briffa, K.R., Jones, P.D. and Kelly, P.M. (1990) Principal component analysis of the Lamb catalogue of daily weather types: Part 2, seasonal frequencies and update to 1987, *International Journal of Climatology*, 10, 549-563.

Brinkmann, W.A.R. (1999) Within-type variability of 700 hPa winter circulation patterns over the Lake Superior basin, *International Journal of Climatology*, 19, 41-58.

Brinkmann, W.A.R. (2000) Modification of a correlation-based circulation pattern classification to reduce within-type variability of temperature and precipitation, *International Journal of Climatology*, 20, 839-852.

Brugger, K.A. (1997) Predicted response of Storglaciaren, Sweden, to climatic warming, *Annals of Glaciology*, 24, 217-222.

Brunetti, M., Colacino, M., Maugeri, M. and Nanni, T. (2001) Trends in the daily intensity of precipitation in Italy from 1951 to 1996, *International Journal of Climatology*, 21, 299-316.

Buishand, T.A. and Brandsma, T. (1997) Comparison of circulation classification schemes for predicting temperature and precipitation in the Netherlands, *International Journal of Climatology*, 17,875-889.

Busuioc, A. and Von Storch, H. (2003) Conditional stochastic model for generating daily precipitation time series, *Climate Research,* 24, 181-195.

Busuioc, A., Von Storch, H. and Schnur, R. (1998) Verification of GCM-generated regional seasonal precipitation for current climate and of statistical downscaling estimates under changing climate conditions, *Journal of Climate,* 12, 258-272.

Cavazos, T. and Hewitson, B. (2002) Relative performance of empirical predictors of daily precipitation. In Rizzoli, A. E. and Jakeman, A. J., (eds.), *Integrated Assessment and Decision Support, Proceedings of the First Biennial Meeting of the International Environmental Modelling and Software Society*, Volume 1, 334- 339. iEMSs, June 2002.

Chapman, W.L. and Walsh, J.E. (1993) Recent variations of sea ice and air temperature in high latitudes, *Bulletin American Meteorological Society*, 74, 1, 33-47.

Chen, D. (2000) A monthly circulation climatology for Sweden and its application to a winter temperature case study, *International Journal of Climatology*, 20, 1067-1076.

Chen, D. and Hellström, C. (1999) The influence of the North Atlantic Oscillation on the regional temperature variability in Sweden: spatial and temporal variations, *Tellus*, 51A, 505-516.

Cheng, S. and Lam. K-C. (2000) Synoptic typing and its application to the assessment of climatic impact on concentrations of sulpher dioxide and nitrogen oxides in Hong Kong, *Atmospheric Environment*, 34, 585-594.

Crane, R (1979) Synoptic controls on the energy budget regime of an ablating fast ice surface, *Archiv FürMeteorologie Geophysik und Bioklimatologie*, Series A, 28, 53-70.

Daultrey, S. (1976) *Principal components analysis, Concepts and Techniques in Modern Geography,* (CATMOG) series, No. 8, Norwich.

Davis, R. and Kalkstein, L.S. (1990) Development of an automated spatial synoptic climatological classification, *International Journal of Climatology*, 10, 769-794.

Delworth T, Manabe S, and Stouffer RJ. (1993) Interdecadal variations of the thermohaline circulation in a coupled ocean–atmosphere model *Journal of Climate,* 6, 1993–2011.

Dyurgerov, M. (2002) *Glacier Mass Balance and Regime: Data of Measurements and Analysis*. Occasional Paper No. 55. *Institute of Arctic and Alpine Research*, University of Colorado.

Dyurgerov, M. (2003) Mountain and subpolar glaciers show an increase in sensitivity to climate warming and intensification of the water cycle, *Journal of Hydrology*, 282, 164-176.

Dyurgerov, M.B. and Meier, M.F. (1999) Analysis of winter and summer glacier mass balances, *Geografiska Annaler*, 81A, 4.

El Dessouky T.M. and Jenkinson, A.F. (1979) Objective daily catalogue of surface pressure, flow and vorticity indices for Egypt and it's use in monthly rainfall forecasting, *Meteorological Research Bulletin*, 11, 1-25.

Elvehøy H., R. Engeset, L.M. Andreassen, J. Kohler, Y. Gjessing and H. Björnson (2002) *Assesment of possible jökulhlaups from Lake Demmevatnet in Norway*. IAHS Publ. No 271, 31-36.

Forbes, J.D. (1853) *Norway and its glaciers visited in 1851; followed by journals of excursions in the High Alps of Dauphiné, Berne and Savoy*, Adam and Charles Black, Edinburgh

Førland, E.J, van Engelen, A., Hanssen-Bauer, I., Heino, R., Ashcroft, J., Dahlström, B., Demarée, G., Frich, P., Jónsson, T., Mietus, M., Müller-Westermeier, G., Pálsdottir, T., Toumenvirta, H., and Vdein, H. (1996) *Changes in normal precipitation in the North Atlantic region*. Klima Report no. 7/96, DNMI.

Førland, E., Roald, L.A., Tveito, O.E .and Hanssen-Bauer, I. (2000) *Past and future variations in climate and runoff in Norway*, Klima Report no. 19/00, DMNI.

Fowler, H.J., Kilsby, C.G. and O'Connell, P.E. (2000) A stochastic rainfall model for the assessment of regional water resource systems under changed climatic conditions, *Hydrology and Earth System Sciences*, 4 (2), 263-282.

Frakes, B. and Yarnal, B. (1997) A procedure for blending manual and correlation-based synoptic classifications. *International Journal of Climatology*, 17, 1381-1396.

Frich, P. (Co-ordinator), H. Alexandersson, J. Ashcroft, B. Dahlström, G. Demarée, A. Drebs, A. van Engelen, E.J. Førland, I. Hanssen-Bauer, R. Heino, T. Jónsson, K. Jonasson, L. Keegan, P.Ø. Nordli, Schmith, T. Steffensen, H. Tuomenvirta, O.E. Tveito, (1996) *North Atlantic Climatological Dataset (NACD Version 1) -Final Report*. DMI Scientific Report 96-1, 47 pp.

Galambosi, A, Duckstein, L and Bogardi, I. (1996) Evaluation and analysis of daily atmospheric circulation patterns of the 500 hPa pressure field over the southwestern USA, *Atmospheric Research*, 40 49-76.

Goodess, C.M. and Palutikof, J.P. (1998) Development of daily rainfall scenarios for Southeast Spain using a circulation-type approach to downscaling, *International Journal of Climatology*, 10, 1051-1083.

Gordon, C., Cooper, C., Senior, C.A.. Banks, H., Gregory, J.M., Johns, T.C., Mitchell, J.F.B.and Wood, R.A. (2000) The simulation of SST, sea ice extents and ocean heat transports in a version of the Hadley Centre coupled model without flux adjustments *Climate Dynamics*, 16 (2-3), 147-168.

Greene, J.S. and Kalkstein, L.S. (1996) Quantitative analysis of summer air masses in the Eastern United States and an application to human mortality, *Climate Research*, 7, 43-53.

Greuell, W. (1989) *Glaciers and climate*. Ph.D.-thesis, Institute of Marine and Atmospheric Sciences, Rijksuniversiteit Utrecht, Unpublished.

Greuell, W. and Oerlemans, J. (1986) Sensitivity studies with a mass balance model including temperature profile calculations inside the glacier, *Zeitschrift Für Gletscherkunde und Glazialgeologie*, 22, 2,101-124.

Greuell, W., and Böhm, R. (1998) 2m temperatures along melting mid-latitude glaciers, and implications for the sensitivity of the mass balance to variations in temperature, *Journal of Glaciology*, 44 (146), 9-21.

Haeberli, W. (2004) Glaciers and ice caps: historical background and strategies of world-wide monitoring. In: Bamber, J.L. and Payne A.J. (eds): *Mass Balance of the Cryosphere*. Cambridge University Press, Cambridge, 559-578.

Hanssen-Bauer, I. and Forland, E.J. (1998a) Long-term trends in precipitation and temperature in the Norwegian Arctic: can they be explained by changes in atmospheric circulation patterns?, *Climate Research*, 10, 143-153.

Hanssen-Bauer, I. and Førland, E.J. (1998b) *Annual and seasonal precipitation variations in Norway 1896-1997*. Report no. 27/98 Klima, DNMI.

Hanssen-Bauer, I. and Førland, E.J., Haugen, J.E. and Tveito, O.E. (2003) *Temperature and precipitation scenarios for Norway: Comparison of results from empirical and dynamical downscaling*, Report 06/03, RegClim: Regional Climate Development under Global Warming.

Hastenrath, S. (1992) Ice-flow and mass changes of Lewis Glacier, Mount Kenya, East Africa, 1986-90: observations and modelling, *Journal of Glaciology*, 38, 128, 36-43.

Hess, P. and Bresowsky, H. (1977) *Katalog der Großwetterlagen Europas (1881-1976)*, Berichte des Deutschen Wetterdienstes, Offenbach am Main.

Hewitson, B.C. and Crane, R.G. (1996) Climate downscaling: techniques and application, *Climate Research*, 7, 85-95

Hodge, S.M., Trabant, D.C., Krimmel, R.M., Heinrichs, T.A., March, R.S. and Josberger, E.G. (1998) Climate variations and changes in mass of three glaciers in western North America, *Journal of Climate*, 11, 2161-2179.

Hoel, A and Werenskiold, W. (1962) *Glaciers and Snowfields in Norway,* Skrifter No. 114, Norsk Polarinstitutt, Oslo University Press, Oslo.

Hoinkes, H. (1968) Glacier variation and weather, *Journal of Glaciology*, 7 (49), 3-19.

Holland, W.R., Capotondi, A., and Holland, M.M. (1995) Advances in ocean modeling for climate change research, *Rev. Geophys.,* Supplement, US National Report to the IUGG, 1991-1994, 33, 1411-1424.

Hooker, B.L and Fitzharris, B.B (1999) The correlation between climatic parameters and the retreat of Franz Josef Glacier, New Zealand, *Global and Planetary Change*, 22, 39-48.

Hoppe, H. and Kiely, G. (1999) Precipitation over Ireland-Observed change since 1940, *Phys. Chem. Earth* (B), 24, (1-2), 91-96.

Hurrell, J.W. (1995) Decadal trends in the North Atlantic Oscillation, regional temperatures and precipitation, *Science*, 269, 676-679.

Hurrell, J.W. and Dickson, R.R. (2001) Climate variability over the North Atlantic, in Stenseth, N.C. Ottersen, G. Hurrell, J.W. and Belgrano, A. (eds.) *Ecological effects of climate variations in the North Atlantic*, Oxford University Press, 1-30.

Huth, R. (2001) Disaggregating climatic trends by classification of circulation patterns *International Journal of Climatology*, 21, 135-153.

Huth, R. (2003) Sensitivity of local daily temperature change estimates to the selection of downscaling models and predictors, *Journal of Climate*, 17 640-652.

IPCC (2001a) *Climate Change 2001: Synthesis Report.* Watson, R.T., (Ed.). Cambridge University Press, UK. 184 pp.

IPCC (2001b) *Climate Change 2001: The Scientific Basis.* Contribution of Working Group I to the Third Assessment Report of the Intergovernmental Panel on Climate Change (IPCC). Houghton, J. T., Ding, Y., Griggs, D.J.,

Noguer, M., van der Linden, P. J. and Xiaosu, D. (Eds.). Cambridge University Press, UK. 944 pp.

IPCC (2001c) *Climate Change 2001: Impacts, Adaptation, and Vulnerability.* Contribution of Working Group II to the Third Assessment Report of the Intergovernmental Panel on Climate Change (IPCC). McCarthy, J.J., Canziani, O.F., Leary, N.A., Dokken, D.J., White, K. S. (Eds.). Cambridge University Press, UK. 1042 pp.

Jenkinson, A.F. and Collison, P. (1977) *An initial climatology of gales over the North Sea, Synoptic Climatology Branch Memorandum No. 62*, Meteorological Office, London.

Jóhannesson, T. (1997) The response of two Icelandic glaciers to climatic warming computed with a degree-day glacier mass balance model coupled to a dynamical glacier model, *Journal of Glaciology*, 42, 143,3 21-327.

Jóhannesson, T., Jónsson, T., Källén, E. and Kaas, E. (1995) Climate change scenarios for the Nordic countries, *Climate Research*, 5, 181-195.

Johnston, R.J. (1978) *Multivariate statistical analysis in Geography*, Longman Group Limited, London.

Jolliffe, I.T. (1990) Principal components analysis: A beginner's guide-I. Introduction and application, *Weather*, 45, 375-382.

Jolliffe, I.T. (1993) Principal component analysis: A beginners's guide-II Pitfalls and Extensions, *Weather*, 48, 246-253.

Jones, P., Hulme, M. and Briffa, K.R. (1993) A comparison of lamb circulation types with an objective classification scheme, *International Journal of Climatology*, 13, 655-663.

Jones, P.D., D.E. Parker, T.J. Osborn, and K.R. Briffa. (2001) Global and hemispheric temperature anomalies--land and marine instrumental records. In *Trends: A Compendium of Data on Global Change*. Carbon Dioxide Information Analysis Center, Oak Ridge National Laboratory, U.S. Department of Energy, Oak Ridge, Tenn., U.S.A.

Kadota, T., Fujita, K., Seko, K., Kayastha, R.B. and Ageta, Y. (1997) Monitoring and prediction of shrinkage of a small glacier in the Nepal Himalaya, *Annals of Glaciology*, 24,90-94.

Kalkstein, L.S. and Corrigan, P. (1986) A synoptic climatological approach for geographical analysis: Assessment of sulpher dioxide concentrations, *Annals of the Association of American Geographers*, 76 (3), 381-395.

Kalkstein, L.S., Barthel, C.D., Greene, J.S. and Nichols, M.C. (1996) A new spatial synoptic classification: application to air mass analysis, *International Journal of Climatology*, 16, 983-1004.

Kalkstein, L.S., Dunne, P.C. and Vose, R.S. (1990) Detection of climate change in the Western North American Arctic using a synoptic climatological approach, *Journal of Climate*, 3, 10, 1153-1167.

Kalkstein, L.S., Tan, G. and Skindlov, J.A. (1987) An evaluation of three clustering procedures for use in synoptic climatological classification, *Journal of Climate and Applied Meteorology*, 26, 717-730.

Karl, T.R., Wang, W.-C., Schlesinger, M.E., Knight, R.W and Portman, D. (1990) A method of relating general circulation model simulated climate to the observed local climate. Part I: Seasonal statistics, *Journal of Climate*, 3, 1053-1079.

Kattenburg, A., Giorgi, F., Grassl, H., Meehl, G.A., Mitchell, J.F.B., Stouffer, R.J., Tokioka, T., Weaver, A.J. and Wigley, T.M.L. (1996) Climate Models - Projections of Future Climate In. *Climate Change 1995 The Science of Climate Change, The Second Assessment Report of the IPCC: Contribution to Working Group 1*. Eds Houghton J.T., Meira Filho L.G., Callander B.A., Harris N., Kattenburg A., and Maskell K. Cambridge University Press 285-357.

Kaufmann, R.K., Snell, S.E,, Gopal, S. and Dezzani, R. (1999) The significance of synoptic patterns identified by the Kirchhofer technique: A Monte Carlo approach, *International Journal of Climatology*, 19, 619-626.

Kerschner, H. (1997) Statistical modelling of equilibrium line altitudes of Hintereisferner, central Alps, Austria, 1859-present, *Annals of Glaciology*, 24, 111-115.

Kidson, J.W. (1997) The utility of surface and upper air data in synoptic climatological specification of surface climatic variables, *International Journal of Climatology*, 17, 399-413.

Kidson, J.W. (2000) An analysis of New Zealand synoptic types and their use in defining weather regimes, *International Journal of Climatology*, 20, 299-316.

Kiely, G. (1999) Climate change in Ireland from precipitation and streamflow observations, *Advances in Water Resources*, 23, 141-151.

Kilsby, C.G., Cowpertwait, P.S.P., O'Connell, P.E. and Jones, P.D. (1998) Predicting rainfall statistics in England and Wales using atmospheric circulation variables, *International Journal of Climatology*, 18, 523-539.

Kim,J.-W., Chang, J.-T., Baker, N.L., Wilks, D.S. and Gates, W.L. (1984) The statistical problem of climate inversion: determination of the relationship between the local and large-scale climate, *Monthly Weather Review*, 112, 2069-2077.

Kirchhofer, W. (1973) Classification of European 500 mb patterns, *Arbeitsbericht der Schweizerischen Meteorologischen Zentralanstalt*, No. 43, Geneva.

Kjøllmoen, B. (Ed) (2003) *Glaciological investigations in Norway in 2002*. Norwegian Water Resources and Energy Directorate, Norway.

Klein Tank, A. M. G., Wijngaard, J. B., Können, G. P., Böhm, R., Demarée, G., Gocheva, A., Mileta, M., Pashiardis, S., Hejkrlik, L., Kern-Hansen, C., Heino, R., Bessemoulin, P., Müller-Westermeier, G., Tzanakou, M., Szalai S., Pálsdóttir, T., Fitzgerald, D., Rubin, S., Capaldo, M., Maugeri, M., Leitass, A., Bukantis, A., Aberfeld, R.,. van Engelen, A. F. V, Forland, E., Mietus, M., Coelho, F., Mares, C., Razuvaev, V., Nieplova, E., Cegnar, T., Antonio López, J., Dahlström, B., Moberg, A., Kirchhofer, W., Ceylan, A., Pachaliuk, O., Alexander, L. V. and Petrovic, P. (2002) Daily dataset of 20th-century surface air temperature and precipitation series for the European Climate Assessment., *International Journal of Climatology*, 22, 1441-1453.

Kuhn, M. (1989) The response of the equilibrium line altitude to climate fluctuations: theory and observations, in Oerlemans,J. (ed) *Glacier Fluctuation and Climate Change*, Kluwer, Dordrecht.

Kuhn, M., Schlosser, E. and Span, N. (1997) Eastern Alpine glacier activity and climatic records since 1860, *Annals of Glaciology*, 24, 164-168.

Kyselý, J. and Huth, R., (2003) Recent changes in atmospheric circulation over Europe detected by objective and subjective methods. In: Proc. 83rd AMS Annual Meeting [CD-ROM], American Meteorological Society, Boston, 5 pp.

Lamb, H.H. (1972) British Isles weather types and a register of daily sequence of circulation patterns, 1861-1971, *Geophysical Memoir*, HMSO, London.

Lamb, H.H. (1982) *Climate, history and the modern world*, Methuen, University Press, Cambridge.

Lamont, G.N., Chinn, T.J. and Fitzharris, B.B. (1999) Slopes of glacier ELAs in Southern Alps of New Zealand in relation to atmospheric circulation patterns, *Global and Planetary Change*, 22, 209-219.

Laumann, T. and Reeh, N. (1993) Sensitivity to climate change of the mass balance of glaciers in southern Norway, *Journal of Glaciology*, 39, 133, 656-665.

Laumann, T. and Tvede, M. (1989) Simulation of the effects of climate changes on a glacier in western Norway, Reprint from 'Conference on Climate and water', Helsinki 11-15th September.

Linderson, M-L (2001) Objective classification of atmospheric circulation over southern Scandinavia, *International Journal of Climatology*, 21,155-169.

Lliboutry, L. (1974) Multivariate statistical analysis of glacier annual balances, *Journal of Glaciology*, 13, 69, 371-392.

Lund, I.A. (1963) Map-pattern classification by statistical methods, *Journal of Applied Meteorology*, 2 56-65.

Marshall, J. and Kushnir, Y. (1997) *A 'white paper' on Atlantic Climate Variability*, http://geoid.mit.edu/accp/avehtml.html

Marshall, J., Kushnir, Y., Battisti, D., Chang, P., Czaja, A., Dickson, R., Hurrell, J., McCartney, M., Saravanan, R. and Visbeck, M. (2001) North Atlantic Climate Variability: Phenomena, Impacts and Mechanisms, *International Journal of Climatology*, 21, 1863-1898.

Maslanik, J.A., Serreze, M.C. and Barry, R.G. (1996) Recent decreases in Arctic summer ice cover and linkages to atmospheric circulation anomalies, *Geophysical Research Letters*, 23, 13, 1677-1680.

Mayes, J.C. (1991) Regional airflow patterns in the British Isles, *International Journal of Climatology* 11,473-491.

McCabe, G.J. and Fountain, A.G. (1995) Relations between atmospheric circulation and mass balance of South Cascade Glacier, Washington, U.S.A., *Arctic and Alpine Research*, 27 (3), 226-233.

Meier, M (1965) Glaciers and climate. In Wright, H.E. Jnr. and Frey, D.G. (eds) *The Quaternary of the United States*. Princeton University Press, Princeton, 795-805.

Moses,T., Kiladis,G.N., Diaz,H.F. and Barry,R.G. (1987) Characteristics and frequency of reversals in mean sea level pressure in the North Atlantic Sector and their relationship to long-term temperature trends, *Journal of Climatology*, 7 , 13-30.

Muller, R.A. (1977) A synoptic climatology for environmental baseline analysis: New Orleans, *Journal of Applied Meteorology*, 16, 20-33.

Murphy, J. (2000) Predictions of climate change over Europe using statistical and dynamical downscaling techniques, *International Journal of Climatology*, 20, 489-501.

Mysak, L.A., and Power, S.B. (1991) Greenland Sea ice and salinity anomalies and interdecadal climate variability, *Climatological Bulletin, 25*, 81-91.

Neale, S.M. and Fitzharris, B.B. (1997) Energy balance and synoptic climatology of a melting snowpack in the Southern Alps, New Zealand, *International Journal of Climatology*, 17, 1595-1609.

Nesje, A. and Dahl, S.O. (1991) Holocene glacier variations of Blåisen, Hardangerjøkulen, central southern Norway, *Quaternary Research*, 35, 25-40

Nesje, A. and Dahl, S.O. (2000a) *Glaciers and environmental change*, Arnold, London

Nesje, A. and Dahl, S.O. (2000b) Are the North Atlantic and Arctic Oscillation reflected in Scandinavian glacier mass balance records?, *PAGES*, 8, (2), 15.

Nesje, A., Lie, Ø., and Dahl, S.O. (2000) Is the North Atlantic Oscillation reflected in Scandinavian glacier mass balance records?, *Journal of Quaternary Science*, 15 (6), 587-601.

Nye, J. F. (1960) The response of glaciers and ice sheets to seasonal and climate changes, *Proc. R. Soc. London*, 256, 559-584.

Nye, J. F. (1963a) On the theory of the advance and retreat of glaciers, *Geophys. J. Royal Astron. Soc.* 7, 431-456.

Nye, J. F. (1963b) The response of a glacier to changes in the rate of nourishment and wastage, *Proc. Royal Soc. A* 275, 87-112.

Nye, J. F. (1965) A numerical method of inferring the budget history of a glacier from its advance and retreat, *Journal of Glaciology*, Vol. 5, No. 41, 589-607.

O'Hare, G. and Sweeney, J.C. (1993) Lamb's circulation types and British weather: an evaluation, *Geography*, 78, 43-60.

Oerlemans, J. (1986) An attempt to simulate historic front variations of Nigardsbreen, Norway, *Theoretical and Applied Climatology*, 37, 126-135.

Oerlemans, J. (1988) Simulation of historic glacier variations with a simple climate-glacier model, *Journal of Glaciology,* 34, 118, 333-341.

Oerlemans, J. (1997a) Climate sensitivity of Franz Josef Glacier, New Zealand, as revealed by numerical modelling, *Arctic and Alpine Research,* 29, 2 233-239.

Oerlemans, J. (1997b) A flowline model for Nigardsbreen, Norway: projection of future glacier length based on dynamic calibration with the historic record, *Annals of Glaciology*, 24, 382-389.

Oerlemans, J. (1998) Modelling glacier fluctuations, In Haeberli, W., Hoelzle, M. and Suter, S. (Eds.), *Into the second century of worldwide glacier monitoring. Studies and Reports in Hydrology*, No. 56, 85 – 96. UNESCO.

Oerlemans, J. (2000) Analysis of a three year meteorological record from the ablation zone of Morteratschgletscher, Switzerland: energy and mass balance, *Journal of Glaciology*, 46, 155, 571-579.

Oerlemans, J. *Modelling valley glaciers*, Institute For Marine and Atmospheric Research, The Netherlands, Unpublished.

Oerlemans, J. and Fortuin, J. P. F. (1992) Sensitivity of glaciers and small ice caps to greenhouse warming, *Science*, 258; 115–117.

Oerlemans, J. and Hoogendoorn, N.C. (1989) Mass-balance gradients and climatic change, *Journal of Glaciology,* 35, 121, 399-405.

Oerlemans, J. and Reichert, B. K. (2000) Relating glacier mass balance to meteorological data by using a seasonal sensitivity characteristic (SSC), *Journal of Glaciology, 46*, 1-6.

Paaske, E. (ed) (2002) *The energy sector and water resources in Norway 2002*, Ministry of Petroleum and Energy, Oslo, Norway (http://www.mpe.dep.no)

Palutikof, J.P., Goodess, C.M., Watkins, S.J. and Holt, T. (2002) Generating rainfall and temperature scenarios at multiple sites: Examples from the Mediterranean, *Journal of Climate*, 15, 24, 3529-3548.

Paterson, W.S.B. (1981) *The Physics of glaciers* (2nd edition), Pergamon Press, Oxford.

Pelfini, M. and Smiraglia, C. (1997) Signals of 20th-century warming from the glaciers in the Central Italian Alps, *Annals of Glaciology*, 24, 350-354.

Pettitt, A.N. (1979) A non-parametric approach to the change-point problem, *Applied Statistics*, 28, 2, 126-135.

Pohjola, V.A. and Rodgers, J.C. (1997a) Atmospheric circulation and variations in Scandinavian Glacier Mass Balance, *Quaternary Research*, 47, 29-36.

Pohjola, V.A. and Rodgers, J.C. (1997b) Coupling between the atmospheric circulation and extremes of the mass balance of Storglaciären, northern Scandinavia, *Annals of Glaciology*, 24, 229-233.

Raper, S.C.B., Briffa, K.R. and Wigley, T.M.L. (1996) Glacier change in northern Sweden from AD 500: a simple geometric model of Storglaciaren, *Journal of Glaciology*, 42 (141), 341-351.

Rhines, P.B. (1994) Climate change in the Labrador Sea, its convection and circulation, Proceedings from the principal investigators meetings, Atlantic Climate Change Program (ACCP), Princeton, May 9th-11th, 1994.

Rodgers, J.C. (1990) Patterns of low-frequency monthly sea level pressure variability (1899-1986) and associated wave cyclone frequencies, *Journal of Climate*, 3, 1364-1379.

Romero, R., Ramis, C. and Guijarro, J.A. (1999a) A classification of the atmospheric circulation patterns producing significant daily rainfall in the Spanish Mediterranean are *International Journal of Climatology*, 19, 95-112.

Romero, R., Sumner, G., Ramis, C. and Genovés, A. (1999b) A classification of the atmospheric circulation patterns producing significant daily rainfall in the Spanish Mediterranean are *International Journal of Climatology*, 19, 765-785.

Schlosser, E. (1997) Numerical simulation of fluctuations of Hintereisferner, Ötztal Alps, since AD 1850, *Annals of Glaciology*, 24, 199-202.

Schmeits, M.J. and Oerlemans, J. (1997) Simulation of the historical variations in length of Unterer Grindwaldgletscher, Switzerland, *Journal of Glaciology*, 43, 143, 152-164.

Sheridan, S.C. (2002) The redevelopment of a weather-type classification scheme for North America, *International Journal of Climatology*, 22, 51-68.

Six, D., Reynaud, L. and Letréguilly, A. (2001) Bilans de masse des glaciers alpins et scandinaves, leur relations avec l'oscillation de climat de l'Atlantique nord, *Earth and Planetary Sciences*, 333, 693-698.

Slonosky, V.C., Jones, P.D. and Davies, T.D. (2000) Variability of the surface atmospheric circulation over Europe, 1774-1995, *International Journal of Climatology*, 20, 1875-1897.

Smith, K. (1995) Precipitation over Scotland, 1757-1992: Some aspects of temporal variability, *International Journal of Climatology*, 15, 543-556.

Sneyers, R. (1992) On the use of statistical analysis for the objective determination of climate change, *Meteorol. Zeitschrift*, N.F. 1, 247-256.

Sweeney, J.C. (1985) The changing synoptic origins of Irish precipitation, *Institute of British Geographers*, 10, 467-480.

Sweeney, J.C. (1987) Controls on the climate of Ireland, *Geographical Viewpoint*, 16, 60-71.

Tangborn, W. (1980) Two models for estimating climate-glacier relationships in the North Cascades, Washington, U.S.A, *Journal of Glaciology*, 25 (91), 3-21.

Torsnes, I., Rye, N. and Nesje, A. (1993) Modern and Little Ice Age equilibrium line altitudes on outlet valley glaciers from Jostedalsbreen, Western Norway: an evaluation of different approaches to their calculation, *Arctic and Alpine Research*, 25, 2, 106-116.

Trigo, R.M. and DaCamara, C.C. (2000) Circulation weather types and their influence on the precipitation regime in Portugal, *International Journal of Climatology*, 20, 1559-1581.

Tuomenvirta, H., Drebs, A., Førland, E., Tveito, O.E., Alexandersson, H., Vaarby Laursen, E. and Jónsson, T. (2001) *Nordklim data set 1.0- description and illustrations*. DNMI Klima Report no. 08/01. Norwegian Meteorological Institute, Oslo

Tvede, A.M. and Laumann, T. (1997) Glacial variations on a meso-scale: examples from glaciers in the Aurland Mountains, southern Norway, *Annals of Glaciology*, 24, 130-134.

Tveito, O.E. (1996) *Trends and variability in North Atlantic pressure series*. DMNI-Report No. 27/96 Klima, Norwegian Meteorological Institute, Oslo.

Valla, F. and Piedallu, C. (1997) Volumetric variations of Glacier de Sarennes, French Alps, during the last two centuries, *Annals of Glaciology*, 24, 361-366.

Van De Wal, R. and Oerlemans, J. (1995) Response of a valley glacier to climate change and kinematic waves: a study with a numerical ice-flow model, *Journal of Glaciology*, 41, 137, 142-152.

Vincent, C. and Vallon, M. (1997) Meteorological controls on glacier mass balance: empirical relations suggested by measurements on glacier de Sarennes, France, *Journal of Glaciology*, 43, 143, 131-137.

Von Storch, H. (1999) On the use of 'inflation' in statistical downscaling, *Journal of Climate*, 12, 3503-3506.

Von Storch, H., Zorita, E. and Cusbach, U. (1993) Downscaling of global climate change estimates to regional scales: An application to Iberian rainfall in wintertime, *Journal of Climate*, 6, 1161-1171.

Wallinga, J. and Van De Wal, R. (1998) Sensitivity of Rhonegletscher, Switzerland, to climate change: experiments with a one-dimensional flowline model, *Journal of Glaciology*, 44, 147, 383-393.

Washington, R., Hodson, A., Isaksson, E., and MacDonald, O. (2000) Northern hemisphere teleconnection indices and the mass balance of Svalbard glaciers, *International Journal of Climatology*, 20, 473-487.

Weber, G-R. (1997) Spatial and temporal variations of 300hPa temperatures in the Northern Hemisphere between 1966 and 1993, *International Journal of Climatology*, 17, 171-185.

Werner, P.C., Gerstengarbe, F-W., Fraedrich, K. and Oesterle, H. (2000) Recent climate change in the North Atlantic/European sector, *International Journal of Climatology*, 20, 463-471.

Wibig, J. (1999) Precipitation in Europe in relation to circulation patterns at the 500 hPa level, *International Journal of Climatology*, 19, 253-269.

Wigley, T.M.L., Jones, P.D., Briffa, K.R. and Smith, G. (1990) Obtaining sub-grid scale information from coarse-resolution general circulation model output, *Journal of Geophysical Research*, 95 (D2), 1943-1953.

Wilby, R.L. (1992) The influence of variable weather patterns on river water quantity and quality regimes, *International Journal of Climatology*, 13, 447-459.

Wilby, R.L. (1997) Non-stationarity in daily precipitation series: implications for GCM downscaling using atmospheric circulation indices, *International Journal of Climatology*, 17, 439-454.

Wilby, R.L. (1998) Modeling low-frequency rainfall events using airflow indicies, weather patterns and frontal frequencies, *Journal of Hydrology*, 212-213, 380-392.

Wilby, R.L. and Dawson, C.W. (2001) Using SDSM — *A decision support tool for the assessment of regional climate change impacts*. User Manual.

Wilby, R.L., Dawson, C.W. and Barrow, E.M. (2002) SDSM- a decisions support tool for the assessment of regional climate change impacts, *Environmental Modelling and Software*, 17, 147-159.

Wilby, R.L., Hay, L.E. and Leavesley, G.H. (1999) A comparison of downscaled and raw GCM output: implications for climate change scenarios in the San Juan River basin, Colorado, *Journal of Hydrology*, 225, 67-91.

Wilby, R.L., Wigley, T.M.L. (2000) Precipitation predictors for downscaling: Observed and general circulation model relationships, *International Journal of Climatology*, 20, 641-661.

Wilby, R.L., Wigley, T.M.L., Conway, D., Jones, P.D., Hewitson, B.C., Main, J. and Wilks, D.S. (1998) Statistical downscaling of general circulation model output: a comparison of methods, *Water Resources Research*, 34, 2995-3008.

Wilks, D. (1995) *Statistical methods in the atmospheric sciences*. Academic Press Limited, London.

Wilks, D. (1998) Multisite generalization of a daily stochastic precipitation generation model, *Journal of Hydrology*, 210,178-191.

Wilks, D.S. and Wilby, R.L (1999) The weather generation game: a review of stochastic weather models, *Progress in Physical Geography*, 23 (3), 329-357.

Winkler, J.A., Palutikof, J.P., Andresen, J.A. and Goodess, C.M. (1997) The simulation of daily temperature series from GCM output. Part II: Sensitivity analysis of an empirical transfer function methodology, *Journal of Climate*, 10, 2514-2532.

Yarnal, B. (1982) *The relationship between synoptic scale atmospheric circulation and glacier mass balance in south-western Canada*. Unpublished Ph.D thesis, Simon Fraser University.

Yarnal, B (1984) Synoptic-scale atmospheric circulation over British Columbia in relation to the mass balance of Sentinel Glacier, *Annals of the Association of American Geographers*, 74, 3, 375-392.

Yarnal, B. (1993) *Synoptic Climatology in Environmental Analysis*, Belhaven Press, London.

Yarnal, B. Comrie, A.C., Frakes, B., and Brown, D.P. (2001) Developments and prospects in synoptic climatology, *International Journal of Climatology*, 21, 1923-1950.

Zorita, E. and Von Storch, H. (1998) The analog method as a simple statistical downscaling technique: comparison with more complicated methods, *Journal of Climate*, 12, 2474-2489.

Zorita. E., Hughes, J.P., Lettemaier, D.P. and Von Storch, H. (1995) Stochastic characterisation of regional circulation patterns for climate model diagnosis and estimation of local precipitation, *Journal of Climate*, 8, 1023-1042.

Zuo, Z. and Oerlemans, J. (1997) Numerical modelling of the historic front variation and the future behaviour of the Pasterze glacier, Austria, *Annals of Glaciology*, 24, 234-241.

Appendix I

VV Horizontal visibility at surface

Code	km	m	Code	km	m	Code	km	m	Code	km	Code	km	m	
00	<0.1	<100	20	2.0	2000	40	4.0	4000	60	10	80	30		
01	0.1	100	21	2.1	2100	41	4.1	4100	61	11	81	35		
02	0.2	200	22	2.2	2200	42	4.2	4200	62	12	82	40		
03	0.3	300	23	2.3	2300	43	4.3	4300	63	13	83	45		
04	0.4	400	24	2.4	2400	44	4.4	4400	64	14	84	50		
05	0.5	500	25	2.5	2500	45	4.5	4500	65	15	85	55		
06	0.6	600	26	2.6	2600	46	4.6	4600	66	16	86	60		
07	0.7	700	27	2.7	2700	47	4.7	4700	67	17	87	65		
08	0.8	800	28	2.8	2800	48	4.8	4800	68	18	88	70		
09	0.9	900	29	2.9	2900	49	4.9	4900	69	19	89	>70		
10	1.0	1000	30	3.0	3000	50	5.0	5000	70	20	90	<0.05		<50
11	1.1	1100	31	3.1	3100	51			71	21	91	0.05		50
12	1.2	1200	32	3.2	3200	52			72	22	92	0.2		200
13	1.3	1300	33	3.3	3300	53	not used		73	23	93	0.5		500
14	1.4	1400	34	3.4	3400	54			74	24	94	1		1000
15	1.5	1500	35	3.5	3500	55			75	25	95	2		2000
16	1.6	1600	36	3.6	3600	56		6	76	26	96	4		4000
17	1.7	1700	37	3.7	3700	57		7	77	27	97	10		
18	1.8	1800	38	3.8	3800	58		8	78	28	98	20		
19	1.9	1900	39	3.9	3900	59		9	79	29	99	>=50		

Notes:
(1)If the visibility is between two of the distances given in the table, the code figure for the lower distance is reported e.g. a visibility of 470 m is reported as 04
(2)When VV=00 the actual visibility is reported by the extra group 1V'f'/V'f'f' in Section 5

(Source: http://www.weather.org.uk/resource/vvcode.htm)

Appendix II

Winter

	Component					
	1	2	3	4	5	6
pres 00	-0.16	0.93	0.13	-0.17		
pres 06	-0.19	0.96	0.06	-0.13		
pres 12	-0.19	0.97				
pres 18	-0.18	0.95				
tmp 00	0.83		0.14	0.38	0.20	
tmp 06	0.87		0.18	0.31	0.22	
tmp 12	0.86	0.12	0.24	0.24	0.26	
tmp 18	0.84	0.11	0.27	0.14	0.30	0.12
rho 00	0.86	0.10		0.33		
rho 06	0.90	0.10		0.22		
rho 12	0.90	0.10	0.14			
rho 18	0.88		0.16		0.10	0.18
cld 00	0.70	-0.10	-0.16		0.08	-0.50
cld 06	0.71	-0.13		-0.24	0.18	-0.36
cld 12	0.63	-0.15		-0.41	0.37	
cld 18	0.58	-0.13		-0.48	0.36	0.16
vis 00	-0.66		0.39		0.17	0.42
vis 06	-0.72		0.32	0.20	0.16	0.32
vis 12	-0.68		0.27	0.42	0.14	
vis 18	-0.64		0.21	0.52		-0.23
vv 00	0.33		0.60		-0.38	-0.14
vv 06	0.31		0.73	-0.13	-0.33	
vv 12	0.26		0.75	-0.24	-0.23	
vv 18	0.19		0.68	-0.19	-0.12	
uu 00	0.68	0.18	-0.36	0.17	-0.27	
uu 06	0.75	0.18	-0.33	0.11	-0.33	0.13
uu 12	0.78	0.15	-0.25		-0.33	0.24
uu 18	0.75	0.13	-0.18	-0.10	-0.27	0.32

Table II-1 Bodo Component matrix with six extracted components. Values less than 0.1 are not displayed. Pres-pressure; tmp-temperature; rho-specific humidity; cld-cloud amount; vis-visibility; *vv*-south scalar; *uu*-west scalar

	Component					
	1	2	3	4	5	6
pres 00	-0.23	-0.66	0.66	-0.14		
pres 06	-0.23	-0.72	0.64			
pres 12	-0.22	-0.76	0.59			
pres 18	-0.20	-0.77	0.54			
tmp 00	0.77	0.23	0.35	0.33		
tmp 06	0.81	0.26	0.36	0.22		
tmp 12	0.79	0.29	0.41	0.15		-0.11
tmp 18	0.75	0.29	0.45		0.11	-0.15
rho 00	0.82		0.21	0.28	-0.13	
rho 06	0.88		0.22	0.17		0.10
rho 12	0.88		0.24		0.08	
rho 18	0.83	0.10	0.27		0.20	
cld 00	0.68				-0.45	-0.10
cld 06	0.69			-0.27	-0.29	-0.18
cld 12	0.65	0.11		-0.37		-0.37
cld 18	0.59			-0.38	0.12	-0.43
vis 00	-0.57	0.30	0.23	0.12	0.52	-0.18
vis 06	-0.61	0.30	0.24	0.29	0.39	-0.18
vis 12	-0.55	0.31	0.30	0.46		-0.12
vis 18	-0.56	0.25	0.23	0.52	-0.22	
vv 00	-0.12	0.51	0.38	-0.25		0.31
vv 06	-0.19	0.55	0.44	-0.37		0.32
vv 12	-0.28	0.47	0.50	-0.36		0.24
vv 18	-0.27	0.37	0.47	-0.22	-0.14	0.16
uu 00	0.66	-0.32	-0.13	0.23		0.24
uu 06	0.73	-0.31	-0.16	0.16	0.11	0.32
uu 12	0.75	-0.25	-0.16		0.30	0.29
uu 18	0.70	-0.17	-0.13	-0.11	0.42	0.20

Table II-2 Orlandet Component matrix with six extracted components. Values less than 0.1 are not displayed. Pres-pressure; tmp-temperature; rho-specific humidity; cld-cloud amount; vis-visibility; *vv*-south scalar; *uu*-west scalar

	Component				
	1	2	3	4	5
pres 06	-0.44	0.49	0.71	0.11	0.12
pres 12	-0.47	0.52	0.70		
pres 18	-0.48	0.53	0.67		
tmp 06	0.84	0.35		-0.13	-0.18
tmp 12	0.79	0.44	0.15	-0.11	-0.16
tmp 18	0.85	0.36	0.14	-0.11	
rho 06	0.87	0.21		-0.11	
rho 12	0.90	0.21	0.16	-0.11	
rho 18	0.89	0.15	0.16	-0.11	0.15
cld 06	0.47	-0.42	0.23	-0.13	
cld 12	0.54	-0.44	0.22	-0.15	0.20
cld 18	0.45	-0.39	0.12	-0.13	0.29
vis 06		0.67	-0.42	-0.16	0.40
vis 12	-0.19	0.73	-0.45	-0.11	0.19
vis 18		0.69	-0.46	-0.16	0.33
vv 06	0.33			0.54	0.24
vv 12	0.35			0.63	0.41
vv 18	0.32			0.54	0.49
uu 06	0.21	0.25	-0.19	0.31	-0.49
uu 12	0.29	0.25	-0.18	0.40	-0.47
uu 18	0.27	0.21	-0.14	0.39	-0.34

Table II-3 Skabu Component matrix with five extracted components. Values less than 0.1 are not displayed. Pres-pressure; tmp-temperature; rho-specific humidity; cld-cloud amount; vis-visibility; *vv*-south scalar; *uu*-west scalar

	Component			
	1	2	3	4
pres 06	-0.33		0.88	0.29
pres 12	-0.31		0.92	0.22
pres 18	-0.26		0.93	0.17
tmp 06	0.75	0.53	0.16	-0.11
tmp 12	0.76	0.58	0.16	
tmp 18	0.75	0.56	0.12	
rho 06	0.81	0.40	0.14	-0.15
rho 12	0.83	0.44	0.11	
rho 18	0.80	0.46		
cld 06	0.64			0.32
cld 12	0.64		-0.19	0.48
cld 18	0.57		-0.18	0.52
vis 06	-0.51	0.53		-0.12
vis 12	-0.56	0.55	0.12	-0.29
vis 18	-0.53	0.49	0.17	-0.38
vv 06	-0.45	0.54	-0.27	0.30
vv 12	-0.55	0.58	-0.20	0.31
vv 18	-0.57	0.52		0.19
uu 06	0.65	-0.27	0.23	-0.24
uu 12	0.70	-0.29	0.18	-0.26
uu 18	0.71	-0.22		

Table II-4 Nordstraum Component matrix with four extracted components. Values less than 0.1 are not displayed. Pres-pressure; tmp-temperature; rho-specific humidity; cld-cloud amount; vis-visibility; *vv*-south scalar; *uu*-west scalar

Summer

	Component					
	1	2	3	4	5	6
pres 00		-.306	.876		.243	
pres 06		-.326	.912		.195	
pres 12	-.110	-.304	.922		.153	
pres 18	-.159	-.262	.897		.140	
tmp 00	.534	.662	.121			
tmp 06	.767	.482	.148			
tmp 12	.877	.252	.163			
tmp 18	.860	.198	.194		-.110	.161
rho 00	.327	.730	.198	-.331	-.108	
rho 06	.415	.730	.205	-.306		
rho 12	.453	.718	.204	-.230		
rho 18	.501	.653	.188	-.145		
cld 00	-.567	.319	-.119	-.226		.473
cld 06	-.595	.362	-.151	-.162	.282	.352
cld 12	-.577	.419	-.192		.447	.103
cld 18	-.456	.425	-.226	.101	.468	
vis 00	.522	-.365	-.193	.309	.252	-.271
vis 06	.585	-.428	-.196	.300	.124	
vis 12	.537	-.557	-.144	.106		.189
vis 18	.443	-.585			-.214	.360
vv 00		.420	.161	.515	-.345	.270
vv 06		.391	.151	.648	-.289	.175
vv 12	-.147	.502		.655		.132
vv 18	-.150	.470		.624	.135	
uu 00	-.682		.236	-.142	-.389	.107
uu 06	-.756	.119	.204	-.161	-.339	
uu 12	-.656	.206	.241		-.265	-.345
uu 18	-.540	.264	.183	.191	-.103	-.503

Table II-5 Bodo Component matrix with six extracted components. Values less than 0.1 are not displayed. Pres-pressure; tmp-temperature; rho-specific humidity; cld-cloud amount; vis-visibility; *vv*-south scalar; *uu*-west scalar

	Component					
	1	2	3	4	5	6
pres 00	-.297	.671	-.118	.615		
pres 06	-.360	.667		.634		
pres 12	-.371	.641		.658		
pres 18	-.371	.605		.650		
tmp 00	.593	.570	.257	-.142		
tmp 06	.455	.724		-.227		
tmp 12		.850		-.312		
tmp 18	.123	.838		-.254		-.131
rho 00	.546	.447	.497	-.152		.134
rho 06	.532	.550	.431	-.173		.136
rho 12	.615	.454	.327		.125	
rho 18	.601	.473	.190	-.109	.305	.117
cld 00	.498	-.418	.277	.230	-.125	-.126
cld 06	.536	-.456	.204	.315		-.130
cld 12	.576	-.495		.251	.300	
cld 18	.567	-.385	-.142	.155	.431	.214
vis 00	-.502	.176	-.440	-.233	.279	.273
vis 06	-.559	.181	-.417	-.325	.231	.302
vis 12	-.700	.195	-.179	-.322		.170
vis 18	-.715	.139		-.242	-.267	
vv 00	.665		-.230	.114	-.499	.177
vv 06	.680		-.395	.134	-.379	.234
vv 12	.656	.105	-.492	.111	-.134	.279
vv 18	.613		-.475	.137		.297
uu 00	-.326	-.238	.489	.160	.264	.174
uu 06	-.354	-.166	.578	.105		.324
uu 12	-.447	-.161	.506		-.227	.426
uu 18	-.355	-.216	.480		-.333	.274

Table II-6 Flesland Component matrix with seven extracted components. Values less than 0.1 are not displayed. Pres-pressure; tmp-temperature; rho-specific humidity; cld-cloud amount; vis-visibility; *vv*-south scalar; *uu*-west scalar

	Component			
	1	2	3	4
pres 06	.176	.775	.376	.416
pres 12		.792	.438	.411
pres 18		.757	.482	.377
tmp 06	.804	-.231	.335	-.119
tmp 12	.903		.206	-.146
tmp 18	.897		.191	
rho 06	.640	-.414	.511	
rho 12	.637	-.394	.527	
rho 18	.688	-.353	.452	
cld 06	-.561	-.353		.347
cld 12	-.458	-.533		.394
cld 18	-.368	-.505		.310
vis 06	.414	.424	-.340	-.289
vis 12	.333	.535	-.354	-.362
vis 18	.216	.501	-.314	-.264
vv 06	.663	-.102	-.372	.222
vv 12	.658	-.137	-.386	.293
vv 18	.629		-.371	.325
uu 06	-.627		.339	-.234
uu 12	-.603		.385	-.343
uu 18	-.577		.328	-.354

Table II-7 Nordstraum Component matrix with four extracted components. Values less than 0.1 are not displayed. Pres-pressure; tmp-temperature; rho-specific humidity; cld-cloud amount; vis-visibility; *vv*-south scalar; *uu*-west scalar

	Component					
	1	2	3	4	5	6
pres 00	.136	-.510	.755	.231	-.182	
pres 06		-.525	.798	.210	-.148	
pres 12		-.483	.834	.210		
pres 18		-.433	.828	.213		
tmp 00	.640	.524	.177			.134
tmp 06	.846	.321	.133			
tmp 12	.924					
tmp 18	.885					.216
rho 00	.541	.590	.290	-.201		.152
rho 06	.645	.539	.289	-.226		
rho 12	.627	.484	.291	-.213		-.153
rho 18	.676	.360	.230	-.155		-.136
cld 00	-.462	.432			-.251	.438
cld 06	-.531	.493			-.357	.180
cld 12	-.476	.543		.236	-.357	-.106
cld 18	-.316	.528		.239	-.324	-.326
vis 00	.235	-.470	-.358	.223		-.367
vis 06	.282	-.581	-.400	.148		-.142
vis 12	.231	-.666	-.345			.213
vis 18	.101	-.622	-.268			.465
vv 00	.309	.241		.565	.252	.146
vv 06	.473	.101	-.194	.624	.202	
vv 12	.337	.283	-.226	.666	-.122	.188
vv 18	.269	.310	-.170	.592	-.135	.102
uu 00	-.588	.154	.255		.281	.357
uu 06	-.674	.259	.270		.333	.222
uu 12	-.574	.255	.279	.117	.543	-.114
uu 18	-.418	.324	.160	.222	.473	-.320

Table II-8 Orlandet Component matrix with six extracted components. Values less than 0.1 are not displayed. Pres-pressure; tmp-temperature; rho-specific humidity; cld-cloud amount; vis-visibility; *vv*-south scalar; *uu*-west scalar

	Component					
	1	**2**	**3**	**4**	**5**	**6**
pres 06	.808		-.355	-.178		.387
pres 12	.801	-.118	-.378	-.170		.404
pres 18	.772	-.147	-.387	-.151	.102	.403
tmp 06	.575	.633			.146	-.251
tmp 12	.844	.331				-.272
tmp 18	.849	.313				-.201
rho 06	.305	.830		.222	.121	
rho 12	.194	.848		.294	.115	
rho 18	.103	.832		.308		.144
cld 06	-.615	.310		.180	.107	.337
cld 12	-.676	.362		.182		.372
cld 18	-.592	.341		.164		.310
vis 06	.484	-.400	.451	.441		.149
vis 12	.520	-.416	.463	.468		.105
vis 18	.505	-.388	.449	.490		.128
vv 06		.305	.464	-.365	-.219	.204
vv 12	.109	.342	.561	-.447	-.300	.119
vv 18	.113	.313	.525	-.380	-.318	.232
uu 06		-.109	.209		.579	.152
uu 12			.367	-.249	.675	
uu 18			.387	-.280	.587	

Table II-9 Skabu Component matrix with five extracted components. Values less than 0.1 are not displayed. Pres-pressure; tmp-temperature; rho-specific humidity; cld-cloud amount; vis-visibility; *vv*-south scalar; *uu*-west scalar

Appendix III

Daily mean sea level pressure for air mass clusters based on NCEP Reanalysis data

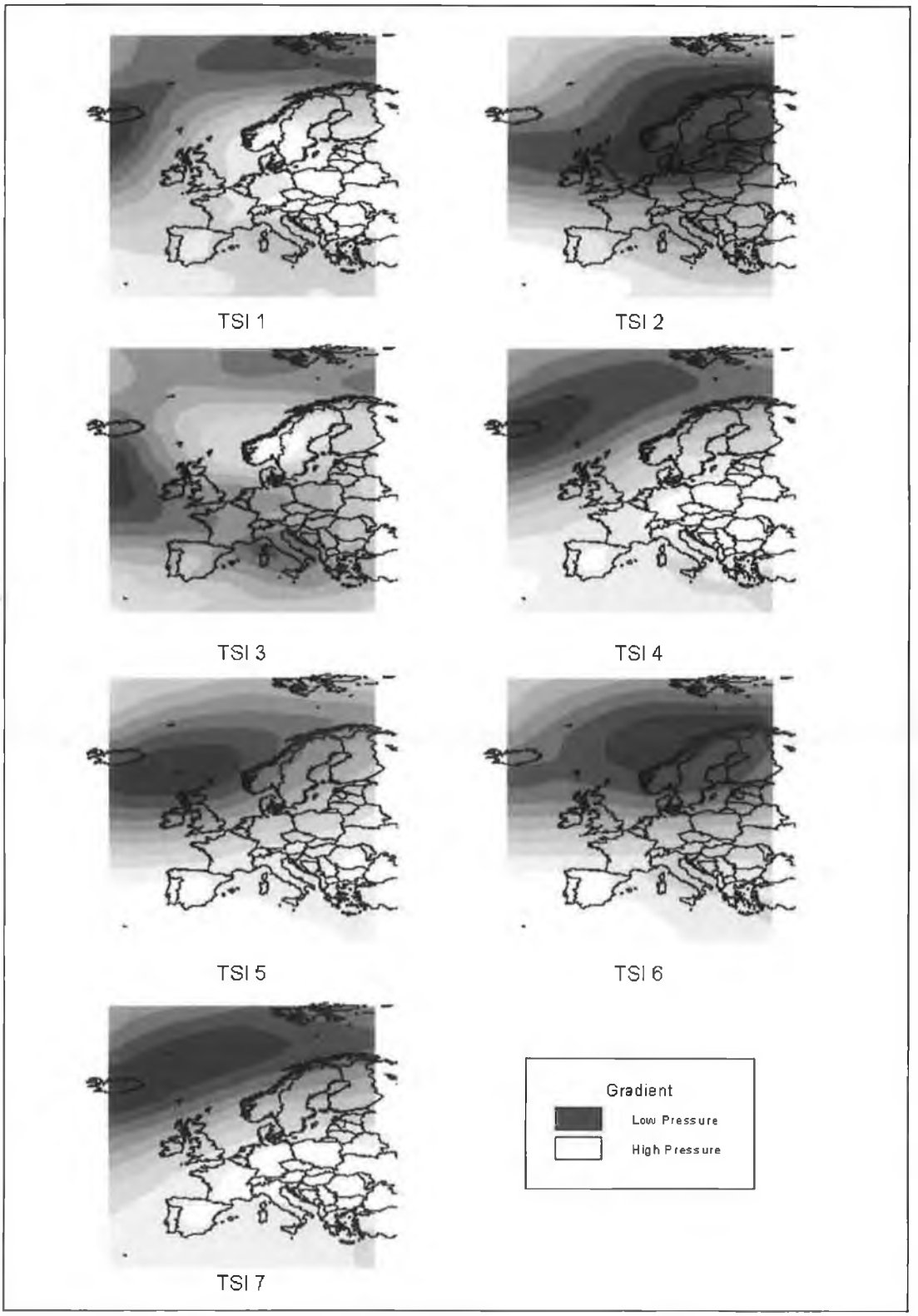

Figure III-1 Daily mean sea level pressure for air mass clusters from Flesland (DJF) 1968-1997

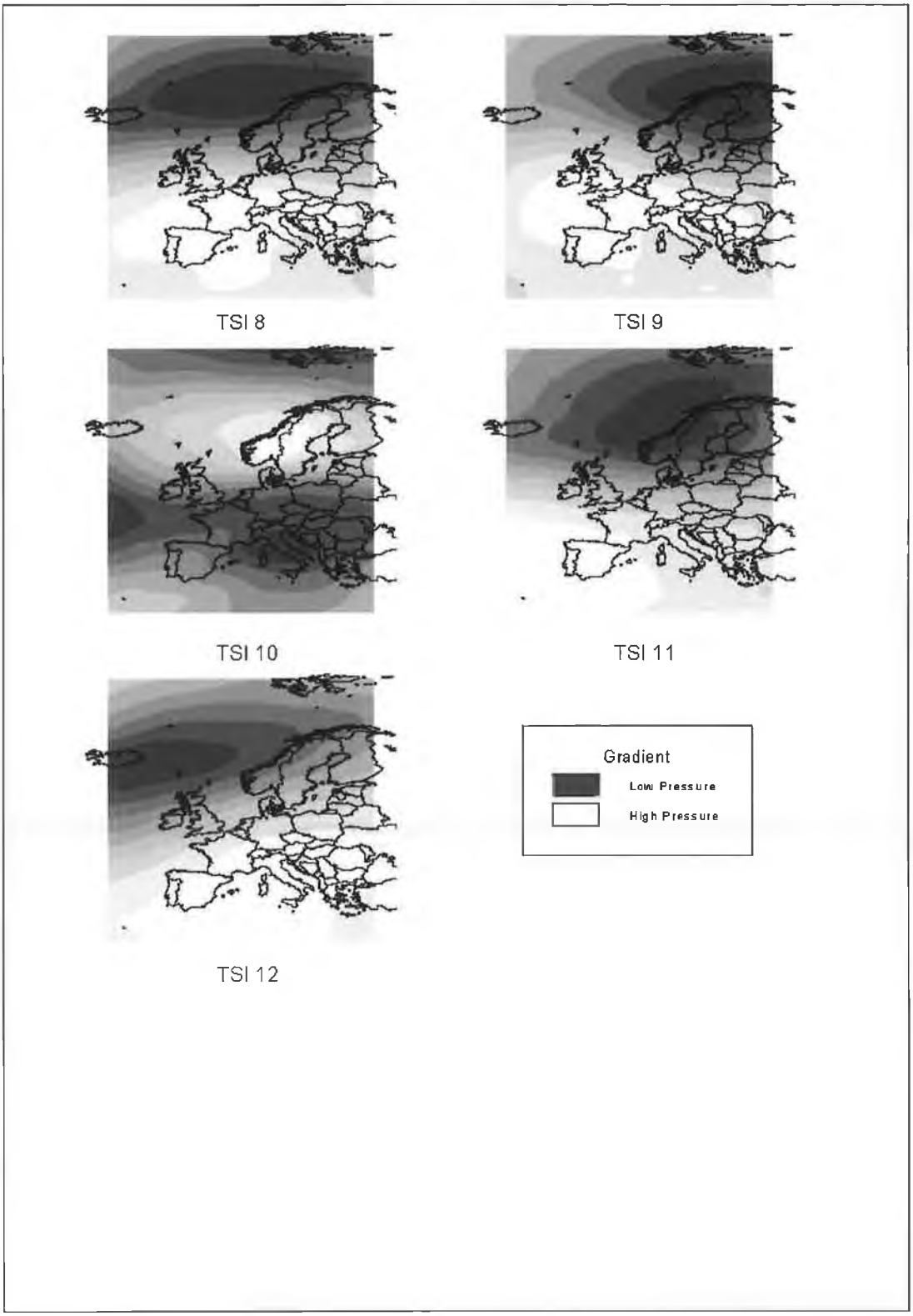

Figure III-2 Daily mean sea level pressure for air mass clusters from Flesland (DJF) 1968-1997

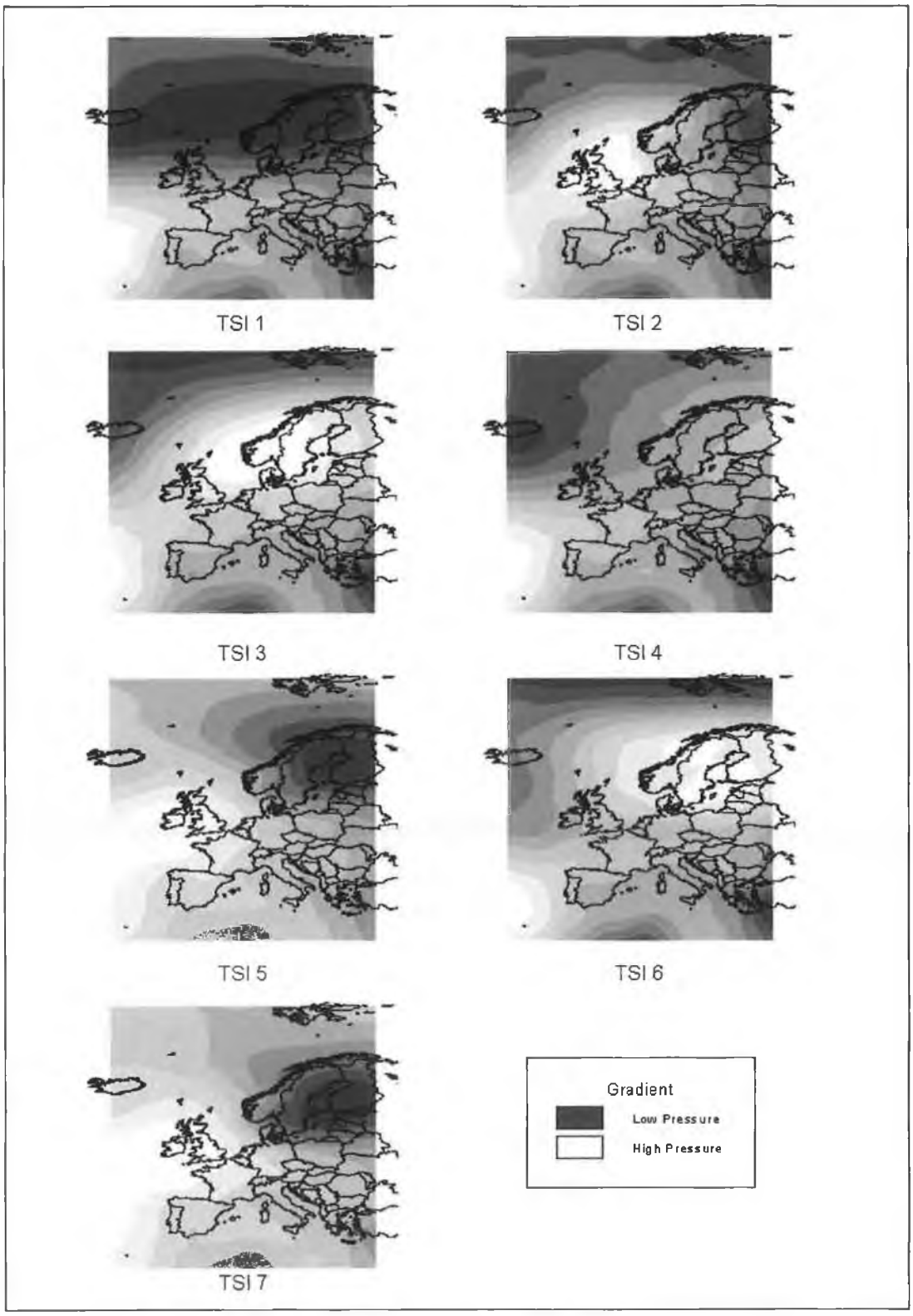

Figure III-3 Daily mean sea level pressure for air mass clusters from Skabu (JJA) 1968-1997

Appendix IV

Winter

Percentiles of GCM (x-axis) and NCEP (y-axis) predictor variables

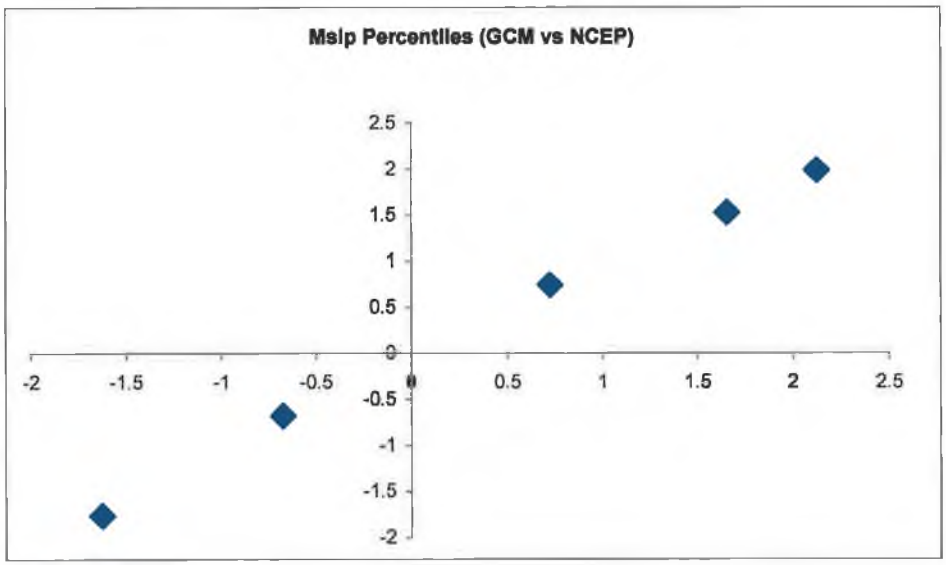

Figure IV-1 Comparison of GCM and NCEP percentiles of mslp

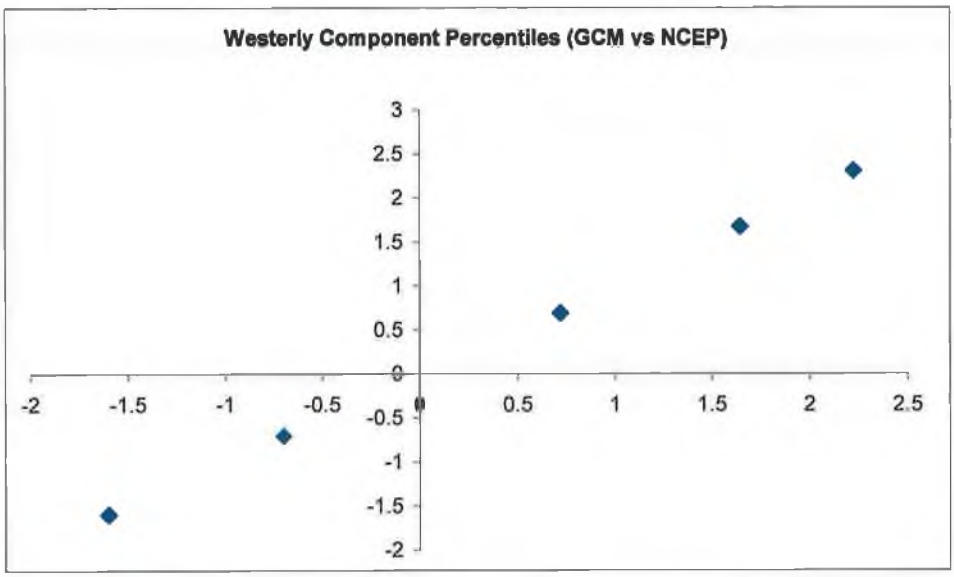

Figure IV-2 Comparison of GCM and NCEP percentiles of the westerly flow component

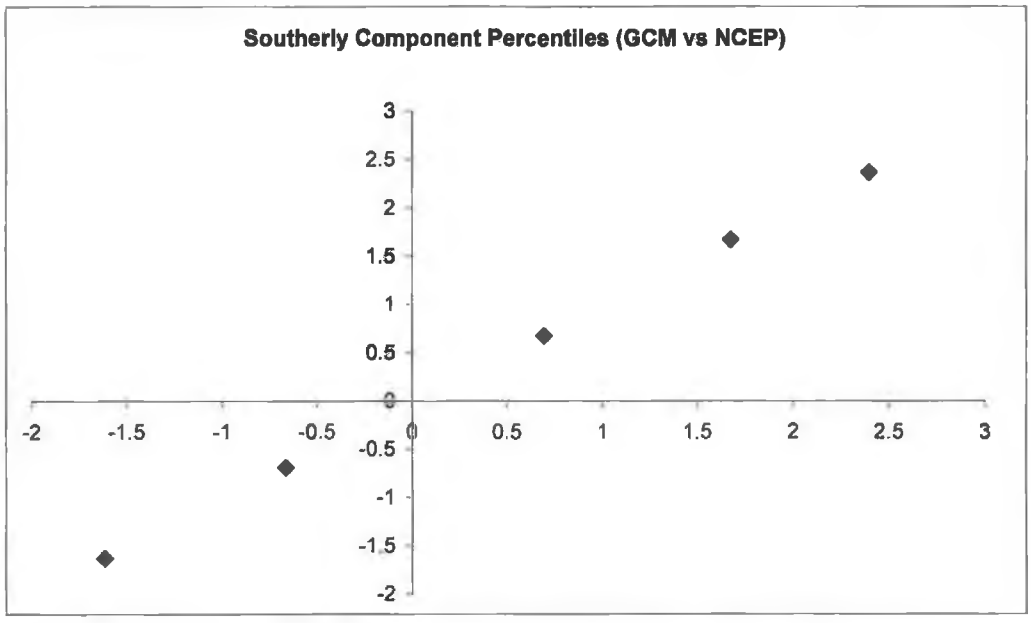

Figure IV-3 Comparison of GCM and NCEP percentiles of the southerly flow component

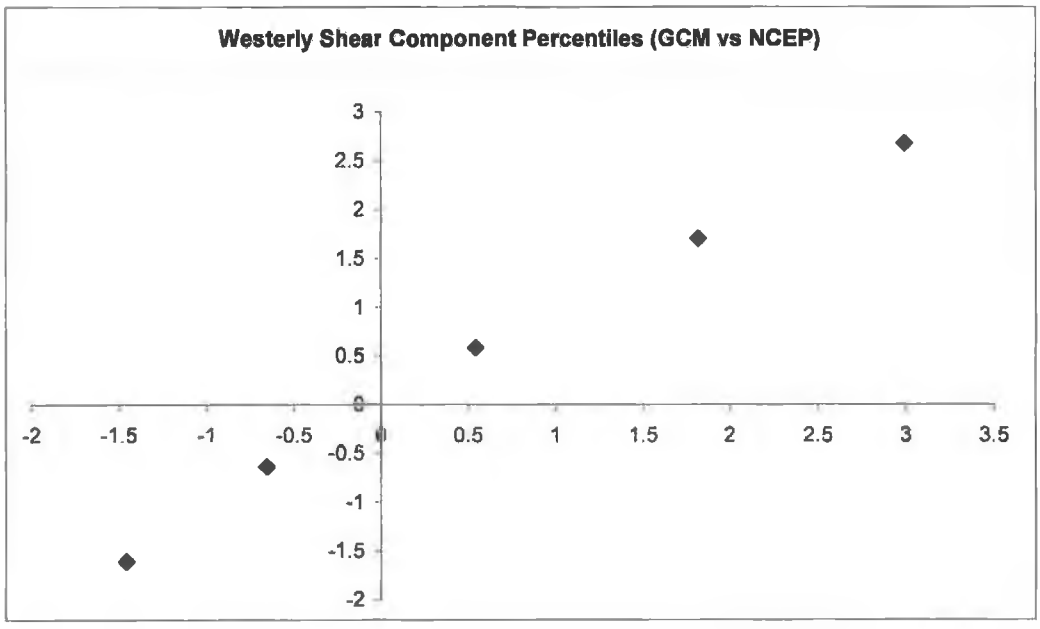

Figure IV-4 Comparison of GCM and NCEP percentiles of westerly shear vorticity

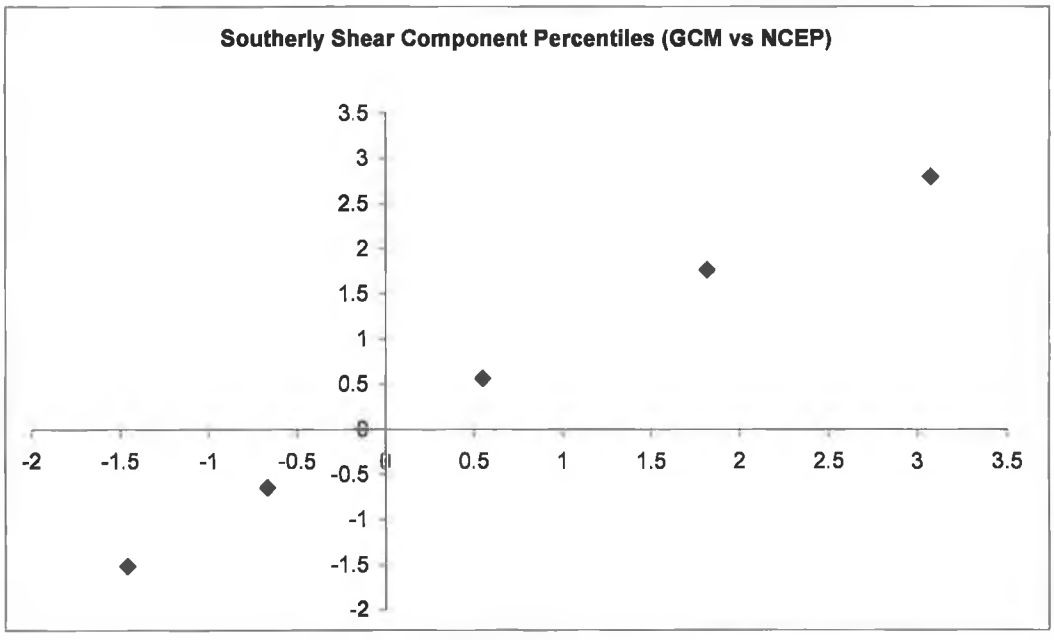

Figure IV-5 Comparison of GCM and NCEP percentiles of southerly shear vorticity

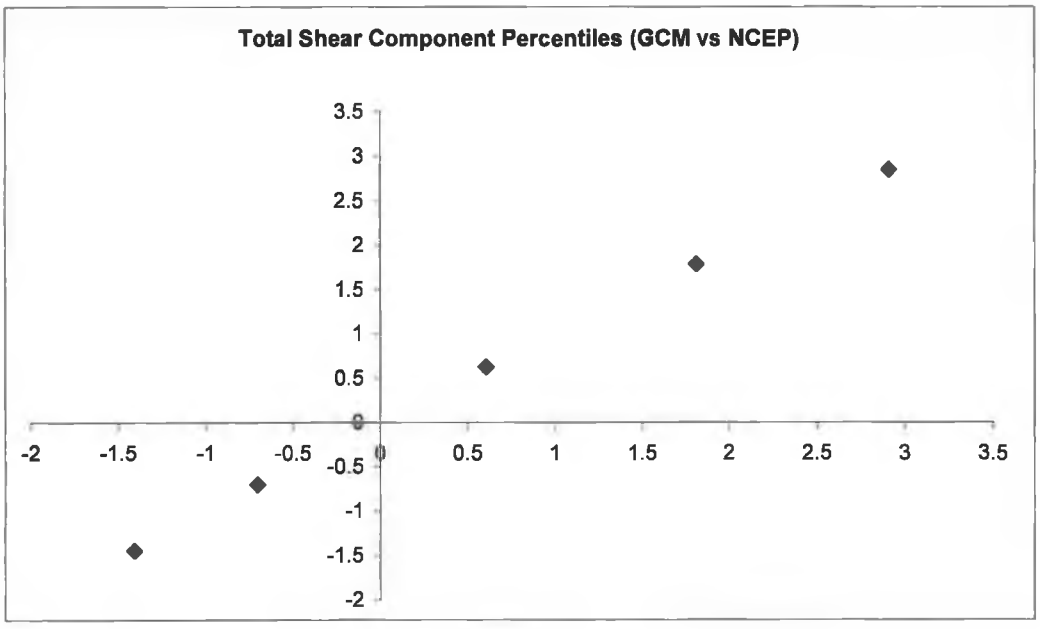

Figure IV-6 Comparison of GCM and NCEP percentiles of total shear vorticity

Summer

Percentiles of GCM (x-axis) and NCEP (y-axis) predictor variables

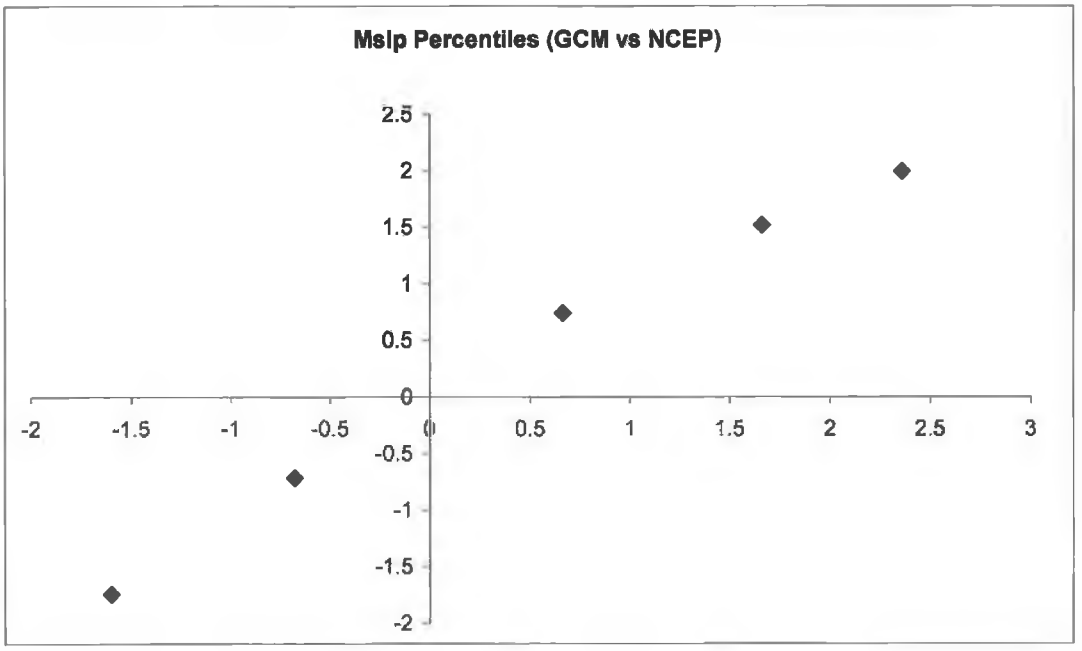

Figure IV-7 Comparison of GCM and NCEP percentiles of mslp

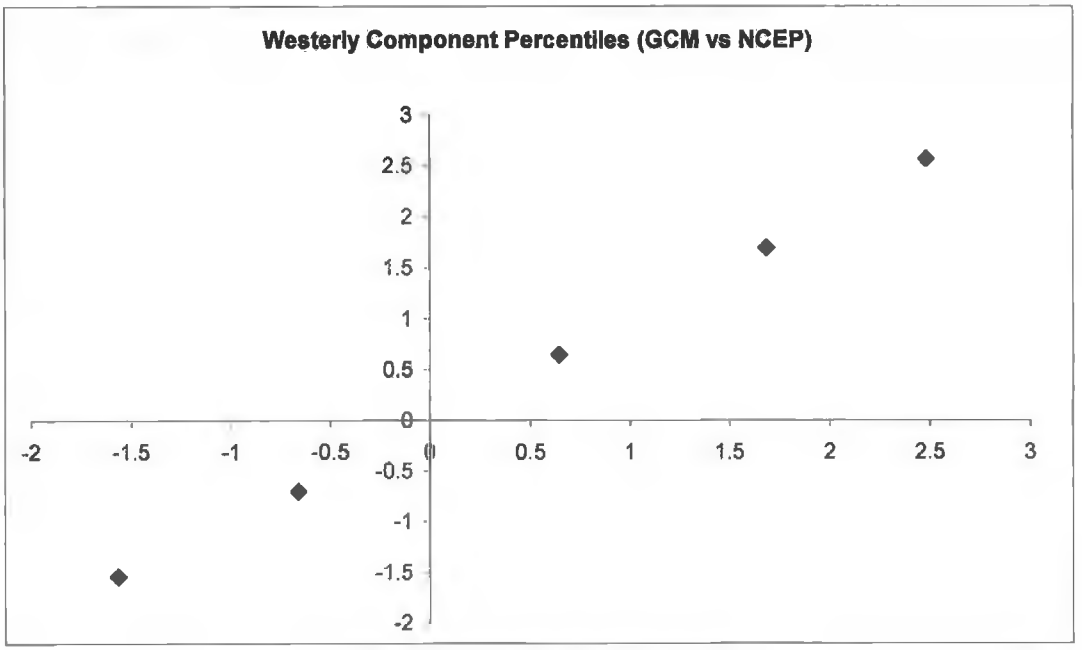

Figure IV-8 Comparison of GCM and NCEP percentiles of the westerly flow component

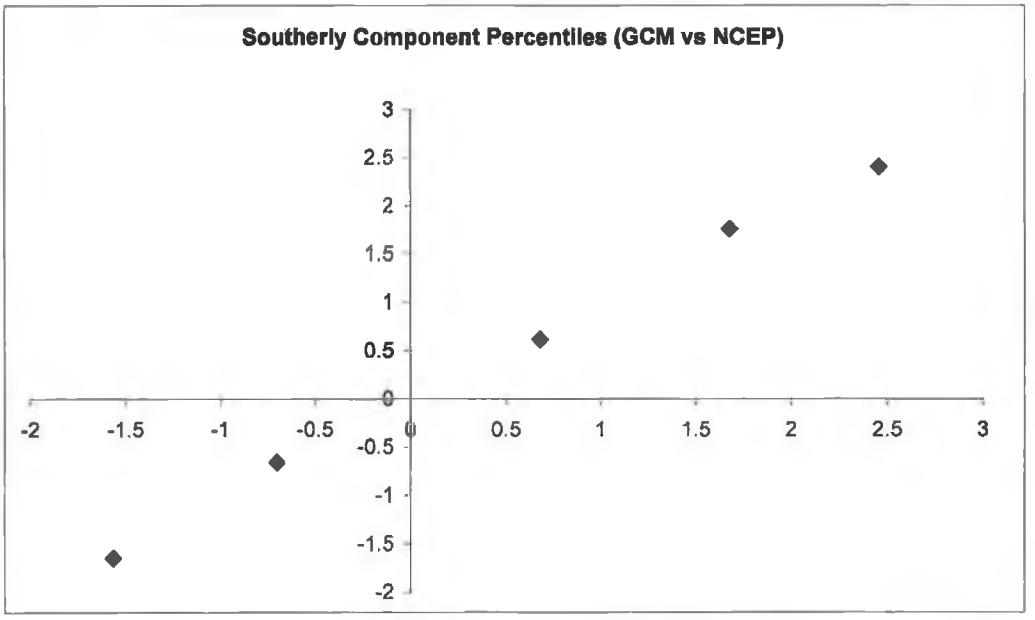

Figure IV-9 Comparison of GCM and NCEP percentiles of the southerly flow component

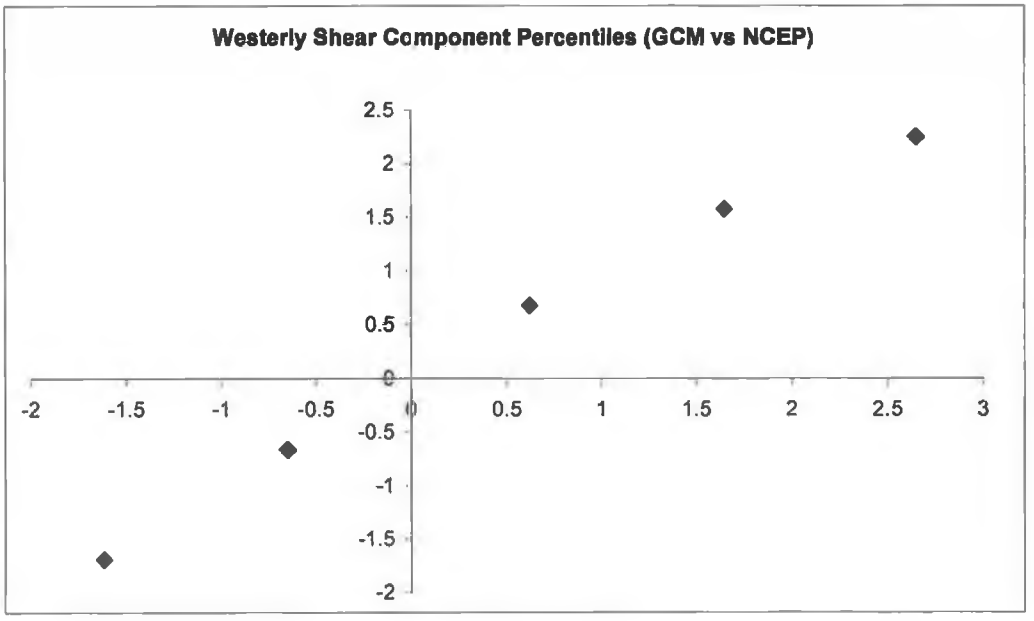

Figure IV-10 Comparison of GCM and NCEP percentiles of the westerly shear vorticity

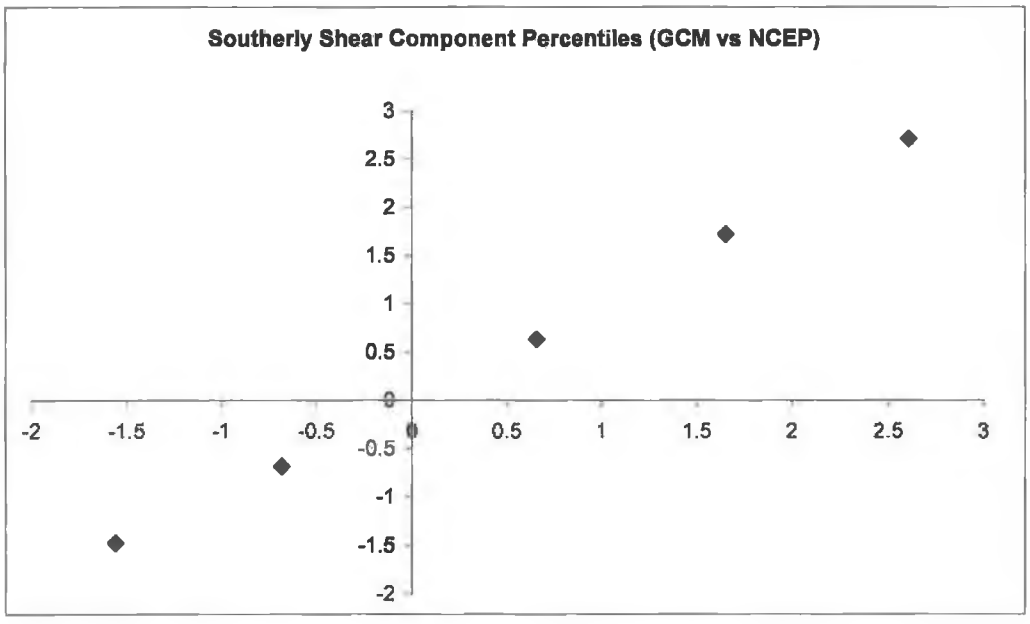

Figure IV-11 Comparison of GCM and NCEP percentiles of southerly shear vorticity

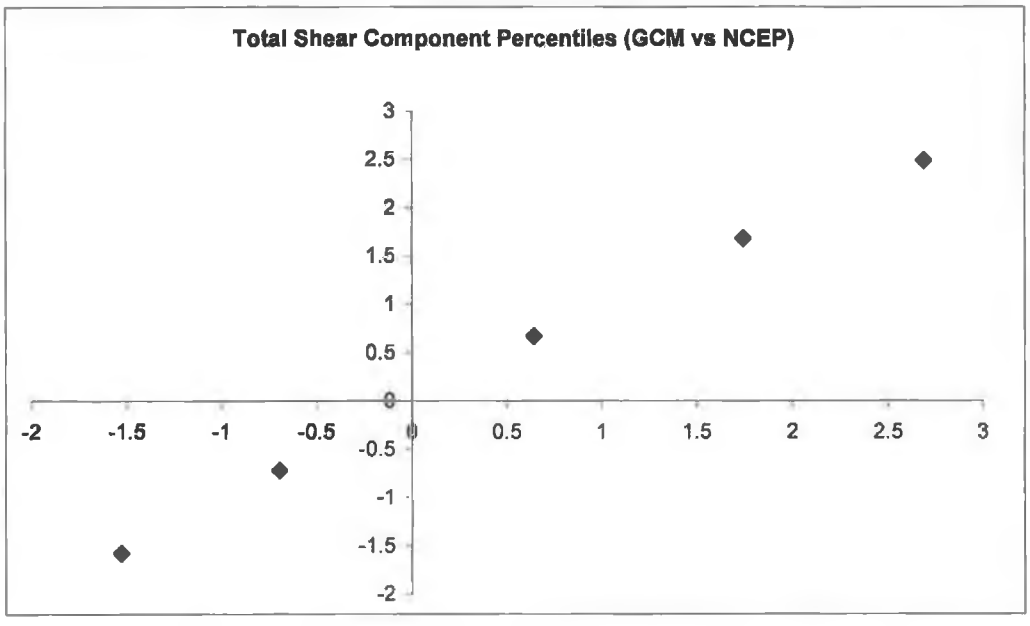

Figure IV-12 Comparison of GCM and NCEP percentiles of total shear vorticity

Appendix V

Flow diagram summarising main steps employed in methodology

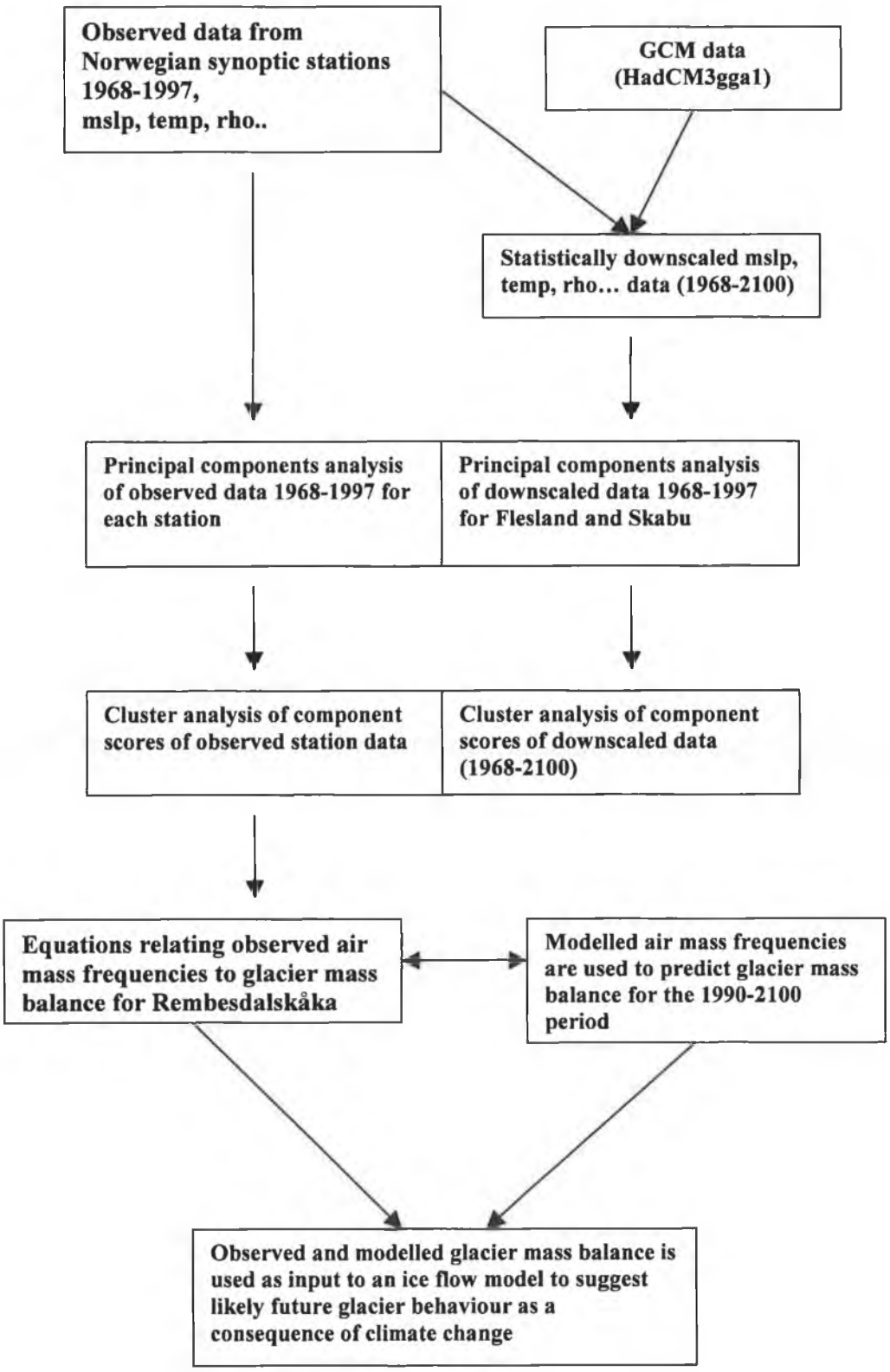

Appendix VI

Ice flow model Programme

```
#!/usr/bin/perl
# Glacier Model programme written by Jason Doran and Rowan Fealy
# Based on equations in Oerlemans 1997
use Math::BigFloat;
$datafile="glacier_data.csv";
```

Programme info and location of input data file

```
$delta_X= 200;          #distance interval
my $delta_T = 0.01; #Time interval
my $hgt = Math::BigFloat->new("1.11111111111111111111111111111");

my $fd=0.06e-15;                # flow parameter 1 This value will need to be adjusted
my $fs=1.79e-12;                # flow parameter 2 This value will need to be adjusted
my $roma=711428401649.511;      # pressure density of ice ((910kg/m-3) * gravity
                                #(9.81m/s2))^3
```

Setting grid and time intervals and specifying the constants

```
# Read in Bed Elevation, Bed Width, Lambda and Height
# Values vary over space only

my %sp=(); #Initialise spatial hash

open (DATA,"$datafile");

my $i = 0;              # A given space step
my $j = 1;              # A given time loop

while (<DATA>) {
        chomp;
        (my $bedElev, my $woBed, my $lambda, $hgt) = split (",");
        @height = (0, $hgt); #$hgt is at element one not element zero

        $sp{$i} = {
                'b'     => $bedElev,
                'wo'=> $woBed,
                'l'     => $lambda,
                'h'     => [@height]
        };

        #$sp{$i}{ab} = (-1 / ($sp{$i}{wo} + ($sp{$i}{l} * $sp{$i}{h}[1])));

        $i++
}
```

Reads the input data files over the space interval, i. Sets H as an array value.

```
my $start = 1;
my $end = $i - 2;
my $endj = 200000; #Says when to stop initialisation
```

Sets start and end of iterations for i and j.

```
close(DATA);

$i=1;

while ($j <= $endj){

        # Calculate New Height.
        # This is done at one given time (j)

        my %spcalc=(); #Initialise spatial hash for calculations
                        #Loop first over the i and then j
                        #for ($i = 1; $i <= $end; $i++) {

#Work out Diffusion equations for D{i} (width + Lambda*Height) * (Fd * (pg)**3 *
H**5 * slope**2) + (Fs * pg**3 * H**3 * slope**2)

        for ($i = 1; $i <= $end; $i++) {

$spcalc{$i}{slope} = (($sp{$i+1}{b} + $sp{$i+1}{h}[$j]) - ($sp{$i-1}{b} + $sp{$i-
        1}{h}[$j])) / (2 * $delta_X);

$spcalc{$i}{Di} = ($sp{$i}{wo} + ($sp{$i}{l} * 0.5 * $sp{$i}{h}[$j])) * ( ($fd *
$roma  * p($sp{$i}{h}[$j],5) * p($spcalc{$i}{slope},2)) + ($fs * $roma *
        p($sp{$i}{h}[$j],3) * p($spcalc{$i}{slope},2)) );

                                        }

$i=1;

# Works out D at i-.5 and i+.5

for ($i = 1; $i <= $end; $i++) {
$spcalc{$i-0.5}{b_Plus_h} = (($sp{$i}{b} + $sp{$i}{h}[$j]) - ($sp{$i-1}{b} +
$sp{$i-1}{h}[$j])) / $delta_X;

$spcalc{$i+0.5}{b_Plus_h} = (($sp{$i+1}{b} + $sp{$i+1}{h}[$j]) - ($sp{$i}{b} +
$sp{$i}{h}[$j])) / $delta_X;
```

```
$spcalc{$i-0.5}{D} = ($spcalc{$i-0.5}{b_Plus_h}) * (($spcalc{$i}{Di} +
$spcalc{$i-1}{Di}) / 2);

$spcalc{$i+0.5}{D} = ($spcalc{$i+0.5}{b_Plus_h}) * (($spcalc{$i+1}{Di} +
$spcalc{$i}{Di}) / 2);
                }
$i=1;
```

Calculates diffusion for each i-½ and i+½ and reads it into an array

```
# Works out d/dx(D d/dx(B+h)

for ($i = 1; $i <= $end; $i++) {

        $sp{$i}{d_ij} = ( ($spcalc{$i+0.5}{D}) - ($spcalc{$i-0.5}{D}) ) / $delta_X;
        $sp{$i}{a} = ($sp{$i}{d_ij} / ($sp{$i}{wo} + ($sp{$i}{l} *
$sp{$i}{h}[$j])));
                        }
        $i=1;
```

Calculates the change in D for i

```
# Calculate Mass Balance as a function of Height

if ($j <= 10000) {
        for ($i = 1; $i <= $end; $i++) {

        if ( (($sp{$i}{h}[$j] + $sp{$i}{b}) >= 1850) ) {
         ($mb{$i}{m} = 2.5395 + (-0.0081 * (($sp{$i}{b} + $sp{$i}{h}[$j])-1650 ))
);
                                                        }
         elsif (($sp{$i}{h}[$j] + $sp{$i}{b}) > 1800) {
         ($mb{$i}{m} = 1.1668 + (-0.0012 * (($sp{$i}{b} + $sp{$i}{h}[$j]) - 1650)
));
                }

         elsif (($sp{$i}{h}[$j] + $sp{$i}{b}) < 1800) {
         ($mb{$i}{m} = -0.1262 + (0.00942 * (($sp{$i}{b} + $sp{$i}{h}[$j]) - 1650)
));
                }

                        }
        }
elsif ($j > 10000) {
        for ($i = 1; $i <= $end; $i++) {

        if ( (($sp{$i}{h}[$j] + $sp{$i}{b}) >= 1850) ) {
         ($mb{$i}{m} = 2.5395 + (-0.0081 * (($sp{$i}{b} + $sp{$i}{h}[$j])-1650 ))
);
```

```
                                                    }
        elsif (($sp{$i}{h}[$j] + $sp{$i}{b}) > 1800) {
        ($mb{$i}{m} = 1.1668 + (-0.0012 * (($sp{$i}{b} + $sp{$i}{h}[$j]) - 1650)
));
                }

        elsif (($sp{$i}{h}[$j] + $sp{$i}{b}) < 1800) {
        ($mb{$i}{m} = -0.1262 + (0.00942 * (($sp{$i}{b} + $sp{$i}{h}[$j]) - 1650)
));
                }

                                                }
                                }
```

For time, j, less than a value, mass balance is equal to … for j greater than or equal to a value, mass balance is equal to…

```
                                $i=1;

                        # Works out DH/dt

                        for ($i = 1; $i <= $end; $i++) {

                        $sp{$i}{Dh_Dt} = ($sp{$i}{a}) + ($mb{$i}{m} / 0.9); # line
118
                                                #print " $sp{$i}{d_ij},
$sp{$i}{Dh_Dt},";
                                }

                        $i=1;
```

Calculates the rate of change of H over time

```
                                # Driving Stress Ud Us

#$sp{$i}{ud} = ( $fd * $roma * p($spcalc{$i}{slope},3) * p($sp{$i}{h},4) );
#$sp{$i}{us} = ( $fs * $roma * p($spcalc{$i}{slope},3) * p($sp{$i}{h},2) );


# Calculate new H

for ($i = 1; $i <= $end; $i++) {

$sp{$i}{a}, MB, $mb{$i}{m}, Dh/dt, $sp{$i}{Dh_Dt},";


 my $newj = $j + 1; #rf1

$sp{$i}{h}[$newj] = $sp{$i}{h}[$j] + ($sp{$i}{Dh_Dt} * $delta_T);
```

```
$sp{0}{h}[$newj] = $sp{1}{h}[$newj] ;#rf resetting height value at 0

                        print " $i , $j,";


if (($sp{$i}{h}[$newj] + $sp{$i}{b}) < $sp{$i}{b}) {
        ($sp{$i}{h}[$newj] = 0);
                                                }
        print " $sp{$i}{h}[$newj] \n";

        } #END for $i <= $end
```

Calculates new H, resets i to 1, ie the start of the glacier, iterates time, j, by 1

```
        $i=1;
                $newj =$j;
                $j++;

                #print " $j \n";

} #END

#Start and end Values are included for computations but not required
#Delete first and last key value from spatial hash
delete $spcalc{$start - 0.5};
delete $spcalc{$end + 0.5};
```

Values at i-½ and i+½ are required for boundary conditions and are deleted

```
#Print Stuff out now
sub numerically { $a<=>$b; }

sub p(){
        my $power=shift;
        my $factor=shift;
        my $result=$power;
        for (my $i=1; $i<$factor; $i++) {
                $result = $result * $power
        }
        return $result;
}

exit;
```